universität wien

DISSERTATION / DOCTORAL THESIS

Titel der Dissertation / Title of the Doctoral Thesis

„Synthesis and Biological Evaluation of Potential PET Tracers for the Muscarinic Acetylcholine Receptors“

verfasst von / submitted by

Marius Ozenil, BSc, MSc

angestrebter akademischer Grad / in partial fulfilment of the requirements for the degree of

Doktor der Naturwissenschaften (Dr. rer. nat.)

Wien, 2021 / Vienna 2021

Studienkennzahl lt. Studienblatt / degree programme code as it appears on the student record sheet:	A 796 605 419
Dissertationsgebiet lt. Studienblatt / field of study as it appears on the student record sheet:	Chemie
Betreut von / Supervisor:	Assoz. Prof. Mag. Dr. Wolfgang Wadsak, Privatdoz.

A scientist in his laboratory is not only a technician: he is also a child placed before natural phenomena which impress him like a fairy tale.

Marie Skłodowska-Curie
Madrid, 1933

Acknowledgment

I want to express my gratitude to Wolfgang Wadsak for supervising this doctoral thesis and for giving me the opportunity to work on radiotracer development in the Division of Nuclear Medicine at the Medical University of Vienna. Besides his evident experience in this field of research, I am very grateful for his approachable and joyful nature, which made me feel welcome from the very first moments.

My sincere thanks go to Verena Pichler, who guided me through this work all the way from the introduction into carbon-11 syntheses to the acceptance of the final manuscript. She conceptualized and led this research and irrespectively contributed by performing experiments. Her purposefulness, endurance and effectiveness were a true motivation.

I also wish to thank all my colleagues at the Division of Nuclear Medicine, especially Babsi, Cecile, Chrysoula, Eva, Julia K., Julia R., Julia V., Karsten, Kate, Lukas, Marie B., Marie N., Neydher, Resi, Sarah and Stefan, for fruitful discussions and for generating an amicable work environment. Special thanks go to Chrysoula, Neydher, Resi and Sarah for their support and for sharing their invaluable experience in pursuing a PhD in radiochemistry or radiopharmacy.

Furthermore, I want to thank my colleagues from the Department of Pharmaceutical Chemistry at the University of Vienna, Gini, Jonas, Markus and Marlon, for their support and ‘synthetic advices’.

I would also like to extend my gratitude to the diploma students Daniela, Julia, Kathi and Lukas for their invaluable experimental support.

Last but not least, I want to thank my family and friends for their support and unforgettable moments throughout these years. Needless to say, my biggest gratitude goes to my wife Sonja and my son Alexander for their deep love and for making me enjoy every single day of the last years.

Abstract

Muscarinic acetylcholine receptors (mAChRs) are G protein-coupled receptors, which appear as five subtypes (M1-M5). Considering their fundamental role in the nervous system and their involvement in many neurodegenerative disorders, mAChRs are an interesting target for molecular imaging. However, currently available mAChR PET tracers are only suitable to a limited extent, especially with respect to their subtype selectivity. Within this work 18 novel derivatives of the naturally occurring alkaloid arecoline were synthesized, chemically characterized and evaluated with a competitive radioligand binding assay toward all mAChR subtypes. Diphenylmethyl esters of arecaidine showed a strongly increased mAChR M1 affinity (from K_i = 20 µM to K_i = 3 nM) compared to arecoline and a promising subtype selectivity for mAChR M1 (up to 140-fold over M2). Radiolabeling of *N*-desmethyl precursors with [^{11}C]CH_3I afforded six carbon-11 labeled products in high radiochemical purity and good yield. Metabolic stability, insensitivity toward the off-target acetylcholinesterase and other preclinical parameters of the diphenylmethyl esters of arecaidine pointed toward a successful tracer, but autoradiography and a direct radioligand binding assay on living cells revealed unacceptable nonspecific binding. Hydrobenzoin esters of arecaidine were designed in the quest to lower lipophilicity while maintaining mAChR affinity. *In vitro* experiments and molecular docking revealed a pronounced dependence of mAChR M1 affinity on stereochemistry. Carbon-11 radiolabeling of the most potent *R*,*R*-isomer (K_i = 99 nM) is ongoing and will elucidate if the lowered lipophilicity results in reduced nonspecific binding. As a secondary finding of this thesis, a structural isomer of the mAChR M1 antagonist pirenzepine, which was unwittingly sold as pirenzepine, was discovered. The isomer was found to originate from an acid-catalyzed rearrangement and showed a tremendously decreased affinity towards mAChR M1. Furthermore, this thesis contains research which results improved the synthesis of routinely produced PET tracers.

Zusammenfassung

Muskarinische Acetylcholinrezeptoren (mAChRs) sind G-Protein-gekoppelte Rezeptoren, die als fünf Subtypen (M1-M5) vorkommen. In Anbetracht ihrer grundlegenden Rolle im Nervensystem und ihrer Bedeutung bei vielen neurodegenerativen Erkrankungen sind mAChRs ein interessantes Zielprotein für die molekulare Bildgebung. Derzeit verfügbare mAChR-PET-Tracer sind jedoch nur in begrenztem Umfang geeignet, insbesondere hinsichtlich ihrer Subtypen-Selektivität. In dieser Arbeit wurden 18 neue Derivate des natürlich vorkommenden Alkaloids Arecolin synthetisiert, chemisch charakterisiert und mit einem kompetitiven Radioliganden-Bindungsassay gegenüber allen mAChR-Subtypen untersucht. Arecaidindiphenylmethylester zeigten eine stark erhöhte mAChR M1-Affinität (von K_i = 20 µM zu K_i = 3 nM) im Vergleich zu Arecolin und eine vielversprechende Subtypen-Selektivität für mAChR M1 (bis zu 140-fach gegenüber M2). Durch radioaktive Markierung von *N*-Desmethyl-Vorläufersubstanzen mit [^{11}C]CH_3I konnten sechs Kohlenstoff-11-markierte Produkte in hoher radiochemischer Reinheit und guter Ausbeute hergestellt werden. Die metabolische Stabilität, Insensitivität gegenüber dem Off-Target-Protein Acetylcholinesterase und andere präklinische Parameter der Arecaidindiphenylmethylester deuteten auf einen erfolgreichen Tracer hin. Autoradiographie und ein direkter Radioliganden-Bindungsassay an lebenden Zellen zeigten jedoch eine inakzeptable unspezifische Bindung. Um die Lipophilie zu senken und gleichzeitig die mAChR-Affinität aufrechtzuerhalten, wurden Hydrobenzoinester des Arecaidins entwickelt. In-vitro-Experimente und molekulares Docking dieser Ester zeigten eine ausgeprägte Abhängigkeit der mAChR M1-Affinität von der Stereochemie. Die Kohlenstoff-11-Radiomarkierung des affinsten *R*,*R*-Isomers (K_i = 99 nM) ist noch nicht abgeschlossen und wird zeigen, ob die verringerte Lipophilie zu einer verringerten unspezifischen Bindung führt. Als sekundärer Befund dieser Arbeit wurde ein Strukturisomer des mAChR M1-Antagonisten Pirenzepin entdeckt, welches unwissentlich als Pirenzepin in den Handel gebracht wurde. Es wurde festgestellt, dass diese Isomer durch eine säurekatalysierte Umlagerung entsteht und eine enorm verringerte Affinität zu mAChR M1 aufweist. Darüber hinaus enthält diese Arbeit Forschungsergebnisse, welche die Synthese routinemäßig hergestellter PET-Tracer verbesserten.

Table of contents

1. Introduction 1
   1.1. Nuclear medicine 1
   1.2. PET 2
   1.3. Prerequisites for PET nuclides 3
   1.4. Carbon-11 5
   1.5. Designing small molecules as brain PET tracers 6
   1.6. Muscarinic Acetylcholine Receptors 8
   1.7. Development of mAChR ligands 8
   1.8. Arecoline – a mAChR ligand with high relevance for this thesis 10
   1.9. Muscarinic acetylcholine receptors as therapeutic targets 12
   1.10. PET tracer development for *in vivo* CNS muscarinic acetylcholine receptor imaging 13
   1.11. *in vivo* peripheral muscarinic acetylcholine receptor imaging 18
2. Aim 19
3. Results and discussion 20
   3.1. Enhanced arecoline derivatives as muscarinic acetylcholine receptor M1 ligands for potential application as PET radiotracers 22
   3.2. Synthesis, biological and computational evaluation of antagonistic, chiral hydrobenzoin esters of arecaidine targeting mAChR M1 41
   3.3. Pirenzepine's doppelgänger: Momentous rearrangement of the most prominent muscarinic M1 antagonist 54
   3.4. Pitfalls and solutions of the fully-automated radiosynthesis of [^{11}C]metoclopramide... 64
   3.5. Molar activity – The keystone in ^{11}C-radiochemistry: An explorative study using the gas phase method 79
   3.6. The Radiopharmaceutical Chemistry of Carbon-11: Tracers and Applications 86
4. Conclusion and outlook 103
5. Literature references 106
6. List of figures and tables 112
7. Supporting information 113

1. Introduction

1.1. Nuclear medicine

Nuclear medicine is a branch of medicine in which radionuclides, frequently coupled to a molecule of interest, are applied to the human body as unsealed sources. The used medical formulations, radiopharmaceuticals, are most commonly administered intravenously. The radiopharmaceutical consists of a chemical entity which accumulates at the region of interest and the radionuclide, which – depending on the mode of decay – allows for imaging and/or therapy.[1] **Therapeutic nuclides** most often are α- or β^--emitters, which are characterized by a high linear energy transfer, allowing them to deliver high doses within a small range of tissue. Half-lives are usually between hours and days, which allows for delivery flexibility and simultaneously makes sure that treated patients can leave the isolation within an acceptable time frame.[2] The β^--emitter iodine-131 is one of the oldest and still most commonly applied therapeutic radionuclides.[2] Iodide is strongly accumulated in thyroid tissue, which is the rational of the $[^{131}I]I^-$ therapy for the treatment of several thyroid diseases. In this case the plain iodide ion adopts two roles: Firstly, it is the targeting vector, which ensures that the radiopharmaceutical reaches its designated tissue. Secondly, it is the radionuclide, which releases the therapeutic radiation. Within the last years, radionuclide therapy has strongly been boosted by investments from big players of the pharmaceutical industry.[3] Nevertheless, diagnosis remains the more common application of nuclear medicine.[4] **Diagnostic nuclides** are required to emit radiation, which is far ranging enough to be detectable from outside the body and at the same time expose the body to a dose as low as possible. In scintigraphy a steady gamma camera captures a two-dimensional image of the distribution of a γ-emitting radiopharmaceutical in the organ of interest or also in the whole body. Considering that radiation from all depths of the subject is summed up in a single pixel on the plane detector, activity of the background tissue adds up to the desired signal, which in turn degrades the image contrast. In single photon emission computed tomography (SPECT) the emitted radiation is detected from various angles, thus allowing the calculation of a three-dimensional, tomographic image.[5] ^{99m}Tc is the most common medical radionuclide and is used in about 80 percent of all nuclear medicine procedures worldwide. It is readily available from a radionuclide generator and emits 140 keV photons during isomeric transition to ^{99}Tc with a half-life of 6 h. The generator yields $[^{99m}Tc]TcO_4^-$, which can be directly used for thyroid scans or reduced and converted to complexes for many different applications.[6] Depending on the posed medical question and tracer pharmacokinetics, nuclear imaging can be performed statically or dynamically. In static imaging a timely almost constant activity distribution is recorded over time and merged in a single image. In dynamic imaging a changing activity distribution is recorded as a series of frames.

Early time points, which generally show strong changes of activity distribution over time, are often recorded with a high frame rate, whereas the frame rate can be reduced for later, more static time points.[5]

1.2. PET

In positron emission tomography (PET) β^+-emitting radiopharmaceuticals are employed. During β^+-decay a proton of a proton-rich nucleus is converted to a neutron while emitting a positron and an electron neutrino (Equation 1).

$$ {}^{A}_{Z}X \rightarrow {}^{A}_{Z-1}Y + e^+ + \nu_e $$

Equation 1: β^+-decay

Upon collision of the emitted positron with an electron, two almost colinear 511 keV photons are released in opposing directions and registered simultaneously by a ring of scintillation detectors arranged around the subject. Therefore, the location of the β^+-decay can be traced back to the volume between the opposed coincidence detectors, which is also called the line of response (LOR). Unlike the gamma cameras used in scintigraphy and SPECT, coincidence detectors do not require absorptive collimation; consequently, the sensitivity of PET is about two to three orders of magnitude higher.[5] Early PET scanners contained only a single ring of detectors around the subject, which restricted the observable coincidence events to annihilation photons perpendicular to the body axis. Modern PET scanners contain multiple rings of detectors, forming a cylinder around the subject (Figure 1). This allows the scanner to register a greater number of coincidence events and hence further increases the sensitivity. Most state-of-the-art PET scanners come in combination with other imaging techniques such as computer tomography (CT) or magnetic resonance imaging (MRI). This allows for a reliable overlay of functional and anatomical images, as the scans can be performed in immediate sequence, without requiring the subject to change position.

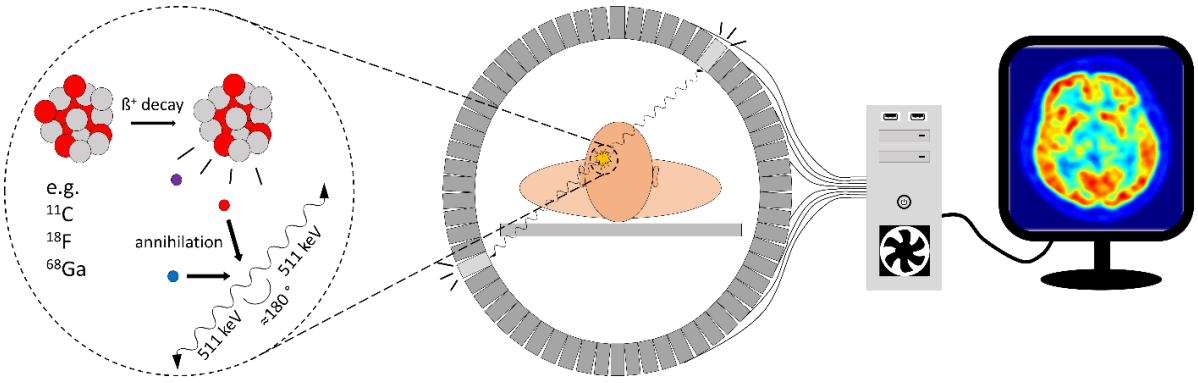


Figure 1: Principle of a PET scan.

2-[^{18}F]Fluoro-2-deoxy-D-glucose (2-[^{18}F]FDG) is by far the most commonly used PET tracer and therefore often referred to as the working horse of PET. PET imaging using 2-[^{18}F]FDG is crucial for a plethora of diagnostic procedures in oncology, neurology, cardiology and inflammatory conditions.[7] 2-[^{18}F]FDG is a fluorinated analogue of glucose, which also acts as a substrate for the GLU transporters. Cells with a higher energy demand often have upregulated GLU transporters and therefore show an increased uptake of 2-[^{18}F]FDG. Inside the cell 2-[^{18}F]FDG can be phosphorylated by hexokinase, the first enzyme of the glycolysis. However, 2-[^{18}F]FDG-6-phosphate lacks the hydroxyl group on position 2 and hence cannot be further metabolized by glycolysis, resulting in metabolic trapping of 2-[^{18}F]FDG-6-phosphate in cells with high glucose uptake (Figure 2)[8].

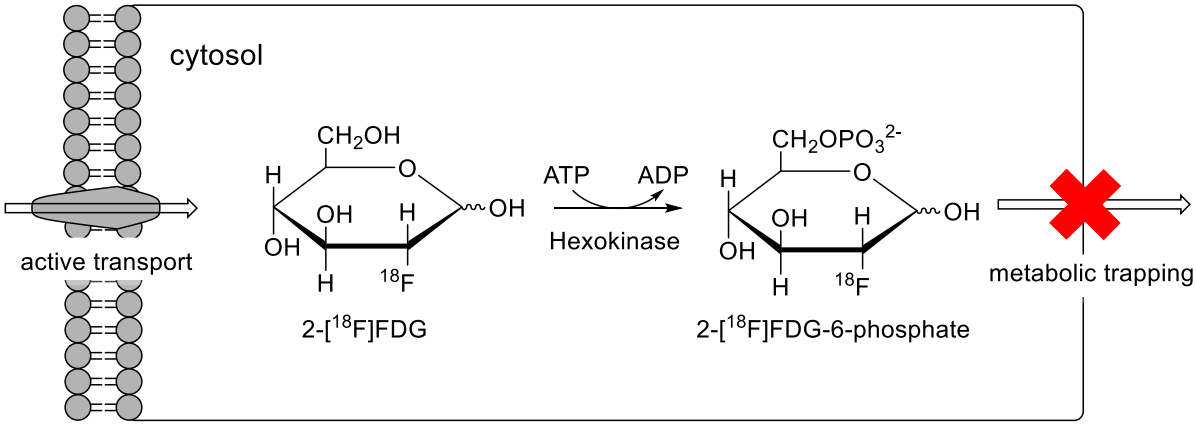


Figure 2: Main cellular metabolism of 2-[^{18}F]FDG trapping.

Although this picture of 2-[^{18}F]FDG is widely accepted and has become textbook knowledge, a less trivial 2-[^{18}F]FDG metabolism was observed in more detailed studies.[9]

1.3. Prerequisites for PET nuclides

Properties of some common radionuclides used in PET imaging are listed in Table 1.

Several factors contribute to the suitability of a radionuclide for PET imaging. Most obviously the nuclide has to undergo **β$^+$-decay with a high probability** and should not have an additional gamma-line close to 511 keV, which could impair quantitative accuracy. Most well-established PET radionuclides feature a β$^+$-decay probability close to 100%. Zirconium-89 displays a β$^+$-decay probability of only 23%; however, as the gamma-line resulting from electron capture (23%) is strongly above the annihilation photon energy, it can be easily gated off by the PET scanner. Still, this comes with an increased radiation burden compared to exclusively β$^+$-decaying nuclides.[10]

The total energy Q of the β$^+$-decay is shared as kinetic energy between the positron and the electron neutrino. Consequently, positrons arising from β$^+$-decay show a continuous distribution of kinetic energy, with a limit of Q. However, β$^+$-decaying nuclides which are characterized

by a high Q value also feature a higher average positron energy and hence a longer positron range.[11] The **positron range** is different between β^+-decaying nuclides and should be as low as possible as it sets a physical limit for the resolution of PET.[12]

The **half-life** of the nuclide should parallel the timescale of the targeted biological phenomenon. Nuclides with a short half-life are suitable for radiotracers with a fast pharmacokinetic, *e.g.* the very short-living radiopharmaceuticals $[^{13}N]NH_3$, $[^{15}O]H_2O$ and $[^{82}Rb]Rb^+$ are used for myocardial perfusion imaging.[13] Short half-life is both a blessing and a curse. On the one hand, high initial doses can be applied while maintaining low radiation burden for the patient and persons the patient encounters later. On the other hand, the nuclide source has to be in close proximity to the scanner and preparation as well as quality control of the product has to be performed at a great pace. Long-living nuclides like ^{89}Zr (3.3 d) and ^{64}Cu (12.7 h) can be found at the other side of the spectrum. These nuclides find their main application in immuno-PET as their long half-life matches well with the pharmacokinetics of antibodies and antibody conjugates.[14]

Chemical methods to reliably and **unimpededly incorporate the PET nuclide** to the radiotracer molecule must be available. Non-metallic PET nuclides like carbon-11 and fluorine-18 can be attached to a radiotracer molecule *via* covalent bonds, which allows to insert a radiolabel to the molecule of interest with no or only minor structural changes. Metallic PET nuclides require a chelator to be attached to the molecule of interest, which induces a structural change. With increasing size of the labeled molecule, this change becomes increasingly insignificant; consequently, metallic PET nuclides are predominantly used for labeling molecules of high molecular weight, such as peptides and proteins.

Besides these physical and chemical properties, the **availability** of the PET nuclide in combination with the **cost of** its **production** is an important factor. PET nuclides are predominantly produced by cyclotrons and radionuclide generators. A cyclotron accelerates small charged particles (most commonly hydride ions) by alternating the potential of surrounding D-shaped electrodes while being constrained to a circular orbit by an external magnetic field. Upon reaching the outermost orbit, the particles are extracted and directed to the target material. In case of accelerated hydride ions, this process usually involves a stripping foil, which removes the associated electrons and thus produces a plain proton beam. Installation and operation of an on-site medical cyclotron comes with a considerable financial effort, which restricts the availability of cyclotron-produced, short-lived nuclides (*e.g.* ^{11}C, ^{13}N, ^{15}O) to specialized centers.[15] The most frequently used PET nuclide fluorine-18 is produced by proton bombardment of $[^{18}O]H_2O$ and can be transported to regional PET centers because of its longer half-life.

In radionuclide generators a mother nuclide with a longer half-life is immobilized on a stationary phase and reaches transient equilibrium with a shorter-lived daughter. Through exploitation of the daughter's different chemical properties, it can be eluted from the generator. Comparably

low investment costs, low space requirement and ease of use are big advantages of radionuclide generators. However, as of now, only two generator-derived PET nuclides with GMP compliance are available: ^{82}Rb and ^{68}Ga. In an effort to overcome cyclotron dependency, the latter has recently attracted keen attention from the radiopharmaceutical industry as well as from academic researchers.[16]

Table 1: Properties of common PET nuclides.[17–19]

	Half-life	β^+ decay mode	Max. positron range (mm)	Production	Example of a relevant PET tracer
^{11}C	20.4 min	100%	4.1	^{14}N(p,α)^{11}C	[^{11}C]methionine[20]
^{13}N	9.98 min	100%	5.4	^{16}O(p,α)^{13}N	[^{13}N]NH_3[21]
^{15}O	2.03 min	100%	8.0	^{14}N(d,n)^{15}O	[^{15}O]H_2O[22]
^{18}F	109.8 min	97%	2.4	^{18}O(p,n)^{18}F	2-[^{18}F]FDG
^{68}Ga	68.0 min	89%	9.0	^{68}Ge/^{68}Ga gen.	[^{68}Ga]Ga-DOTATATE[23]
^{82}Rb	1.25 min	96%	16.5	^{82}Sr/^{82}Rb gen.	[^{82}Rb]RbCl[24]
^{89}Zr	78.4 h	23%	3.8	^{89}Y(p,n)^{89}Zr	[^{89}Zr]Zr-DFO-Trastuzumab[25]

1.4. Carbon-11

Carbon is the central element of organic chemistry and constitutes the majority of molecules that build up living organisms. As such, radioactive carbon isotopes enable radiolabeling of pivotal, highly bio-relevant structures without changing their structure at all. However, the short half-life sets high requirements on the swiftness of the reactions and on the synthesis module's degree of automation. The gas target during proton irradiation for carbon-11 production is commonly filled with naturally abundant N_2 (mainly ^{14}N) and traces of naturally abundant O_2 (mainly ^{16}O). Carbon-11 produced in such a target gas mixture exists as [^{11}C]CO_2, which can be directly used for labeling reactions (*e.g.* using Grignard chemistry[26]) or can be converted to secondary synthons (Figure 3). [^{11}C]CH_3I is the most commonly used carbon-11 synthon and can be synthesized automatically in various commercially available synthesis modules. [^{11}C]CH_3I can be formed *via* the "wet" chemistry method or the "gas-phase" method. In the "wet" chemistry method [^{11}C]CO_2 is trapped in solution of $LiAlH_4$ in tetrahydrofuran and thereby reduced to [^{11}C]CH_3OH. After evaporation of the solvent, hydroiodic acid is added to the precipitate and heated to 90 °C. The resulting [^{11}C]CH_3I is distilled off and passed over $NaOH/P_2O_5$ to remove HI and H_2O. Although this method is reliable in terms of radiochemical yields, it suffers from limited molar activity caused by contaminations of atmospheric CO_2 in $LiAlH_4$.[27] In the nowadays more commonly used "gas-phase" method [^{11}C]CO_2 is trapped on a molecular sieve and

reduced to [^{11}C]CH_4 in the presence of H_2 and a Ni catalyst at 400 °C. [^{11}C]CH_4 then undergoes iodination with I_2 at 720-740 °C. To improve the overall yield, this step is commonly performed in circulation, so that unreacted [^{11}C]CH_4 can be recycled.[27,28]

In the majority of applications [^{11}C]CH_3I is used to introduce a [^{11}C]methyl group to nucleophilic functionalities, such as alcohols, amines, phenols or thiols *via* an S_N2 reaction. To increase the reactivity for reactions with demanding nucleophiles, [^{11}C]CH_3I can be converted to [^{11}C]CH_3OTf by passage through an AgOTf column. Although less commonly applied, [^{11}C]CH_3I can also be used for different reactions, such as the formation of C-C bonds *via* Pd-mediated Stille and Suzuki cross-coupling.[29] The chemistry of carbon-11 is discussed in more detail in chapter 3.6.

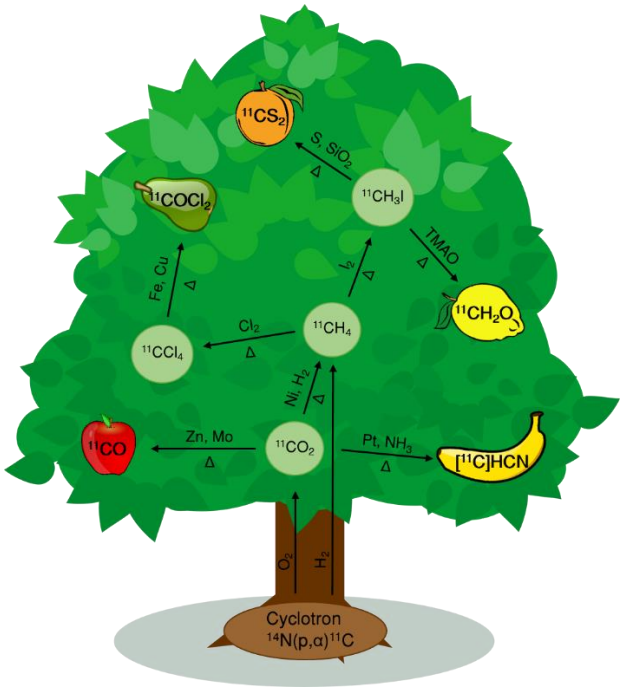


Figure 3: Reaction pathways to carbon-11 synthons. Own work, also published.[27]

1.5. Designing small molecules as brain PET tracers

Over the last decades a plethora of small molecules of PET tracers have been developed for brain imaging. Besides the aforementioned 2-[^{18}F]FDG, nowadays commonly used small molecules radiotracers include [^{11}C]PIB for imaging cerebral beta-amyloid plaques[30], [^{11}C]raclopride for imaging the cerebral D_2 dopamine receptor[31], [^{11}C]methionine for imaging amino acid uptake in glioma[20] and [^{11}C]DASB for imaging cerebral serotonin transporters[32].

A. D. Gee *et al.* recently summarized following design and test criteria for the development of small molecules as radiopharmaceutical vectors (Table 2).[33]

Table 2: Design and test criteria for the discovery and development of small molecule radiotracers.

Design criteria	Test criteria
• Choosing an appropriate target • High affinity and selectivity for the target • Ease of radiosynthesis • Maximizing target accessibility while minimizing non-displaceable binding	• Good signal-to-noise ratio *in vivo* • Good *in vivo* pharmacokinetics • *In vivo* distribution and pharmacology consistent with literature reports • Low levels of radiolabeled metabolites in the region of interest • High sensitivity toward the target

Design criteria can be evaluated prior radiolabeling and they support the identification of proper candidates for PET tracer development. Test criteria consist of properties that can be assessed by *in vitro* and *in vivo* experiments using the labeled compound to determine its potential utility as radiotracer.

For a PET tracer to be of clinical relevance most obviously also the chosen **molecular target** should be of clinical interest and there should be relevant clinical questions associated with that molecular target. Furthermore, the target has to be expressed at a sufficient concentration to allow for successful imaging. Although sensitivity generally is a major strength of PET imaging, review of the established radiotracers reveals that – with only some exceptions – the lowest B_{max} that can be successfully imaged is around 1 nM. Additionally, the size of the expressing tissue should at least exceed the resolution of the PET scanner (2-5 mm) to avoid underestimation of the signal through the partial volume effect.[33] The B_{max} strongly influences the required **affinity** of the radiotracer. With decreasing target expression levels (decreasing B_{max}) the affinity must increase accordingly (K_D decrease) to maintain the target-to-background ratio. As a rule of thumb, a minimum K_D/B_{max} ratio of 10 should be reached to achieve sufficient contrast *in vivo*.[34] Ideally, the radiotracer should be fully **selective** and thus only bind to the desired target. However, if the radiotracer binds to more than one target, the location, B_{max} and the affinity to the off-target must be considered. Radiochemistry of carbon-11 and fluorine-18 is a continuously evolving field, which has given rise to a wide variety of labeling reactions. Still, caused by the relatively short half-life, not all thinkable small molecules can be labeled with organic PET nuclides. **Ease of the radiochemistry** therefore remains an important factor when choosing a molecule for PET tracer development.[35] Diffusion or active transport of the PET tracer to the tissue of interest is a fundamental property in order to **maximize target accessibility**. Considering intravenous application, the blood-brain barrier (BBB) imposes a significant challenge for the target accessibility of brain radiotracers. The BBB comprises active transporters to satisfy the brain's need for important, highly polar molecules, such as amino

acids and glucose. Nevertheless, the vast majority of brain radiotracers do not fulfill the structural requirements to act as substrates for these transports and therefore rely on passive diffusion through the BBB, whereas [^{11}C]methionine and 2-[^{18}F]FDG are notable exceptions. A lot of research effort has been put in predicting a drug's likelihood to penetrate the BBB *a priori*. In addition to other physico-chemical properties, lipophilicity quantified by the logP value is frequently used as indicator for BBB permeability. Several desirable logP ranges have been proposed; however, when applied to the entity of brain permeable radiotracers there are numerous false positives and false negatives. In fact, a recent study concludes that the total polar surface area (tPSA), which can be calculated from any given chemical structure within seconds, displays a higher predictive power for the BBB permeability of radiotracers.[36] Additionally, efflux transporters, most notably the P-glycoprotein, can negatively affect the target accessibility of the radiotracer.[37]

1.6. Muscarinic Acetylcholine Receptors

Muscarinic Acetylcholine Receptors (mAChRs) are a group of G protein-coupled receptors, which bind the endogenous ligand acetylcholine and can also by activated by the fungal toxin muscarine. Alongside with nicotinic acetylcholine receptors, they mediate the cholinergic neurotransmission. Considering their regulatory functions in the central nervous system, glandular secretion, smooth muscle contraction and heart rate, mAChRs adopt a pivotal role in human physiology.[38] mAChRs are divided into five subtypes (M1-M5), which are expressed throughout the central and peripheral nervous system. Subtypes M1, M4 and M5 are mainly found in the central nervous system, whereas M2 and M3 also show high expression levels in the periphery.[39] Subtypes with odd numbers (M1, M3 and M5) are predominantly coupled to $G_{q/11}$ proteins, whereas even-numbered subtypes preferentially signal through $G_{i/o}$ proteins.[38] As of now the exact functional role of the different subtypes and their interplay within the same body system remains poorly defined.[40] This can partly be attributed to a lack of small molecules that can inhibit or activate specific mAChR subtypes with high selectivity.[38]

1.7. Development of mAChR ligands

Based on their location of binding, mAChR ligands can be divided in orthosteric, allosteric and bitopic ligands.[38] **Orthosteric ligands** bind to the same pocket as the endogenous ligand acetylcholine. The orthosteric binding site of the mAChRs is deeply buried within the transmembrane core as illustrated in the crystal structure of mAChR M1 (Figure 4) and is covered with a tyrosine lid.[38] In the region of the orthosteric pocket, crystal structures of the other mAChR subtypes show an overall very similar picture, which is not surprising when considering the

high degree of sequence homology between the subtypes.[41] Most well-known mAChR ligands (*e.g.* scopolamine, atropine, QNB)[42] bind to the orthosteric pocket. Orthosteric mAChR ligands generally bear a high affinity and a well-defined structure-activity relationship,[38] which are major advantages for PET tracer development. Furthermore, tritiated orthosteric mAChR ligands are commercially available (*e.g.* [^{3}H]NMS, [^{3}H]QNB),[43] which allows for straightforward affinity determination of novel unlabeled, orthosteric ligands. Based on their pharmacology, orthosteric mAChR ligands can be divided into agonists (activation of the receptor), antagonists (competitive inhibition of agonist) and inverse agonists (induces opposite pharmacological response).[44]

Allosteric ligands bind to a different part of the receptor, compared to the endogenous ligand. The vast majority of allosteric mAChR ligands bind to the cone above the orthosteric binding pocket, when viewing the receptor from the extracellular side (Figure 4). Allosteric mAChR ligands typically feature a superior subtype selectivity, which however comes at the cost of limited receptor affinity.[38] Based on their pharmacology, allosteric mAChR ligands can be basically divided into positive allosteric modulators (PAMs, increasing the affinity of orthosteric ligands), negative allosteric modulators (NAMs, lowering the affinity of orthosteric ligands) and neutral allosteric modulators.[45]

The pros and cons of orthosteric ligands versus allosteric ligands are highlighted by the comparison of the two well-studied ligands scopolamine and BQCA (Table 3).

Table 3: Binding parameters of well-known mAChR ligands given in nM. Data of scopolamine is given as K_i values from a competitive radioligand binding assay using [^{3}H]NMS. Values of BQCA are given as inflection point of ACh efficacy potentiation as measured by calcium mobilization.

compound	binding site	M1	M2	M3	M4	M5	lit.
scopolamine	orthosteric	1.1	2.0	0.44	0.8	2.07	[42]
BQCA	allosteric	845	>100000	>100000	>100000	>100000	[46]

In an attempt to combine the favorable properties of orthosteric and allosteric mAChR ligands, the concept of **bitopic ligands** has recently attracted strong research interest. This class of compounds is designed to simultaneously bridge both binding sites of a single receptor and aims to achieve subtype selectivity through the allosteric binding and affinity through the orthosteric binding. Although this concept seems simple and yet ingenious, its practical implementation remains cumbersome in many cases.[38] THRX-160209 can be considered a successful example of the bitopic concept.[47] However, the chemical characteristic of this class of compounds, such as the high molecular weight, indicates poor BBB permeability. Generally, there is not always consensus in the literature whether a ligand should be considered orthosteric or bitopic. In fact, several compounds which were initially described as orthosteric ligands later were reclassified as allosteric ligands.

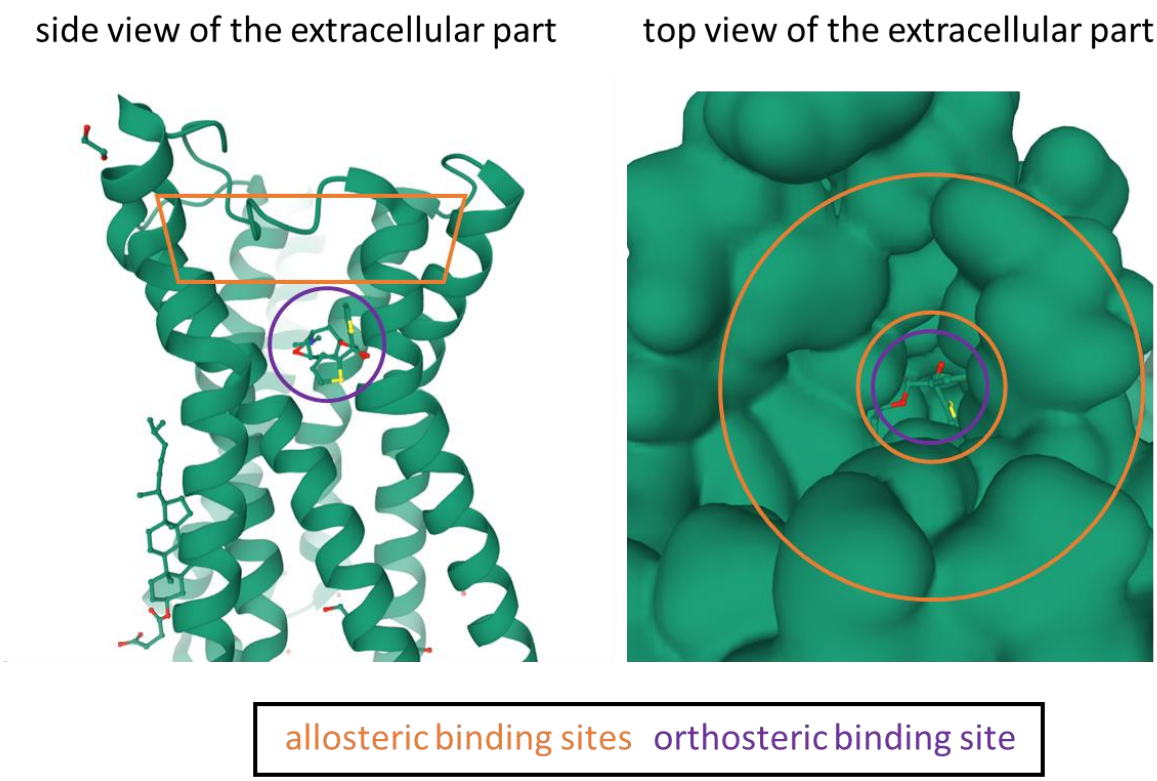


Figure 4: Graphical illustration of the mAChR M1 crystal structure PDB:5CXV[41] using Mol*.[48] The approximal location of the orthosteric binding site and the allosteric binding sites are highlighted. The receptor structure contains the co-crystallized orthosteric antagonist tiotropium, which is displayed in 'ball and stick' style. In the side view the protein is displayed as cartoon and in the top view it is displayed as Gaussian surface.

1.8. Arecoline – a mAChR ligand with high relevance for this thesis

Many orthosteric mAChR ligands occur as natural products in poisonous plants or fungi. Famous examples include muscarine found in *Amanita muscaria* (fly agaric) and atropine in *Atropa belladonna* (deadly nightshade). One of the less famous naturally occurring mAChR ligands – at least in the Western world – is the less toxic and psychoactive alkaloid arecoline. **Arecoline** is the major effective constituent in the fruits of *Areca catechu*, which are the fourth most commonly used drug after nicotine, alcohol and caffeine worldwide (Figure 5).[49] *Areca catechu* is mainly consumed in Southeast Asia, where also more than one million tons of its fruits are produced annually.[50] Typically, the fruits are consumed by chewing them wrapped in betel leaves coated with slaked lime, which gives the users euphoria, a sense of wellbeing, warmth, increased alertness and enhanced capability to work. However, this comes at the cost of many long-term side effects such as cancers of mouth and of esophagus, immunosuppression, hypothyroidism, prostate hyperplasia and infertility.[51] Tooth decay and permanently stained deep red tooth are the most visible side effects (Figure 5).



Figure 5: Top left: kiosk selling fruits of *Areca catechu* in Myanmar (own photograph), top right: user of Areca catechu with red-stained teeth (reproduced with permission of Gunda Wörlein, https://indojunkie.com/), bottom left: fruits of *Areca catechu* hanging in a kiosk in Myanmar (own photograph), bottom right: peeled fruit of *Areca catechu* (own photograph).

Despite these negative properties, fruits of *Areca catechu* are used in traditional Chinese medicine to treat tapeworm infections and arecoline was shown to improve the memory of patients suffering a variety of neurodegenerative diseases.[49] Being a BBB permeable but low affinity (K_i in the low micromolar range) mAChR agonist, arecoline may also act as a lead compound for the development of diagnostic or therapeutic mAChR ligands.[49] When comparing the structure of arecoline with other mAChR ligands (Figure 6) and unsuccessful ligands[52], it becomes clear that no space-demanding residues should be introduced at this part of the molecule. However, thinking of the secondary amine as precursor, the *N*-methyl group appears feasible for carbon-11 labeling using [^{11}C]CH_3I. Consequently, the *O*-methyl group of arecoline remains to tune its physico-chemical properties toward a suitable PET tracer.

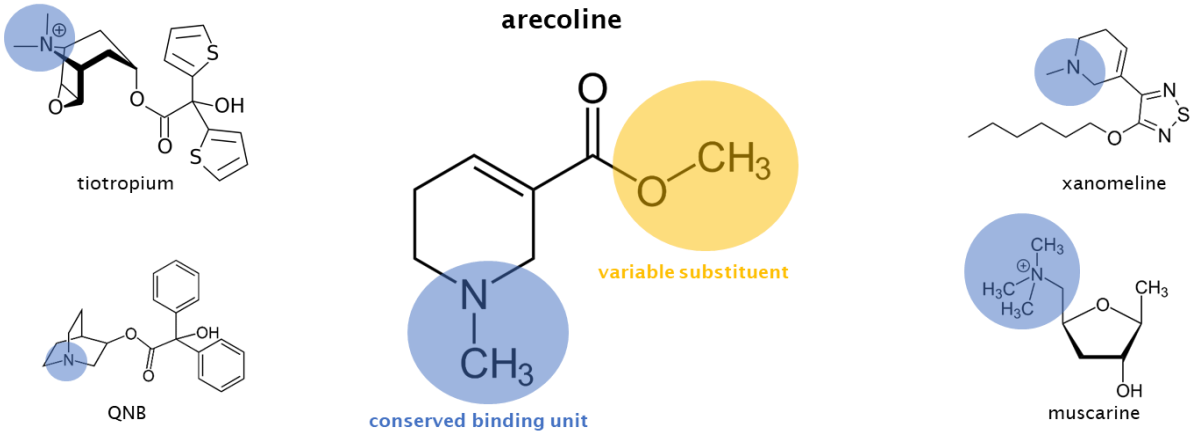


Figure 6: Structures of arecoline and some well-known orthosteric mAChR ligands.

1.9. Muscarinic acetylcholine receptors as therapeutic targets

Muscarinic ligands are clinically approved for the treatment in several different body parts, *e.g.* atropine for treatment of bradycardia[53], scopolamine for pupil dilatation and preventing motion sickness[54], butylscopolamine bromide (Buscopan) for treatment of crampy abdominal pain[55], ipratropium for treatment of COPD and asthma[56], pirenzepine for treatment of peptic ulcers[57], benztropine for treatment of Parkinson symptoms[58] and solifenacin for treatment of overactive bladder[59]. Adverse effects of mAChR antagonist are often linked to blockade of others than the desired mAChR subtype, which highlights the importance of subtype selectivity for mAChR drug development.[60]

However, considering their central role in the CNS, mAChR drugs have not yet found a proportionate clinical application for the treatment of CNS disorders.

Loss of cholinergic function is of high relevance in the cognitive impairment associated with Alzheimer's disease (AD). Accordingly, the overwhelming majority of clinically approved drugs for the symptomatic treatment of AD target the cholinergic system (*e.g.* tacrine, rivastigmine, galantamine, donepezil)[61]. As of today, all of them act as inhibitors of acetylcholineesterase and are associated with a relatively small symptomatic benefit along many side effects. Despite extensive research, especially on the M1 subtype, drugs targeting the mAChRs directly have not yet reached clinical approval in AD treatment.[61,62] mAChRs are also regarded as a promising target in the treatment of schizophrenia.[61] For example the mAChR M1 agonist xanomeline showed reasonable efficacy in the treatment of schizophrenia symptoms[63], but gastrointestinal side effects hamper its clinical application.[64]

1.10. PET tracer development for *in vivo* CNS muscarinic acetylcholine receptor imaging

The development of mAChR radiotracers started as early as 1982. An overview of the described mAChR radiotracer is depicted in Figure 7. (*R*,*S*)-[^{125}I]IQNB was the first radioligand used in the mapping of central mAChRs. It is a radioiodinated version of the highly affine chemical warfare agent 3-quinuclidinyl benzilate (QNB), which was studied extensively and stockpiled by the U.S. Army as incapacitating agent. Undoubtedly, high target affinity is a fundamental prerequisite in radiotracer development as it is the driving force to obtain the desired high target-to-nontarget ratio in imaging. However, when assuming the k_{on} to be constant, according to the kinetic definition of the equilibrium dissociation constant ($K_D = k_{off}/k_{on}$), high affinity comes with a slow off rate.[33] This 'second face' of high target affinity is assumed to compromise the *in vivo* radiotracer distribution of (*R*,*S*)-[^{125}I]IQNB, which strongly suffered from dependence of blood flow and transport across the BBB. As a consequence, (*R*,*S*)-[^{125}I]IQNB scans required two visits to the clinic and required pharmacokinetic modelling to separate the parameters of flow and transport from receptor density. Following a mAChR radiotracer like (*R*,*S*)-[^{125}I]IQNB over time, the aim of mAChR *in vivo* imaging studies often evolves from mapping the distribution of mAChRs[65] over studying differences between healthy and diseased subjects[66] to studying the effect of diseases treatment.[67] Although promising differences in receptor density between healthy and diseased brains could be shown in the majority of clinical studies, no impact on clinical care could be delineated from these measurements. Additionally, the lack of mAChR subtype selectivity as well as the limited resolution and sensitivity of SPECT hindered broad application of (*R*,*S*)-[^{125}I]IQNB.[68] Nevertheless, regarding all human *in vivo* mAChR imaging studies from the 1980s until now, (*R*,*S*)-[^{125}I]IQNB remains the most applied radiotracer;[69] however, not a single (*R*,*S*)-[^{125}I]IQNB study after 2007 is reported. From a radiochemical perspective [*carbonyl*-^{11}C]QNB is interesting because of its labeling procedure, which involves formation of [^{11}C]benzylic acid from [^{11}C]CO_2 and the benzophenone dianion followed by esterification with 3-quinuclidinol using 1,1'-carbonyldiimidazole.[70]

mAChR targeting PET tracers, [^{11}C]scopolamine[71], [^{11}C]benztropine[72], [^{11}C]TRB[73], [^{11}C]NMPB[74] developed between 1988 and 1993 suffer from similar problems: E.g. [^{11}C]scopolamine showed clear differences in cerebral cortical and cerebellar uptake. However, within the measurable time frame of up to 2 h post-injection, the cerebral cortical radiotracer distribution did not correspond to the anticipated receptor densities. Analysis *via* kinetic modeling resulted in good agreement with expectations based on *in vitro* studies; however, the authors concluded that the limited precision of the method may hinder its widespread clinical application.[71]

The frequently observed flow dependent radiotracer distribution shifted the goal of mAChR radiotracer development from compounds with high affinity to compounds with slightly reduced affinity, allowing to reach steady after bolus injection or equilibrium after infusion.[68] Expression levels of the different subtypes in human brain are rarely reported; however, based on the mAChR density of M1 and M2 in human brain[75] it was estimated that a radioligand K_D of about 3-50 nM is suitable for imaging CNS mAChRs *in vivo*.[76]

[^{11}C]NMPB acted as lead compound for the synthesis of congeners with *N*-ethyl ([^{11}C]4-EPB) and *N*-propyl ([^{11}C]4-PPB) residues instead of *N*-methyl[77], which however did not advance to human studies. Similarly, regioisomers of [^{11}C]NMPB regarding the piperidyl position were studied, which eventually yielded (+)-[^{11}C]3-MPB as a more favorable mAChR radiotracer because of its quicker kinetic and higher specific uptake in monkey scans.[78] (+)-[^{11}C]3-MPB was used to study humans suffering from chronic fatigue syndrome and showed reduced binding in the group of mAChR autoantibody positive subjects.[79]

Although studied extensively in humans, PET tracers originating in the previous millennium did rarely aim for subtype selectivity, which renders them unattractive for current clinical mAChR imaging studies. This is not caused by inadvertence in the radiotracer development, but because the existence of five different mAChR subtypes was just about to be recognized around that time,[80] not to mention the unknowingness of their collective expression in human brain.[81]

One of the earliest example of a subtype selective mAChR radiotracer is [^{18}F]FP-TZTP. Based on its K_i values for M1 (7.4 nM) and M2 (2.2 nM), [^{18}F]FP-TZTP can hardly be considered subtype selective; however, comparing *in vitro* binding between heart and brain tissue, [^{18}F]FP-TZTP exhibited M2 subtype selectivity. *In vivo* subtype selectivity could not be proven by the traditional pharmacological methods because of the uniform cerebral expression of M2 receptors and the lack of other M2 selective ligands which could be used for blocking experiments. Yet, *ex vivo* autoradiography using subtype selective knockout mice confirmed the *in vivo* M2 selectivity.[82] Imaging studies in monkeys applying physostigmine, an acetylcholinesterase inhibitor, revealed sensitivity of [^{18}F]FP-TZTP binding to endogenous acetylcholine concentration. Consequently, [^{18}F]FP-TZTP scans should be regarded as measurement of the muscarinic systems biology, rather than just M2 receptor distribution.[68] Cerebral distribution volumes of [^{18}F]FP-TZTP were shown to significantly correlate with human age.[83] However, its discrepancy between *in vitro* K_is and *in vivo* subtype selectivity is not yet fully understood but thought to be caused by a small but statistically significant slower M2 receptor off-rate.[84] This highlights the importance of studying binding kinetics in addition to binding affinity when pursuing subtype-selective mAChR radiotracer development.

[^{11}C]Xanomeline and [^{11}C]butylthio-TZTP were, despite their similar structure compared to [^{18}F]FP-TZTP, originally described as M1 ligands. However, later studies revealed an evenly

good affinity of xanomeline for mAChR M4.[85] In human imaging studies these PET ligands showed poor selectivity for mAChRs over sigma sites.[86]

The mAChR M1 targeting PET radioligand [^{11}C]GSK1034702 is innovative in two ways. Firstly, it is the first mAChR radioligand developed to target an allosteric binding site of a mAChR receptor. Secondly, in difference to all previous mAChR PET ligands its main goal is not receptor mapping nor diagnosis. Instead, [^{11}C]GSK1034702 was synthesized and applied in human studies for evaluating blood-brain barrier permeability to de-risk the drug development process of GSK1034702 for the treatment of cognitive disorders. The observed good brain uptake of [^{11}C]GSK1034702 discharged possible development risks and provided a support to advance the drug in the next stage of clinical development. Nevertheless, the authors concluded that [^{11}C]GSK1034702 might not be a suitable PET ligand due to the limited specific binding, which results from relatively low affinity (pEC_{50} = 8.1) or low molar activity (≈ 9 GBq/µmol).[87] Although developed as an allosteric ligand, GSK1034702 was also shown to displace the orthosteric ligand [^{3}H]NMS (K_i = 960 nM)[88] and therefore nowadays is considered as bitopic ligand.[89]

AF150(S) is an M1 selective mAChR agonist and was evaluated as potential therapeutic in animal models of neurological diseases. Despite its moderate affinity (K_D = 200 nM), Buiter *et al.* labeled the compound with carbon-11 and evaluated its use as PET tracer *via* rat brain autoradiography, *ex vivo* biodistribution and metabolite analysis in brain and blood. The authors concluded that the observed rapid metabolism, radioactive metabolites, hydrophobicity and relatively low binding affinity may be challenging for PET studies.[90] *In vivo* imaging studies using [^{11}C]AF150(S) revealed binding enhancement in brain with increasing concentration of AF150(S).[91]

Recently, Malmquist *et al.* modified the structure of (+)-[^{11}C]3-MPB by substituting one of the phenyl groups with cyclopentyl.[92] Based on its rapid kinetic in monkey brain, the (*S*,*R*) isomer was deemed most promising. Although the K_i of all four possible stereoisomers toward mAChR M1 was determined, no affinities for subtypes M2-M5 were reported. However, when comparing the blocking using scopolamine (not subtype selective) with the blocking using pirenzepine (M1 subtype selective) in human brain autoradiography, involvement of M2-M5 in the binding of (*S*,*R*)-[^{11}C]1-(methylpiperidin-3-yl)2-cyclopentyl-2-hydroxy-2-phenylacetate is evident.[92]

LSN3172176 is a bitopic ligand developed by Elli Lilly, which shares several chemical features with GSK1034702. Although [^{3}H]NMS displacement from M1-M5 membrane preparations attested LSN3172176 M1 selectivity, no M1 selectivity was evident when performing saturation binding using [^{3}H]LSN3172176.[88] *In vivo* studies in monkeys using [^{11}C]LSN3172176 and pretreatment with scopolamine reduced radioligand binding to levels indistinguishable from the mAChR devoid cerebellum. Also, pretreatment with the M1 selective partial agonist AZD6088 strongly reduced cerebral radioligand binding but not as quantitative as scopolamine.

[^{11}C]LSN3172176 is rapidly metabolized in monkeys: 15 min post-injection 71% of the radioactivity is found as more polar radiometabolites. Based on its high specific brain signal paired with appropriate kinetics in rhesus monkey brain, [^{11}C]LSN3172176 was advanced to human studies for further evaluation.[93]

The group of Craig W. Lindsley at the Vanderbilt University has extensively optimized mAChR M4 positive allosteric modulators (PAMs).[94] Eventually this led to the high affinity PAM VU0467485, which was deemed suitable as PET tracer candidate.[95] However, no specific binding could be observed in rat brain autoradiography in self-blocking experiments using [^{11}C]VU0467485. Two closely related congeners, in which a single hydrogen was substituted with a fluorine, were also carbon-11 labeled and evaluated using autoradiography. Interestingly, both showed a drastic increase in specific binding. [^{11}C]M_4R-1023, the congener with the highest specific binding as observed in autoradiography, was chosen for *in vivo* imaging of rats. Due to its low brain uptake [^{11}C]M_4R-1023 is no likely candidate for further preclinical evaluation; nevertheless, it may act as starting point for further chemical optimization.[95]

[^{11}C]MK-6884 is the most recently reported potential mAChR radiotracer studied i*n vivo* and is under development by Merck & Co. It arose from optimization of binding affinity and balancing of physicochemical properties from a lead series of potent M4 PAMs. *In vivo* imaging studies on monkeys showed rapid BBB penetration and activity distribution according to the known expression pattern of cerebral mAChR M4 with the highest uptake in the striatum. Intravenous injection of a different M4 PAM resulted in significant reduction of radiotracer binding, indicating specific binding. *In vitro* autoradiography on rat brain sections using a tritiated compound of a similar chemotype showed that radiotracer only binds in presence of an agonist (carbachol).[96] This supports that [^{11}C]MK-6884 only binds to activated receptors; however, no *in vivo* study proofing or falsifying this hypothesis was performed. A clinical study using [^{11}C]MK-6884 was completed in 2019[97] albeit no results have been published yet.

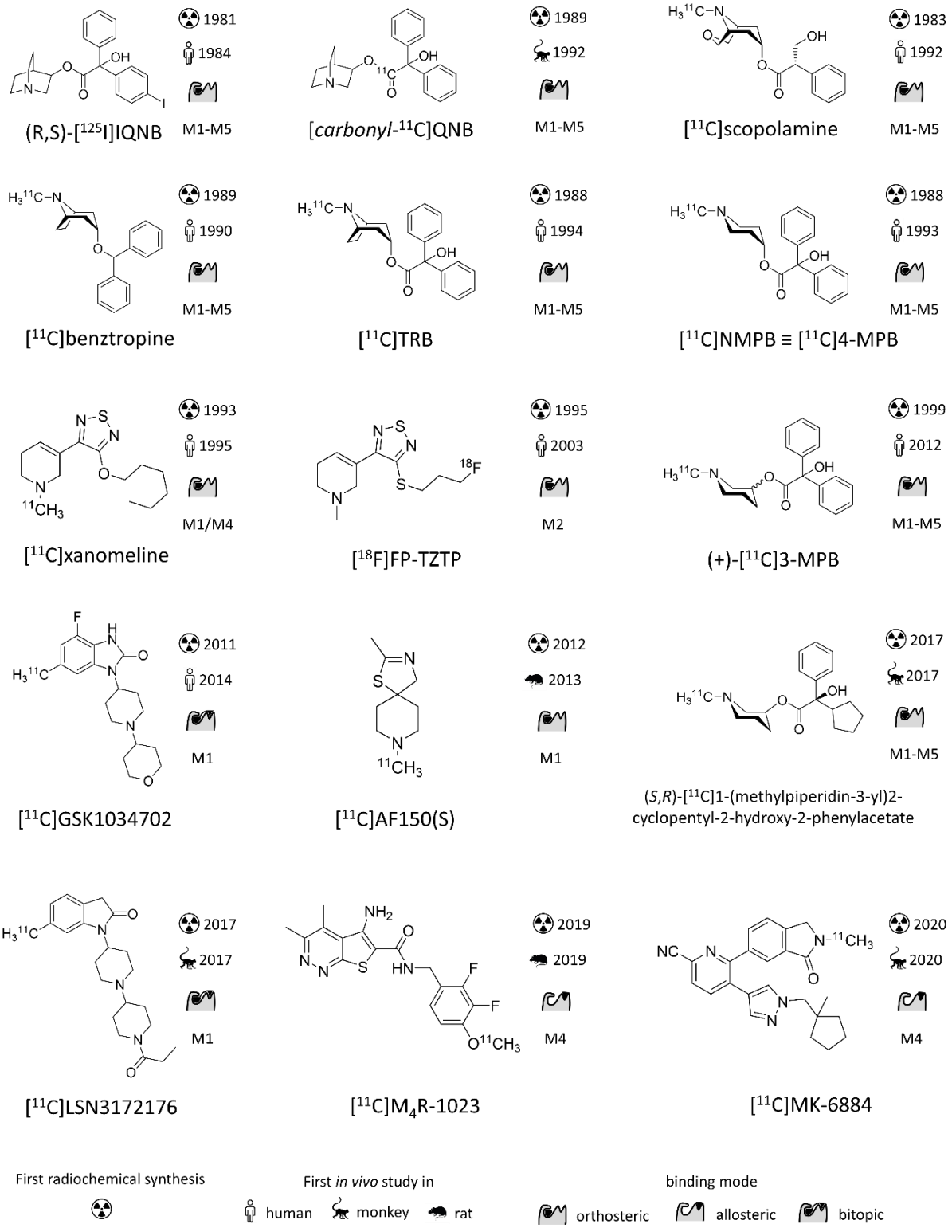


Figure 7: Structures and binding properties of mAChR ligands previously evaluated as imaging probes. Emphasis is given on more recent developments. First synthesis: (*R*,*S*)-[^{125}I]IQNB[98], [*carbonyl*-^{11}C]QNB[70], [^{11}C]scopolamine[99], [^{11}C]benztropine[100], [^{11}C]TRB[101], [^{11}C]NMPB[102], [^{11}C]xanomeline[103], [^{18}F]FP-TZTP[104], (+)-[^{11}C]3-MPB[105], [^{11}C]GSK1034702[106], [^{11}C]AF150(S),[90] (*S*,*R*)-[^{11}C]1-methylpiperidin-3-yl)2-cyclopentyl-2-hydroxy-2-phenylacetate[92], [^{11}C]LSN3172176[107], [^{11}C]M$_4$R-1023[95], [^{11}C]MK-6884[96]. First in man/animal: (*R*,*S*)-[^{125}I]IQNB[65], [*carbonyl*-^{11}C]QNB[108], [^{11}C]scopolamine[71], [^{11}C]benztropine[72], [^{11}C]TRB[73], [^{11}C]NMPB[74], [^{11}C]xanomeline[86], [^{18}F]FP-TZTP[83], (+)-[^{11}C]3-MPB[79], [^{11}C]GSK1034702[87], [^{11}C]AF150(S),[91] (*S*,*R*)-[^{11}C]1-methylpiperidin-3-yl)2-cyclopentyl-2-hydroxy-2-phenylacetate[92], [^{11}C]LSN3172176[107], [^{11}C]M$_4$R-1023[95], [^{11}C]MK-6884[96]

One of the main lessons that can be learned from the last decades of mAChR radiotracer development is that lipophilicity and affinity have to be balanced carefully in order to receive a feasible compromise of signal-to-noise ratio, flow independency, nonspecific binding and BBB permeability (Figure 8).

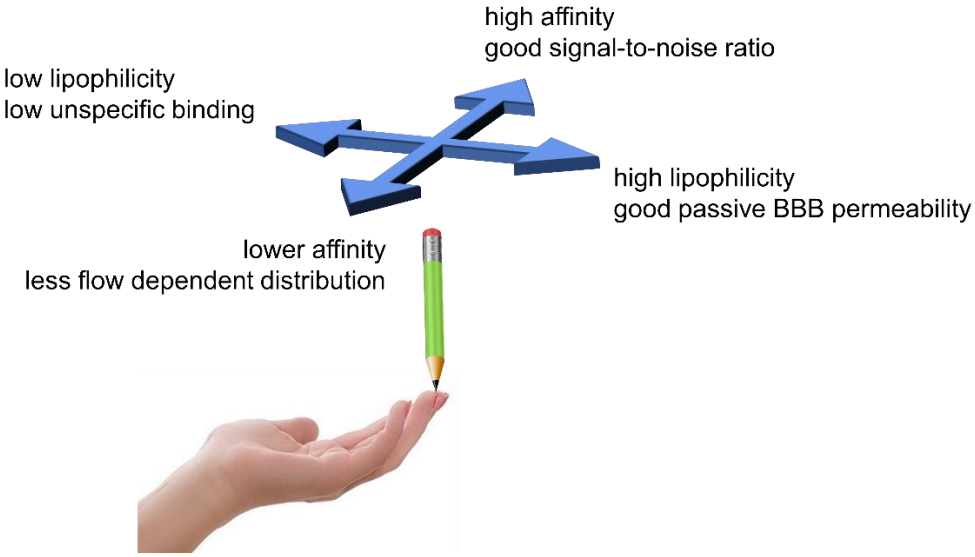


Figure 8: General influence of affinity and lipophilicity on imaging properties in mAChR PET tracer development.

1.11. *in vivo* peripheral muscarinic acetylcholine receptor imaging

With some exceptions the vast majority of *in vivo* mAChR imaging studies targets the CNS; although, mAChRs are also of high relevance in the peripheral nervous system.[109] *N*-methylated QNB ([^{11}C]MQNB) was used *e.g.* to study mAChRs in human heart. Featuring a positively charged quaternary ammonium, [^{11}C]MQNB is unable to penetrate the BBB and therefore can only bind to peripheral mAChRs.[110] So far, the limited axial field-of-view of PET scanners made it inefficient to additionally follow the peripheral radiotracer distribution in neuroimaging studies. Considering the advent of whole-body PET scanners[111], much more information of peripheral mAChR radiotracer distribution might be available in the future. In view of the overexpression of mAChRs in a wide variety of cancer types[112], it is conceivable that mAChR PET radiotracers might also find application in cancer imaging. High expression of mAChR M3 recently was identified as a biomarker in patients with non-small cell lung cancer.[113] However, as of now, no *in vivo* studies imaging mAChRs as biomarkers in malignancies were reported.

2. Aim

Despite their biological importance, no PET tracer targeting the mAChRs has yet found widespread clinical application, which can be contributed to the suboptimal properties of currently available molecules. In essence, this doctoral thesis aims to investigate the suitability of arecoline derivatives as potential PET tracers for mAChRs.

To reach this objective, the research work can be divided into following parts:

1. Design and synthesis of potential mAChR ligands: The synthesis of novel arecoline derivatives, which are eligible for carbon-11 labeling, should be planned and performed. The products should be obtained in a purity which allows for biological testing (≥95%) and investigated by analytical methods to prove the desired molecular structures. Furthermore, *N*-desmethyl precursors should be synthesized to enable subsequent radiolabeling.
2. Affinity determination toward the mAChR subtypes: The affinity of the synthesized compounds should be assessed in competitive radioligand binding assay toward each individual subtype.
3. Radiolabeling: A carbon-11 labeling method for arecoline derivatives should be established using *N*-desmethyl precursors. Reaction parameters should be optimized to set up a robust, automated labeling procedure, which yields the carbon-11 product in sufficient purity and quantity for preclinical evaluation.
4. Preclinical evaluation: The suitability of the carbon-11 labeled compounds as mAChR PET tracers should be evaluated by a broad spectrum of preclinical methods. Undesired properties revealed within this step should feed back to part 1.

Additionally, this doctoral thesis aims to increase the robustness of carbon-11 radiosynthesis presented by the established PET tracer [^{11}C]metoclopramide and to contribute to an analysis of the factors influencing the molar activity of carbon-11 labeled compounds in general.

3. Results and discussion

The research building up this thesis was published in peer-reviewed scientific journals or is under review at such as listed below. Following three works contain the research of this dissertation in the narrower sense.

1.

Ozenil, M.; Pacher, K.; Balber, T.; Vraka, C.; Roller, A.; Holzer, W.; Spreitzer, H.; Mitterhauser, M.; Wadsak, W.; Hacker, M.; Pichler, V. Enhanced Arecoline Derivatives as Muscarinic Acetylcholine Receptor M1 Ligands for Potential Application as PET Radiotracers. *European Journal of Medicinal Chemistry* **2020**, *204*, 112623. https://doi.org/10.1016/j.ejmech.2020.112623.

2.

Ozenil, M.; Aronow, J.; Piljak, D.; Vraka, C.; Holzer, W.; Spreitzer, H.; Wadsak, W.; Hacker, M.; Pichler, V. Synthesis, Biological, and Computational Evaluation of Antagonistic, Chiral Hydrobenzoin Esters of Arecaidine Targeting mAChR M1. *Pharmaceuticals* **2020**, *13*, 437. https://doi.org/10.3390/ph13120437

3.

Ozenil, M.; Skos, L.; Roller, A.; Gajic, N.; Holzer, W.; Spreitzer, H.; Platzer-Ozenil, S.; Vraka, C.; Hacker, M.; Wadsak, W.; Pichler, V.
Manuscript not submitted.

Furthermore, the author of this dissertation contributed to following publications in the field of PET Tracer development with experimental and manuscriptal work.

4.

Pichler, V.; **Ozenil, M.**; Bamminger, K.; Vraka, C.; Hacker, M.; Langer, O.; Wadsak, W. Pitfalls and Solutions of the Fully-Automated Radiosynthesis of [11C]Metoclopramide. *EJNMMI radiopharm. chem.* **2019**, *4* (1), 31. https://doi.org/10.1186/s41181-019-0083-2.

5.

Pichler, V.; Zenz, T.; Philippe, C.; Vraka, C.; Berrotéran-Infante, N.; Pfaff, S.; Nics, L.; **Ozenil, M.**; Langer, O.; Willeit, M.; Traub-Weidinger, T.; Lanzenberger, R.; Mitterhauser, M.; Hacker, M.; Wadsak, W. Molar Activity – The Keystone in 11C-Radiochemistry: An Explorative Study Using the Gas Phase Method. *Nuclear Medicine and Biology* **2018**, *67*, 21–26. https://doi.org/10.1016/j.nucmedbio.2018.09.003.

6.

Pichler, V.; Berroterán-Infante, N.; **Ozenil, M.**; Pfaff, S.; Philippe, C., Wadsak, W. (2019) *The Radiopharmaceutical Chemistry of Carbon-11: Tracers and Applications.* In: Lewis J., Windhorst A., Zeglis B. (eds) Radiopharmaceutical Chemistry. Springer, Cham. https://doi.org/10.1007/978-3-319-98947-1_12

3.1. Enhanced arecoline derivatives as muscarinic acetylcholine receptor M1 ligands for potential application as PET radiotracers

Marius Ozenil,[1] Katharina Pacher,[1] Theresa Balber,[1,2] Chrysoula Vraka,[1] Alexander Roller,[3] Wolfgang Holzer,[4] Helmut Spreitzer,[4] Markus Mitterhauser,[1,2] Wolfgang Wadsak,[1,5] Marcus Hacker,[1] Verena Pichler[1]

[1] Department of Biomedical Imaging and Image-guided Therapy, Division of Nuclear Medicine, Medical University of Vienna, Austria

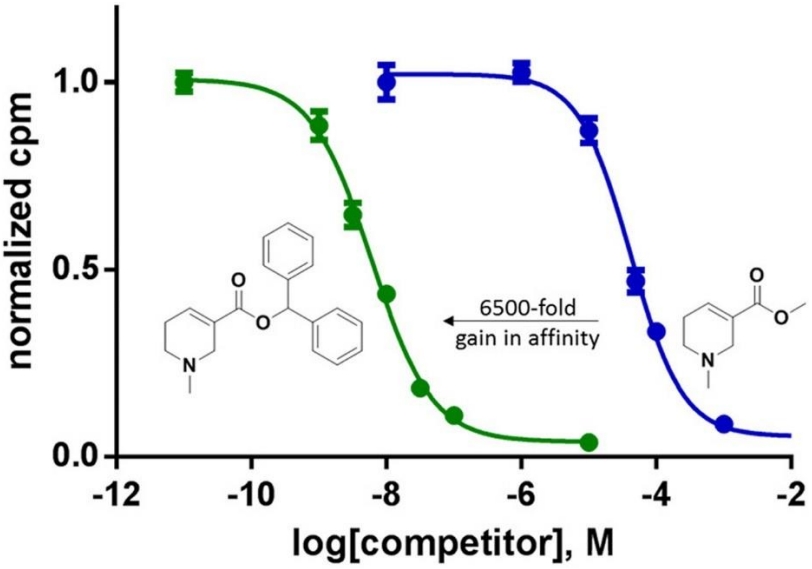
[2] Ludwig Boltzmann Institute Applied Diagnostics, Vienna, Austria

[3] X-ray Structure Analysis Centre, Faculty of Chemistry, University of Vienna, Austria

[4] Department of Pharmaceutical Chemistry, Faculty of Life Sciences, University of Vienna, Austria

[5] CBmed GmbH - Center for Biomarker Research in Medicine, Graz, Austria

Graphical abstract



The doctoral candidate synthesized all fifteen novel arecoline derivatives, radiolabeled six compounds with carbon-11, performed an extensive preclinical evaluation of the most promising candidates and largely wrote the manuscript.

European Journal of Medicinal Chemistry 204 (2020) 112623

Contents lists available at ScienceDirect

European Journal of Medicinal Chemistry

journal homepage: http://www.elsevier.com/locate/ejmech

Enhanced arecoline derivatives as muscarinic acetylcholine receptor M1 ligands for potential application as PET radiotracers

Marius Ozenil [a], Katharina Pacher [a], Theresa Balber [a, b], Chrysoula Vraka [a], Alexander Roller [c], Wolfgang Holzer [d], Helmut Spreitzer [d], Markus Mitterhauser [a, b], Wolfgang Wadsak [a, e], Marcus Hacker [a], Verena Pichler [a, *]

[a] Department of Biomedical Imaging and Image-guided Therapy, Division of Nuclear Medicine, Medical University of Vienna, Austria
[b] Ludwig Boltzmann Institute Applied Diagnostics, Vienna, Austria
[c] X-ray Structure Analysis Centre, Faculty of Chemistry, University of Vienna, Austria
[d] Department of Pharmaceutical Chemistry, Faculty of Life Sciences, University of Vienna, Austria
[e] CBmed GmbH - Center for Biomarker Research in Medicine, Graz, Austria

ARTICLE INFO

Article history:
Received 28 May 2020
Received in revised form
17 June 2020
Accepted 18 June 2020
Available online 19 July 2020

Keywords:
Muscarinic acetylcholine receptors
PET
Carbon-11
Neuroimaging

ABSTRACT

Supported by their involvement in many neurodegenerative disorders, muscarinic acetylcholine receptors (mAChRs) are an interesting target for PET imaging. Nevertheless, no radiotracer is established in clinical routine. Within this work we aim to develop novel PET tracers based on the structure of arecoline. Fifteen novel arecoline derivatives were synthesized, characterized and tested for their affinity to the mAChRs M1-M5 and the conceivable off-target acetylcholinesterase. Five arecoline derivatives and arecoline were labeled with carbon-11 in good yields. Arecaidine diphenylmethyl ester (**3b**), arecaidine bis(4-fluorophenyl)methyl ester (**3c**) and arecaidine (4-bromophenyl)(4-fluorophenyl)methyl ester (**3e**) showed a tremendous gain in mAChR affinity compared to arecoline and a pronounced subtype selectivity for M1. Metabolic stability and serum protein binding of [^{11}C]**3b** and [^{11}C]**3c** were in line with properties of established brain tracers. Nonspecific binding of [^{11}C]**3c** was prevalent in kinetic and endpoint experiment on living cells as well as in autoradiography on native mouse brain sections, which motivates us to decrease the lipophilicity of this substance class prior to *in vivo* experiments.
© 2020 The Author(s). Published by Elsevier Masson SAS. This is an open access article under the CC BY-NC-ND license (http://creativecommons.org/licenses/by-nc-nd/4.0/).

1. Introduction

Muscarinic acetylcholine receptors (mAChRs) are G-protein coupled receptors, which bind acetylcholine as endogenous ligand. Naming of the mAChRs is based on the additional activation by the fungal toxin muscarine. Their involvement in neurotransmission of the central nervous system as well as in the regulation of heart rate, muscle contraction and glandular secretion assigns mAChRs a pivotal role in physiology [1]. Conversely, alterations in mAChR signal transduction are involved in neurological disorders such as Schizophrenia, Alzheimer's or Parkinson's disease [2]. mAChRs are divided into five subtypes (M1–M5), all of which are expressed in the human brain. M1, M4 and M5 are expressed only in certain brain areas, whereas M2 and M3 are abundant throughout the brain [3]. The subtypes are classified by their activation of G proteins from the $G_{q/11}$ (M1, M3 and M5) or $G_{i/o}$ family (M2 and M4) [1]. Comparison of the crystal structures of M1–M4 proteins showed high similarity, which leads to difficulties in the development of subtype selective mAChR ligands [4]. A closer relation of M1 to M4 [5] was found compared to the structural relation of M1 to M3, which potentially explains that the clinically relevant antagonist pirenzepine displays a higher affinity to M1 and M4 than M2 and M3 [6]. The neurotransmitter acetylcholine binds to the orthosteric binding site, which is highly conserved and sterically demanding. As a consequence, a huge amount of ligands described in literature for mAChR are positive allosteric modulators (PAMs) [7]. However, most of them suffer from limited affinity [1].

The naturally occurring alkaloid arecoline exhibits orthosteric partial agonist properties toward mAChRs and is found in the betel nut. Its stimulating effects in the central nervous system underline its ability to cross the blood brain barrier [8]. Although arecoline is also known to have activity on selected nicotinic acetylcholine receptors [8], derivatization with typical muscarinic moieties as

* Corresponding author.
E-mail address: verena.pichler@meduniwien.ac.at (V. Pichler).

https://doi.org/10.1016/j.ejmech.2020.112623
0223-5234/© 2020 The Author(s). Published by Elsevier Masson SAS. This is an open access article under the CC BY-NC-ND license (http://creativecommons.org/licenses/by-nc-nd/4.0/).

applied within this work is strongly expected to deliver muscarinic selectivity. The inhibitor constants (K_i) of arecoline toward mAChRs were determined to be in the range of 15–77 μM [9], which is certainly insufficient for mAChRs positron emission tomography (PET) imaging. However, arecoline might act as a suitable lead structure for the development of high affinity mAChR ligands [10]. A typical pharmacophore in the orthosteric mAChR M1 binding motif displays a 'cationic head' which interacts with the Asp105A residue[11]. In arecoline this feature is represented by the protonated tertiary amine. Derivatives of arecoline should not contain bulky residues on the amine in order to maintain the critical cationic head. In fact, studies on previously synthesized arecoline derivatives confirmed that replacement of the *N*-methyl group of arecoline resulted in reduction or a complete loss of agonistic activity [12]. Instead it appears feasible to use the *N*-methyl position unchanged, leaving the *O*-methyl position open for chemical derivatization. The *O*-methyl position is moreover the attack point for esterases leading to arecaidine as metabolite [13]. Moreover, the introduction of carbon-11 at the *N*-methyl position does not alter the investigated structure leading to similar behaviour as the unlabeled preclinically investigated compound and open up the possibility for application in PET. PET is a non-invasive imaging modality and can be used to study receptor distribution and occupancy in brain or the peripheral nervous system. Considering the mAChR density in brain, it can be estimated that the affinity constant for a mAChR tracer should be around 3–50 nM for *in vivo* imaging [14,15]. Numerous animal and human imaging studies of mAChRs have been undertaken in healthy and diseased brain. Till now, no protocol has been established in clinical routine. Considering that acetylcholine was the first neurotransmitter to be discovered, even further presses the question why mAChR-imaging has not yet found its way into clinics. On the one hand, this can be attributed to the current lack of impact on clinical decisions derived from information obtained from mAChRs imaging [10]. On the other hand, the ongoing research effort put on novel radiotracers for mAChRs (Fig. 1) emphasizes that imaging properties of current radiotracers are still to be improved.

In the early days of mAChR tracer development, ligands with excessive affinity (*e.g.* [^{11}C]scopolamine [16] (**I**) [^{11}C]benztropine [17]), heavily caused flow-dependent accumulation. More recent mAChR tracer developments, [^{11}C]GSK1034702 [18] (**II**) and (*S*,*R*)-1-methylpiperidin-3-yl)2-cyclopentyl-2-hydroxy-2-phenylacetate [19] (**III**), suffer from low specific *in vivo* binding and the agonist [^{11}C]AF150(S) [20] (**IV**) was deemed challenging for *in vivo* applications because of its rapid metabolism and limited binding affinity. Furthermore, one of the main challenges in current mAChR tracer development remains subtype selectivity [21], since for the majority of mAChR ligands subtype selectivity and affinity have been contradictory properties [1]. The high affinity M4 PAM [^{11}C] VU0467485 (**V**) and two of its congeners overcome this discrepancy, yet limited specific binding and insufficient BBB permeability stopped their further development[22]. [^{11}C]LSN3172176 (**VI**) can currently be considered as the most promising candidate for clinical mAChR M1 imaging and was just advanced to human studies for further evaluation [23]. A BBB penetrant selective mAChR M1 PET tracer would not only allow to investigate the molecular pathology of brain diseases, but also facilitate the discovery of drugs for therapeutic applications[23].

In this study, we aim to significantly enhance the potency of arecoline derivatives by synthesis of a set of orthosteric compounds targeting the mAChR M1. We investigated their physico-chemical behaviour and affinity toward all five muscarinic acetylcholine receptors. The most successful candidates of this preclinical screening showed affinity in the low nanomolar range, and were radiolabeled with carbon-11 for further pharmacological characterization toward radiotracer development for PET.

2. Results and discussion

2.1. Synthesis of arecoline-based low molecular weight compounds

Starting from arecaidine (1-methyl-3,6-dihydro-2*H*-pyridine-5-carboxylic acid) and 4-methylmorpholine-2-carbonitrile a set of fifteen compounds was synthesized and six precursors required for potential radiolabeling with carbon-11 were prepared from *N*-protected guvacine. Fig. 2 and Fig. 3 outline the synthetic routes for arecoline derivatives (**1**–**3**). **1a** was prepared by methylation of *N*-Fmoc guvacine in presence of Na_2CO_3. Esters **1b**–**c** were prepared by reacting *N*-Fmoc guvacine with alcohols activated as trichloroacetimidate. **1j** was prepared *via* the acid chloride route. Activation of *N*-protected or unprotected arecaidine with *N*,*N*′-dicyclohexylcarbodiimide and subsequent spontaneous migration of the acyl residue gave the *N*-substituted urea derivatives **1k** and **3k**. Fmoc deprotection by diethylamine afforded compounds **2a**–**c** and **2j**–**k**. Precursor **2i** was obtained by Boc removal in presence of trifluoroacetic acid. **1i** and **3b**–**j** were synthesized *via*

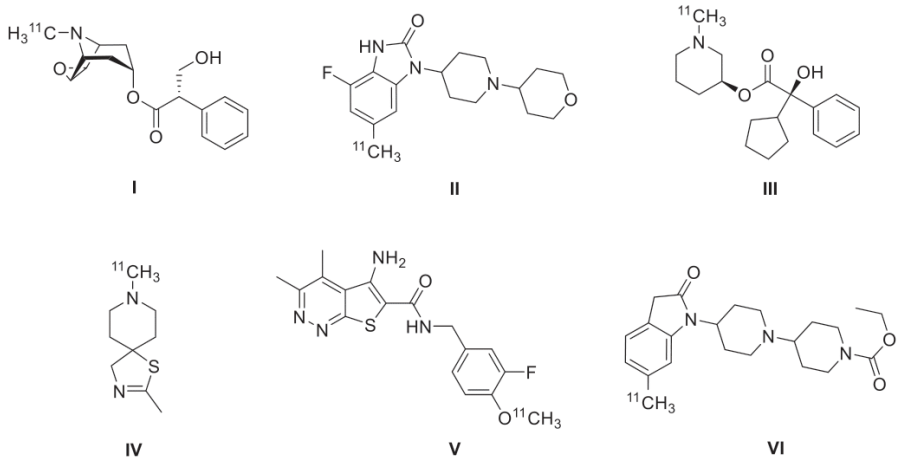


Fig. 1. Structures of carbon-11 radioligands investigated as mAChR PET tracers.

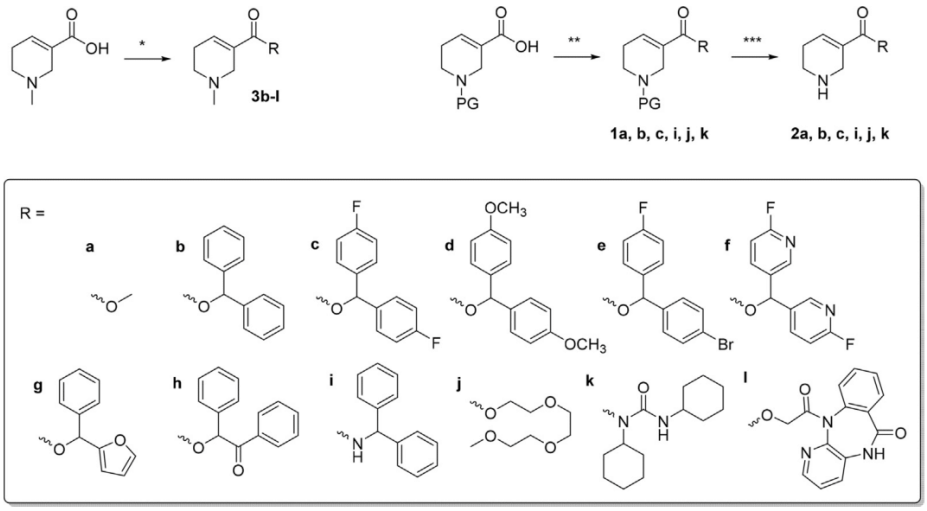


Fig. 2. Synthesis overview of arecoline derivatives (**3b**–**l**) and their N-desmethyl congeners (**2a**,**b**,**c**,**i**,**j**,**k**).* **3b**–**g**: 1. CDI, DMF 2. Na^+R^-, 3–25%; **3h**–**j**: 1. CDI, DMF, 2. RH, 3–18%; **3k**: DCC, DMF, 69%; **3l**: 1. NaH in DMF, 2. NaI, 11-(chloroacetyl)-5,11-dihydro-6H-pyrido[2,3-b][1,4]benzodiazepin-6-one, 13%. ** **1a**: PG = Fmoc, Na_2CO_3, CH_3I, DMF, 96%; **1b**–**c**: PG = Fmoc, RC(=NH)CCl_3, DCM, 87–93%; **1i**: PG = Boc, CDI, DMF, 2. RH, 12%; **1j**: PG = Fmoc, 1. $SOCl_2$, 2. RH, 93%; **1k**: PG = Fmoc, DCC, DMF, 48%. *** **2a**,**b**,**c**,**j**,**k**: DEA, ACN, 63–93%; **2i**: TFA, DCM, 79%.

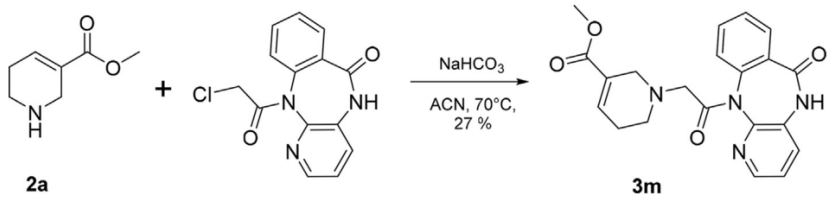


Fig. 3. Synthesis of the arecoline derivative **3m** by nucleophilic substitution.

carbonyldiimidazol-mediated coupling. **3l**–**m** were prepared by alkylation with an α-chloro amide. Preparative chromatography using an alpha-1-acid glycoprotein stationary phase allowed for chiral resolution of **3e**.

The protected precursor compounds (**1**) were synthesized in good to excellent yields, whereas the synthesis of the non-radioactive reference compounds (**3**) was more demanding leading to only moderate yields. This difference in yields can be explained by two factors, resulting from the zwitterionic characteristics of arecaidine compared to *N*-Fmoc guvacine. Firstly, the limited solubility of arecaidine in most organic solvents necessitated DMF-compatible esterification procedures. Secondly, arecaidine's interionic interactions can reduce the access of the activating reagent to the carboxylic group.

Derivatives of 4-methylmorpholine-2-carboxylic acid (**6**–**7**) were prepared as congeners with decreased lipophilicity compared to **3b** and **3i** (Fig. 4). **6** was prepared by Ritter reaction in formic acid [24] from **4**. **8** was prepared by Grignard reaction with benzylmagnesium bromide from **4**. Carbonyldiimidazol-mediated coupling of **5** with sodium diphenylmethanolate afforded **7**. Surprisingly, compounds **4** and **5** were not literature reported. Synthesis of **4** could be realized by addition of *N*-methylethanolamine to 2-chloro acrylonitrile and subsequent base cyclization, using an adopted procedure of Kopach et al. [25] Acidic hydrolysis of the nitrile **4** afforded compound **5**.

Precursors (**2**) and non-radioactive reference compounds (**3, 6**–**8**) were fully characterized by 2D-NMR spectroscopy, HRMS and UV-HPLC. Regarding benzhydryl derived compounds, the shift and multiplicity of the benzylic proton signal is influenced by the type of the neighboring element and hence the type of carbonyl compound. Esters (**3b**–**g**, **7**) show a singlet at 6.86–7.00 ppm, whereas the amides **3i** and **6** exhibited a high field shifted signal at 6.28 ppm and 6.25 ppm respectively. Furthermore, the type of carbonyl compound influences the shielding of the respective vinylic proton of the arecaidine backbone. For the ester derivatives (**3b**–**h**, **3j**, **3l**) a multiplet at 6.87–7.32 ppm was observed, compared to a high field shifted mutliplet at 6.15–6.56 ppm for the amide derivatives (**3i**, **k**). In HRMS measurements all analyzed compounds could be ionized in positive mode yielding $[M+H]^+$ and/or $[M+Na]^+$ cations of expected masses.

Compound **3k** and **5** were isolated as monocrystals and analyzed by X-ray single crystal diffraction analysis. The compounds crystalized in an orthorhombic crystal system (space group Pna21) and in a monoclinic crystal system (space group P21/n), respectively. A detailed description is shown in the Supporting Information.

2.2. Subtype selectivity analysis toward muscarinic acetylcholine receptors

Inhibition constants (K_i) against mAChR subtypes of arecoline, **3b**–**m** and **6**–**8** were determined with a competitive radioligand binding assay applying the common mAChR ligand *N*-methyl-[^{3}H] scopolamine ([^{3}H]NMS). Arecoline, **3d**, **3j**–**m** and **8** feature

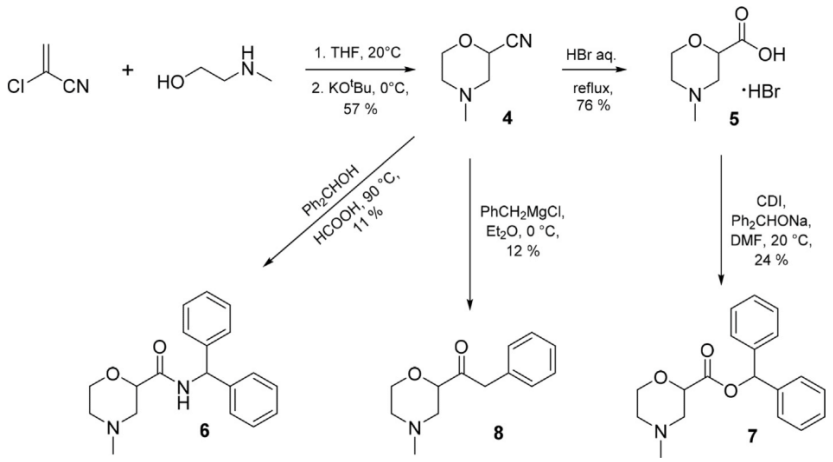


Fig. 4. Synthesis of 4-methylmorpholine-2-carbonitrile (**4**) and its related carboxylic acid (**5**). **4** and **5** were used for the synthesis of potential mAChR ligands **6**–**8**.

inhibition constants in the micromolar range or higher against all mAChR subtypes, whereas **3b**, **3c, 3e**–**i**, **6** and **7** show a drastically increased affinity with values in the submicromolar to low nanomolar range (Table 1).

No specific competitive binding could be observed on membranes prepared from wild type CHO cells (negative control), proving the high specificity of these ligands in the competitive radioligand binding assay. The determined inhibition constants for arecoline (**3a**) match well with previously reported data [9].

3l–**m** are conjugates of the arecoline backbone with the clinically applied M1-selective antagonist pirenzepine and were designed to promote subtype M1 selectivity. However, their low affinity excluded them from further development. Exchange of the *O*-methyl group of arecoline with a diphenylmethyl (**3b**), bis(4-fluorophenyl)methyl (**3c**) or (4-bromophenyl)(4-fluorophenyl) methyl (**3e**) moiety led to a tremendous increase of affinity toward all subtypes to levels suitable for PET tracers. Structures with fluorine substituents were investigated to enable potential use of fluorine-18 for radiolabeling. The affinity dropped strongly when arecaidine was substituted with 4-methylmorpholine-2-carboxylic acid (**6**, **7**). Enantiomers of **3e** show a distinct affinity profile, with a twofold difference in M1 affinity being the most notable difference ($p = 0.007$). Interestingly, **3b**, **3c** and **3e** show a preference for subtype M1, whereas arecoline (**3a**) shows a higher affinity for subtype M2 compared to M1. The derivatization of arecoline with diphenylmethyl moieties affected the subtype selectivity to such an extent that also in the overall subtype selectivity profile the difference in affinity is the highest between M1 and M2 for **3b** (35-fold), **3c** (140-fold), (−)-**3e** (36-fold) and (+)-**3e** (86-fold). From a thermodynamical perspective, the similar target densities of the subtypes in human brain [26] paired with the strong subtype selectivity for M1 over M2 should lead to an equally strong subtype selectivity in *in vivo* imaging. In **3b** and **3c** the subtype selectivity of M1 over M3-M5 is less pronounced (between 2.7-fold and 18-fold), which might appear insufficient for subtype-selective *in vivo* imaging. However, [^{18}F]FP-TZTP, which is a known *in vivo* M2 selective tracer, features only 3.4-fold selectivity of the M1 over the M2 receptor *in vitro* [27]. Ravasi et al. [28] proposed, that *in vivo* M2 selectivity of [^{18}F]FP-TZTP is caused by the slower k_{off} from M2 compared to the other subtypes. This highlights the importance of ligand-receptor kinetics for mAChR tracer development and motivated us to study the *in vitro* kinetics of [^{11}C]**3c** (see section Interactions of [^{11}C]**3c** with CHO-M1 cells).

2.3. Specificity analysis of competing electric eel acetylcholinesterase (EeAChE) affinity and metabolism

Compounds **3a**–**m** and **6**–**8** could unintentionally act as ligand

Table 1
Inhibition constants (K_i) given in nM, n ≥ 3, determined by [^{3}H]NMS competition binding.

	M1	M2	M3	M4	M5
3a	20,300 ± 2400	3800 ± 890	16,700 ± 5900	4700 ± 410	7000 ± 570
3b	3.1 ± 0.5	110 ± 39	56 ± 22	16 ± 4	14 ± 1
3c	5.0 ± 1.6	710 ± 110	77 ± 28	19 ± 5	32 ± 5
3d	>4700	>4500	>2200	>3300	>2600
(−)-**3e**	15.6 ± 2.1	560 ± 110	56 ± 10	64 ± 11	42 ± 23
(+)-**3e**	7.8 ± 1.7	670 ± 70	52 ± 6	42 ± 2	27 ± 5
3f	850 ± 240	1480 ± 40	690 ± 170	720 ± 420	690 ± 70
3h	270 ± 130	3300 ± 500	1240 ± 210	1200 ± 500	800 ± 190
3i	153 ± 60	>4500	1500 ± 290	400 ± 74	580 ± 130
3j	148,000 ± 35,000	>4500	>2200	>3300	>2600
3k	204,000 ± 53,000	>4500	>2200	>3300	>2600
3l	>4700	>4500	>2200	>3300	>2600
3m	>4700	>4500	>2200	>3300	>2600
6	610 ± 50	>4500	>2200	>3300	>2600
7	710 ± 90	>4500	>2200	>3300	>2600
8	>4700	>4500	>2200	>3300	>2600

or substrate for AChE (acetylcholinesterase), which would cause specificity problems. AChE is a certainly conceivable off-target in the development of orthosteric ligands for mAChRs and especially of interest for arecoline-derived compounds when considering the structural similarity to the known AChE-inhibitors neostigmine and pyridostigmine [29]. Inhibition constants (K_i) against EeAChE (acetylcholinesterase from *Electrophorus electricus*) of **3a**–**m** and **6**–**8** and tacrine as positive control were determined by Ellman's assay. The obtained K_i of the positive control tacrine was 30 ± 10 nM, which corresponds well to the range of literature reported values [30] (for graphs see Supporting Information, Fig. S7). For **3a**–**m** and **6**–**8** no inhibition compared to the blank could be perceived in the c_{ATI}/(sec/OD) diagram at the highest concentration tested (16.5 μM). Graphs are shown in the Supporting Information, Fig. S6. Furthermore, a two-way ANOVA followed by a Dunnett's multiple comparisons test revealed that the slopes are not significantly different ($\alpha > 0.05$), which allows to conclude that the K_i against EeAChE of **3a**–**m** and **6**–**8** is higher than 16.5 μM.

Interestingly, no significant EeAChE metabolism could be observed for arecoline derivatives **3a**–**m** and **6**–**8** under these conditions, not even after 60 min of incubation ($\alpha > 0.05$). Overall, it was ruled out that **3a**–**m** and **6**–**8** are EeAChE substrates under the used assay conditions. Additionally, **3a**–**m** and **6**–**8** did not show any EeAChE inhibitory effects at concentrations up to 25 μM.

Concluding, the investigated set of mAChR ligands exhibits high specificity against the target of choice as they were neither inhibitors nor substrates to the off-target EeAChE.

2.4. HPLC-log$P_{ow}^{pH7.4}$ determination and structure-activity relationship

Although the predictive factor of HPLC-log$P_{ow}^{pH7.4}$ for prediction of blood brain barrier penetration is critically discussed in literature [31–33], still this value is broadly determined in drug development. The HPLC-log$P_{ow}^{pH7.4}$ as a measure for the affinity of compounds to a lipophilic stationary phase allows estimation of nonspecific binding in fatty tissue, other lipophilic tissues or plasma protein binding and was therefore analyzed.

The HPLC-log$P_{ow}^{pH7.4}$ value was determined chromatographically and tPSA was calculated (Table 2). All target compounds (**3a**–**m** and **6**–**8**) exhibited HPLC-logP values in the range of established BBB permeable brain tracers [31] and **3a**–**k** and **6**–**8** exhibit a tPSA (total polar surface area) < 60 Å^2, supporting BBB penetration [34].

For identification of the most promising compounds in terms of subtype selectivity independent from the absolute value, the ratio values of the K_i of M4/M1 was correlated with the ones for M3/M1. Three main groups could be recognized showing low subtype selectivity (Fig. 5A, blue), intermediate preference for M1 (Fig. 6A, red) and high preference for M1 subtype (Fig. 5A, green). The three compounds with the highest preference for the M1 subtype were as follows in increasing order: **3i** < **3c** < **3b**. Obviously, the diphenylmethyl moiety was crucial to achieve highly improved subtype selectivity against the mAChR-M1 subtype compared to arecoline. Notable is also the enantiomeric selectivity of (+)-**3e** over (−)-**3e** for mAChR-M1 giving the opportunity to fine-tune the affinities *via* stereochemistry.

Correlation of the pK_i toward M1 and the log$P_{ow}^{pH7.4}$ values showed a logarithmic trend of affinity and lipophilicity ($R^2 = 0{,}56$). However, as the K_i of compounds **3d**, **3l**, **3m** and **8** toward M1 was higher than the concentration range of the experiment, only a trend analysis was possible. Especially, the analysis of the enantiomers (+)-**3e** and (−)-**3e** exemplarily shows, that an increase in affinity is possible without an alteration in lipophilicity and underlines the importance of enantiomeric selectivity for the binding to mAChR M1.

Overall, the most promising compounds in terms of subtype selectivity, absolute affinity against mAChR M1 and tPSA were **3b** and **3c**, which were further evaluated for radiolabeling with carbon-11. The isostere **3i** was additionally used for comparison purposes in metabolic studies.

Table 2
Overview of substance parameters. tPSA was calculated using ChemBioDraw 13.0.2.3021.

	tPSA [Å^2]*	HPLC-log$P_{ow}^{pH7.4}$
3a	29.54	−1.62 ± 0.62
3b	29.54	3.32 ± 0.04
3c	29.54	3.62 ± 0.08
3d	48.00	3.07 ± 0.04
3e	29.54	4.12 ± 0.15
3f	54.26	1.91 ± 0.17
3g	38.77	3.66 ± 0.08
3h	46.61	2.94 ± 0.05
3i	32.34	2.25 ± 0.12
3j	57.23	−0.70 ± 0.54
3k	52.65	2.24 ± 0.13
3l	91.31	0.57 ± 0.37
3m	91.31	0.96 ± 0.31
6	41.57	2.30 ± 0.12
7	38.77	2.79 ± 0.05
8	29.54	1.00 ± 0.30

2.5. Docking studies

Docking of protonated **3c** in the active center of mAChR M1 (PDB: 5CXV) [5] supports that it adopts a similar binding pose compared to tiotropium (Fig. 6A).

In this pose tiotropium as well as protonated **3c** feature electrostatic interaction of the quaternary ammonium cation with ASP105A and hydrophobic interactions of the aromatics to several apolar amino acid side chains. In the docked binding pose of tiotropium ASN382A acts as hydrogen bond donor and acceptor for the hydroxyl and carbonyl moiety, whereas in protonated **3c** the carbonyl acts as hydrogen bond acceptor for CYS407A. Additionally, protonated **3c** features hydrogen bonds to SER109A and THR189A (Fig. 6C). Hydrogen bonds to organic fluorine have low binding energies, yet they are known to affect chemical behavior [35] and can hence potentially influence ligand binding.

Furthermore, we performed molecular docking of protonated **3b** and **3i** in order to get a molecular insight into the reason for the approx. 50-fold higher mAChR M1 binding affinity of **3b**.

Unexpectedly, in these docking experiments **3i** (lowest estimated binding energy: −20.3 kcal/mol; lowest binding affinity score: −31.4) performed even slightly better than **3b** (−20.2 kcal/mol; −26.9). Consequently, we assume that the experimentally observed loss of affinity of **3i** compared to **3b** is not based on the lack of a suitable conformer inside the binding pocket caused by the more rigid amide bond, but rather results from reduced flexibility during its way to the active center. Furthermore, also electronical differences of the neighboring moieties between **3b** and **3i**, as observed by NMR spectroscopy, could affect the capability of the ligands to reach the binding pocket.

2.6. Radiolabeling of the most promising compounds with carbon-11

The most promising compounds **3b** and **3c** regarding subtype selectivity, receptor specificity and physico-chemical parameters were chosen for radiolabeling. The radiolabelling of **3i** was performed for the analysis of metabolites obtained by liver microsomes. All other compounds were radiolabeled to show the

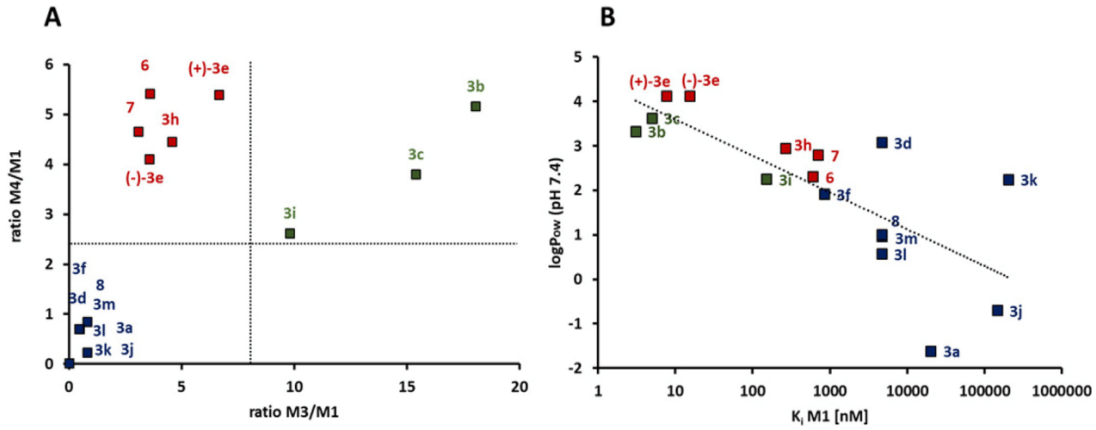


Fig. 5. (A) **Evaluation of the subtype selectivity by comparison of the ratio values of M4/M1 and M3/M1**. The analysis identified a group of compounds with low subtype selectivity (blue), compounds with intermediate (red) and high preference for M1 (green). (B) **Correlation of the pK_i toward M1 and the HPLC-$logP_{ow}$** (pH 7.4). A logarithmic trend was observed showing that higher lipophilicity leads to higher affinities.

substrate scope of the chosen reaction conditions. First small scale reaction were performed to investigate the optimal labeling conditions. Subsequently, fully-automated radiosyntheses were set up to study metabolism, plasma protein binding and cell binding.

Small scale reactions of compounds **2a**, **2b** and **2j** with [^{11}C]CH_3I yielded [^{11}C]**3a**, [^{11}C]**3b** and [^{11}C]**3j** (Fig. 7) in good yields in both solvents, ACN (Table 3) and DMSO (Table 4) as determined by RP-HPLC without further purification. When using ACN, radiochemical yields [36] significantly increased with reaction time and temperature. In DMSO, labeling was almost quantitative at both tested reaction times and temperatures. Thus, DMSO at 20 °C for 2 min was initially chosen for implementation of the automated radiosynthesis.

The fully automated syntheses comprised of the preparation of [^{11}C]CH_3I, reaction with the respective precursor, semi-preparative purification as well as formulation to physiological conditions was set up for compounds **3a**, **3b**, **3c**, **3i**, **3j** and **3k**. Although the small-scale reaction showed complete conversion at room temperature in DMSO, for the fully-automated synthesis the reaction temperature was increased to 80 °C, because unreacted [^{11}C]CH_3I was observed during semi-preparative HPLC of the crude reaction mixture at 20 °C for all compounds. Precursor **2k** features two potential nucleophilic sites that could react with [^{11}C]CH_3I (see Supporting Information).

In total 32 large-scale batches of carbon-11 compounds were produced (Table 5). Due to different semi-preparative HPLC runtimes the overall synthesis time from end of bombardment varies slightly among the products and ranges between 40 and 45 min, which is approximately two half-lives of carbon-11 ($t_{1/2} = 20$ min). Precursors (**2**) were employed in a roughly 100-fold excess compared to [^{11}C]CH_3I. The radiochemical purity as determined by HPLC exceeded 96% in all batches and pH and osmolality were determined to be in the physiological range. All radiolabeled compounds showed high purity and physico-chemical parameters as determined in the quality control were in accordance with the guidelines of the European Pharmacopoeia for radiopharmaceutical preparations [37].

We showed that **3a**–**c** and **3i**–**k** can be carbon-11 labeled straightforwardly in high yields, independent of the carbonyl substituent (R). The high yields of the radiosynthesis of all tested compounds enable a potential application for at least two patients per synthesis.

2.7. Physico-chemical parameters and pharmacological behavior of radiolabeled compounds

Human liver microsome metabolism was studied with compounds [^{11}C]**3b**, [^{11}C]**3c** and [^{11}C]**3i**. For all of them the main radiometabolite was identified as [^{11}C]arecaidine and the rate of its formation was found out to be heavily dependent on the structure of the parent compound (Fig. 8). [^{11}C]**3i** was almost unaffected by human liver microsomes, whereas 30% [^{11}C]**3b** and 53% [^{11}C]**3c** were unmetabolized after 1 h. Furthermore, a second radiometabolite with a retention time between arecaidine and the parent compound was observed for all three compounds (Supporting Information, Table S2, Fig. S8). This metabolite never represented more than 10% of the total activity and was identified as arecaidine ethyl ester ($C_9H_{15}NO_2$), based on HPLC-HRMS measurements (Supporting Information) of nonradioactive incubations of **3b** with human liver microsomes. Formation of the ethyl ester can be explained by the presence of EtOH in the tracer formulation. *In vivo* experiments are expected to be unaffected by [^{11}C]arecaidine ethyl ester formation, rationalized by the concomitant stronger dilution of EtOH. Considering the expected low transport of [^{11}C]arecaidine across the blood brain barrier [38] and the low affinity to all mAChRs, we are confident that ester cleavage in the liver will not interfere with neuroimaging but can potentially affect applications in the peripheral nervous system.

Serum protein binding of [^{11}C]**3b**, [^{11}C]**3c** and [^{11}C]**3i** was studied by ultrafiltration, demonstrating 5.8 ± 1.0%, 9.0 ± 1.2% and 18.2 ± 0.4% ($n \geq 3$, ±sd) free fraction, respectively. The measured serum protein binding is comparable to established brain tracers [39], substantiating the possible utilization of [^{11}C]**3b**, [^{11}C]**3c** and [^{11}C]**3i** for *in vivo* imaging. Plasma stability of [^{11}C]**3c** was 94 ± 2% after 60 min ($n = 3$).

To reduce tracer metabolism, we exchanged the ester for an amide bond (**3i**), which resulted in drastic improvement of metabolic stability. However, the mAChR affinity of **3i** is much lower compared to its bioisostere **3b**. To sum it up, [^{11}C]**3b** and [^{11}C]**3c** represent the most promising substances of this series regarding mAChR PET tracer development. Comparing these two, [^{11}C]**3c** stands out, because of its higher *in vitro* metabolic stability and M1 subtype selectivity.

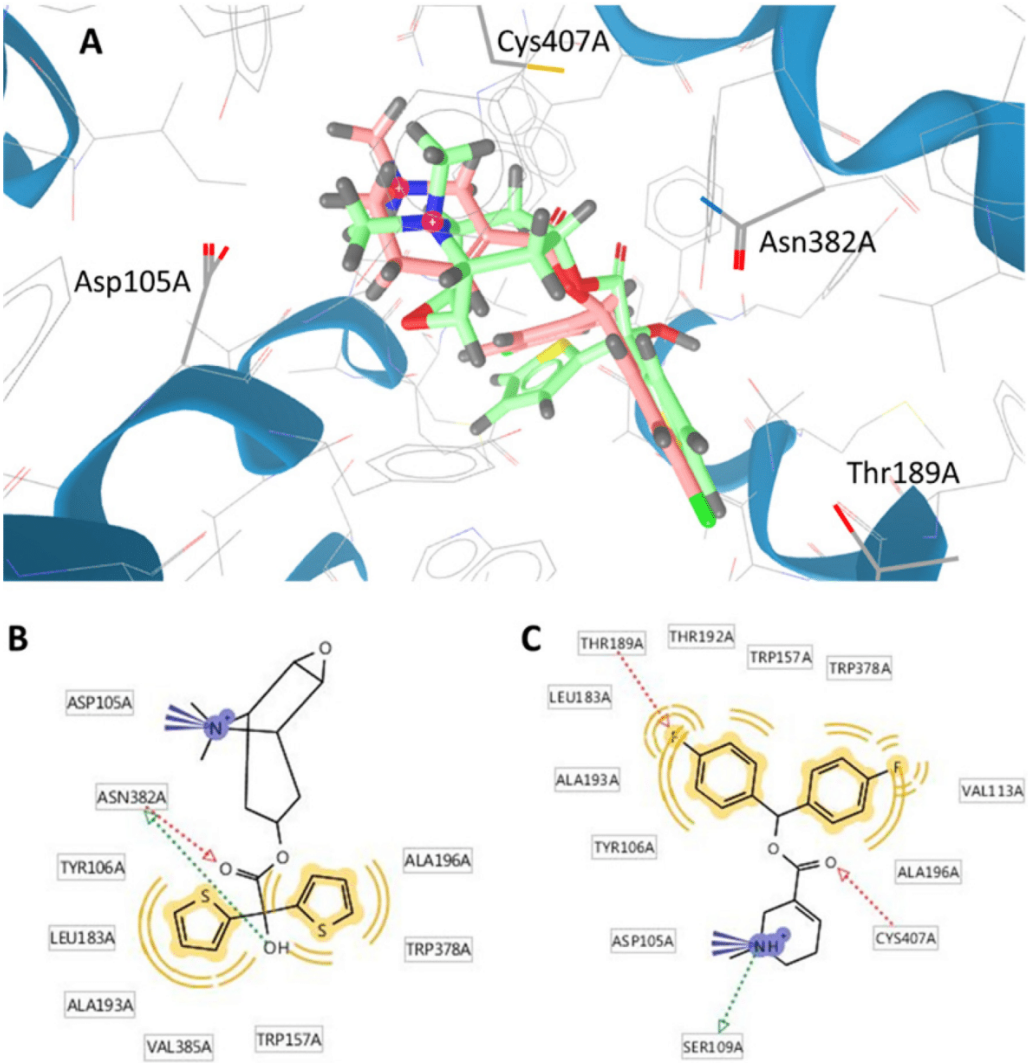


Fig. 6. A: Lowest binding energy docking poses of **3c** (salmon, −20.0 kcal/mol) and tiotropium (light green, −22.4 kcal/mol) in the orthosteric binding site of human M1 mAChR. Ser109A is covered by the docked ligands. B,C: Pharmacophore-derived interactions of tiotropium (B) and **3c** (C) with the binding pocket environment calculated and visualized with LigandScout.

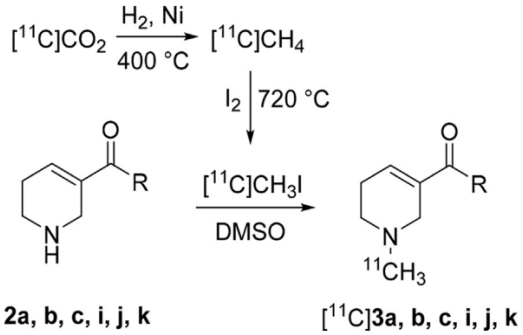


Fig. 7. Reaction scheme of the radiochemical labeling.

Table 3
Non-isolated radiochemical yields [%] in ACN as determined by radio-HPLC (ND = not determined, n = 1). ACN was not investigated as solvent for labeling of [^{11}C]**3j**, because an almost quantitative non-isolated radiochemical yield was observed using DMSO (Table 4).

	[^{11}C]3a		[^{11}C]3b		[^{11}C]3j	
	20 °C	70 °C	20 °C	70 °C	20 °C	70 °C
2 min	23	55	37	58	ND	ND
5 min	33	81	45	68	ND	ND

Table 4
Non-isolated radiochemical yields [%] in DMSO as determined by radio-HPLC (n = 1).

	[^{11}C]3a		[^{11}C]3b		[^{11}C]3j	
	20 °C	120 °C	20 °C	120 °C	20 °C	120 °C
2 min	92	91	79	87	98	95
5 min	93	91	87	85	96	94

Table 5
Production parameters of carbon-11-labeled compounds. Yield is related to the estimated starting activity of [^{11}C]CO_2.

n	[^{11}C]3a	[^{11}C]3b	[^{11}C]3c	[^{11}C]3i	[^{11}C]3j	[^{11}C]3k
	3	5	19	2	1	2
yield (GBq)	5.9 ± 1.0	5.3 ± 1.6	3.8 ± 1.3	2.7 ± 2.0	7.2	4.3 ± 1.0
RCY (%)	18.7 ± 2.7	17.4 ± 6.8	12.9 ± 3.8	8.6 ± 4.8	21.1	13.2 ± 2.4
A_m at EOS (GBq/μmol)	58 ± 17	93 ± 80	122 ± 115	30 ± 6	43	132 ± 36

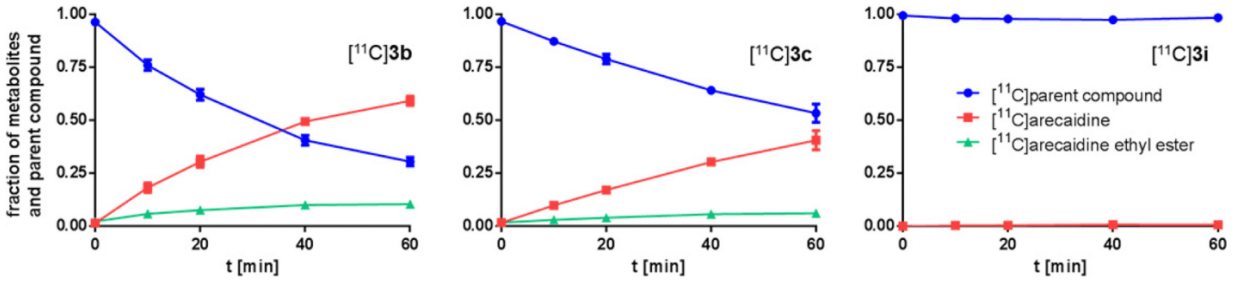


Fig. 8. Metabolic stability of compounds [^{11}C]**3b**, [^{11}C]**3c** and [^{11}C]**3i** against human liver microsomes. Error bars represent standard deviation of n = 3 ([^{11}C]**3b** and [^{11}C]**3c**) or n = 2 ([^{11}C]**3i**) incubations of individual batches.

2.8. Interactions of [^{11}C]3c with CHO-M1 cells

The kinetics of the interaction of [^{11}C]**3c** with living CHO-M1 cells was studied using LigandTracer. On the first view promising binding curves, reaching equilibrium in 8–15 min, were obtained. However, the observed binding did not reach saturation at a concentration 100-fold above K_i but showed a rather linear equilibrium signal increase with concentration (maximum concentration of 10 × K_i shown in Fig. S9A for the sake of readability). Furthermore, CHO-M1 cells preblocked with 10 μM scopolamine showed essentially the same binding kinetics as unblocked CHO-M1 cells Fig. S9A). Additionally, the binding curvature appeared independent on [^{11}C]**3c** concentration (Fig. S9B). Considering these observations, we concluded that the binding observed in the LigandTracer experiments cannot exclusively be explained by the interaction of **3c** with mAChR M1.

To study this further, we performed a direct radioligand binding assay using [^{11}C]**3c** and investigated the binding behavior of blocked CHO-M1 cells versus unblocked CHO-M1 cells at three different concentrations in six-well plates (Fig. 9). At a radioligand concentration of 0.3 nM blocking with 10 μM scopolamine and 10 μM pirenzepine significantly reduced the binding of [^{11}C]**3c** to CHO-M1 cells. However, CHO cells lacking the M1 receptor (blank) show an overall lower radioligand binding compared to the blocked CHO-M1 cells. Hence, the observed [^{11}C]**3c** binding is not fully blockable with the used concentrations and reference ligands. With increasing concentrations of **3c** blocking with scopolamine and pirenzepine becomes less effective, leading to no significant difference in radioligand binding between unblocked and blocked CHO-M1 cells at 3 nM and 30 nM of **3c**.

As control, the similar assay was performed at ≤ 4 °C to investigate the ligand binding without active process contributions (Fig. 9) [40]. At CHO-M1 cells ≤ 4 °C [^{11}C]**3c** binding is reduced to the same extent as in blocked CHO-M1 cells, indicating that active cellular processes are involved in the binding of [^{11}C]**3c** to living cells.

The extent of specific binding is limited to the amount of expressed target, whereas nonspecific binding increases linearly

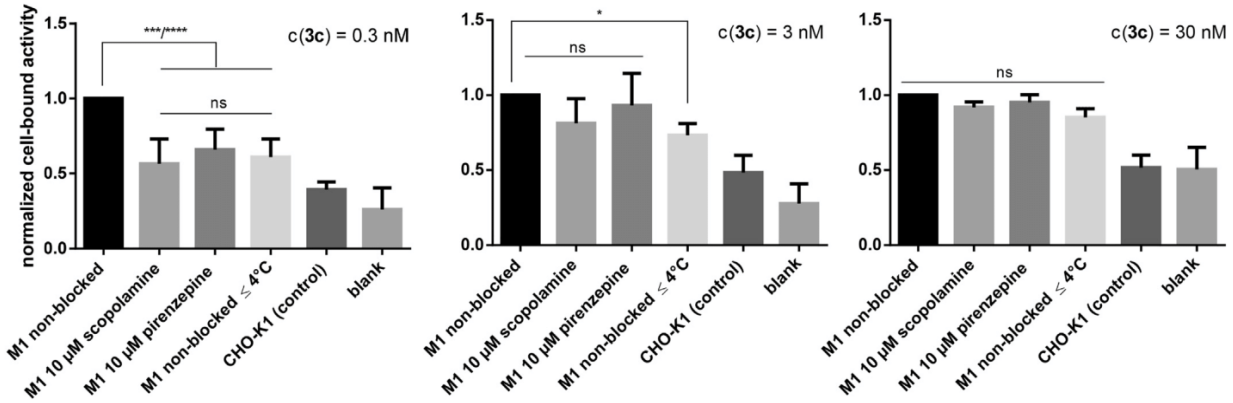


Fig. 9. [^{11}C]**3c** binding to CHO cells. Data are displayed normalized to the binding on the non-blocked CHO-M1 cells. Groups were compared using an ordinary one-way ANOVA and Tukey's multiple comparisons test, with a single pooled variance (*: P ≤ 0.05, ***: P ≤ 0.001, ****: P ≤ 0.0001, ns: not significant, n ≥ 3). At all tested [^{11}C]**3c** concentrations the normalized cell-bound activity of the CHO–K1 control cells was not significantly different from the blank.

with the radioligand concentration and is not saturable. Thus, the specific binding was only visible at a low radioligand concentration (0.3 nM), while at higher concentrations (3 nM, 30 nM) mostly nonspecific binding was detected.

2.9. In vitro autoradiography

Total binding of [^{11}C]pirenzepine (15 nM) was reduced to background signal in the presence of 10 μM scopolamine or atropine confirming that the brain sections and the used procedure allows the visualization of specific binding to mAChRs. However, neither of the blocking agents significantly reduced the radioactive signal derived from total [^{11}C]**3c** (30 nM) binding in a total of 30 brain sections derived from different brain regions of two different subjects, demonstrating only nonspecific binding (Fig. 10).

Also at a concentration close to the K_D [^{11}C]**3c** (3 nM) did not show a difference between baseline and blocking, whereas [^{11}C]pirenzepine at a concentration close to the K_D (15 nM) clearly showed specific binding.

3. Conclusion

Despite the pivotal role of mAChRs in human physiology and disease, non-invasive external imaging thereof has not yet found its way into clinical routine. Constrained imaging properties of the currently available mAChR PET tracers demand improvement in order to correspond to the clinical needs. In search of an improved PET tracer for mAChRs fifteen novel arecoline-derived compounds were synthesized, characterized and tested for their affinity toward mAChRs and EeAChE. Conjugation of arecaidine to diphenylmethyl-containing structures afforded K_i values in the low nanomolar range, which is suitable for the application as mAChR PET probe. Besides, the difference in affinity of (+)-**3e** and (−)-**3e** underline the applicability of stereochemistry to impact mAChR M1 ligand development. Moreover, all tested compounds were shown to neither act as orthosteric ligand nor substrate for the off-target AChE. Fully-automated carbon-11-labeling procedures for [^{11}C]**3a**–**c** and [^{11}C]**3i**–**k** were developed and the most promising candidates underwent further studies to assess their metabolic stability and serum protein binding, where [^{11}C]**3b** and [^{11}C]**3c** showed suitable properties for future tracer development. Real-time and endpoint radioligand binding studies using [^{11}C]**3c** on living cells as well as *in vitro* autoradiography on mouse brain sections revealed pronounced nonspecific binding, which motivates us to reduce the lipophilicity for future tracer candidates of similar structure prior to *in vivo* studies. Although the observed nonspecific binding of [^{11}C]**3c** restrains this compound from acting as imaging agent, it can still be considered as mAChR M1 ligand for purposes where nonspecific binding is less of a problem, *e.g.* therapeutics [41].

4. Experimental section

4.1. Materials

Diphenylmethyl trichloroacetimidate [42], furan-2-yl(phenyl) methanol [43], arecaidine [44] and *N*-Boc-guvacine [44] were synthesized as published previously. *N*-Fmoc-guvacine (≥98%, Santa Cruz Biotechnology), arecoline hydrobromide (XA BC-Biotech), scopolamine hydrobromide (Sigma-Aldrich), pirenzepine dihydrochloride (≥98%, Sigma-Aldrich), diethylamine (DEA, > 99%, Fisher Scientific), thionylchloride (≥99%, Sigma-Aldrich), triethylene glycol monomethyl ether (95%, Aldrich), diphenylmethanol (99%, Aldrich), 4,4′-dimethoxybenzhydrol (98+%, Alfa Aesar), 4,4′-difluorobenzhydrol (98+%, Alfa Aesar), (4-bromophenyl)(4-fluorophenyl)methanol (fluorochem), benzhydrylamine (97%, Alfa Aesar), *N*,*N*′-dicyclohexylcarbodiimide (DCC, 99%, Alfa Aesar), 1,1′-carbonyldiimidazole (CDI, reagent grade, Sigma Aldrich), iodomethane (CH_3I, ≥ 99%, Sigma-Aldrich), trichloroacetonitrile (98%, Alfa Aesar), 1,8-diazabicyclo[5,4,0]undec-7-en (>97%, Merck-Schuchardt), 11-(chloroacetyl)-5,11-dihydro-6H-pyrido[2,3-b][1,4]benzodiazepine-6-one (abcr), trifluoroacetic acid (99%, Alfa Aesar), aq. HBr (48%, Sigma Aldrich), formic acid

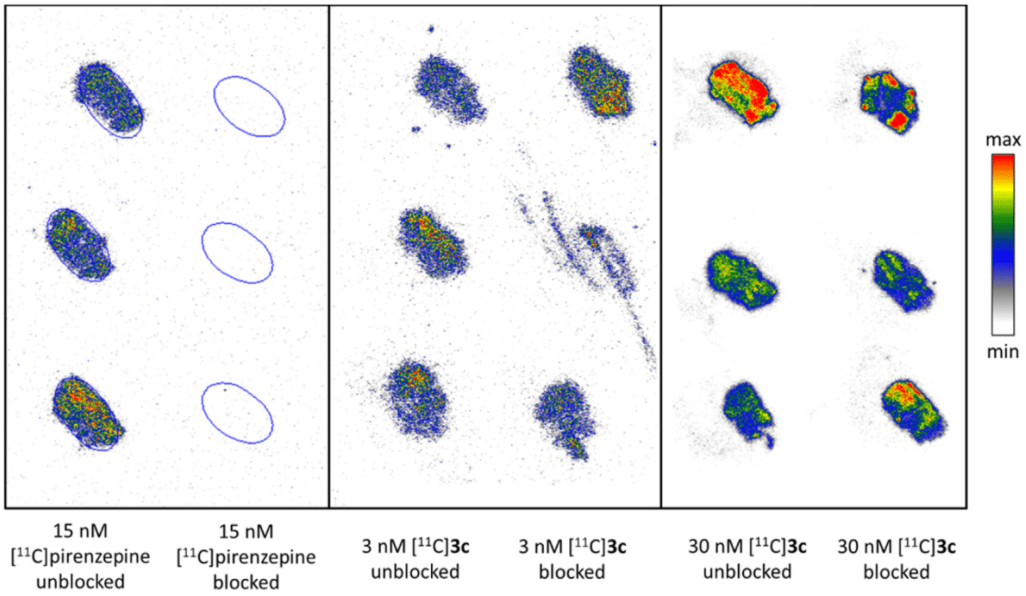


Fig. 10. Autoradiography of mice brain sections. Blocking was performed by co-incubation with 10 μM scopolamine. The signal at 15 nM [^{11}C]pirenzepine blocked is below limit of detection and the position of the invisible sections is therefore marked with a blue ellipse. Radioactivity is displayed as a linear color gradient. Sections separated in boxes are derived from different experiments, allowing only semi-quantitative analysis.

(≥95%, Merck), 2-chloroacrylonitrile (98%, Sigma Aldrich), 2-(methylamino)ethanol (99%, Alfa Aesar), KO^{t}Bu (≥98%, Sigma Aldrich), 5,5′-dithiobis-(2-nitrobenzoic acid) (DTNB, ≥98%, Carl Roth), acetylthiocholine iodide (ATI, ≥ 98%, Sigma Aldrich), tacrine hydrochloride (≥98%, Santa Cruz Biotechnology), acetylcholinesterase from *Electrophorus electricus* (1323 units/mg, Sigma Aldrich), sodium hydride (NaH, 60% dispersion in mineral oil, Aldrich), Mg turnings (≥99%, Sigma Aldrich), benzyl chloride (>99%, Merck), 5-bromo-2-fluoropyridine (>98%, TCI), ethyl formate (97%, Sigma Aldrich), dibromoethane (>98%, Merck), sodium carbonate (Na_2CO_3, anhydrous for analysis, Merck), sodium bicarbonate ($NaHCO_3$, ≥98%, Fluka), sodium iodide (NaI, 99.5%, Merck), poly(-ethyleneimine) (PEI, 50% in H_2O, Fluka), *N*,*N*-dimethylformamide (DMF, 99.8% extradry over molecular sieve, Acros), acetonitrile (ACN, Sigma Aldrich), dichloromethane (DCM, EMPROVE® ESSENTIAL, Merck), *n*-hexane (PE, Hi-PerSolv CHROMANORM, VWR), ethyl acetate (EE, 99.9%, VWR), diethyl ether (Et_2O, 100%, VWR), ethanol (EMROVE® exp, Merck), dimethylsulfoxide (DMSO, ≥ 99.9%, Sigma Aldrich) and C18 Sep-Pak (WAT020515, Waters) cartridges were purchased and used as received. Solvents indicated as "dry" were stored over molecular sieves for a minimum of 2 days. Reaction progress was monitored by pre-coated TLC sheets ALUGRAM® Xtra SIL G/UV254 (0.20 mm silica gel 60 with fluorescent indicator). Silica gel on TLC plates (0.25 mm, 20 × 20 cm, 99571 Sigma Aldrich) was used for preparative separation unless stated otherwise. In indicated cases aluminiumoxide 60 F_{254} neutral (Merck) was used for preparative TLC. [*N*-methyl-^{3}H]scopolamine methyl chloride (2.964 TBq/μmol, 37 MBq, in 1 mL ethanol) was purchased from PerkinElmer.

4.2. Instrumentation

NMR samples were measured in chloroform-d ($CDCl_3$, ≥99.8%, stabilized with silver foil, Sigma Aldrich) at 25 °C. The center of the (residual) solvent signal was used as an internal standard which was related to TMS with δ 7.26 ppm (^{1}H in $CDCl_3$) and δ 77.0 ppm (^{13}C in $CDCl_3$). ^{19}F NMR spectra were referenced *via* Ξ ratio and gsHMBC spectra of ^{15}N were referenced against neat, external CH_3NO_2. Unless stated otherwise full and unambiguous assignment of NMR signals was achieved by combination of standard NMR techniques, such as COSY, NOESY, APT, HSQC and HMBC experiments. NMR spectra of intermediates were recorded with a Bruker Avance III 200 spectrometer (200 MHz for ^{1}H). NMR spectra of final compounds were recorded with a Bruker Avance III 400 spectrometer (400 MHz for ^{1}H, 100 MHz for ^{13}C, 40 MHz for ^{15}N and 376 MHz for ^{19}F) or a Bruker Avance III 600 spectrometer (600 MHz for ^{1}H, 150 MHz for ^{13}C and 565 MHz for ^{19}F). Mass spectra were obtained on a Bruker maXis 4G instrument (ESI-TOF, HRMS). All newly synthesized or tested compounds (**1a**–**8**) passed a pan assay interference compounds filter [45]. An Agilent 1260 Infinity HPLC System with a flow of 1 mL/min and XBridge Shield RP18 2.5 μm, 50 × 3.0 mm column was used for determination of the radiochemical yield in the small scale reactions, quality control of the radiotracers as well as for the assessment of the tracer stability in formulation (further parameters shown in Table 6). LogP measurements were performed and interpreted as published recently [31] on an Agilent HPLC system consisting of an autosampler (series 1100), pump (series 1200), diode array detector (series 1100) and a radiodetector (Ramona, Elysia-Raytest) using an apHERA (5 μm, 10 × 6 mm) stationary phase. All tested compounds (**3a**–**m**, **6**–**8**) were shown to have a purity exceeding 95% as analyzed by the logP HPLC method without addition of toluene and triphenylene. The same HPLC System was used for the analysis of human liver microsomes metabolites with an XSelect™ (HSS T3, 3.5 μm, 100 × 4.6 mm) stationary phase, a flow of 1 mL/min and a gradient program (0.0–3.0 min: 95% pH 9.3, 5% ACN; 5.0–14.0 min: X % pH 9.3, 100-X % ACN; 15.0–16.0 min: 95% pH 9.3, 5% ACN; with X being 50, 45 and 63 for compounds **3b**, **3c** and **3i**, respectively). For the analysis of EeAChE metabolism a similar gradient was used: 0.0–3.0 min: 98% pH 9.3, 2% ACN; 5.0–14.0 min: 40% pH 9.3, 60% ACN; 15.0–16.0 min: 98% pH 9.3, 2% ACN. The used eluent buffer is a 25 mM $NH_4H_2PO_4$ solution set to pH 9.3 with NaOH. The LOQ given in Table 6 was estimated based on the standard deviation of the response and the slope [46].

Table 6
Separation conditions for analytical HPLC as part of radiotracer quality control and for the concentration determination of the **3e** enantiomers.

Compound	Eluent	$k_{prec.}$	$k_{prod.}$	LOQ [μg/mL]
3a	20% ACN, 80% pH 9.3	1.20	2.67	0.88
3b	60% ACN, 40% pH 9.3	2.00	3.53	1.05
3c	60% ACN, 40% pH 9.3	1.93	3.73	1.07
3e	75% ACN, 25% pH 9.3	–	2.35	1.20
3i	40% ACN, 60% pH 9.3	2.53	4.60	1.83
3j	20% ACN, 80% pH 9.3	1.80	3.67	1.99
3k	50% ACN, 50% pH 9.3	1.53	2.67	0.76

CHO–K1 cells stably transfected with human muscarinic receptors M1-M5 were obtained from Missouri University of Science and Technology cDNA Resource Center (Cell Catalog#: CEM1000000, CEM2000000, CEM3000000, CEM4000000, CEM5000000) and cultivated in Ham's F12 Nutrient Mixture (Gibco, Life Technologies Limited) containing 10% FBS (Gibco, Life Technologies Limited), 250 μg/mL Geneticin® (G418, Thermo Fisher) at 37 °C and 5% CO_2 in a cell incubator. Gibco™ Trypsin-EDTA (0.05%) was used for passaging cells. Untransfected CHO–K1 cells were obtained from ATCC and cultivated like described above but in media free of Geneticin®. Protease Inhibitor Cocktail powder (P2714-1BTL, Sigma-Aldrich) was dissolved in 10 mL water and used as such. The protein concentration of membrane suspensions was determined with Pierce™ BCA Protein Assay Kit (Thermo Scientific) on a BioTek Synergy HTX multi-mode reader. A M-36 tygon tubed Cell Harvester (Brandel®) and Whatman™ GF/B filters were used for the filtration of radioligand binding assays. Filter disks were counted with 2 mL Ultima Gold™ (high flashpoint LSC cocktail, PerkinElmer) using a 300 SL Automatic TDCR liquid Scintillation Counter (HIDEX) in CPM mode. LigandTracer grey and yellow (ridgeview instruments ab, Sweden) with LigandTracer Control V2.0.1 and TraceDrawer V1.8.1 were used for measuring real-time kinetic on living cells.

A GE PETtrace 860 cyclotron (General Electric Medical System, Sweden) was used for the production of [^{11}C]CO_2 by a^{14}N(p, α)^{11}C reaction in gas target filled with N_2 + 1% O_2 (Topline, Messer) at a beam current of 65 μA. Transformation to [^{11}C]CH_3I, radiolabeling of the precursor and tracer purification were carried out in a TRACERlab™ FX C Pro synthesizer using the built in semi-preparative HPLC system featuring a Linear Instruments Model 200 UV/Vis detector and a LaPrep HPLC pump (VWR) [47].

Metabolic stability was studied with Corning® Gentest™ HLM, ~20-Donor Pool, Mixed Gender microsomes and Corning® Gentest™ NADPH Regenerating System, Solution A and B. Pooled Human Serum (Innovative Research, Inc.), Centrifree®, Ultracel®PL Regenerated Cellulose Centrifugal filters (Merck Millipore), Microcon®-10 Ultracel®PL-10 Regenerated Cellulose 10,000 NMWL Centrifugal Filters and a 2480 Wizard^2 Automatic Gamma Counter (PerkinElmer) were used for determination of serum protein binding.

4.3. Synthesis

1-(9*H*-fluoren-9-yl)methyl 3-methyl 1,2,5,6-tetrahydropyridine-1,3-dicarboxylate (*N*-Fmoc-guvacoline) (1a). *N*-Fmoc-guvacine (50.0 mg, 0.143 mmol) and Na_2CO_3 (18.2 mg, 0.172 mmol) were suspended in dry DMF (5 mL) for 30 min at 20 °C. CH_3I (100 μL, 1.61 mmol) was added dropwise and the reaction mixture was stirred o/n. The reaction mixture was poured on H_2O (60 mL) and extracted with Et_2O (3x 30 mL). The combined organic layers were washed with H_2O (2x 15 mL), dried with Na_2SO_4, filtered and evaporated to give **1a** (49.8 mg, 96%) as a highly viscous oil.

^{1}H NMR (200 MHz, $CDCl_3$) δ 7.77 (d, J = 7.3 Hz, 2H), 7.59 (d, J = 7.3 Hz, 2H), 7.40 (t, J = 7.3 Hz, 2H), 7.31 (t, J = 7.3 Hz, 2H), 7.08 (s, 1H), 4.46 (d, J = 6.8 Hz, 2H), 4.27 (t, J = 6.8 Hz, 1H), 4.22–4.17 (m, 2H), 3.79 (s, 3H), 3.52 (brs, 2H), 2.29 (brs, 2H).

Methyl 1,2,5,6-tetrahydropyridine-3-carboxylate (guvacoline) (2a). 1a (49.8 mg, 0.137 mmol) was dissolved in ACN (3 mL), diethylamine (300 μL, 2.91 mmol) was added and the reaction mixture was stirred for 2.5 h at 20 °C. The reaction mixture was evaporated to about 1 mL and the product was isolated by preparative TLC (PE:EE = 1:6 + 1% DEA; R_f = 0.13–0.33) and appeared as yellowish oil (17.9 mg, 93%).

^{1}H NMR (400 MHz, $CDCl_3$) δ 7.04 (m, 1H, H-4), 3.73 (s, 3H, O–CH_3), 3.55 (m, 2H), 2.93 (t, J = 5.7 Hz, 2H, H-6), 2.28–2.21 (m, 2H, H-5).* ^{13}C NMR (100 MHz, $CDCl_3$) δ 166.5 (C=O), 138.3 (C-4), 130.3 (C-3), 51.5 (O–CH_3), 44.1 (C-2), 41.9 (C-6), 26.2 (C-5). HRMS (ESI) calcd for $C_7H_{12}NO_2$ ($M + H^+$) 142.0863, found 142.0876. *The guvacoline ^{1}H NH signal could not be found.

3-benzhydryl 1-(9*H*-fluoren-9-yl)methyl 1,2,5,6-tetrahydropyridine-1,3-dicarboxylate (1b). *N*-Fmoc-guvacine (50.0 mg, 0.143 mmol) and diphenylmethyl trichloroacetimidate (61.1 mg, 0.186 mmol) were dissolved in dry DCM (2 mL) and stirred at 20 °C under argon for 16 h. The product was isolated *via* preparative TLC (PE:EE = 3:1; R_f = 0.25–0.56) and formed white crystals (64.3 mg, 87%).

^{1}H NMR (200 MHz, $CDCl_3$) δ 7.74 (brs, 2H), 7.58 (brs, 2H), 7.46–7.20 (m, 14H), 6.99 (brs, 1H), 4.52–4.05 (m, 5H), 3.54 (brs, 2H), 2.32 (brs, 2H), 2.06 (s, 1H).

Benzhydryl 1,2,5,6-tetrahydropyridine-3-carboxylate (2b). 1b (64.3 mg, 0.125 mmol) was dissolved in ACN (3 mL), diethylamine (300 μL, 2.91 mmol) was added and the reaction mixture was stirred for 2 h at 20 °C. The reaction mixture was evaporated to about 1 mL and the product was isolated by preparative TLC (PE:EE = 1:1 + 1% DEA; R_f = 0.12–0.28) and appeared as yellowish wax (32.5 mg, 89%).

^{1}H NMR (400 MHz, $CDCl_3$) δ 7.34 (m, 8H, Ph H-2,3,5,6), 7.28 (m, 2H, Ph H-4), 7.20 (m, 1H, H-4), 6.94 (s, 1H, $CHPh_2$), 3.65 (m, 2H, H-2), 2.96 (t, J = 5.7 Hz, 2H, H-6), 2.30 (m, 2H, H-5).* ^{13}C NMR (100 MHz, $CDCl_3$) δ 164.7 (C=O), 140.3 (Ph C-1), 138.9 (C-4), 130.0 (C-3), 128.5 (Ph C-3,5), 127.9 (Ph C-4), 127.0 (Ph C-2,6), 76.7 ($CHPh_2$), 43.8 (C-2), 41.7 (C-6), 26.0 (C-5). HRMS (ESI) calcd for $C_{19}H_{20}NO_2$ ($M + H^+$) 294.1489, found 294.1487. *The guvacoline ^{1}H NH signal could not be found.

Bis(4-fluorophenyl)methyl 2,2,2-trichloroacetimidate. Bis(4-fluorophenyl)methanol (220 mg, 1.00 mmol), trichloroacetonitrile (10.0 mL, 10.0 mmol) and 1,8-diazabicyclo(5.4.0)undec-7-ene (0.10 mmol, 15 μL) were stirred in dry DCM at 20 °C under argon for 1.5 h. Volatiles were evaporated and the residue was purified by silica column chromatography (PE:EE = 80:1 + 3% TEA). The product appeared as white crystals (358 mg, 98%).

^{1}H NMR (200 MHz, $CDCl_3$) δ 8.45 (brs, 1H), 7.45–7.32 (m, 4H), 7.13–6.98 (m, 4H), 6.92 (s, 1H).

Bis(4-fluorophenyl)methyl 1-(2-(9*H*-fluoren-9-yl)acetyl)-1,2,5,6-tetrahydropyridine-3-carboxylate (1c). *N*-Fmoc-guvacine (40.0 mg, 0.115 mmol) and bis(4-fluorophenyl)methyl 2,2,2-trichloroacetimidate. (54.2 mg, 0.149 mmol) were dissolved in dry DCM (3 mL) and stirred at 20 °C under argon for 16 h. The product was isolated *via* preparative TLC (PE:EE = 7:2; R_f = 0.26–0.51) and formed white crystals (57 mg, 93%).

^{1}H NMR (200 MHz, $CDCl_3$) δ 7.74 (brs, 2H), 7.57 (d, J = 7.4 Hz, 2H), 7.44–7.18 (m, 9H), 7.10–6.98(m, 4H), 6.94 (s, 1H), 4.50–4.38 (m, 2H), 4.32–4.21 (m, 3H), 3.53 (brs, 2H), 2.33 (brs, 2H).

Bis(4-fluorophenyl)methyl 1,2,5,6-tetrahydropyridine-3-carboxylate (2c). 1c (57.1 mg, 0.107 mmol) was dissolved in ACN (3 mL), diethylamine (300 μL, 2.91 mmol) was added and the reaction mixture was stirred for 2 h at 20 °C. The reaction mixture was evaporated to about 1 mL and the product was isolated by preparative TLC (PE:EE = 1:1 + 1% DEA; R_f = 0.08–0.25) and appeared as yellowish oil (23.7 mg, 63%).

^{1}H NMR (400 MHz, $CDCl_3$) δ 7.29 (m, 4H, Ph H-2,6), 7.18 (m, 1H, H-4), 7.03 (m, 4H, H-3,5), 6.89 (s, 1H, $CHPh_2$), 3.64 (m, 2H, H-2), 2.97 (t, J = 5.8 Hz, 2H, H-6), 2.33 (m, 2H, H-5).* ^{13}C NMR (100 MHz, $CDCl_3$) δ 164.5 (C=O), 162.4 (d, J = 247.1 Hz, Ph C-4), 139.2 (C-4), 135.9 (d, J = 3.2 Hz, Ph C-1), 129.6 (C-3), 128.8 (d, J = 8.2 Hz, Ph C-2,6), 115.5 (d, J = 21.7 Hz, Ph C-3,5), 75.5 ($CHPh_2$), 43.7 (C-2), 41.6 (C-6), 25.9 (C-5). ^{19}F NMR (377 MHz, $CDCl_3$) δ −113.9 (m, Ph-F). HRMS (ESI) calcd for $C_{19}H_{18}F_2NO_2$ ($M + H^+$) 330.1300, found 330.1302. *The guvacoline ^{1}H NH signal could not be found.

***Tert*-butyl 5-(benzhydrylcarbamoyl)-1,2,3,6-tetrahydropyridine-1-carboxylate (1i).** *N*-Boc-guvacine (40.0 mg, 0.176 mmol) and CDI (28.5 mg, 0.176 mmol) were stirred in dry THF (3 mL) at 20 °C under argon for 30 min. Benzhydrylamine (45 μL, 0.264 mmol) was added and the reaction was stirred for 72 h. The reaction mixture was evaporated to 0.5 mL, the formed precipitate was removed by filtration and the filtrate purified *via* preparative TLC (PE:EE = 5:2; R_f = 0.32–0.49). The product appeared as colorless oil (8.0 mg, 12%).

^{1}H NMR (200 MHz, $CDCl_3$) δ 7.40–7.16 (m, 10H), 6.64 (brs, 1H), 6.34–6.14 (m, 2H), 4.22–4.12 (m, 2H), 3.49 (t, J = 5.6 Hz, 2H), 2.34–2.20 (m, 2H), 1.46 (s, 9H).

***N*-(diphenylmethyl)-1,2,5,6-tetrahydropyridine-3-carboxamide (2i). 1i** (8.0 mg, 0.020 mmol) was stirred in DCM (2 mL) containing TFA for 1.5 h at 20 °C. The volatiles were removed by evaporation, the solid residue was taken up in saturated Na_2CO_3 solution and extracted with DCM (3x 2 mL). The extract was dried with Na_2SO_4, filtered and evaporated to yield a colorless oil (4.7 mg, 79%).

^{1}H NMR (400 MHz, $CDCl_3$) δ 7.33 (m, 4H, Ph H-3,5), 7.27 (m, 2H, Ph H-4), 7.23 (m, 4H, Ph H-2,6), 6.62 (m, 1H, H-4), 6.29 (d, J = 7.8 Hz, 1H, $CHPh_2$), 6.21 (brd, J = 7.8 Hz, 1H, CONH), 3.61 (m, 2H, H-2), 2.93 (t, J = 5.7 Hz, 2H, H-6), 2.21 (m, 2H, H-5).* ^{13}C NMR (100 MHz, $CDCl_3$) δ 166.2 (C=O), 141.5 (Ph C-1), 134.2 (C-3), 131.1 (C-4), 128.7 (Ph C-3,5), 127.5 (Ph C-4), 127.4 (Ph C-2,6), 56.8 ($CHPh_2$), 44.3 (C-2), 42.1 (C-6), 25.7 (C-5). ^{15}N NMR (41 MHz, $CDCl_3$) δ −260.2 (CONH).** HRMS (ESI) calcd for $C_{19}H_{21}N_2O$ ($M + H^+$) 293.1648, found 293.1649. *The guvacoline ^{1}H NH signal could not be found. ** The guvacoline ^{15}N signal could not be found.

1-(9*H*-fluoren-9-yl)methyl 3-{2-[2-(2-methoxyethoxy)ethoxy]ethyl} 1,2,5,6-tetrahydropyridine-1,3-dicarboxylate (1j). *N*-Fmoc-guvacine (50.0 mg, 0.143 mmol) was suspended in dry DCM (2 mL) and $SOCl_2$ (250 μL, 3.45 mmol) was added by syringe. The mixture was sonicated for 40 min at 20 °C. Evaporation of the volatiles yielded the acyl chloride, which was heated to 50 °C with triethylene glycol monomethyl ether (1 mL, 6.25 mmol) for 1 h. The reaction mixture was poured on H_2O (30 mL) and extracted with Et_2O (5x 15 mL). The combined organic layers were washed with H_2O (2x 10 mL), dried with Na_2SO_4, filtered and evaporated to give **1j** (66.0 mg, 93%) as a viscous, slightly yellow oil.

^{1}H NMR (200 MHz, $CDCl_3$) δ 7.76 (d, J = 7.2 Hz, 2H), 7.58 (d,

J = 7.2 Hz, 2H), 7.40 (t, J = 7.2 Hz, 2H), 7.31 (t, J = 7.2 Hz, 2H), 7.10 (s, 1H), 4.45 (d, J = 6.3 Hz, 2H), 4.38–4.18 (m, 5H), 3.80–3.47 (m, 12H), 3.37 (s, 3H), 2.29 (brs, 2H).

2-[2-(2-methoxyethoxy)ethoxy]ethyl 1,2,5,6-tetrahydropyridine-3-carboxylate (2j). 1j (66.0 mg, 0.133 mmol) was dissolved in ACN (3 mL), diethylamine (300 μL, 2.91 mmol) was added and the reaction mixture was stirred for 2 h at 20 °C. The reaction mixture was evaporated to about 1 mL and the product was isolated by preparative TLC (EE + 1% DEA; R_f = 0.14–0.48) and appeared as yellowish oil (31.8 mg, 87%).

^{1}H NMR (400 MHz, $CDCl_3$) δ 7.07 (m, 1H, H-4), 4.29 (m, 2H, TEG H-1), 3.73 (m, 2H, TEG H-2), 3.68–3.63 (m, 6H, TEG H-3,4,5), 3.55 (m, 2H, H-2), 3.54 (m, 2H, TEG H-6), 3.38 (s, 3H, OCH_3), 2.92 (t, J = 5.7 Hz, 2H, H-6), 2.27–2.20 (m, 2H, H-5).* ^{13}C NMR (100 MHz, $CDCl_3$) δ 165.9 (C═O), 138.6 (C-4), 130.3 (C-3), 71.9 (TEG C-6), 70.62 (TEG C-3)**, 70.61 (TEG C-4)**, 70.57 (TEG C-5), 62.9 (TEG C-2), 59.0 (OCH_3), 44.0 (C-2), 41.9 (C-6), 26.2 (C-5). HRMS (ESI) calcd for $C_{13}H_{24}NO_5$ (M + H^+) 274.1649, found 274.1647. *The guvacoline ^{1}H NH signal could not be found. **indistinguishable.

(9*H*-fluoren-9-yl)methyl 5-{[3-cyclohexyl(cyclohexylcarbamoyl)amino]carbonyl}-1,2,3,6-tetrahydropyridine-1-carboxylate (1k). *N*,*N*′-Dicyclohexylcarbodiimide (20.7 mg, 0.100 mmol) was added to a stirred solution of *N*-Fmoc-guvacine (31.9 mg, 0.0913 mmol) in 1 mL dry DMF at 20 °C. After 1.5 h more *N*,*N*′-Dicyclohexylcarbodiimide (10.0 mg, 0.0483 mmol) was added. After 20 h the reaction mixture was poured on water (10 mL) and extracted with Et_2O (3x 10 mL). The combined organic layers were dried with Na_2SO_4, filtered, evaporated and purified *via* preparative TLC (PE:EE = 2:1; R_f = 0.44–0.66). The product was obtained as white, crystalline solid (24.4 mg, 48%).

^{1}H NMR (200 MHz, $CDCl_3$) δ 7.77 (d, J = 7.2 Hz, 2H), 7.58 (d, J = 7.2 Hz, 2H), 7.40 (t, J = 7.2 Hz, 2H), 7.31 (t, J = 7.2 Hz, 2H), 6.25 (brs, 2H), 4.49–4.33 (m, 2H), 4.32–4.17 (m, 3H), 4.05 (brs, 1H), 3.55 (brs, 3H), 2.20 (brs, 2H), 2.00–1.05 (m, 18H).

***N*-cyclohexyl-*N*-(cyclohexylcarbamoyl)-1,2,5,6-tetrahydropyridine-3-carboxamide (2k). 1k** (24.4 mg, 0.0439 mmol) was dissolved in ACN (3 mL), diethylamine (300 μL, 2.91 mmol) was added and the reaction mixture was stirred for 3 h at 20 °C. The reaction mixture was evaporated to about 1 mL and the product was isolated by preparative TLC (DCM:MeOH = 12:1; R_f = 0.06–0.22) and appeared as slightly yellowish oil (12.5 mg, 85%).

^{1}H NMR (400 MHz, $CDCl_3$) δ 6.74 (d, J = 7.5 Hz, 1H, CONH), 6.21 (m, 1H, H-4), 4.02 (m, 1H, Cy1 H-1), 3.62 (m, 1H, Cy2 H-1), 3.58 (m, 2H, H-2), 2.97 (t, J = 5.8 Hz, 2H, H-6), 2.17 (m, 2H, H-5), 1.95 (m, 2H, Cy1 H-2a,6a), 1.90 (m, 2H, Cy2 H-2a,6a), 1.79 (m, 2H, Cy1 H-3a,5a), 1.75 (m, 2H, Cy1 H-2b,6b), 1.70 (m, 2H, Cy2 H-3a,5a), 1.61 (m, 2H, Cy1,2 H-4a), 1.35 (m, 2H, Cy2 H-3b,5b), 1.27 (m, 2H, Cy1 H-3b,5b), 1.18 (m, 2H, Cy2 H-2b,6b), 1.17 (m, 2H, Cy1,2 H-4b).* ^{13}C NMR (100 MHz, $CDCl_3$) δ 171.1 (C═O), 154.2 (NCON), 135.6 (C-3), 128.0 (C-4), 57.0 (Cy1 C-1), 49.8 (Cy2 C-1), 44.4 (C-2), 41.8 (C-6), 32.7 (Cy2 C-2,6), 30.9 (Cy1 C-2,6), 26.3 (Cy1 C-3,5), 25.4 (Cy1 C-4), 25.3 (Cy2 C-4), 24.7 (Cy2 C-3,5), 24.6 (C-5). ^{15}N NMR (41 MHz, $CDCl_3$) δ −256.7 (CONHCy2).** HRMS (ESI) calcd for $C_{19}H_{32}N_3O_2$ (M + H^+) 334.2489, found 334.2492. *The guvacoline ^{1}H NH signal could not be found. ** The guvacoline and imide ^{15}N signals could not be found.

Sodium diphenylmethanolate. Diphenylmethanol (300 mg, 1.62 mmol) was dissolved in dry THF (10 mL) and sodium (100 mg, 4.35 mmol) was added. The mixture was slightly heated until the gas evolution stopped. Excessive sodium was removed and the suspension was concentrated under reduced pressure. The waxy residue was dissolved in dry DMF (3.35 mL) and used for the synthesis of **3b** and **7** without characterization. **sodium 4,4′-difluordiphenylmethanolate**, **sodium 4,4′-dimethoxydiphenylmethanolate**, **sodium (4-bromophenyl)(4-fluorophenyl)methanolate**, **bis(6-fluoropyridin-3-yl)methanolate** and **furan-2-yl(phenyl)methanolate** were prepared accordingly.

Benzhydryl 1-methyl-1,2,5,6-tetrahydropyridine-3-carboxylate (3b). Arecaidine (20.0 mg, 0.142 mmol) was suspended in dry DMF (2 mL) and heated gently until almost everything dissolved. CDI (23.0 mg, 0.142 mmol) was added as solid. After 15 min sodium diphenylmethanolate (0.59 mL of a 0.1 g/mL solution, 0.284 mmol) was added and the reaction mixture was stirred for 18 h at 20 °C. The reaction mixture was poured on water (10 mL) and extracted with DCM (3x 10 mL). The organic phase was concentrated under reduced pressure and purified by preparative TLC (EE; R_f = 0.29–0.50). The product was obtained as colorless oil (8.3 mg, 19%).

^{1}H NMR (400 MHz, $CDCl_3$) δ 7.34 (m, 8H, Ph H-2,3,5,6), 7.28 (m, 2H, Ph H-4), 7.15 (m, 1H, H-4), 6.94 (s, $CHPh_2$), 3.21 (m, 2H, H-2), 2.51 (t, J = 5.6 Hz, 2H, H-6), 2.40 (m, 2H, H-5), 2.42 (s, 3H, NCH_3). ^{13}C NMR (100 MHz, $CDCl_3$) δ 164.7 (C═O), 140.3 (Ph C-1), 138.3 (C-4), 129.1 (C-3), 128.5 (Ph C-3,5), 127.8 (Ph C-4), 127.1 (Ph C-2,6), 53.2 (C-2), 50.8 (C-6), 45.8 (NCH_3), 26.8 (C-5). ^{15}N NMR (41 MHz, $CDCl_3$) δ −349.7 (NCH_3). HRMS (ESI) calcd for $C_{20}H_{22}NO_2$ (M + H^+) 308.1645, found 308.1656.

Bis(4-fluorophenyl)methyl 1-methyl-1,2,5,6-tetrahydropyridine-3-carboxylate (3c). Arecaidine (20.0 mg, 0.142 mmol) was suspended in dry DMF (3 mL) and heated gently until almost everything dissolved. CDI (23.0 mg, 0.142 mmol) was added as solid. After 1 h sodium 4,4′-difluordiphenylmethanolate (0.69 mL of a 0.1 g/mL solution, 0.284 mmol) was added and the reaction mixture was stirred for 60 h at 20 °C. The reaction mixture was poured on water (10 mL) and extracted with EE (2x 20 mL). The organic phase was washed with water (10 mL), dried over Na_2SO_4, concentrated under reduced pressure and purified by preparative TLC (EE; R_f = 0.18–0.45). The product was obtained as colorless oil (4.4 mg, 9%).

^{1}H NMR (600 MHz, $CDCl_3$) δ 7.28 (m, 4H, Ph H-3,5), 7.14 (m, 1H, H-4), 7.03 (m, 4H, Ph H-2,6), 6.90 (s, 1H, $CHPh_2$), 3.22 (m, 2H, H-2), 2.54 (t, J = 5.6 Hz, 2H, H-6), 2.44 (s, 3H, NCH_3), 2.43 (m, 2H, H-5). ^{13}C NMR (151 MHz, $CDCl_3$) δ 164.6 (C═O), 162.5 (d, J = 247.0 Hz, Ph C-4), 138.7 (C-4), 136.0 (d, J = 3.0 Hz, Ph C-1), 129.0 (d, J = 8.3 Hz, Ph C-2,6), 128.8 (C-3), 115.6 (d, J = 22.1 Hz, Ph C-3,5), 75.6 ($CHPh_2$), 53.1 (C-2), 50.8 (C-6), 45.7 (NCH_3), 26.7 (C-5). HRMS (ESI) calcd for $C_{20}H_{20}F_2NO_2$ (M + H^+) 344.1457, found 344.1462.

Bis(4-methoxyphenyl)methyl 1-methyl-1,2,5,6-tetrahydropyridine-3-carboxylate (3d). Arecaidine (30.0 mg, 0.213 mmol) was suspended in dry DMF (4 mL) and heated gently until almost everything dissolved. CDI (34.5 mg, 0.213 mmol) was added as solid. After 1 h sodium 4,4′-dimethoxydiphenylmethanolate (1.13 mL of a 0.1 g/mL solution, 0.426 mmol) was added and the reaction mixture was stirred for 24 h at 20 °C. The reaction mixture was poured on water (10 mL) and extracted with EE (2x 20 mL). The organic phase was washed with water (10 mL), dried over Na_2SO_4, concentrated under reduced pressure and purified by preparative TLC (EE; R_f = 0.18–0.45). The product was obtained as colorless oil (2.8 mg, 4%).

^{1}H NMR (400 MHz, $CDCl_3$) δ 7.24 (m, 4H, Ph H-2,6), 7.11 (m, 1H, H-4), 6.88 (s, 1H, $CHPh_2$), 6.86 (m, 4H, Ph H-3,5), 3.79 (s, 6H, OCH_3), 3.20 (m, 2H, H-2), 2.51 (t, J = 5.7 Hz, 2H, H-6), 2.41 (s, 3H, NCH_3), 2.38 (m, 2H, H-5). ^{13}C NMR (100 MHz, $CDCl_3$) δ 164.8 (C═O), 159.1 (Ph C-4), 138.0 (C-4), 132.7 (Ph C-1), 129.1 (C-3), 128.4 (Ph C-2,6), 113.8 (Ph C-3,5), 76.2 ($CHPh_2$), 53.1 (C-2), 50.7 (C-6), 45.7 (NCH_3), 26.6 (C-5). HRMS (ESI) calcd for $C_{20}H_{26}NO_4$ (M + H^+) 368.1856, found 368.1855.

(4-bromophenyl)(4-fluorophenyl)methyl 1-methyl-1,2,5,6-

tetrahydropyridine-3-carboxylate (3e). Arecaidine (40.0 mg, 0.284 mmol) was suspended in dry DMF (5 mL) and heated gently until almost everything dissolved. CDI (46.1 mg, 0.284 mmol) was added as solid. After 30 min sodium (4-bromophenyl)(4-fluorophenyl)methanolate (1.72 mL of a 0.1 g/mL solution, 0.568 mmol) was added and the reaction mixture was stirred for 2 weeks at 20 °C. The reaction mixture was poured on water (15 mL) and extracted with EE (2x 25 mL). The organic phase was washed with water (10 mL), dried over Na_2SO_4, concentrated under reduced pressure and purified by preparative TLC (EE; R_f = 0.28–0.42). The product was obtained as slightly yellow oil (28.4 mg, 25%).

^{1}H NMR (400 MHz, $CDCl_3$) δ 7.46 (m, 2H, Ph-Br H-3,5), 7.28 (m, 2H, Ph-F H-2,6), 7.19 (m, 2H, Ph-Br H-2,6), 7.13 (m, 1H, H-4), 7.02 (m, 2H, Ph-F H-3,5), 6.86 (s, 1H, $CHPh_2$), 3.18 (m, 2H, H-2), 2.51 (t, J = 5.6 Hz, 2H, H-6), 2.41 (s, 3H, NCH_3), 2.40 (m, 2H, H-5). ^{13}C NMR (100 MHz, $CDCl_3$) δ 164.4 (C═O), 162.4 (d, J = 247.2 Hz, Ph-F C-4), 139.1 (Ph-Br C-1), 138.7 (C-4), 135.6 (d, J = 3.2 Hz, Ph-F C-1), 131.7 (Ph-Br C-3,5), 128.9 (d, J = 8.3 Hz, Ph-F C-2,6), 128.6 (Ph-Br C-2,6), 122.0 (Ph-Br C-4), 115.5 (d, J = 21.6 Hz, Ph-F C-3,5), 75.4 ($CHPh_2$), 53.1 (C-2), 50.7 (C-6), 45.7 (NCH_3), 26.7 (C-5). ^{19}F NMR (377 MHz, $CDCl_3$) δ −113.7 (m). ^{15}N NMR (41 MHz, $CDCl_3$) δ −349.8 (NCH_3). HRMS (ESI) calcd for $C_{20}H_{20}BrFNO_2$ ($M + H^+$) 404.0656, found 404.0668.

The racemic product was resolved on an AGP 0.3 cmØ × 5 cm 5 μM column using 12% 2-propanol in 10 mM NH_4Ac pH 5.8 at a flow of 0.5 mL/min (Fig. S5, Supporting Information). 2 μL of a 10 mg/mL solution in 2-propanol was injected 10 times resulting in baseline separation of the enantiomers. The pooled fractions were diluted with the same amount of water, subjected to solid phase extraction and eluted with ethanol (10 mL). Using a PerkinElmer 341 polarimeter with a 1 dm cell, (−) was assigned to the enantiomer with the stronger interaction to the stationary phase and (+) was assigned to the enantiomer with the weaker interaction to the stationary phase.

Bis(6-fluoropyridin-3-yl)methanol. Mg turnings (345 mg, 14.2 mmol) were stirred in dry THF (10 mL) and activated with $BrCH_2CH_2Br$ (two drops). 5-bromo-2-fluoropyridine (500 mg, 2.84 mmol) in dry THF (2 mL) was added dropwise at 20 °C and the reaction mixture was refluxed for 45 min. Ethyl formate (115 μL, 1.42 mmol) in Et_2O (3 mL) was added dropwise at 20 °C and the reaction mixture was stirred for further 30 min. The reaction mixture was poured on sat. aq. NH_4Cl (20 mL) and extracted with EE (3x 15 mL) The combined organic phases were dried with Na_2SO_4 and evaporated. Preparative TLC (EE, R_f = 0.18–0.33, when developed twice) afforded the product (54 mg, 17%) as yellow wax.

^{1}H NMR (200 MHz, $CDCl_3$) δ 8.21 (m, 2H, H-2), 7.76 (m, 2H, H-4), 6.93 (m, 2H, H-5), 5.95 (s, 1H, $CHPyr_2$), 3.18 (brs, 1H, OH). ^{13}C NMR (50 MHz, $CDCl_3$) δ 163.4 (d, J = 240.8 Hz, C-6), 145.9 (d, J = 15.0 Hz, C-2), 139.8 (d, J = 8.2 Hz, C-4), 136.3 (d, J = 4.6 Hz, C-3), 110.0 (d, J = 37.4 Hz, C-5), 70.7 ($CHPyr_2$). HRMS (ESI) calcd for $C_{11}H_8F_2N_2NaO$ ($M + Na^+$) 245.0495, found 245.0497.

Bis(6-fluoropyridin-3-yl)methyl 1-methyl-1,2,5,6-tetrahydropyridine-3-carboxylate (3f). Arecaidine (30.0 mg, 0.213 mmol) was suspended in dry DMF (4 mL) and heated gently until almost everything dissolved. CDI (34.5 mg, 0.213 mmol) was added as solid. After 1 h sodium bis(6-fluoropyridin-3-yl)methanolate (1.04 mL of a 0.1 g/mL solution, 0.426 mmol) was added and the reaction mixture was stirred for 24 h at 20 °C. The reaction mixture was poured on water (15 mL) and extracted with EE (3x 15 mL). The organic phase was washed with water (10 mL), dried over Na_2SO_4, concentrated under reduced pressure and purified by preparative TLC (EE; R_f = 0.08–0.10) as well as preparative TLC on alox (PE:EE = 2:1), yielding the product as colorless oil (1.8 mg, 3%).

^{1}H NMR (500 MHz, $CDCl_3$) δ 8.24 (m, 2H, Pyr H-2), 7.74 (m, 2H, Pyr H-4), 7.32 (m, 1H, H-4), 7.00 (s, 1H, $CHPyr_2$), 6.99 (m, 2H, Pyr H-6), 4.21 (m, 1H, H-2), 3.54 (m, 1H, H-6) 3.48 (m, 1H, H-2), 3.32 (m, 1H, H-5), 2.92 (s, 3H, NCH_3), 2.91 (m, 1H, H-6), 2.58 (m, 1H, H-5). ^{13}C NMR (125 MHz, $CDCl_3$) δ 163.63 (d, J = 240.5 Hz, Pyr C-6), 163.59 (d, J = 240.5 Hz, Pyr C-6), 162.1 (C═O), 146.7 (d, J = 7.7 Hz, Pyr C-2), 146.6 (d, J = 7.7 Hz, Pyr C-2), 140.17 (d, J = 7.5 Hz, Pyr C-4), 138.6 (C-4), 131.8 (d, J = 4.6 Hz, Pyr C-3), 131.5 (d, J = 4.6 Hz, Pyr C-3), 123.2 (C-3), 110.3 (d, J = 37.4 Hz, Pyr C-5), 110.2 (d, J = 37.4 Hz, Pyr C-5), 72.5 ($CHPyr_2$), 50.3 (C-2), 49.3 (C-6), 43.2 (NCH_3), 23.1 (C-5). ^{19}F NMR (471 MHz, $CDCl_3$) δ −66.6 (ddd, J = 17.1 Hz, J = 7.0 Hz, J = 2.3 Hz). HRMS (ESI) calcd for $C_{18}H_{18}F_2N_3O_2$ ($M + H^+$) 346.1362, found 346.1366.

Furan-2-yl(phenyl)methyl 1-methyl-1,2,5,6-tetrahydropyridine-3-carboxylate (3g). Arecaidine (40.0 mg, 0.284 mmol) was suspended in dry DMF (5 mL) and heated gently until almost everything dissolved. CDI (46.1 mg, 0.284 mmol) was added as solid. After 20 min sodium furan-2-yl(phenyl)methanolate (1.11 mL of a 0.1 g/mL solution, 0.568 mmol) was added and the reaction mixture was stirred for 60 h at 20 °C. The crude reaction mixture was purified by semipreparative HPLC with Two injections of 1.5 mL each were performed and the product fractions were immediately collected on DCM. The combined organic phases were dried with brine and $MgSO_4$, filtered and evaporated, yielding the product as a yellowish oil (6 mg, 15%). This work-up procedure was chosen due to the observed instability of this compound on silica and alox stationary phases. The isolated compound was sufficiently stable for chemical characterization. Despite storage at −20 °C, HPLC analysis prior to planned affinity measurements revealed inacceptable decomposition, excluding it from further evaluation.

^{1}H NMR (400 MHz, $CDCl_3$) δ 7.43 (m, 2H, Ph H-2,6), 7.40 (m, 1H, Fur H-5), 7.37 (m, 2H, Ph H-3,5), 7.35 (m, 1H, Ph H-4), 7.12 (m, 1H, H-4), 6.96 (s, 1H, CHPhFur), 6.31 (dd, J = 3.3 Hz, J = 1.9 Hz, 1H, Fur H-4), 6.19 (d, J = 3.3 Hz, 1H, Fur H-3), 3.19 (m, 2H, H-2), 2.50 (m, 2H, H-6), 2.41 (s, 3H, NCH_3), 2.38 (m, 2H, H-5). ^{13}C NMR (100 MHz, $CDCl_3$) δ 164.5 (C═O), 152.4 (Fur C-2), 143.2 (Fur C-5), 138.5 (C-4), 137.5 (Ph C-1), 128.8 (C-3), 128.5 (Ph C-3,5), 128.3 (Ph C-4), 127.1 (Ph C-2,6), 70.3 (CHPhFur), 53.1 (C-6), 50.7 (C-6), 45.7 (NCH_3), 26.6 (C-5). ^{15}N NMR (41 MHz, $CDCl_3$) δ −349.5 (NCH_3). HRMS (ESI) calcd for $C_{18}H_{20}NO_3$ ($M + H^+$) 298.1438, found 298.1433.

2-oxo-1,2-diphenylethyl 1-methyl-1,2,5,6-tetrahydropyridine-3-carboxylate (3h). Arecaidine (40.0 mg, 0.284 mmol) was suspended in dry DMF (5 mL) and heated gently until almost everything dissolved. CDI (46.1 mg, 0.284 mmol) was added as solid. After 1 h (±)-benzoin (121 mg, 0.568 mmol) was added and the reaction mixture was stirred for 5 days at 20 °C. The reaction mixture was poured on water (15 mL) and extracted with EE (3x 15 mL). The combined organic phases were dried over Na_2SO_4 and concentrated under reduced pressure. Half of the resulting residue was purified by preparative TLC (EE; R_f = 0.17–0.40), yielding the product as colorless oil (12.0 mg, 3%).

^{1}H NMR (400 MHz, $CDCl_3$) δ 7.95 (m, 2H, COPh H-2,6), 7.51 (m, 1H, COPh H-4), 7.48 (m, 2H, Ph H-2,6), 7.40 (m, 2H, COPh H-3,5), 7.37 (m, 1H, Ph H-4), 7.35 (m, 2H, Ph H-3,5), 7.17 (m, 1H, H-4), 6.91 (s, 3H, CHPh), 3.20 (m, 2H, H-2), 2.52 (m, 2H, H-6), 2.41 (s, 3H, NCH_3), 2.40 (m, 2H, H-5). ^{13}C NMR (100 MHz, $CDCl_3$) δ 193.9 (COPh), 165.0 (COO), 139.2 (C-4), 134.7 (COPh C-1), 133.8 (Ph C-1), 133.4 (COPh C-4), 129.2 (Ph C-4), 129.1 (Ph C-3,5), 128.8 (COPh C-2,6), 128.62 (COPh C-3,5), 128.56 (Ph C-2,6), 128.2 (C-3), 77.3 (CHPh), 52.9 (C-2), 50.6 (C-6), 45.6 (NCH_3), 26.6 (C-5). HRMS (ESI) calcd for $C_{21}H_{22}NO_3$ ($M + H^+$) 336.1594, found 336.1600.

***N*-benzhydryl-1-methyl-1,2,5,6-tetrahydropyridine-3-carboxamide (3i).** Arecaidine (20.0 mg, 0.142 mmol) was suspended in dry DMF (3 mL) and heated gently until almost everything dissolved. CDI (23.0 mg, 0.142 mmol) was added as solid.

After 1 h benzhydrylamine (52.0 mg, 0.284 mmol) was added and the reaction mixture was stirred for 18 h at 20 °C. DMF was evaporated under reduced pressure and the residue was purified by preparative TLC (DCM:MeOH = 20:1; R_f = 0.36–0.47 when developed twice; subsequently: DCM:MeOH = 30:1, analytical TLC plate, R_f = 0.11–0.27). The product was obtained as colorless oil (5.3 mg, 12%).

^{1}H NMR (400 MHz, $CDCl_3$) δ 7.33 (m, 4H, Ph H-3,5), 7.27 (m, 2H, Ph H-4), 7.23 (m, 4H, Ph H-2,6),6.56 (m, 1H, H-4), 6.28 (m, 2H, $CHPh_2$, NH), 3.26 (m, 2H, H-2), 2.57 (t, J = 5.7 Hz, 2H, H-6), 2.44 (s, 3H, NCH_3), 2.38 (m, 2H, H-5). ^{13}C NMR (100 MHz, $CDCl_3$) δ 165.8 (C═O), 141.4 (Ph C-1), 132.4 (C-3), 130.1 (C-4), 128.7 (Ph C-3,5), 127.5 (Ph C-4), 127.4 (Ph C-2,6), 56.9 ($CHPh_2$), 53.2 (C-2), 50.8 (C-6), 45.5 (NCH_3), 25.8 (C-5). ^{15}N NMR (41 MHz, $CDCl_3$) δ −260.3 (CONH), −348.9 (NCH_3). HRMS (ESI) calcd for $C_{20}H_{22}N_2NaO$ ($M + Na^+$) 329.1624, found 329.1634.

2-[2-(2-methoxyethoxy)ethoxy]ethyl 1-methyl-1,2,5,6-tetrahydropyridine-3-carboxylate (3j). Arecaidine (20.0 mg, 0.142 mmol) was suspended in dry DMF (2 mL) and CDI (23.0 mg, 0.142 mmol) was added as solid. The suspension was gently heated until a solution was obtained. Triethylene glycol monomethyl ether (50 μL, 0.312 mmol) was added and the reaction mixture was stirred for 60 h at rt. The solvent was evaporated and the residue was purified by preparative TLC (PE:EE = 2:1; R_f = 0.22–0.38). The product was obtained as colorless oil (7.2 mg, 18%).

^{1}H NMR (400 MHz, $CDCl_3$) δ 7.03 (m, 1H, H-4), 4.29 (m, 2H, TEG H-1), 3.73 (m, 2H, TEG H-2), 3.66 (m, 4H, TEG H-3,4), 3.65 (m, 2H, TEG H-5), 3.55 (m, 2H, TEG H-6), 3.38 (s, 3H, OCH_3), 3.17 (m, 2H, H-2), 2.52 (t, J = 5.6 Hz, 2H, H-6), 2.42 (s, 3H, NCH_3), 2.38 (m, 2H, H-5). ^{13}C NMR (100 MHz, $CDCl_3$) δ 165.6 (C═O), 137.8 (C-4), 128.7 (C-3), 71.9 (TEG C-6), 70.62 (TEG C-3)*, 70.61 (TEG C-4)*, 70.58 (TEG C-5)*, 69.2 (TEG C-2), 63.6 (TEG C-1), 59.0 (OCH_3), 53.1 (C-2), 50.7 (C-6), 45.6 (NCH_3), 26.5 (C-5). ^{15}N NMR (41 MHz, $CDCl_3$) δ −349.7 (NCH_3). HRMS (ESI) calcd for $C_{14}H_{26}NO_5$ ($M + H^+$) 288.1805, found 288.1815. *indistinguishable.

***N*-cyclohexyl-*N*-(cyclohexylcarbamoyl)-1-methyl-1,2,5,6-tetrahydropyridine-3-carboxamide (3k).** Arecaidine (30.0 mg, 0.213 mmol) and diphenylmethanol (78.3 mg, 0.425 mmol) were suspended in dry DMF (1.5 mL) and dry DCM (0.5 mL). DMAP (3 mg, 0.025 mmol) was added at 20 °C and the reaction mixture was cooled to 0 °C. DCC (48.2 mg, 0.234 mmol) was added as solution in DMF (0.5 mL) and the reaction mixture was stirred at 0 °C for 10 min, at 20 °C for 40 min and at 70 °C for 30 min. The solvent was evaporated and the residue was purified by preparative TLC (DCM:MeOH = 11:1; R_f = 0.20–0.50). The product was obtained as off-white solid (50.9 mg, 69%). Crystals suitable for single-crystal X-ray crystallography were grown from $CDCl_3$/hexane by slow evaporation of solvents. Crystallographic analysis is described in the Supporting Information.

^{1}H NMR (400 MHz, $CDCl_3$) δ 6.77 (d, J = 7.5 Hz, 1H, NH), 6.15 (m, 1H, H-4), 4.01 (m, 1H, Cy1 H-1a), 3.63 (m, 1H, Cy2 H-1a), 3.13 (m, 2H, H-2), 2.51 (t, J = 5.7 Hz, 2H, H-6), 2.39 (s, 3H, NCH_3), 2.28 (m, 2H, H-5), 2.03 (m, 2H, Cy1 H-2a,6a), 1.91 (m, 2H, Cy2 H-2a,6a), 1.78 (m, 2H, Cy1 H-3a,5a), 1.73 (m, 2H, Cy1 H-2b,6b), 1.69 (m, 2H, Cy2 H-3a,5a), 1.60 (m, 2H, Cy1,2 H-4a), 1.35 (m, 2H, Cy2 H-3b,5b), 1.27 (m, 2H, Cy1 H-3b,5b), 1.17 (m, 4H, Cy1,2 H-4b, Cy2 H-2b,6b). ^{13}C NMR (100 MHz, $CDCl_3$) δ 171.5 (C═O), 154.3 (NCON), 134.3 (C-3), 127.6 (C-4), 57.7 (Cy1 C-1), 54.1 (C-2), 50.9 (C-6), 49.6 (Cy2 C-1), 45.6 (NCH_3), 32.7 (Cy2 C-2,6), 30.9 (Cy1 C-2,6), 26.3 (Cy1 C-3,5), 25.54 (C-5), 25.47 (Cy1 C-4)*, 25.3 (Cy2 C-4)*, 24.7 (Cy2 C-3,5). ^{15}N NMR (41 MHz, $CDCl_3$) δ −350.7 (NCH_3). HRMS (ESI) calcd for $C_{20}H_{34}N_3O_2$ ($M + H^+$) 348.2646, found 348.2654. *indistinguishable.

Note: The initial intention of this reaction was the synthesis of **3b**, however, the *N*-acylurea was isolated under the given conditions. For the synthesis of **3k** the addition of diphenylmethanol can be omitted.

2-oxo-2-(6-oxo-5,6-dihydro-11*H*-benzo[*e*]pyrido[3,2-*b*][1,4]diazepin-11-yl)ethyl 1-methyl-1,2,5,6-tetrahydropyridine-3-carboxylate (3l). Arecaidine (19.6 mg, 0.139 mmol) was suspended in dry DMF (3 mL) and heated gently until almost everything dissolved. NaH (8.3 mg of a 60% dispersion, 0.208 mmol) was added and the mixture was stirred for 1 min. 11-(chloroacetyl)-5,11-dihydro-6*H*-pyrido[2,3-*b*][1,4]benzodiazepin-6-one (40.0 mg, 0.139 mmol) and NaI (20.8 mg, 0.139 mmol) was added and the mixture was heated to 70 °C for 1 h. DMF was evaporated *in vacuo*, the residue was suspended in DCM and filtered. The product was isolated from the filtrate by preparative TLC (DCM:MeOH = 12:1; R_f = 0.19–0.38) and appeared as white solid (6.9 mg, 13%).

^{1}H NMR (600 MHz, $CDCl_3$) δ 9.74 (brs, 1H, CONH), 8.31 (brs, 1H, Ar H-2), 7.96 (d, J = 7.7 Hz, 1H, Ar H-7), 7.63 (m, 2H, Ar H-9,10), 7.62 (dd, J = 7.9 Hz, J = 1.6 Hz, 1H, Ar H-4), 7.43 (m, 1H, Ar H-8), 7.33 (dd, J = 7.9 Hz, J = 4.8 Hz, 1H, Ar H-3), 6.88 (m, 1H, H-4), 5.02 (m, 1H, $COCH_2$), 4.71 (d, J = 12.5 Hz, 1H, $COCH_2$), 3.20 (d, J = 16.2 Hz, 1H, H-2), 3.02 (d, J = 16.2 Hz, 1H, H-2), 2.55 (m, 1H, H-6), 2.45 (m, 1H, H-6), 2.39 (s, 3H, NCH_3), 2.35 (m, 2H, H-5). ^{13}C NMR (151 MHz, $CDCl_3$) δ 167.6 (NHCO), 166.8 (NCO), 164.7 (COO), 145.6 (Ar C-11a), 145.3 (Ar C-2), 140.3 (Ar C-10a), 139.0 (C-4), 133.5 (Ar C-9), 131.5 (Ar C-7), 130.9 (Ar C-4a), 130.6 (Ar C-4), 128.4 (Ar C-8,10), 127.9 (C-3), 124.7 (Ar C-3), 62.8 (CH_2O), 52.9 (C-2), 50.7 (C-6), 45.6 (NCH_3), 26.5 (C-5).* HRMS (ESI) calcd for $C_{21}H_{21}N_4O_4$ ($M + H^+$) 393.1557, found 393.1563.

* one quaternary carbon (Ar C-6a) could not be found.

Methyl 1-(2-oxo-2-(6-oxo-5,6-dihydro-11*H*-benzo[*e*]pyrido[3,2-*b*][1,4]diazepin-11-yl)ethyl)-1,2,5,6-tetrahydropyridine-3-carboxylate (3m). Guvacoline (9.0 mg, 0.0638 mmol) was dissolved in dry ACN (3 mL) and $NaHCO_3$ (5.4 mg, 0.0638 mmol) and 11-(chloroacetyl)-5,11-dihydro-6*H*-pyrido[2,3-*b*][1,4]benzodiazepin-6-one (18.3 mg, 0.0638 mmol) were added. The reaction mixture was stirred for 20 min at 70 °C and for 60 h at 20 °C, filtered and purified by preparative TLC (EE; R_f = 0.16–0.32). The product was obtained as off-white solid (6.7 mg, 27%).

^{1}H NMR (400 MHz, $CDCl_3$) δ 9.60 (brs, 1H, CONH), 8.29 (brs, 1H, Ar H-2), 7.96 (m, 1H, Ar H-7), 7.64 (m, 2H, Ar H-9,10), 7.55 (dd, J = 7.9 Hz, J = 1.3 Hz, 1H, Ar H-4), 7.44 (m, 1H, Ar H-8), 7.28 (dd, J = 7.9 Hz, J = 4.7 Hz, 1H, Ar H-3), 6.87 (m, 1H, H-4), 3.66 (m, 1H, $COCH_2$), 3.63 (s, 3H, OCH_3), 3.40 (d, J = 15.0 Hz, 1H, $COCH_2$), 3.18 (m, 1H, H-2), 2.94 (m, 1H, H-2), 2.56 (m, 1H, H-6), 2.36 (m, 1H, H-6), 2.20 (m, 1H, H-5), 2.05 (m, 1H, H-5). ^{13}C NMR (151 MHz, $CDCl_3$) δ 169.6 (NHCO), 168.0 (NCO), 166.0 (COO), 147.2 (Ar C-11a), 144.9 (Ar C-2), 140.7 (Ar C-10a), 137.5 (C-4), 133.4 (Ar C-9), 131.3 (Ar C-7), 130.6 (Ar C-4a), 129.8 (Ar C-4), 128.7 (Ar C-6a), 128.5 (Ar C-10), 128.1 (Ar C-8), 123.9 (Ar C-3), 60.3 ($COCH_2$), 51.5 (OCH_3), 50.8 (C-2), 48.3 (C-6), 26.3 (C-5). HRMS (ESI) calcd for $C_{21}H_{21}N_4O_4$ ($M + H^+$) 393.1557, found 393.1565.

4-methylmorpholine-2-carbonitrile (4). A solution of 2-chloroacrylonitrile (1.37 mL, 17.1 mmol) in dry THF (3 mL) was added to a stirred solution of *N*-methylethanolamine (1.38 mL, 17.1 mmol) in dry THF (3 mL). After 40 min the solution was cooled to 0 °C and KO^{t}Bu (1.92 g, 17.1 mmol) was added in portions. The reaction mixture was stirred for 10 min on ice, before THF was removed under reduced pressure. The crude product was purified by Kugelrohr distillation to yield a colorless liquid (1.24 g, 57%).

^{1}H NMR (400 MHz, $CDCl_3$) δ 4.59 (m, 1H, H-2), 4.00 (m, 1H, H-6), 3.75 (m, 1H, H-6), 2.70 (m, 1H, H-3), 2.56 (m, 1H, H-5), 2.52 (m, 1H, H-3), 2.32 (m, 1H, H-5), 2.31 (s, 3H, NCH_3). ^{13}C NMR (151 MHz, $CDCl_3$) 117.1 (CN), 65.0 (C-6), 64.2 (C-2), 56.6 (C-3), 54.1 (C-5), 46.0 (NCH_3). HRMS (ESI) calcd for $C_6H_{11}N_2O$ ($M + H^+$) 127.0866, found 127.0869.

2-carboxy-4-methylmorpholin-4-ium bromide (5). 4 (1.24 g, 9.83 mmol) was refluxed in H_2O (6 mL) containing 48% aq. HBr

solution (6 mL) for 1.5 h. The reaction mixture was evaporated to dryness. The product was separated from NH_4Br by fractional crystallization from H_2O and drying in high vacuum at 50 °C. The product appeared as white crystals (1.68 g, 76%) suitable for single crystal X-ray crystallography.

^{1}H NMR (400 MHz, D_2O) 4.52 (m, 1H, H-2), 4.26 (m, 1H, H-6), 3.98 (m, 1H, H-3), 3.91 (m, 1H, H-6), 3.56 (m, 1H, H-5), 3.20 (m, 1H, H-5), 3.19 (m, 1H, H-3), 2.99 (s, 3H, NCH_3). ^{13}C NMR (151 MHz, D_2O) 171.1 (COOH), 72.8 (C-2), 64.3 (C-6), 54.3 (C-3), 53.1 (C-5), 44.2 (NCH_3). HRMS (ESI) calcd for $C_6H_{12}NO_3$ ($M + H^+$) 146.0812, found 146.0815.

***N*-benzhydryl-4-methylmorpholine-2-carboxamide (6). 4** (100 mg, 0.793 mmol) and diphenylmethanol (146 mg, 0.793 mmol) were stirred in formic acid (2 mL) at 90 °C for 5 days. The reaction mixture was cooled to 20 °C, poured on water (15 mL) and extracted with DCM (3x10 mL). The organic phases were combined, dried with Na_2SO_4 and half of the total volume was subjected to preparative TLC (EE, R_f = 0.04–0.13). The product appeared as off-white, crystalline solid (13 mg, 11%).

^{1}H NMR (400 MHz, $CDCl_3$) δ 7.33 (m, 4H, Ph H-3,5), 7.27 (m, 2H, Ph H-4), 7.23 (m, 4H, Ph H-2,6), 7.19 (brd, J = 8.5 Hz, 1H, CONH), 6.25 (d, J = 8.5 Hz, 1H, $CHPh_2$), 4.14 (dd, J = 10.7 Hz, J = 2.7 Hz, 1H, H-2), 3.94 (m, 1H, H-6), 3.75 (m, 1H, H-6), 3.24 (m, 1H, H-3), 2.71 (m, 1H, H-5), 2.34 (s, 3H, NCH_3), 2.17 (m, 1H, H-5), 2.01 (m, 1H, H-3). ^{13}C NMR (100 MHz, $CDCl_3$) δ 168.7 (CONH), 141.30 (Ph C-1), 141.28 (Ph C-1), 128.66 (Ph C-3,5), 128.64 (Ph C-3,5), 127.50 (Ph C-4), 127.44 (Ph C-2,6), 127.42 (Ph C-4), 127.26 (Ph C-2,6), 75.2 (C-2), 66.3 (C-6), 56.9 (C-3), 56.1 ($CHPh_2$), 54.2 (C-5), 45.8 (NCH_3). ^{15}N NMR (41 MHz, $CDCl_3$) δ −259.3 (CONH), −345.7 (NCH_3). HRMS (ESI) calcd for $C_{19}H_{23}N_2O_2$ ($M + H^+$) 311.1754, found 311.1759.

Benzhydryl 4-methylmorpholine-2-carboxylate (7). 5 (80.0 mg, 0.354 mmol) was suspended in dry DMF (3 mL) and heated gently until almost everything dissolved. CDI (86.1 mg, 0.531 mmol) was added as solid. After 30 min sodium diphenylmethanolate (2.2 mL of a 0.1 g/mL solution, 1.06 mmol) was added and the reaction mixture was stirred for 18 h at 20 °C. The reaction mixture was poured on water (30 mL) and extracted with EE (3x 15 mL). The organic phase was concentrated under reduced pressure and half of it was purified by preparative TLC (PE:EE = 1:1; R_f = 0.16–0.35). The product was obtained as colorless oil (13.0 mg, 24%).

^{1}H NMR (400 MHz, $CDCl_3$) δ 7.34 (m, 4H, Ph H-2,6), 7.33 (m, 4H, Ph H-3,5), 7.29 (m, 2H, Ph H-4), 6.98 (s, 1H, $CHPh_2$), 4.31 (dd, J = 8.9 Hz, J = 2.9 Hz, 1H, H-2), 4.03 (m, 1H, H-6), 3.70 (m, 1H, H-6), 2.95 (m, 1H, H-3), 2.55 (m, 1H, H-5), 2.34 (m, 1H, H-3), 2.31 (s, 3H, NCH_3), 2.26 (m, 1H, H-5). ^{13}C NMR (100 MHz, $CDCl_3$) δ 169.0 (C=O), 139.7 (Ph C-1), 139.6 (Ph C-1), 128.5 (Ph C-3,5), 128.03 (Ph C-4), 127.97 (Ph C-4), 127.2 (Ph C-2,6), 127.0 (Ph C-2,6), 77.3 ($CHPh_2$), 74.4 (C-2), 66.1 (C-6), 56.4 (C-3), 54.3 (C-5), 46.2 (NCH_3). ^{15}N NMR (41 MHz, $CDCl_3$) δ −347.2 (NCH_3). HRMS (ESI) calcd for $C_{19}H_{22}NO_3$ ($M + H^+$) 312.1594, found 312.1589.

1-(4-methylmorpholin-2-yl)-2-phenylethan-1-one (8). Mg turnings (116 mg, 4.76 mmol) were stirred in dry Et_2O (2 mL) and activated with $BrCH_2CH_2Br$ (two drops). Benzyl chloride (602 mg, 4.76 mmol) in dry Et_2O (3 mL) was added dropwise at 20 °C and the reaction mixture was stirred for 30 min. **4** (200 mg, 1.59 mmol) in Et_2O (3 mL) was added dropwise at 0 °C and the reaction mixture was stirred at room temperature for 1.5 h. The reaction was quenched with 1M aq. HCl (4 mL) and subsequently NaOH (0.5 g) was added. The resulting suspension was extracted with Et_2O (3x 10 mL) and combined organic phases were dried with Na_2SO_4 and evaporated. One third of the crude product was purified by preparative TLC (DCM:MeOH = 30:1; R_f = 0.22–0.61), yielding a yellowish oil (14 mg, 12%).

^{1}H NMR (400 MHz, $CDCl_3$) δ 7.31 (m, 2H, Ph H-3,5), 7.25 (m, 1H, Ph H-4), 7.20 (m, 2H, Ph H-2,6), 4.07 (dd, J = 10.3 Hz, J = 2.8 Hz, 1H, H-2), 3.99 (m, 1H, H-6), 3.92 (d, J = 16.0 Hz, 1H, CH_2Ph), 3.87 (d, J = 16.0 Hz, 1H, CH_2Ph), 3.70 (m, 1H, H-6), 2.95 (m, 1H, H-3), 2.63 (m, 1H, H-5), 2.29 (s, 3H, NCH_3), 2.14 (m, 1H, H-5), 1.94 (m, 1H, H-3). ^{13}C NMR (100 MHz, $CDCl_3$) δ 206.6 (C=O), 133.6 (Ph C-1), 129.7 (Ph C-2,6), 128.5 (Ph C-3,5), 126.9 (Ph C-4), 80.1 (C-2), 66.7 (C-6), 56.0 (C-3), 54.5 (C-5), 46.2 (NCH_3), 45.2 (CH_2Ph). ^{15}N NMR (41 MHz, $CDCl_3$) δ −346.8 (NCH_3). HRMS (ESI) calcd for $C_{13}H_{18}NO_2$ ($M + H^+$) 220.1332, found 220.1337.

4.4. M1–M5 affinity determination

Membranes containing human M1, M2, M3, M4 or M5 receptors and CHO-K1 wild type membranes were prepared from the respective cell line according to a protocol adapted from Klotz et al. [48] Cells were grown to confluence in T175 flasks for membrane preparation. The medium was removed and the cell layer was washed with ice-cold PBS and suspended with a cell scraper in 2 mL/flask 10 mM Tris/HCl, 1 mM EDTA-buffer (pH 7.4) and 200 μL/flask of protease inhibitor. Cells were disrupted by passing the suspension through a G29 needle and the resulting homogenate was centrifuged (10 min, 1000×*g*, 4 °C). The supernatant was again centrifuged (30 min, 100,000 g, 4 °C) and the resulting membrane pellet was suspended in 125 μL/flask 50 mM Tris/HCl-buffer (pH 7.4) and stored at −80 °C. In one batch typically ten T175 flasks were processed to membranes. The protein concentration of the membrane suspension was assessed with a photometric BCA assay and ranged from approx. 500–3000 μg/mL.

Stock solutions of compounds for affinity testing were prepared in DMSO and 50 mM Tris/HCl, 10 mM $MgCl_2$, 1 mM EDTA (pH 7.4) was used as assay buffer. The radioligand binding assay was performed in PP test tubes by mixing 5 μL of test compound in DMSO, 50 μL of [*N*-methyl-^{3}H]scopolamine methyl chloride in assay buffer and 445 μL of membrane suspension in assay buffer. 5 μL of 1 μM scopolamine was used instead of test compound to measure the nonspecific binding and 5 μL DMSO were used to assess the maximum binding potential. Effective concentrations of radioligand were 0.2 nM, 0.3 nM, 0.8 nM, 0.2 nM, 1 nM for M1–M5 and 4–30 μg membrane were used per tube. After 1.5 h incubation at 23 °C the membrane bound radioactivity was recovered by filtration through GF/B glass fibre filters pre-soaked in 0.1% PEI and measured in a β-counter.

At least five distinct concentrations of test compound (each pipetted in triplicate) were used to calculate the IC_{50} by a variable slope logistic regression in GraphPad Prism®. Inhibition constants (K_i) were calculated with the Cheng-Prusoff equation, with radioligand K_D values of 0.18 nM, 0.24 nM, 0.23 nM, 0.10 nM and 0.35 nM for M1–M5 as determined in the Supporting Information (Table S1). Results are given as average of at least three independent experiments.

4.5. EeAChE affinity and metabolism

Ellman's assay was performed according to a modified protocol from literature [30]. Briefly, 5 μL sample solution were pipetted in two columns of a flat bottom 96-well-plate and in the first two rows 5 μL water was used as a blank. Then 200 μL of the enzyme solution (0.0682 μg/mL) were added column after column. After 4 min, 48.8 μL of DTNB (0.5 mM) was added. After another minute for each row 48.8 μL of a different concentration of ATI (3 mM, 1.5 mM, 0.75 mM, 0.375 mM or 0.188 mM) was added. After 2 min the plate was placed in the photometric microplate reader, where the absorbance was measured in 10 s intervals for 10 min at 405 nm. For each sample concentration reciprocal ATI concentrations were plotted against the reciprocal slope of the kinetic

measurement (sec/OD) and the resulting slope was plotted against the sample concentrations. The K_i was determined as the negative abscissa intercept of this plot. Graphs are depicted in the Supporting Information, Fig. S6. Every sample was tested in three independent experiments. Sample solutions were prepared by prediluting 10 mM DMSO stock solutions of arecoline, **3b**–**m**, **6**–**8** and tacrine 1:10 in water to suppress the AChE inhibitory effect of DMSO [49].

To study the EeAChE metabolism a solution containing the same concentration of the sample and the enzyme as used in the Ellman's Assay was prepared and incubated at 20 °C for 10 min and 60 min. For the blank water was used instead of enzyme solution. At the given timepoints the solution was quenched with ACN:MeOH = 1:1 and analyzed by RP-HPLC. The sample peak area of the enzyme-containing solution and the blank was compared using a multiple comparisons 2way ANOVA.

4.6. Ligand docking

Ligand docking was performed in LigandScout 4.4_RC6 with a crystal structure of a human M1 mAChR bound to tiotropium [5] using AutoDock 4.2 with default settings. Protonated **3c** and tiotropium were docked to the orthosteric binding site and pharmacophores were generated to compare their interaction with the environment. **3c** features a calculated pKa of 7.99 (MarvinSketch 17.24) and therefore was docked in its protonated form to account for the expected higher abundance of this species under physiological conditions. The used sequence of crystal structure of the M1 receptor features also a small second chain. Mentioned residue numbers are suffixed with 'A' in order to be unambiguous and to stick with the PDB nomenclature.

4.7. Radiochemistry

For small scale reactions [^{11}C]CH_3I was trapped in 1.7 mL solvent. 200 μL of this solution were added to 1 mg of precursor in 200 μL solvent, whereat different solvents, reaction time and temperature were tested. The reaction mixture was quenched with 100 μL H_2O and analyzed with radio-HPLC. The non-isolated radiochemical yield [36] was determined by dividing the AUC of the product by the total AUC.

For automated syntheses [^{11}C]CH_3I was trapped in a reaction vessel containing 1 mg of precursor dissolved in 0.5 mL DMSO. The reaction mixture was heated to 80 °C for 2 min, cooled to 25 °C, quenched with 1 mL HPLC eluent and purified by preparative HPLC (conditions summarized in Table 7). The product fraction was collected in a stirred bulb containing 100 mL water. A solid phase extraction cartridge was used to isolate the product from the predominantly aqueous solution. The immobilized product was washed with 10 mL water, eluted with 1.5 mL ethanol and collected in a glass vial containing 6 mL sterile PBS. Subsequently, the cartridge was furthermore rinsed with 5 mL 0.9% NaCl solution to recover small amounts of remaining product.

4.8. Metabolic stability

15 μL microsomes were preincubated in 257 μL PBS, 15 μL solution A and 3 μL solution B by gently shaking at 37 °C for 10 min. 10 μL of tracer solution was added and 50 μL samples were taken at 0, 10, 20, 40 and 60 min. The samples were immediately quenched wit 50 μL ACN:MeOH = 1:1, centrifuged at 21,500 g for 5 min and 50 μL of the supernatant was analyzed with radio-HPLC. Peak areas of appearing radiometabolites were decay corrected for their retention times and related to the total peak area.

For metabolite identification a solution of **3b** in EtOH (10 mg/mL) was used instead of tracer solution. 50 mM NH_4Ac pH 9.3 was used as mobile phase to allow for HRMS measurement of the collected fraction.

4.9. Serum protein binding

5–20 μL tracer solution (depending on the activity concentration) was incubated with 1 mL human serum or 1 mL PBS for 50 min at 23 °C. Afterwards, 200 μL of the resulting mixture was pipetted on a filter and the total activity was measured prior filtration. Free tracer was separated from protein-bound tracer by ultrafiltration of 200 μL in Centrifree (2100 g, 50 min) or Microcon (14,000 g, 40 min) filters. The amount of free tracer was determined from a measurement of a defined volume of the filtrate (usually 100 μL), which is corrected for time and to the theoretical total volume of 200 μL. The given ff% is corrected for nonspecific binding determined from the PBS measurement. Ultrafiltration of serum was performed in technical triplicates.

4.10. Kinetic studies using LigandTracer

Briefly, the LigandTracer system consists of a tilted, slowly rotating petridish containing medium with radioligand and locally seeded target cells. A radiodetector mounted above the upper part of the tilted dish measures the cell bound activity with every revolution and thus can follow the interaction kinetics between radioligand and cells in real-time.

One day before the experiment 1×10^6 CHO-M1 cells were suspended in a volume of 1 mL medium and pipetted on an area of 1 cm^2 close to the edge of a petri dish. The cells were allowed to attach in the incubator overnight. 20 min prior to the measurement the medium was replaced with 3 mL FBS-free medium. The petri dish was placed on the LigandTracer device and a baseline measurement was started. In case of a preblocking experiment, this medium contained 10 μM scopolamine. The run was paused and carbon-11 labeled product solution was added *via* micropipette to reach the desired concentration and the run was continued until equilibrium was reached (detection time: 5 s, detection delay time: 0 s). A single petri dish was used to follow the interaction at up to three concentrations.

Table 7
Separation conditions for semi-preparative HPLC during radiosynthesis.

Cpd.	Column	Eluent	Flow [mL/min]	$k_{prec.}$	$k_{prod.}$
3a	Supelcosil™ LC-ABZb, 5 μm, 250 × 10 mm	15% ACN, 85% pH 9.3	5.0	3.25	4.88
3j	Supelcosil™ LC-ABZb, 5 μm, 250 × 10 mm	20% ACN, 80% pH 9.3	5.0	1.70	2.37
3b	Supelcosil™ LC-ABZb, 5 μm, 250 × 10 mm	50% ACN, 50% pH 9.3	5.0	2.63	4.60
3c	Supelcosil™ LC-ABZb, 5 μm, 250 × 10 mm	50% ACN, 50% pH 9.3	7.5	3.12	4.60
3i	Nucleodur PolarTec, 5 μm, 250 × 10 mm	45% ACN, 55% pH 9.3	5.0	2.60	3.92
3k	ProntoSIL 120C18 ace-EPS, 5 μm, 250 × 10 mm	60% ACN, 40% pH 6.8	5.0	1.75	3.33

4.11. Direct radioligand binding assay using [^{11}C]3c

One day before the experiment CHO-M1 cells and wild type CHO cells were seeded to six-well plates (2.5×10^5 cells per well). The medium was removed and the cells were incubated with 0.3 nM, 3 nM or 30 nM [^{11}C]**3c** in FBS free medium containing 10 μM scopolamine, 10 μM pirenzepine or no competitor for 20 min at 20 °C. For the experiment at ≤ 4 °C the sixwell plates were put on ice 15 min prior to and during the incubation and the used incubation solutions were put on ice previously. The supernatant was removed and the cells were quickly washed with 3 mL icecold PBS. Cells were detached by shaking them for 10 min with 0.5 mL trypsin at 20 °C. The cell suspensions were transferred to PP test tubes and each well was rinsed with 1 mL medium. The tubes were measured in a gamma counter for 30 s. The resulting count rate of the cell bound activity was corrected for decay and normalized to the incubation without competitor for each concentration. The experiment was performed in technical triplicates.

4.12. In vitro autoradiography

Autoradiography was performed on sagittal mouse brain sections of two different individuals using [^{11}C]**3c** and [^{11}C]pirenzepine as a reference according to a previously published protocol described for [^{3}H]pirenzepine [50]. In brief, thawed and dried *cryo*-sections were pre-incubated in 50 mM KH_2PO_4 buffer (pH 7.4) following radioligand incubation for 40 min using the same buffer at 20 °C. Radioligand concentration was chosen with respect to affinity and molar activity (15 nM [^{11}C]pirenzepine; 3 nM and 30 nM [^{11}C]**3c**). Vicinal sections were co-incubated using 10 μM scopolamine or atropine as blocking agents. To remove unbound radioligand, sections were washed twice in ice-cold assay buffer for 5 min and dipped in ice-cold water. Dry sections were exposed to a phosphor screen in a lightproof cassette overnight. Stored radioactivity was read-out using a Cyclone Phosphor Imager and digital autoradiograms were generated using OptiQuant Software (PerkinElmer).

4.13. Statistical analysis

All experiments were performed in at least three repetitions and values were expressed as mean ± standard deviation, if not stated otherwise. Statistical tests were performed with GraphPadPrism 6.

Author contributions

M.O. and V.P. designed the research concept, performed syntheses and compound characterization, performed preclinical experiments and analyzed the respective data and prepared the manuscript. K.P. performed preclinical experiments, analyzed data and proofread the manuscript. T.B. and C.V. designed and performed preclinical experiments, analyzed data and contributed to the manuscript. A.R. performed and analyzed X-ray experiments and contributed to manuscript preparation. W.H. performed and analyzed NMR experiments and proofread the manuscript. H.S. contributed to compound design and syntheses concept and proofread the manuscript. M.M., W.W. and M.H. contributed to the overall research concept and preparation of the manuscript. All authors have given approval to the final version of the manuscript.

Funding

Funding was provided by the Medical University of Vienna and University of Vienna.

Declaration of competing interest

The authors declare that they have no known competing financial interests or personal relationships that could have appeared to influence the work reported in this paper.

Acknowledgment

Our gratitude goes to Katharina Pallitsch and Prof. Ernst Urban for recording 600 MHz and 500 MHz NMR spectra as well as to Daniel Dobusch for performing the HRMS measurements. We thank Prof. Thierry Langer for providing LigandScout. This work was supported by the Medical Imaging Cluster (MIC). We are grateful for the technical support of Thomas Zenz and Andreas Krcal.

Appendix A. Supplementary data

Supplementary data to this article can be found online at https://doi.org/10.1016/j.ejmech.2020.112623.

References

[1] A.C. Kruse, B.K. Kobilka, D. Gautam, P.M. Sexton, A. Christopoulos, J. Wess, Muscarinic acetylcholine receptors: novel opportunities for drug development, Nat. Rev. Drug Discov. 13 (2014) 549–560, https://doi.org/10.1038/nrd4295.
[2] D. Dencker, M. Thomsen, G. Wörtwein, P. Weikop, Y. Cui, J. Jeon, J. Wess, A. Fink-Jensen, Muscarinic acetylcholine receptor subtypes as potential drug targets for the treatment of schizophrenia, drug abuse and Parkinson's disease, ACS Chem. Neurosci. 3 (2012) 80–89, https://doi.org/10.1021/cn200110q.
[3] P. Abrams, K.-E. Andersson, J.J. Buccafusco, C. Chapple, W.C. de Groat, A.D. Fryer, G. Kay, A. Laties, N.M. Nathanson, P.J. Pasricha, A.J. Wein, Muscarinic receptors: their distribution and function in body systems, and the implications for treating overactive bladder, Br. J. Pharmacol. 148 (2006) 565–578, https://doi.org/10.1038/sj.bjp.0706780.
[4] W.A.C. Burger, P.M. Sexton, A. Christopoulos, D.M. Thal, Toward an understanding of the structural basis of allostery in muscarinic acetylcholine receptors, J. Gen. Physiol. (2018), https://doi.org/10.1085/jgp.201711979 jgp.201711979.
[5] D.M. Thal, B. Sun, D. Feng, V. Nawaratne, K. Leach, C.C. Felder, M.G. Bures, D.A. Evans, W.I. Weis, P. Bachhawat, T.S. Kobilka, P.M. Sexton, B.K. Kobilka, A. Christopoulos, Crystal structures of the M1 and M4 muscarinic acetylcholine receptors, Nature 531 (2016) 335–340, https://doi.org/10.1038/nature17188.
[6] P. Angeli, Trends in Receptor Research: Proceedings of the 8th Camerino-Noordwijkerhout Symposium, Camerino, Italy, 8-12 September 1991, Elsevier Science, Amsterdam, 2014. http://qut.eblib.com.au/patron/FullRecord.aspx?p=1837800. (Accessed 10 May 2019).
[7] S.E. Yohn, P.J. Conn, Positive allosteric modulation of M 1 and M 4 muscarinic receptors as potential therapeutic treatments for schizophrenia, Neuropharmacology 136 (2018) 438–448, https://doi.org/10.1016/j.neuropharm.2017.09.012.
[8] R.L. Papke, N.A. Horenstein, C. Stokes, Nicotinic activity of arecoline, the psychoactive element of "betel nuts", suggests a basis for habitual use and anti-inflammatory activity, PloS One 10 (2015), https://doi.org/10.1371/journal.pone.0140907.
[9] G.Z. Dong, K. Kameyama, A. Rinken, T. Haga, Ligand binding properties of muscarinic acetylcholine receptor subtypes (m1-m5) expressed in baculovirus-infected insect cells, J. Pharmacol. Exp. Therapeut. 274 (1995) 378–384.
[10] W.C. Eckelman, Imaging of muscarinic receptors in the central nervous system, Curr. Pharmaceut. Des. 12 (2006) 3901–3913.
[11] C.C. Felder, F.P. Bymaster, J. Ward, N. DeLapp, Therapeutic opportunities for muscarinic receptors in the central nervous system, J. Med. Chem. 43 (2000) 4333–4353, https://doi.org/10.1021/jm990607u.
[12] M. Wolf-Pflugmann, G. Lambrecht, J. Wess, E. Mutschler, Synthesis and muscarinic activity of a series of tertiary and quaternary N-substituted guvacine esters structurally related to arecoline and arecaidine propargyl ester, Arzneimittelforschung 39 (1989) 539–544.
[13] S. Giri, J.R. Idle, C. Chen, T.M. Zabriskie, K.W. Krausz, F.J. Gonzalez, A metabolomic approach to the metabolism of the Areca nut alkaloids arecoline and aracaidine in the mouse, Chem. Res. Toxicol. 19 (2006) 818–827, https://doi.org/10.1021/tx0600402.
[14] R. Quirion, Cholinergic markers in Alzheimer disease and the autoregulation of acetylcholine release, J. Psychiatry Neurosci. JPN. 18 (1993) 226–234.
[15] W.C. Eckelman, M.R. Kilbourn, C.A. Mathis, Discussion of targeting proteins

in vivo: in vitro guidelines, Nucl. Med. Biol. 33 (2006) 449–451, https://doi.org/10.1016/j.nucmedbio.2006.03.008.
[16] K.A. Frey, R.A. Koeppe, G.K. Mulholland, D. Jewett, R. Hichwa, R.L.E. Ehrenkaufer, J.E. Carey, D.M. Wieland, D.E. Kuhl, B.W. Agranoff, In vivo muscarinic cholingeric receptor imaging in human brain with [11C]scopolamine and positron emission tomography, J. Cerebr. Blood Flow Metabol. 12 (1992) 147–154, https://doi.org/10.1038/jcbfm.1992.18.
[17] S.L. Dewey, R.R. Macgregor, J.D. Brodie, B. Bendriem, P.T. King, N.D. Volkow, D.J. Schlyer, J.S. Fowler, A.P. Wolf, S.J. Gatley, R. Hitzemann, Mapping muscarinic receptors in human and baboon brain using [N-11C-methyl]-benztropine, Synapse 5 (1990) 213–223, https://doi.org/10.1002/syn.890050307.
[18] K. Ridler, V. Cunningham, M. Huiban, L. Martarello, S. Pampols-Maso, J. Passchier, R.N. Gunn, G. Searle, A. Abi-Dargham, M. Slifstein, J. Watson, M. Laruelle, E.A. Rabiner, An evaluation of the brain distribution of [11 C] GSK1034702, a muscarinic-1 (M 1) positive allosteric modulator in the living human brain using positron emission tomography, EJNMMI Res. 4 (2014) 66, https://doi.org/10.1186/s13550-014-0066-y.
[19] J. Malmquist, K. Varnäs, M. Svedberg, F. Vallée, J.S. Albert, S.J. Finnema, M. Schou, Discovery of a novel muscarinic receptor PET radioligand with rapid kinetics in the monkey brain, ACS Chem. Neurosci. (2017), https://doi.org/10.1021/acschemneuro.7b00340.
[20] H.J.C. Buiter, J.E. Leysen, R.C. Schuit, A. Fisher, A.A. Lammertsma, A.D. Windhorst, Radiosynthesis and biological evaluation of the M1 muscarinic acetylcholine receptor agonist ligand [11C]AF150(S), J. Label. Compd. Radiopharm. 55 (2012) 264–273, https://doi.org/10.1002/jlcr.2932.
[21] P. Seeman, B. Madras, Imaging of the Human Brain in Health and Disease, Elsevier, 2013.
[22] X. Deng, A. Hatori, Z. Chen, K. Kumata, T. Shao, X. Zhang, T. Yamasaki, K. Hu, Q. Yu, L. Ma, G. Wang, L. Wang, Y. Shao, L. Josephson, S. Sun, M. Zhang, S. Liang, Synthesis and preliminary evaluation of ^{11} C-labeled VU0467485/AZ13713945 and its analogues for imaging muscarinic acetylcholine receptor subtype 4, ChemMedChem 14 (2019) 303–309, https://doi.org/10.1002/cmdc.201800710.
[23] N.B. Nabulsi, D. Holden, M.-Q. Zheng, F. Bois, S.-F. Lin, S. Najafzadeh, H. Gao, J. Ropchan, T. Lara-Jaime, D. Labaree, A. Shirali, L. Slieker, C. Jesudason, V. Barth, A. Navarro, N. Kant, R.E. Carson, Y. Huang, Evaluation of ^{11} C-LSN3172176 as a novel PET tracer for imaging M $_1$ muscarinic acetylcholine receptors in nonhuman primates, J. Nucl. Med. 60 (2019) 1147–1153, https://doi.org/10.2967/jnumed.118.222034.
[24] G.C. Gullickson, D.E. Lewis, Synthesis of N -benzhydrylamides from nitriles by Ritter reactions in formic acid, Synthesis (2003) 681–684, https://doi.org/10.1055/s-2003-38069.
[25] M.E. Kopach, U.K. Singh, M.E. Kobierski, W.G. Trankle, M.M. Murray, M.A. Pietz, M.B. Forst, G.A. Stephenson, V. Mancuso, T. Giard, M. Vanmarsenille, T. DeFrance, Practical synthesis of chiral 2-morpholine: (4-benzylmorpholin-2-(*S*)-yl)-(tetrahydropyran-4-yl)methanone mesylate, a useful pharmaceutical intermediate, Org. Process Res. Dev. 13 (2009) 209–224, https://doi.org/10.1021/op800247w.
[26] E.P. Lebois, C. Thorn, J.R. Edgerton, M. Popiolek, S. Xi, Muscarinic receptor subtype distribution in the central nervous system and relevance to aging and Alzheimer's disease, Neuropharmacology 136 (2018) 362–373, https://doi.org/10.1016/j.neuropharm.2017.11.018.
[27] D.O. Kiesewetter, J. Lee, L. Lang, S.G. Park, C.H. Paik, W.C. Eckelman, Preparation of 18F-labeled muscarinic agonist with M2 selectivity, J. Med. Chem. 38 (1995) 5–8, https://doi.org/10.1021/jm00001a002.
[28] L. Ravasi, D.O. Kiesewetter, K. Shimoji, G. Lucignani, W.C. Eckelman, Why does the agonist [18F]FP-TZTP bind preferentially to the M2 muscarinic receptor? Eur. J. Nucl. Med. Mol. Imag. 33 (2006) 292–300, https://doi.org/10.1007/s00259-005-1966-x.
[29] J. Luo, S. Chen, S. Min, L. Peng, Reevaluation and update on efficacy and safety of neostigmine for reversal of neuromuscular blockade, Therapeut. Clin. Risk Manag. 14 (2018) 2397–2406, https://doi.org/10.2147/TCRM.S179420.
[30] F.H. Darras, Y.-P. Pang, On the use of the experimentally determined enzyme inhibition constant as a measure of absolute binding affinity, BioRxiv, https://doi.org/10.1101/144204, 2017.
[31] C. Vraka, L. Nics, K.-H. Wagner, M. Hacker, W. Wadsak, M. Mitterhauser, Log P , a yesterday's value? Nucl. Med. Biol. 50 (2017) 1–10, https://doi.org/10.1016/j.nucmedbio.2017.03.003.
[32] M.R. Kilbourn, P.J.H. Scott, Is logP truly dead? Nucl. Med. Biol. 54 (2017) 41–42, https://doi.org/10.1016/j.nucmedbio.2017.08.006.
[33] C. Vraka, M. Mitterhauser, Reconsider logP!, Nucl. Med. Biol. 54 (2017) 42, https://doi.org/10.1016/j.nucmedbio.2017.08.007.
[34] H. Pajouhesh, G.R. Lenz, Medicinal chemical properties of successful central nervous system drugs, NeuroRx 2 (2005) 541–553, https://doi.org/10.1602/neurorx.2.4.541.
[35] P. Champagne, J. Desroches, J.-F. Paquin, Organic fluorine as a hydrogen-bond acceptor: recent examples and applications, Synthesis 47 (2014) 306–322, https://doi.org/10.1055/s-0034-1379537.
[36] H.H. Coenen, A.D. Gee, M. Adam, G. Antoni, C.S. Cutler, Y. Fujibayashi, J.M. Jeong, R.H. Mach, T.L. Mindt, V.W. Pike, A.D. Windhorst, Consensus nomenclature rules for radiopharmaceutical chemistry — setting the record straight, Nucl. Med. Biol. 55 (2017) v–xi, https://doi.org/10.1016/j.nucmedbio.2017.09.004.
[37] European directorate for the quality of medicines (EDQM), general monograph 0125 - radiopharmaceutical preperations, in: Eur. Pharmacopoeia, Council of Europe, Strasbourg, 2016.
[38] D. Lodge, G.A.R. Johnston, D.R. Curtis, S.J. Brand, Effects of the Areca nut constituents arecaidine and guvacine on the action of GABA in the cat central nervous system, Brain Res. 136 (1977) 513–522, https://doi.org/10.1016/0006-8993(77)90075-0.
[39] C. Vraka, S. Mijailovic, V. Fröhlich, M. Zeilinger, E.-M. Klebermass, W. Wadsak, K.-H. Wagner, M. Hacker, M. Mitterhauser, Expanding LogP: present possibilities, Nucl. Med. Biol. 58 (2018) 20–32, https://doi.org/10.1016/j.nucmedbio.2017.11.007.
[40] S. Göschl, H.P. Varbanov, S. Theiner, M.A. Jakupec, M. Galanski, B.K. Keppler, The role of the equatorial ligands for the redox behavior, mode of cellular accumulation and cytotoxicity of platinum(IV) prodrugs, J. Inorg. Biochem. 160 (2016) 264–274, https://doi.org/10.1016/j.jinorgbio.2016.03.005.
[41] G.C. Van de Bittner, E.L. Ricq, J.M. Hooker, A philosophy for CNS radiotracer design, Acc. Chem. Res. 47 (2014) 3127–3134, https://doi.org/10.1021/ar500233s.
[42] I.A.I. Ali, E.S.H.E. Ashry, R.R. Schmidt, Protection of hydroxy groups with diphenylmethyl and 9-fluorenyl trichloroacetimidates– effect on anomeric stereocontrol, Eur. J. Org Chem. 2003 (2003) 4121–4131, https://doi.org/10.1002/ejoc.200300323.
[43] M. Pawlicki, L. Latos-Grażyński, L. Szterenberg, 5,10,15-Triaryl-21,23-dioxacorrole and its isomer with a protruding furan ring, J. Org. Chem. 67 (2002) 5644–5653, https://doi.org/10.1021/jo025773f.
[44] S. Song, S.-F. Zhu, L.-Y. Pu, Q.-L. Zhou, Iridium-catalyzed enantioselective hydrogenation of unsaturated heterocyclic acids, Angew. Chem. 125 (2013) 6188–6191, https://doi.org/10.1002/ange.201301341.
[45] J.B. Baell, G.A. Holloway, New substructure filters for removal of pan assay interference Compounds (PAINS) from screening libraries and for their exclusion in bioassays, J. Med. Chem. 53 (2010) 2719–2740, https://doi.org/10.1021/jm901137j.
[46] ICH Harmonised Tripartite Guideline, Validation of Analytical Procedures: Text and Methodology Q2(R1), 1996.
[47] C. Rami-Mark, N. Berroterán-Infante, C. Philippe, S. Foltin, C. Vraka, A. Hoepping, R. Lanzenberger, M. Hacker, M. Mitterhauser, W. Wadsak, Radiosynthesis and first preclinical evaluation of the novel norepinephrine transporter pet-ligand [11C]ME@HAPTHI, EJNMMI Res. 5 (2015) 34, https://doi.org/10.1186/s13550-015-0113-3.
[48] K.N. Klotz, J. Hessling, J. Hegler, C. Owman, B. Kull, B.B. Fredholm, M.J. Lohse, Comparative pharmacology of human adenosine receptor subtypes - characterization of stably transfected receptors in CHO cells, Naunyn, Schmiedebergs Arch. Pharmacol. 357 (1998) 1–9.
[49] A. Kumar, T. Darreh-Shori, DMSO: a mixed-competitive inhibitor of human acetylcholinesterase, ACS Chem. Neurosci. 8 (2017) 2618–2625, https://doi.org/10.1021/acschemneuro.7b00344.
[50] P. Valuskova, V. Farar, S. Forczek, I. Krizova, J. Myslivecek, Autoradiography of 3H-pirenzepine and 3H-AFDX-384 in mouse brain regions: possible insights into M1, M2, and M4 muscarinic receptors distribution, Front. Pharmacol. 9 (2018) 124, https://doi.org/10.3389/fphar.2018.00124.

3.2. Synthesis, biological and computational evaluation of antagonistic, chiral hydrobenzoin esters of arecaidine targeting mAChR M1

Marius Ozenil,[1] Jonas Aronow,[1] Daniela Piljak,[1] Chrysoula Vraka,[1] Wolfgang Holzer,[2] Helmut Spreitzer,[2] Wolfgang Wadsak,[1,3] Marcus Hacker,[1] Verena Pichler[2]

[1] Department of Biomedical Imaging and Image-guided Therapy, Division of Nuclear Medicine, Medical University of Vienna, Austria
[2] Department of Pharmaceutical Chemistry, Faculty of Life Sciences, University of Vienna, Austria
[3] CBmed GmbH - Center for Biomarker Research in Medicine, Graz, Austria

The doctoral candidate synthesized novel arecoline derivatives, performed their biological and computational evaluation and largely wrote the manuscript.

pharmaceuticals

MDPI

Article

Synthesis, Biological, and Computational Evaluation of Antagonistic, Chiral Hydrobenzoin Esters of Arecaidine Targeting mAChR M1

Marius Ozenil [1], Jonas Aronow [1], Daniela Piljak [1], Chrysoula Vraka [1], Wolfgang Holzer [2], Helmut Spreitzer [2], Wolfgang Wadsak [1,3], Marcus Hacker [1] and Verena Pichler [2,*]

1 Department of Biomedical Imaging and Image-guided Therapy, Division of Nuclear Medicine, Medical University of Vienna, 1090 Vienna, Austria; marius.ozenil@meduniwien.ac.at (M.O.); jonas.aronow@meduniwien.ac.at (J.A.); daniela.piljak@gmx.at (D.P.); chrysoula.vraka@meduniwien.ac.at (C.V.); wolfgang.wadsak@meduniwien.ac.at (W.W.); marcus.hacker@meduniwien.ac.at (M.H.)

2 Department of Pharmaceutical Chemistry, Faculty of Life Sciences, University of Vienna, 1090 Vienna, Austria; wolfgang.holzer@univie.ac.at (W.H.); helmut.spreitzer@univie.ac.at (H.S.)

3 CBmed GmbH—Center for Biomarker Research in Medicine, 8036 Graz, Austria

* Correspondence: verena.pichler@univie.ac.at; Tel.: +43-1-4277-55624

Received: 11 November 2020; Accepted: 27 November 2020; Published: 30 November 2020



Abstract: Muscarinic acetylcholine receptors (mAChRs) are a pivotal constituent of the central and peripheral nervous system. Yet, therapeutic and diagnostic applications thereof are hampered by the lack of subtype selective ligands. Within this work, we synthesized and chemically characterized three different stereoisomers of hydrobenzoin esters of arecaidine by NMR, HR-MS, chiral chromatography, and HPLC-logP. All compounds are structurally eligible for carbon-11 labeling and show appropriate stability in Dulbecco's phosphate-buffered saline (DPBS) and F12 cell culture medium. A competitive radioligand binding assay on Chinese hamster ovary cell membranes comprising the human mAChR subtypes M1-M5 showed the highest orthosteric binding affinity for subtype M1 and a strong influence of stereochemistry on binding affinity, which corresponds to in silico molecular docking experiments. K_i values toward M1 were determined as 99 ± 19 nM, 800 ± 200 nM, and 380 ± 90 nM for the (*R*,*R*)-, (*S*,*S*)-, and racemic (*R*,*S*)-stereoisomer, respectively, highlighting the importance of stereochemical variations in mAChR ligand development. All three stereoisomers were shown to act as antagonists toward mAChR M1 using a Fluo-4 calcium efflux assay. With respect to future positron emission tomography (PET) tracer development, the (*R*,*R*)-isomer appears especially promising as a lead structure due to its highest subtype selectivity and lowest K_i value.

Keywords: muscarinic; drug development; subtype selectivity

1. Introduction

Muscarinic acetylcholine receptors (mAChRs) are G protein-coupled receptors, which are strongly involved in the parasympathetic nervous system's signal transduction. mAChRs appear as five subtypes, which differ in their expression pattern and downstream signaling [1]. However, their conserved orthosteric binding units hamper subtype selective molecular targeting [2]. Current anticholinergic drugs with market approval are mainly antagonists or inverse agonists [3]. Regarding therapeutic applications, mAChR agonists are in clinical use for the treatment of glaucoma [4], Sjögren's syndrome [4], and underactive bladder [5]. mAChR agonists have also been proposed as promising drugs for the treatment of Alzheimer's disease symptoms, hitherto, no compound passed clinical trial phase 3 [6]. Several mAChR antagonists targeting primarily the M1 subtype are used in

medicine mainly for the treatment of Parkinson's disease [7] and peptic ulcers [8]. However, the clinical applicability of mAChR agonists and antagonists is often restrained by side effects related to the activation or inhibition of other mAChR subtypes [7]. Considering the insufficient penetration of the blood–brain barrier as well as unsuitable pharmacokinetics and -dynamics in treatment regimens of e.g., Parkinson's disease, these drugs often merely have peripheral effects on disease symptoms. Hence, as they do not act on the disease origin [9], they do not have the ability to alter disease progression. Therefore, clinical management is solely based on symptomatic treatment.

The pivotal role of mAChRs in human physiology and their involvement in neuropathogenesis is well known, yet the underlying molecular mechanisms remain poorly understood [2]. A suitable positron emission tomography (PET) tracer targeting the mAChRs would allow for in vivo molecular imaging of mAChRs and hence strongly contribute to increase the knowledge in mAChR research. The basic understanding of the molecular mechanism is the only guide to establish personalized precision medicine based on image-guided therapy applications for central nervous system (CNS) diseases. Irrespective of numerous efforts, so far, no mAChR PET radiotracer has found widespread clinical application. Predominantly, this can be attributed to unsuccessful attempts to meet all the stringent requirements such as high affinity (ca. 3–50 nM) [10], subtype selectivity, metabolic stability, in vivo specific binding, and many more [11]. The requirements and parameters defining an effective and safe medication are highly dependent on the purpose (therapy or diagnosis) and the site of action (central or peripheral targets) and have to be considered already during the drug discovery process. In contrast to imaging agents, therapeutic CNS drugs allow less stringent attributes in terms of structure and binding affinity (μM to nM), but toxicology, functionality profile, and functional subtype selectivity are more in the spotlight [9,12].

Concluding, the repertoire of mAChR ligands for both therapy and diagnosis is characterized by a lack of high affinity and simultaneously subtype selective compounds. Diphenylmethyl esters of arecaidine (**a** and **b**, Figure 1) were recently discovered as orthosteric mAChR ligands with low nanomolar affinity and pronounced M1 selectivity. Unfortunately, strong nonspecific binding observed in the preclinical evaluation restrained their use as PET tracers [13]. Considering that nonspecific binding is often caused by hydrophobic interactions [14], this work aims to synthesize and evaluate similar compounds with reduced lipophilicity. In this study, we introduce the synthesis of chiral hydrobenzoin esters of arecaidine, which are fully characterized by nuclear magnetic resonance (NMR) spectroscopy and high resolution-mass spectrometry (HR-MS), and the purity was assessed by chiral and reversed phase-high performance liquid chromatography (HPLC). Physicochemical parameters as well as stability, affinity, and functionality toward mAChRs were assessed by in vitro methods for all synthesized compounds. In order to understand the difference in binding affinities, the binding poses of the novel compounds were assessed by in silico docking studies.

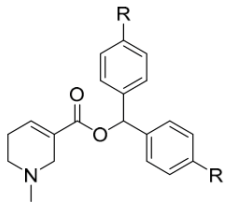


Figure 1. General structure of previously studied diphenylmethyl esters of arecaidine [13].

2. Results and Discussion

2.1. Chemistry

Hydrobenzoin esters of arecaidine were prepared and characterized by NMR spectroscopy, HR-MS, logP, RP-HPLC, and chiral HPLC. The esterification of (*R*,*R*)- and (*S*,*S*)-hydrobenzoin (**d**, **f**) yielded the

enantiomerically pure esters **1** and **2**, whereas esterification with *meso*-hydrobenzoin (**g**) yielded racemic **3** (Figure 2). Previously, arecaidine esters were prepared in low yields via 1,1′-carbonyldiimidazole (CDI)-mediated esterification [13]. Within this work, we describe a transesterification procedure from the readily available arecaidine methyl ester (**e**, arecoline). Regarding the synthesis of hydrobenzoin esters, the transesterification (synthesis of **2**) is characterized by a 70% increased yield and less experimental effort compared to the CDI-mediated esterification (synthesis of **1**). The vicinal coupling constant of the hydrobenzoin part is the most notable difference in NMR spectra between **1** or **2** (7.2 Hz) to **3** (5.8 Hz). Chiral HPLC confirmed that no racemization occurred during both methods (Supporting Information).

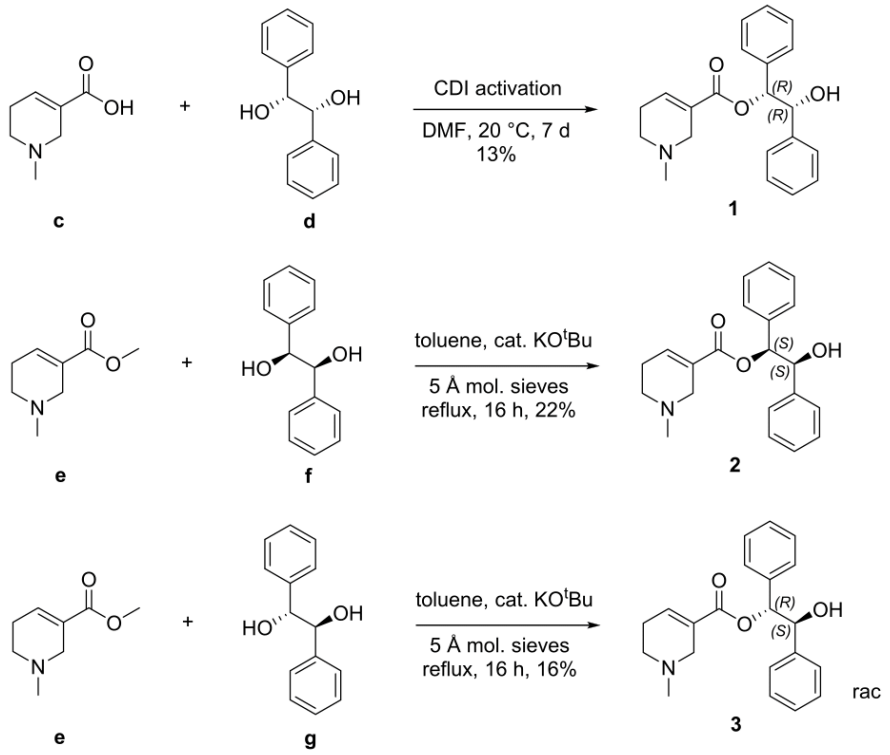


Figure 2. Stereoselective synthesis of hydrobenzoin esters of arecaidine.

2.2. Evaluation of Physico-Chemical Parameters and Stability

HPLC-log$P_{ow}^{pH7.4}$ values were found to be 2.24 ± 0.12 (**1**=**2**) and 2.39 ± 0.10 (**3**), which are much lower compared to arecaidine diphenylmethyl ester (3.32 ± 0.04) [13]. Consequently, **1**, **2**, and **3** are expected to be less prone to nonspecific binding. The predictive power of logP for blood–brain barrier permeability is controversially discussed, and several desirable logP ranges were postulated. However, the HPLC-log$P_{ow}^{pH7.4}$ values of **1**, **2**, and **3** comply with every single favorable logP range compared recently [15]. In addition, other chemical characteristics of **1**, **2**, and **3**, such as molecular weight (337.42 g/mol), number of hydrogen bonds (3 acceptors, 1 donor), polar surface area (49.8 Å^2), rotatable bond count (6), and possession of a tertiary nitrogen with a positive charge at pH 7–8 (calculated pKa = 7.8) are in good accordance with desired properties for CNS active drugs [16]. Furthermore, analysis by SwissADME [17] indicates that **1**, **2**, and **3** are no P-glycoprotein substrates and no PAINS [18] or Brenk [19] alerts were caused.

The stability of **1**, **2**, and **3** in buffer and cell culture medium was investigated because their disintegration could impair biological testing. **1**, **2**, and **3** show a comparable rate of decomposition in Dulbecco's phosphate-buffered saline (DPBS) and Ham's F12 cell culture medium at 37 °C over a time period of 60 h (Figure 3), which is slow enough to allow for biological testing and drug development. For **1**, **2**, and **3**, the decomposition is faster in Ham's F12 cell culture medium compared to DPBS.

After 60 h in DPBS **1**, **2**, and **3** were decomposed to the same extent (not significantly different in Sidak's multiple comparisons test, $\alpha = 0.05$). However, the decomposition of **1** in Ham's F12 cell culture medium was significantly stronger compared to **2** ($p \leq 0.001$) and **3** ($p \leq 0.01$). The different stability of the enantiomers **1** and **2** in Ham's F12 cell culture medium can be attributed to its numerous chiral constituents. Enantioselectivity in the presence of chiral amino acids is frequently observed in organic reactions; still, an unequivocal mechanism often remains obscure [20]. For the potential application as a carbon-11 PET tracer, compounds should exhibit a reasonable stability for at least six half-lifes (i.e., 2 h). The determined stabilities of **1**, **2**, and **3** support further development as a carbon-11 PET tracer, as a linear interpolation between the 0 h and 10 h indicates that only 0.8% and 2.5% are decomposed after 2 h in DPBS and Ham's F12 cell culture medium, respectively.

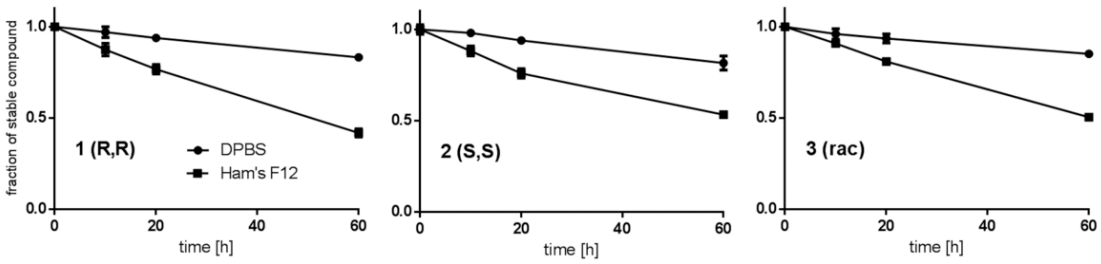


Figure 3. Stability of **1**, **2,** and **3** in Dulbecco's phosphate-buffered saline (DPBS) and Ham's F12 cell culture medium at 37 °C. Error bars represent the standard deviation.

2.3. In Silico Docking Experiments

Based on the in silico docking experiments, the enantiomers **1** and **2** feature substantially different binding poses (Figure 4). In addition to the hydrophobic interactions and the ionic Asp105 interaction, both enantiomers show hydrogen bonds to two amino acid side chains. However, in the predicted binding pose of **1**, the position of the hydroxyl group enables it to act as a hydrogen bond donor and acceptor to Asn382, which is an amino acid that is known to be strongly involved in the binding of high affinity antagonists [21]. Conclusively, **1** exhibits an additional hydrogen bond interaction compared to **2**, which can be seen as an indicator for higher affinity.

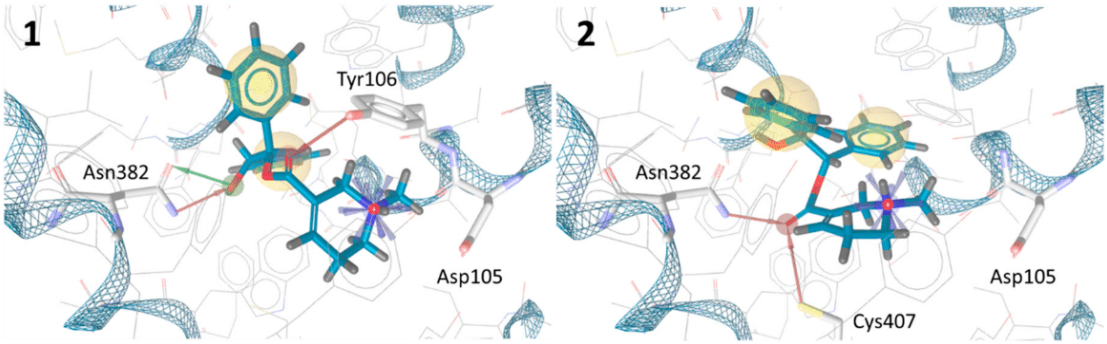


Figure 4. Calculated binding poses of protonated **1** and **2** in the orthosteric binding pocket of human muscarinic acetylcholine receptors (mAChR) M1. Amino acid residues participating in non-hydrophobic interactions are highlighted. **1** shows hydrophobic interactions to Val113, Trp157, Leu183, Ala193, Ala196, Trp378 and **2** to Tyr106, Trp157, Ala193, Ala196, Trp378, Tyr381, and Val385 (not highlighted).

2.4. Biological Evaluation

The expected orthosteric binding of **1**, **2**, and **3** could be confirmed using [*N*-methyl-^{3}H]scopolamine methyl chloride ([^{3}H]NMS) in a competitive radioligand binding assay toward all mAChR subtypes. All competitive binding curves show a monophasic logistic behavior and justify the use of a one-site model (supporting information, Figure S1) [22]. Comparing the subtypes, all tested compounds show

the highest affinity toward M1 followed by M5 and the lowest affinity to M2 (Table 1). However, the methyl ester of the free acid of **1**, **2**, and **3** (**e**, arecoline) shows pronounced mAChR M2 affinity [13], which illustrates the influence of chemical derivatization on subtype selectivity. **1** is considered most promising because it displays the highest affinity to the preferred M1 subtype. Furthermore, **1** shows the strongest subtype selectivity against all subtypes (M1 over M2, M3, M4, and M5) and the highest overall selectivity between M1 and M2 (19-fold) within the tested compounds. Especially, the 7-fold M1 over M4 subtype selectivity has to be mentioned. Although it is the second lowest selectivity compared to the other receptor subtypes, it is even higher than found in pirenzepine (3.5-fold) and trihexyphenidyl (1.6-fold) [23]. The superior mAChR M1 affinity of the (*R*,*R*)-isomer **1** over the (*S*,*S*)-isomer **2** corresponds well to the in silico docking experiments.

Table 1. Inhibition constants (K_i) given in nM, determined by competition binding on cell membranes derived from Chinese hamster ovary (CHO) cells. For data of this work and [13], errors are reported as standard deviation and for [23], errors are reported as standard error. K_i values of this work were determined using [*N*-methyl-^{3}H]scopolamine methyl chloride ([^{3}H]NMS), $n \geq 3$.

	M1	M2	M3	M4	M5	Source
1 (*R*,*R*)	99 ± 19	1900 ± 300	1300 ± 600	700 ± 300	600 ± 75	this work
2 (*S*,*S*)	800 ± 200	8000 ± 2000	1600 ± 300	2700 ± 600	1300 ± 300	this work
3 (*rac*)	380 ± 90	3700 ± 1000	3200 ± 500	1600 ± 200	970 ± 90	this work
arecoline	20,300 ± 2400	3800 ± 890	16,700 ± 5900	4700 ± 410	7000 ± 570	[13]
pirenzepine	8 ± 1	270 ± 10	150 ± 10	28 ± 1	170 ± 10	[23]
trihexyphenidyl	1.6 ± 0.2	7 ± 1	6.4 ± 0.4	2.6 ± 0.4	15.9 ± 0.1	[23]

In terms of mAChR M1 minimum subtype selectivity, **1** performs better than the clinically established mAChR M1 antagonists pirenzepine and trihexyphenidyl (Figure 5) and also better than our recent top candidates for mAChR M1 PET imaging [13]. Given the lower affinity of **1** compared to pirenzepine, antagonistic mAChR M1 treatment with **1** would require a higher dose, which might be well tolerated due to the broader M1 subtype selectivity. Compounds featuring two aromatic rings are very prominent in mAChR drug development. However, to the best of our knowledge, the hydrobenzoin scaffold has only been utilized in a single publication on muscarinic ligand development [24]. In that publication, compounds 18a–c contain the hydrobenzoin scaffold integrated in a 1,4-dioxane ring and also show the highest affinity toward subtype M1. Still, subtype selectivity is narrower compared to the compounds presented herein.

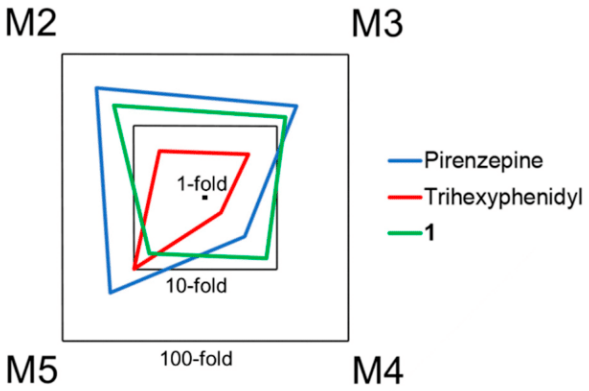


Figure 5. Subtype selectivities related to M1 visualized as radar charts. For each substance, the logarithmic axis represents K_i toward the respective subtype divide by the K_i of M1. Compared to the clinically established M1 antagonists pirenzepine and trihexyphenidyl, **1** shows a pronounced subtype selectivity toward M4, which results in overall broader subtype selectivity. Selectivities of pirenzepine and trihexyphenidyl were calculated based on their literature reported K_i values [23].

The significantly different binding affinities observed between the three stereoisomers underline the general possibility to increase mAChR affinity and subtype selectivity of arecaidine esters via stereochemical variations. In view of the vast majority of achiral small molecules, which have been studied as potential mAChR PET tracers [10], we believe that stereochemistry is a useful yet underappreciated tool to optimize compound properties.

In addition to the assessment of the affinity by means of a radiometric competition binding assay [25] on cellular membranes, the functionality of the synthesized compounds was further evaluated in a cell-based fluorescence assay using Fluo-4 [26]. In contrast to the mAChR agonist carbachol, no increase in calcium release could be induced by incubation with **1**, **2**, and **3** using commercially available Fluo-4 direct calcium flux assay on stably transfected CHO-M1 cells (Figure 6, Panel A). Applying compounds **1**, **2**, **3**, and scopolamine as positive control prior to the treatment with a constant concentration of the signal inducing carbachol clearly illustrates the antagonistic binding of the tested compounds (Figure 6, Panel B). The progression of the effect–concentration curve of both positive controls, carbachol for the agonistic assay and scopolamine for the antagonistic assay, are in good accordance with the results depicted by the manufacturer.

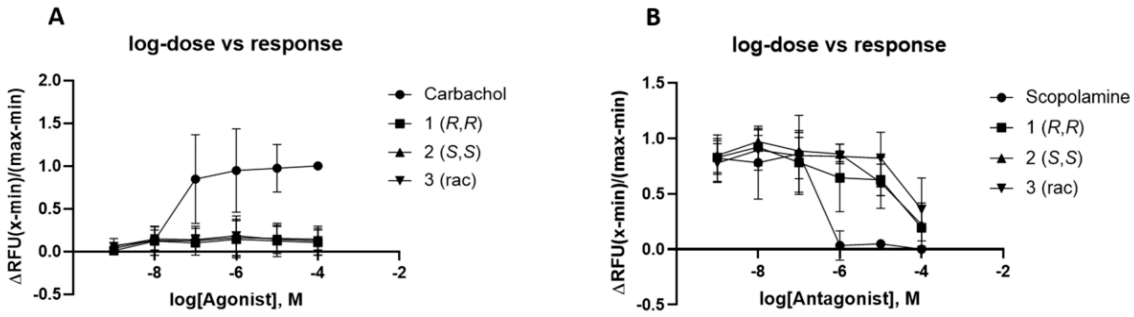


Figure 6. Dose-dependent calcium response to muscarinic 1 (M1) receptor agonists and antagonists. CHO-M1 cells were plated in black clear bottom 96-well plate and incubated overnight. The following day, cells were assayed for a calcium response to carbachol (positive control), **1**, **2**, and **3** using the Fluo-4 Direct™ Calcium Assay Kit. Cells were stimulated for potential agonistic activity (panel A) [27] or cells were treated for potential antagonistic activity, scopolamine (positive control), **1**, **2**, and **3** to block the calcium response elicited by 20 μM carbachol (panel B). Measurements are given in relative fluorescent units (RFU) as the maximum response minus the minimum response divided by the minimum response.

1 has a high binding affinity (K_i-value) to the M1 receptor of 99 ± 19 nM, as assessed by means of the radioligand binding assay, being 2-fold out of the postulated ideal range [10]. As numerous mAChR ligands failed in PET radiotracer development due to too high binding affinity, being a disadvantage in radiotracer kinetics causing flow dependence of tracer accumulation [10], this "borderline" binding affinity should not be a common ground for excluding **1** from further development toward diagnostic application, especially when considering that the targeted mAChR subtype M1 is the most abundant subtype in the cortex [28]. Furthermore, **1** may serve as a lead structure for the development of derivatives with even higher affinity, retaining its suitable selectivity profile and moderate lipophilicity values.

It is an ongoing debate as to whether PET radiotracer targeting GPCRs are preferably agonist or antagonists [29] Agonists per se complicate the PET image analysis as they favorably bind to the activated form of GPCRs. The global picture shows a prevalence for antagonists carried by the easier access and unlikeliness of side effects. Considering the physico-chemical parameters, binding affinities, subtype selectivity, and effective functionality of the here presented subset of compounds, the potential application points into the direction as diagnostic imaging probes over a potential therapeutic application. Potential application as an imaging probe is further supported by the expected ease of carbon-11 radiolabeling of **1**, considering that structurally related arecaidine esters were previously labeled with carbon-11 straightforwardly via reaction of [^{11}C]CH_3I with *N*-desmethyl

precursors [13]. The observed antagonism is advantageous for PET radiotracers, as potential side effects are unlikely. Especially, compound **1** stands out with binding affinities in the nanomolar range and high subtype selectivity, proving the importance of stereochemical adjustments for successful mAChR ligand development.

3. Conclusions

Subtype selectivity represents an ambitious but necessary goal in the development of orthosteric mAChR ligands for therapeutics as well as for diagnostics. Within this work, we synthesized chiral hydrobenzoin esters of arecaidine and investigated their stability and binding properties toward mAChRs. Stereochemistry was shown to have a strong impact on in vitro mAChR M1 affinity, which was also anticipated by in silico molecular docking. Furthermore, the variable affinity toward the other subtypes highlights the relevance of chiral ligands in the quest for subtype selectivity. The antagonistic (*R*,*R*)-isomer **1** shows most promising characteristics to act as a suitable mAChR M1 PET tracer and especially stands out because of its broad subtype selectivity compared to clinically established mAChR M1 antagonists. These properties motivate us to radiolabel **1** with carbon-11 in the future to further evaluate its applicability as brain PET tracer.

4. Experimental

4.1. Materials

Arecaidine was prepared according to the literature [30] from arecoline hydrobromide (XA BC-Biotech). Carbonyldiimidazol (CDI, reagent grade, Sigma Aldrich, St. Louis, MO, USA), (*R*,*R*)-hydrobenzoin (>99%, TCI), (*S*,*S*)-hydrobenzoin (98+%, alfa aesar), *meso*-hydrobenzoin (>98%, TCI), KO^{t}Bu (98%, Sigma Aldrich), dimethylformamide (DMF, 99.8% extra-dry over molecular sieve, Acros), toluene (99.8% anhydrous, Sigma Aldrich, St. Louis, MO, USA), probenecid (>98%, TCI), and DPBS (Gibco, Life Technologies Limited) were used without further purification. Protease Inhibitor Cocktail powder (P2714-1BTL, Sigma-Aldrich, St. Louis, MO, USA) was dissolved in 10 mL water and used as such.

4.2. Instrumentation

NMR samples were measured in deuterated chloroform ($CDCl_3$, ≥99.8%, stabilized with silver foil, Sigma Aldrich) at 25 °C on a Bruker Avance III 400 spectrometer (400 MHz for ^{1}H and 100 MHz for ^{13}C). An assignment of NMR signals was achieved by a combination of standard NMR techniques, such as COSY, NOESY, APT, HSQC, and HMBC experiments. The residual $CHCl_3$ signal was set to 7.26 ppm for ^{1}H spectra and 77.0 ppm for ^{13}C spectra. Coupling constants are given in Hz. Mass spectra were obtained on a Bruker maXis 4G instrument (ESI-TOF, HR-MS). Optical rotation was determined in $CHCl_3$ using a Schmidt + Haensch UniPol L2000 polarimeter with a 1dm cell. An Agilent HPLC system consisting of an autosampler (series 1100), pump (series 1200) and diode array detector (series 1100) was used for the determination of logP using an apHERA (5 µm, 10 × 6 mm) stationary phase [15]. Compounds **1**–**3** were shown to exceed a purity of 95% by gradient run using the logP HPLC method without the addition of toluene and triphenylene and by isocratic runs on an XSelect™ (HSS T3, 3.5 µm, 100 × 4.6 mm) stationary phase at a flow of 1 mL/min (supporting information, Figure S2). Fluorescence measurements were performed on a BioTek Synergy HTX multi-mode reader. A M-36 tygon tubed Cell Harvester (Brandel®) and Whatman™ GF/B filters were used for the filtration of radioligand binding assays. Filter disks were counted with 2 mL Ultima Gold™ (high flashpoint LSC cocktail, PerkinElmer) using a 300 SL Automatic TDCR liquid Scintillation Counter (HIDEX).

4.3. Stability Measurements in DPBS and Cell Culture Media

First, 1089 µL DPBS or Ham's F12 nutrient mixture were mixed with 11 µL of 10 mM stock solution of **1**, **2**, or **3** in DMSO (final DMSO content: 1%) and agitated at 37 °C. Then, 80 µL of the solution was analyzed by UV-HPLC (216 nm) using an XSelect™ (HSS T3, 3.5 µm, 100 × 4.6 mm)

stationary phase and 40% acetonitrile in 25 mM $(NH_4)H_2PO_4$ buffer (pH 9.3) at a flow of 1 mL/min ($k_{1,2}$ = 5.6, k_3 = 5.9). The fraction of stable compounds was calculated as the area under the curve of the compound peak for each combination of compound and matrix related to the 0 h time point with 100%. Three non-consecutive HPLC analyses were performed for each time point, combination of compounds, and matrix.

4.4. Molecular Docking Studies

Molecular docking was performed on a crystal structure of human mAChR M1 [31] using AutoDock 4.2 with default settings in LigandScout 4.4_RC6. **1** and **2** were docked as protonated tertiary amines to consider the expected species under physiological conditions. A pharmacophore of the binding poses exhibiting the expected ionic interaction to Asp105 was created to visualize proposed interactions of **1** and **2** to amino acid side chains.

4.5. Cell Culture

CHO-K1 cells stably transfected with human muscarinic receptors M1–M5 were obtained from The Missouri University of Science and Technology cDNA Resource Center (Cell Catalog#: CEM1000000, CEM2000000, CEM3000000, CEM4000000, CEM5000000) and cultivated in Ham's F12 Nutrient Mixture (Gibco, Life Technologies Limited, Waltham, MA, USA) containing 10% FBS (Gibco, Life Technologies Limited), 250 µg/mL Geneticin® (G418, Thermo Fisher, Waltham, MA, USA) at 37 °C and 5% CO_2 in a cell incubator. Gibco™ Trypsin-EDTA (0.05%) was used for passaging cells. Untransfected CHO-K1 cells were obtained from ATCC and cultivated as described above but in media free of Geneticin®. Powdered protease inhibitor cocktail (P2714-1BTL, Sigma Aldrich, St. Louis, MO, USA) was dissolved in 10 mL water and used as such.

4.6. Affinity Assay Toward mAChRs M1-M5 on CHO Membranes

Cell membranes bearing human mAChRs M1-M5 were prepared as described previously [13]. In short, stably transfected CHO cells were grown to confluence in T175 flasks, washed with ice-cold DPBS, and suspended in 2 mL 10 mM Tris/HCl, 1 mM EDTA-buffer (pH 7.4), and 200 µL protease inhibitor using a cell scraper. A cell homogenate was prepared by passing the cell suspension through a G29 needle and subsequently centrifuged (10 min, 1000× *g*, 4 °C). Ultracentrifugation of the supernatant (30 min, 100,000× *g*, 4 °C) yielded a membrane pellet, which was suspended in 125 µL 50 mM Tris/HCl-buffer (pH 7.4) per T175 flask and stored at −80 °C. Ten confluent T175 flask were processed for one batch.

Inhibition constants (K_i) were determined with a competitive radioligand binding assay using 50 mM Tris/HCl, 10 mM $MgCl_2$, and 1 mM EDTA (pH 7.4) as assay buffer. Then, 5 µL of test compound in DMSO, 50 µL of [*N*-methyl-^{3}H]scopolamine methyl chloride ([^{3}H]NMS) in assay buffer, and 445 µL of membrane suspension diluted in assay buffer were incubated for 90 min at 23 °C. The membrane-bound activity was recovered by filtration through GF/B filter paper pre-soaked in 0.1 % PEI and measured with a liquid scintillation counter. Maximum binding was measured by using 5 µL plain DMSO, and nonspecific binding was measured by using 5 µL 1 µM scopolamine in DMSO. A final concentration of [^{3}H]NMS was 0.2 nM, 0.3 nM, 0.8 nM, 0.2 nM, and 1 nM for M1–M5. Then, 3–12 µL membrane suspension were used per tube. IC_{50} values were calculated by a variable slope logistic regression using at least five distinct concentrations of test compound, pipetted in triplicates. K_i values were calculated using the Cheng–Prusoff equation and following K_D values of [^{3}H]NMS for M1-M5 [13]: 0.18 nM, 0.24 nM, 0.23 nM, 0.10 nM, and 0.35 nM.

4.7. Calcium Efflux Assay for Agonist/Antagonists Discrimination

For the Fluo-4 direct™ calcium assay kit (invitrogen), 100 µL of a 5×10^5 cells/mL suspension of CHO-M1 cells were seeded in black clear bottom 96-well plates (Corning). After settling of the cells for 24 h, the kit was performed according to the supplier's recommendation. In detail, the media was

removed, and 50 µL of Hanks-balanced salt solution (HBSS; Sigma Aldrich) were added, followed by 50 µL of the Fluo-4 buffer solution (including probenecid). The 96-well plates were incubated for 60 min at 37 °C in the dark. For the agonist assay, 100 µL of a double-concentrated dilution series of carbachol (positive control), **1**, **2**, and **3** were added with the end concentration of 100, 10, 1, 0.1, 0.01 and 0.001 µM in duplicates. The relative fluorescence was measured with an excitation wavelength of 494 nm and an emission wavelength of 516 nm. For the antagonist assay, 50 µL of a 4-fold concentrated dilution series of scopolamine hydrochloride (positive control), **1**, **2**, and **3** were added in duplicates. Subsequently a 40 µM stock solution of carbachol was added to all wells, and the relative fluorescence was measured with an excitation wavelength of 494 nm and an emission wavelength of 516 nm. Stock solution of **1**, **2**, and **3** were in DMSO with a final concentration of at most 1% of DMSO. All experiments were performed at least in three repetitions.

4.8. Calculations and Statistics

If not indicated otherwise, all values are depicted as mean ± standard deviation. All quantitative results were analysed by means of MS Excel® 2013. Significance was tested with GraphPad Prims 6 (version 6.07, San Diego, CA, USA).

4.9. Synthesis

(1R,2R)-(+)-2-hydroxy-1,2-diphenylethyl 1-methyl-1,2,5,6-tetrahydropyridine-3-carboxylate (**1**). Arecaidine (40.0 mg, 0.284 mmol, 1.0 equiv) was suspended in dry DMF (5 mL) and heated gently until almost everything dissolved. CDI (46.1 mg, 0.284 mmol, 1.0 equiv) was added as solid. After 1 h (*R*,*R*)-hydrobenzoin (122 mg, 0.568 mmol, 2.0 equiv) was added, and the reaction mixture was stirred for 7 days at 20 °C. The reaction mixture was poured on water (15 mL) and extracted with EtOAc (3 × 15 mL). The combined organic phases were dried over Na_2SO_4 and concentrated under reduced pressure. The resulting residue was purified via preparative thin layer chromatography (TLC) (CH_2Cl_2/MeOH, 90:10) to give the desired product in 13% yield (12.2 mg). ^{1}H NMR (400 MHz, $CDCl_3$): 7.24–7.17 (m, 6H, Ph H-3,4,5), 7.15–7.07 (m, 5H, Ph H-2,6, H-4), 5.92 (d, *J* = 7.2, 1H, Et H-1), 4.95 (d, *J* = 7.2, 1H, Et H-2), 3.20–3.10 (m, 2H, H-2), 2.53–2.47 (m, 2H, H-6), 2.43–2.35 (m, 2H, H-5), 2.39 (s, 3H, CH_3). ^{13}C NMR (101 MHz, $CDCl_3$): δ 164.8 (C=O), 139.2 (Ph C-1), 138.4 (C-4), 136.9 (Ph C-1), 128.8 (C-3), 128.10 (Ph C-3,4,5), 128.03 (Ph C-3,5), 127.97 (Ph C-4), 127.2 (Ph-C-2,6), 127.1 (Ph C-2,6), 79.9 (Et C-1), 77.2 (Et C-2), 53.1 (C-2), 50.6 (C-6), 45.6 (CH_3), 26.6 (C-5). HRMS (ESI+) (m/z): calculated for $C_{21}H_{24}NO_3$ $[M + H]^+$: 338.1751; found 338.1751.

(1S,2S)-(−)-2-hydroxy-1,2-diphenylethyl 1-methyl-1,2,5,6-tetrahydropyridine-3-carboxylate (**2**). Following a modified literature procedure [32], arecoline hydrobromide (200 mg, 0.85 mmol, 1.0 equiv) was dissolved in sat. aq. Na_2CO_3 (5 mL). The aqueous layer was extracted with CH_2Cl_2 (3×), dried (Na_2SO_4), and concentrated under reduced pressure. To a solution of the residual oily free base in PhMe (5 mL), (*S*,*S*)-hydrobenzoin (181 mg, 0.85 mmol, 1.0 equiv), KO^{t}Bu (5 mg, 0.04 mmol, 0.05 equiv), and a spatula of activated 5 Å molecular sieves were added subsequently. The resulting mixture was refluxed for 16 h. Then, it was filtered through a pad of celite, and volatiles were removed under reduced pressure. The crude oil was purified via preparative TLC (EtOAc/*n*-heptane, 70:30 with 3% Et_3N) to give the desired product in 22% yield (63 mg). ^{1}H NMR (400 MHz, $CDCl_3$): δ 7.25–7.19 (m, 6H, Ph H-3,4,5), 7.17–7.06 (m, 5H, Ph H-2,6, H-4), 5.92 (d, *J* = 7.2, 1H, Et H-1), 4.97 (d, *J* = 7.2, 1H, Et H-2), 3.20–3.13 (m, 2H, H-2), 2.53–2.47 (m, 2H, H-6), 2.43–2.36 (m, 2H, H-5), 2.41 (s, 3H, CH_3). ^{13}C NMR (101 MHz, $CDCl_3$): δ 164.8 (C=O), 139.0 (Ph C-1), 138.4 (C-4), 136.8 (Ph C-1), 128.9 (C-3), 128.17 (Ph C-4), 128.15 (Ph C-3,5), 128.09 (Ph C-3,5), 128.05 (Ph C-4), 127.2 (Ph C-2,6), 127.1 (Ph C-2,6), 79.9 (Et C-1), 77.2 (Et C-2), 53.2 (C-2), 50.7 (C-6), 45.7 (CH_3), 26.7 (C-5). HRMS (ESI+) (m/z): calculated for $C_{21}H_{24}NO_3$ $[M + H]^+$: 338.1751; found 338.1758.

Rac. (1S,2R)-2-hydroxy-1,2-diphenylethyl 1-methyl-1,2,5,6-tetrahydropyridine-3-carboxylate (**3**). Following a modified literature procedure [32], arecoline hydrobromide (200 mg, 0.85 mmol, 1.0 equiv) was dissolved in sat. aq. Na_2CO_3 (5 mL). The aqueous layer was extracted with CH_2Cl_2 (3×), dried (Na_2SO_4), and concentrated under reduced pressure. To a solution of the residual oily free base in PhMe (5 mL), *meso*-hydrobezoin (181 mg, 0.85 mmol, 1.0 equiv), KO^{t}Bu (5 mg, 0.04 mmol, 0.05 equiv), and a spatula

of activated 5 Å molecular sieves were added subsequently. The resulting mixture was refluxed for 16 h. Then, it was filtered through a pad of celite, and volatiles were removed under reduced pressure. The crude oil was purified via preparative TLC (EtOAc/*n*-heptane, 70:30 with 3% Et_3N) to give the desired product in 16% yield (46 mg). ^{1}H NMR (400 MHz, $CDCl_3$): δ 7.33–7.26 (m, 6H, Ph H-3,4,5), 7.26–7.22 (m, 4H, Ph H-2,6), 7.03–6.97 (m, 1H, H-4), 5.97 (d, J = 5.8, 1H, Et H-1), 5.03 (d, J = 5.8, 1H, Et H-2), 3.13–3.06 (m, 2H, H-2), 2.53–2.45 (m, 2H, H-6), 2.40 (s, 3H, CH_3), 2.39–2.33 (m, 2H, H-5). ^{13}C NMR (101 MHz, $CDCl_3$): δ 164.5 (C=O), 139.5 (Ph C-1), 138.2 (C-4), 136.6 (Ph C-1), 128.8 (C-3), 128.38 (Ph C-4), 128.26 (Ph C-3,5), 128.08 (Ph C-3,5, Ph C-4), 78.9 (Et C-1), 76.5 (Et C-2), 53.0 (C-2), 50.6 (C-6), 45.6 (CH_3), 26.6 (C-5). HRMS (ESI+) (m/z): calculated for $C_{21}H_{24}NO_3$ $[M + H]^+$: 338.1751; found 338.1755.

Supplementary Materials: The following are available online at http://www.mdpi.com/1424-8247/13/12/437/s1, Figure S1: Exemplary competitive binding curves of **1**, **2**, and **3** on human mAChR M1 expressed on cell membranes of stably transfected CHO cells using [*N*-methyl-^{3}H]scopolamine methyl chloride. Values at 10^{-11} M and 10^{-10} M represent full binding in absence of competitor, Figure S2: Isocratic HPLC chromatograms of compounds **1**–**3**. 35–40% ACN in 25 mM $NH_4H_2PO_4$ buffer pH 9.3 at a flow of 1 mL/min, Figure S3: Chiral chromatography using a an AGP 0.3 cmØ × 5cm 5 µM column operated with 2% IPA in 10 mM NH_4Ac pH 5.8 at a flow of 0.5 mL/min, Figure S4: ^{1}H- and ^{13}C-NMR spectrum of **1**, Figure S5: ^{1}H- and ^{13}C-NMR spectrum of **2**. Figure S6: ^{1}H- and ^{13}C-NMR spectrum of **3**.

Author Contributions: M.O. and J.A. planned and/or performed the syntheses. W.H. performed NMR characterization. M.O., D.P., C.V. and V.P. planned and/or performed biological characterization. M.O., J.A. and V.P. prepared the manuscript. H.S., W.W. and M.H. contributed to the overall research concept and proofread the manuscript. All authors have read and agreed to the published version of the manuscript.

Funding: This research received no external funding.

Acknowledgments: Open Access Funding by the University of Vienna.

Conflicts of Interest: The authors declare no conflict of interest.

References

1. Haga, T. Molecular properties of muscarinic acetylcholine receptors. *Proc. Jpn. Acad. Ser. B Phys. Biol. Sci.* **2013**, *89*, 226–256. [CrossRef] [PubMed]
2. Kruse, A.C.; Kobilka, B.K.; Gautam, D.; Sexton, P.M.; Christopoulos, A.; Wess, J. Muscarinic Acetylcholine Receptors: Novel Opportunities for Drug Development. *Nat. Rev. Drug Discov.* **2014**, *13*, 549–560. [CrossRef] [PubMed]
3. Casarosa, P.; Kiechle, T.; Bakker, R.A. Differential Inverse Agonism at the Human Muscarinic M3 Receptor. In *Methods in Enzymology*; Elsevier: Amsterdam, the Netherlands, 2010; pp. 81–101.
4. Cheng, C.-Q.; Xu, H.; Liu, L.; Wang, R.-N.; Liu, Y.-T.; Li, J.; Zhou, X.-K. Efficacy and Safety of Pilocarpine for Radiation-Induced Xerostomia in Patients with Head and Neck Cancer. *J. Am. Dent. Assoc.* **2016**, *147*, 236–243. [CrossRef] [PubMed]
5. Gaitonde, S.; Malik, R.D.; Christie, A.L.; Zimmern, P.E. Bethanechol: Is It Still Being Prescribed for Bladder Dysfunction in Women? *Int. J. Clin. Pract.* **2019**, *73*, e13248. [CrossRef] [PubMed]
6. Verma, S.; Kumar, A.; Tripathi, T.; Kumar, A. Muscarinic and Nicotinic Acetylcholine Receptor Agonists: Current Scenario in Alzheimer's Disease Therapy. *J. Pharm. Pharmacol.* **2018**, *70*, 985–993. [CrossRef]
7. Xiang, Z.; Thompson, A.D.; Jones, C.K.; Lindsley, C.W.; Conn, P.J. Roles of the M1 Muscarinic Acetylcholine Receptor Subtype in the Regulation of Basal Ganglia Function and Implications for the Treatment of Parkinson's Disease. *J. Pharmacol. Exp. Ther.* **2012**, *340*, 595–603. [CrossRef] [PubMed]
8. Holle, G.E. Pathophysiology and Modern Treatment of Ulcer Disease. *Int. J. Mol. Med.* **2010**, *25*, 483–491. [CrossRef]
9. Gribkoff, V.K.; Kaczmarek, L.K. The Need for New Approaches in CNS Drug Discovery: Why Drugs Have Failed, and What Can Be Done to Improve Outcomes. *Neuropharmacology* **2017**, *120*, 11–19. [CrossRef]
10. Toyohara, J.; Sakata, M.; Ishiwata, K. Human Brain Imaging of Acetylcholine Receptors. In *Imaging of the Human Brain in Health and Disease*; Elsevier: Amsterdam, the Netherlands, 2014; pp. 113–160.
11. Eckelman, W.C.; Kilbourn, M.R.; Mathis, C.A. Discussion of Targeting Proteins in Vivo: In Vitro Guidelines. *Nucl. Med. Biol.* **2006**, *33*, 449–451. [CrossRef]

12. Moulton, B.C.; Fryer, A.D. Muscarinic Receptor Antagonists, from Folklore to Pharmacology; Finding Drugs That Actually Work in Asthma and COPD: Anticholinergics in Treatment of Airway Disease. *Br. J. Pharmacol.* **2011**, *163*, 44–52. [CrossRef]
13. Ozenil, M.; Pacher, K.; Balber, T.; Vraka, C.; Roller, A.; Holzer, W.; Spreitzer, H.; Mitterhauser, M.; Wadsak, W.; Hacker, M.; et al. Enhanced Arecoline Derivatives as Muscarinic Acetylcholine Receptor M1 Ligands for Potential Application as PET Radiotracers. *Eur. J. Med. Chem.* **2020**, *204*, 112623. [CrossRef] [PubMed]
14. Nagar, S.; Korzekwa, K. Commentary: Nonspecific Protein Binding versus Membrane Partitioning: It Is Not Just Semantics. *Drug Metab. Dispos.* **2012**, *40*, 1649–1652. [CrossRef] [PubMed]
15. Vraka, C.; Nics, L.; Wagner, K.-H.; Hacker, M.; Wadsak, W.; Mitterhauser, M. Log P, a Yesterday's Value? *Nucl. Med. Biol.* **2017**, *50*, 1–10. [CrossRef] [PubMed]
16. Pajouhesh, H.; Lenz, G.R. Medicinal Chemical Properties of Successful Central Nervous System Drugs. *NeuroRX* **2005**, *2*, 541–553. [CrossRef]
17. Daina, A.; Michielin, O.; Zoete, V. SwissADME: A Free Web Tool to Evaluate Pharmacokinetics, Drug-Likeness and Medicinal Chemistry Friendliness of Small Molecules. *Sci. Rep.* **2017**, *7*, 42717. [CrossRef]
18. Baell, J.B.; Holloway, G.A. New Substructure Filters for Removal of Pan Assay Interference Compounds (PAINS) from Screening Libraries and for Their Exclusion in Bioassays. *J. Med. Chem.* **2010**, *53*, 2719–2740. [CrossRef]
19. Brenk, R.; Schipani, A.; James, D.; Krasowski, A.; Gilbert, I.H.; Frearson, J.; Wyatt, P.G. Lessons Learnt from Assembling Screening Libraries for Drug Discovery for Neglected Diseases. *ChemMedChem* **2008**, *3*, 435–444. [CrossRef]
20. Nagamine, T.; Inomata, K.; Endo, Y.; Paquette, L.A. Amino Acid Mediated Intramolecular Asymmetric Aldol Reaction to Construct a New Chiral Bicyclic Enedione Containing a Seven-Membered Ring: Remarkable Inversion of Enantioselectivity Compared to the Six-Membered Ring Example. *J. Org. Chem.* **2007**, *72*, 123–131. [CrossRef]
21. Ward, S.D.C.; Curtis, C.A.M.; Hulme, E.C. Alanine-Scanning Mutagenesis of Transmembrane Domain 6 of the M1 Muscarinic Acetylcholine Receptor Suggests That Tyr381 Plays Key Roles in Receptor Function. *Mol. Pharm.* **1999**, *56*, 1031–1041. [CrossRef]
22. Motulsky, H.J.; Neubig, R.R. Analyzing Binding Data. *Curr. Protoc. Neurosci.* **2010**, *52*, 7.5.1–7.5.65. [CrossRef]
23. Bolden, C.; Cusack, B.; Richelson, E. Antagonism by Antimuscarinic and Neuroleptic Compounds at the Five Cloned Human Muscarinic Cholinergic Receptors Expressed in Chinese Hamster Ovary Cells. *J. Pharmacol. Exp. Ther.* **1992**, *260*, 576–580. [PubMed]
24. del Bello, F.; Bonifazi, A.; Giorgioni, G.; Piergentili, A.; Sabbieti, M.G.; Agas, D.; Dell'Aera, M.; Matucci, R.; Górecki, M.; Pescitelli, G.; et al. Novel Potent Muscarinic Receptor Antagonists: Investigation on the Nature of Lipophilic Substituents in the 5- and/or 6-Positions of the 1,4-Dioxane Nucleus. *Med. Chem.* **2020**, *63*, 5763–5782. [CrossRef] [PubMed]
25. Maguire, J.J.; Kuc, R.E.; Davenport, A.P. Radioligand Binding Assays and Their Analysis. In *Receptor Binding Techniques*; Davenport, A.P., Ed.; Humana Press: Totowa, NJ, USA, 2012; pp. 31–77.
26. Ma, Q.; Ye, L.; Liu, H.; Shi, Y.; Zhou, N. An Overview of Ca^{2+} Mobilization Assays in GPCR Drug Discovery. *Expert Opin. Drug Discov.* **2017**, *12*, 511–523. [CrossRef] [PubMed]
27. Crittenden, C.; Dolzer, J.; Huan, B.; Yu, M.; Lydford, S.; Huggins, C. Cell Based Assays on the FLIPR$^{TETRA®}$ System: Comparison of the FLIPR® Calcium 5 Assay Kit to Other Fluorescence Based Calcium Flux Assays. In *Molecular Devices Scientific Poster*; Molecular Devices, Inc.: San Jose, CA, USA, 2017.
28. Zeeberg, B.R. Pharmacokinetic computer simulations of the relationship between in vivo and in vitro neuroreceptor subtype selectivity of radioligands. *Nucl. Med. Biol.* **1999**, *26*, 803–809. [CrossRef]
29. Colom, M.; Vidal, B.; Zimmer, L. Is There a Role for GPCR Agonist Radiotracers in PET Neuroimaging? *Front Mol. Neurosci.* **2019**, *12*, 255. [CrossRef]
30. Song, S.; Zhu, S.-F.; Pu, L.-Y.; Zhou, Q.-L. Iridium-Catalyzed Enantioselective Hydrogenation of Unsaturated Heterocyclic Acids. *Angew. Chem. Int. Ed.* **2013**, *52*, 6072–6075. [CrossRef]
31. Thal, D.M.; Sun, B.; Feng, D.; Nawaratne, V.; Leach, K.; Felder, C.C.; Bures, M.G.; Evans, D.A.; Weis, W.I.; Bachhawat, P.; et al. Crystal Structures of the M1 and M4 Muscarinic Acetylcholine Receptors. *Nature* **2016**, *531*, 335–340. [CrossRef]

32. Murthy, K.S.K.; Rey, A.W.; Tjepkema, M. Enantioselective Synthesis of 3-Substituted-4-Aryl Piperidines Useful for the Preparation of Paroxetine. *Tetrahedron Lett.* **2003**, *44*, 5355–5358. [CrossRef]

Publisher's Note: MDPI stays neutral with regard to jurisdictional claims in published maps and institutional affiliations.

© 2020 by the authors. Licensee MDPI, Basel, Switzerland. This article is an open access article distributed under the terms and conditions of the Creative Commons Attribution (CC BY) license (http://creativecommons.org/licenses/by/4.0/).

3.3. Pirenzepine's doppelgänger: Momentous rearrangement of the most prominent muscarinic M1 antagonist

Marius Ozenil,[1] Lukas Skos,[1] Alexander Roller,[2] Natalie Gajic,[2] Wolfgang Holzer,[3] Helmut Spreitzer,[3] Sonja Platzer-Ozenil,[4] Chrysoula Vraka,[1] Marcus Hacker,[1] Wolfgang Wadsak,[1,5] Verena Pichler[3]

[1] Department of Biomedical Imaging and Image-guided Therapy, Division of Nuclear Medicine, Medical University of Vienna, Austria
[2] X-ray Structure Analysis Centre, Faculty of Chemistry, University of Vienna, Austria
[3] Department of Pharmaceutical Chemistry, Faculty of Life Sciences, University of Vienna, Austria
[4] Faculty of Chemistry, University of Vienna, Austria
[5] CBmed GmbH - Center for Biomarker Research in Medicine, Graz, Austria

The doctoral candidate discovered the described rearrangement reaction, studied the reaction as well as the resulting compounds with a wide variety of methods and largely wrote the manuscript.

Pirenzepine's doppelgänger: Momentous rearrangement of the most prominent muscarinic M1 antagonist

Marius Ozenil,[1] Lukas Skos,[1] Alexander Roller,[2] Natalie Gajic,[2] Wolfgang Holzer,[3] Helmut Spreitzer,[3] Sonja Platzer-Ozenil,[4] Chrysoula Vraka,[1] Marcus Hacker,[1] Wolfgang Wadsak,[1,5] Verena Pichler[3,*]

[1] Department of Biomedical Imaging and Image-guided Therapy, Division of Nuclear Medicine, Medical University of Vienna

[2] X-ray Structure Analysis Centre, Faculty of Chemistry, University of Vienna

[3] Department of Pharmaceutical Chemistry, Faculty of Life Sciences, University of Vienna

[4] Faculty of Chemistry, University of Vienna

[5] CBmed GmbH - Center for Biomarker Research in Medicine, Graz

*corresponding author

Abstract

Drug safety is top priority to prevent any event that may cause or lead to inappropriate medication; although, these events continuously occurred throughout history until today. In this study, we describe a novel rearrangement product of the clinically established muscarinic acetylcholine receptor ligand pirenzepine, which entered the commercially supply chain under the wrong label of being pirenzepine. The rearrangement occurs under highly acidic conditions, which were previously believed to be suitable for the dihydrochloride formation of pirenzepine. The affinity of the rearrangement product is significantly decreased for pirenzepine and the structurally related telenzepine. Fortunately, reaction kinetics proved that no rearrangement takes place in gastric acid, which therefore is no safety issue for human administration. The commercial supply of false compounds, even of well-described and often used compounds like pirenzepine used as reference compounds in drug development, needs to be considered to guarantee solid basic research and data integrity.

Introduction

The chemical industry is currently being reshaped by globalization and several emerging market players have now become global leaders.[1] In the western market of laboratory chemicals this is characterized by a boom of chemical distributors[2], which act as importers of bulk quantities from companies around the world and subsequently sell small quantities to research and development institutions. Regarding the product quality, it should be beneficial that at least two different companies, the manufacturer and the distributor, assess the product quality. As chemical distributor within the European Union under REACH it is common to place chemicals on the European market without any further analytical process.[3] For active pharmaceutical ingredients, import into the European Union requires higher standards and all active substances must have been manufactured under good manufacturing practice (GMP). As active pharmaceutical ingredients are chemicals by their very nature, reliable quality control of the chemical identity is the fundament of drug safety. Nevertheless, at least hundreds of deadly incidents have been caused by confusion of chemicals in products of the pharmaceutical industry. For example, in 2008, Baxter processed heparin containing oversulfated chondroitin sulfate from a commercial supplier[4] and diethylene glycol which was falsely specified as glycerine has been used in the production of cough syrup between 1992 and 2007.[5]

Pirenzepine is a well-established parasympatholytic drug, which is in clinical use since the late 1970's.[6] It acts as antagonist for the muscarinic acetylcholine receptors (mAChRs), with a strong preference for the mAChR subtype M1. Due to its inability to cross the blood brain barrier, pirenzepine triggers only peripheral mAChRs. Pirenzepine is best known for its long history as inhibitor of gastric acid secretion and motility in the treatment of gastric and duodenal ulcers.[7] Besides these classical applications, pirenzepine is effective for controlling myopia progression in children[8] and is currently undergoing a phase II clinical trial for the treatment of peripheral neuropathy[9]. The relevance of pirenzepine roots back to the early days of mAChR research, when its observed different binding affinities gave evidence for the existence of mAChR subtypes.[10] Since then pirenzepine is broadly used in biological assays to differentiate between M1 and the other mAChR subtypes.[11,12] Consequently, this has led to the fact that a significant amount of knowledge regarding mAChR subtypes is tightly linked to the chemical structure of pirenzepine.

Like many therapeutically used amines, pirenzepine (**1**) is mainly used as its hydrochloride. Pirenzepine dihydrochloride (**2**) is widely available as pure compound and the active pharmaceutical ingredient of more than 25 trade names.[13–15] The synthesis of pirenzepine dihydrochloride was firstly patented by Dr Thomae GmbH[16] and many alternative synthesis procedures were reported since then (Figure 1).[17–21] Budesinsky *et al.*[22] reported an unexpected formation of a side product (**3**) during the synthesis of **1**, in which the 5,11-dihydro-6*H*-pyrido-[2,3-*b*][1,4]benzodiazepin-6-one part rearranges to 6-amino-5,5*a*-dihydro-11*H*-pyrido[2,1-*b*]quinazolin-11-one. Generally, the well-studied class of β-lactam antibiotics illustrates that lactams can be prone to hydrolysis[23] and rearrangement[24], especially when under high ring strain. Despite intensive investigations on the synthesis of pirenzepine, only few works report experimental details of the final step, the reaction of pirenzepine to its dihydrochloride (Figure 1).[16,20,21] Furthermore, pirenzepine acts as a lead structure for the development of novel mAChR ligands. The most notable examples which arose from this strategy are the mAChR M1 antagonist telenzepine[25], the M2/M4 antagonist AF-DX-384[26] and the M2 antagonists AF-DX 116[27] and AQ-RA 741[28].

Requiring pirenzepine as agent for displacement studies for investigating the mAChR M1[29], we bought pirenzepine dihydrochloride from a fine chemical distributor. However, it turned out that the received compound did not contain pirenzepine dihydrochloride at all, but later was identified as structural

isomer. Within this work we characterized this structural isomer, revealed the reaction leading to its formation, studied its mAChR affinity profile and traced back the origin of its production.

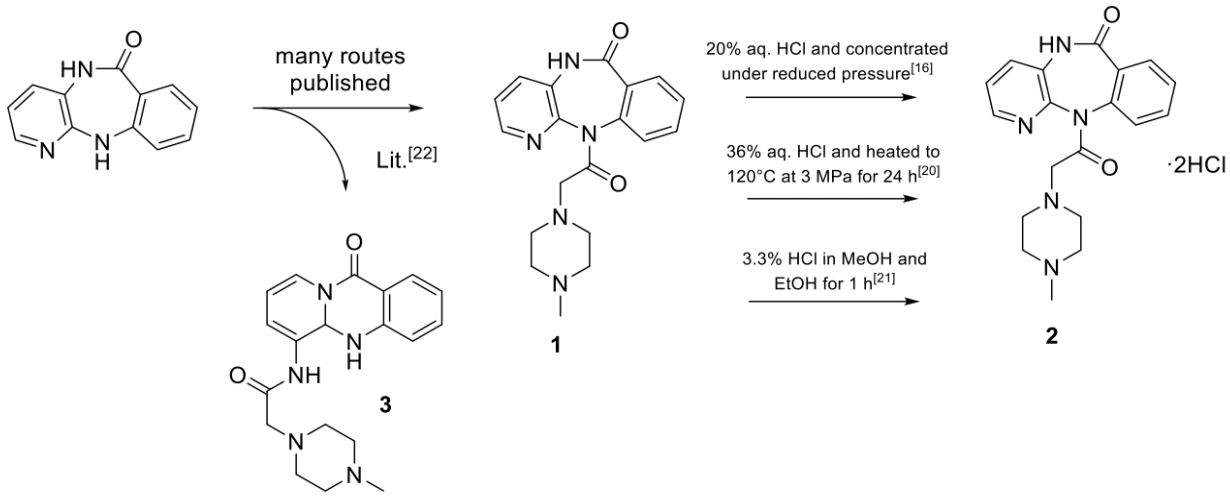


Figure 1: *Overview of synthetic routes of pirenzepine dihydrochloride. Emphasis is given on the synthetic conditions for the formation of the dihydrochloride.*

Results and discussion

Chemistry

X-ray measurements revealed the true structure (**4**) of a commercially obtained pirenzepine dihydrochloride (**2**) sample, which has not yet been reported in literature. **4** and **2** are constitutional isomers and hence cannot be distinguished by mass spectrometry without molecular fragmentation. However, ^{1}H-, ^{13}C-, ^{15}N-NMR spectroscopy, IR spectroscopy, melting point and RP-HPLC allow for a clear differentiation (Supporting Information).

In search for a synthetic access to **4** we revealed that aqueous acidic conditions combined with moderately increased temperature result in rearrangement of **2** to **4**. When **2** is reacted in 0.1 M aqueous HCl at 37 °C, 55 °C or 75 °C overnight, **4** is only formed in traces (<1 %). However, in strong excess of aqueous HCl (6 M) the rearrangement was shown to follow a pseudo first order kinetic with a quantitative conversion (Figure 2). Consequently, **4** must be much lower in free energy compared to **2**, which also correlates to their minimized MMFF94 energies of 583 kJ/mol and 762 kJ/mol, respectively. We propose that this reaction proceeds via lactam hydrolysis and subsequent condensation of the resulting primary amine with the exocyclic carbonyl group (Figure 3). The intermediate (in brackets) was never observed experimentally, which underlines its reactiveness and indicates, that the prior amide hydrolysis is the rate determining step. This is further supported by the observed high activation energy (83.2±1.9 kJ/mol), which is common for acidic amide bond cleavages (78.6-89.9 kJ/mol)[30]. The exchange of an oxygen atom with an heavy oxygen by utilization of [^{18}O]H_2O during the rearrangement reaction supports the proposed reaction scheme (Figure S8).

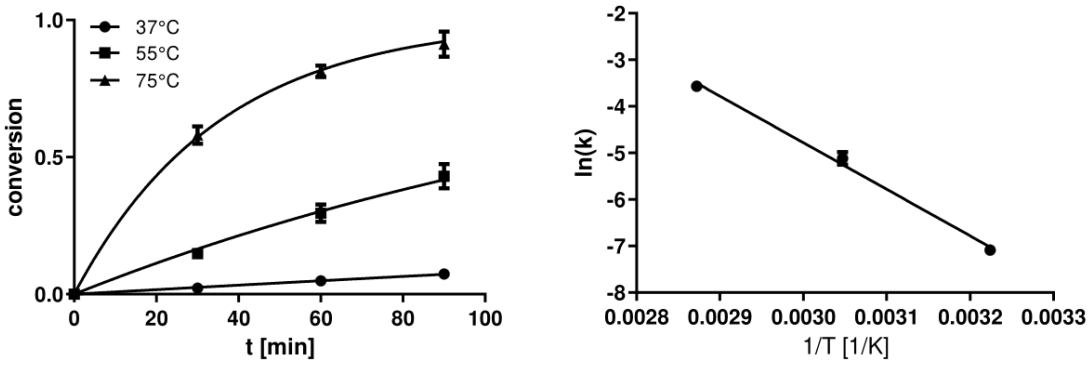


Figure 2: *Kinetic data of the rearrangement of **2** in 6 M HCl at an initial concentration of 50 µg/mL as determined by HPLC. Error bars indicate the standard deviation of n=3 measurements. Left: The kinetic profile of the rearrangement shows the conversion of **2** to **4** as function of time at different temperatures. The conversion is calculated normalized to the maximum area under the curve of **4**. The rearrangement follows a pseudo first order kinetic with half lifes of 25±2 min (75 °C), 117±16 min (55 °C) and 830±30 min (37 °C). Right: Arrhenius plot illustrating a linear relationship between inverse temperature and logarithm of the rate constants. The activation energy of the reaction was delineated from the slope: 83.2±1.9 kJ/mol.*

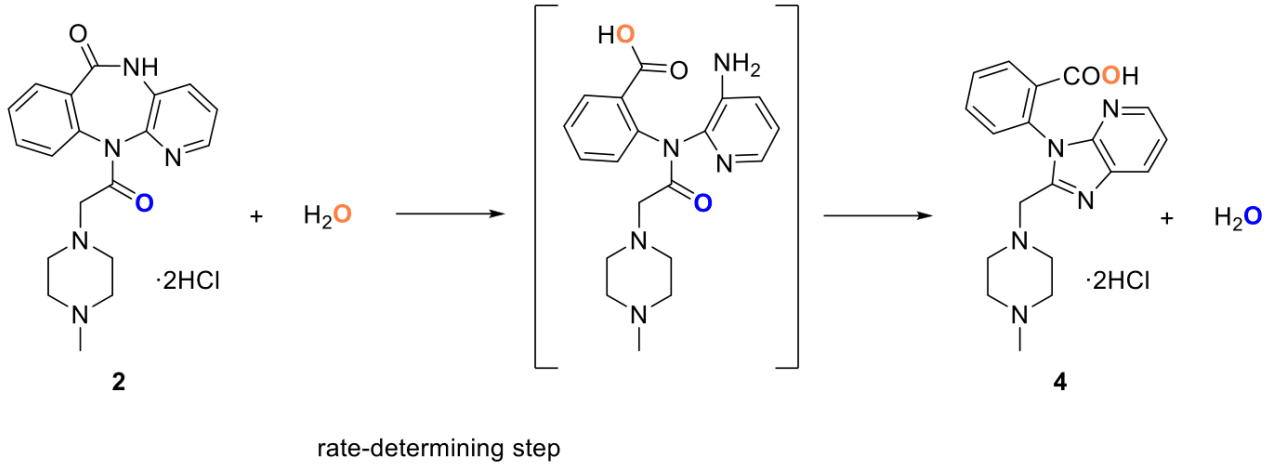


Figure 3: *Reaction scheme showing the proposed reactive intermediate. Oxygens in the carboxylic acid group are indistinguisable, but for reasons of clarity only one of them is coloured like the hydrolyzing water.*

Given that pirenzepine is used as oral drug and that the rearrangement takes place in acidic aqueous solution, we investigated whether isomerization of **2** to **4** can occur in gastric environment. Fortunately, neither simulated gastric fluid (0.08 M aq. HCl, 1 g/L NaCl and 1.6 g/L pepsin) nor equimolar aqueous HCl solution caused detectable isomerization of **2** to **4** after 6 h at 37 °C. These results indicate that pirenzepine is sufficiently kinetically inert to prevent formation of pharmacological relevant doses of **4** in the stomach, leaving pirenzepine's doppelgänger a sole problem of chemical production and distribution. Pure, crystalline **2** heated to 100 °C for 12 h did not result in formation of **4** in detectable amounts, indicating that isomerization as a result of improper handling during delivery is not to be expected.

Conditions under which pirenzepine undergoes this rearrangement are typical conditions for the formation of hydrochlorides. Review of the chemical literature showed that in the patent of Suzhou Homesun Pharmaceutical Co., Ltd[20] even harsher conditions (36% HCl, 120 °C, 3 MPa) are used for the dihydrochloride formation of pirenzepine. Manufacturers following this procedure will inevitably and unintentionally produce **4** instead of **2** in quantitative yields. Milder conditions[16,21] for the formation of **2** must be chosen to avoid formation of **4**.

Pirenzepine dihydrochloride batches from several distributors of fine chemicals (Table S1) and pharmaceuticals (Table S2) were qualitatively analyzed using UV-HPLC and two affected chemical distributors were revealed (sample #2 and #3). Frequently, certificates of analysis provided by distributors contain only superficial parameters like appearance, assay and melting point. However, no substantive analytical data allowing a solid proof of the chemical structure are presented. The main pillar of quality control for assay determination is HPLC, but we should question this overreliance on a separation method that cannot provide structural information. Finally, in close collaboration with the distributors the chemical was removed from their product portfolio.

All tested pharmaceutical products containing pirenzepine were shown to contain the expected constitutional isomer (**2**). According to entries in online pharmacies, Suzhou Homesun Pharmaceutical Co., Ltd also provides pirenzepine tablets[31,32]; however, no sample could be obtained by European pharmaceutical wholesalers.

Telenzepine, a thienobenzodiazepine congener of pirenzepine, was shown to undergo an analog rearrangement yielding **6**, which was characterized by NMR spectroscopy and X-ray diffraction analysis. Based on mass spectrometry data, this rearrangement was proposed previously.[33] It is assumable that also other acyl-diazepinones (*e.g.* AF-DX 116, AF-DX 384, AQ-RA 741) are prone to this rearrangement. From a synthetic chemist's perspective, the quantitative conversion of the rearrangement of pirenzepine highlights the potential applicability of the acyl diazepinone rearrangement as a useful tool for the synthesis of other *N*-substituted imidazoles.

Determination of affinities toward mAChR M1-M5

Table 1: *K_i-values (nM) as determined by a competitive radioligand binding assay using [N-methyl-^{3}H]scopolamine methyl chloride ([^{3}H]NMS) on CHO cell membranes containing human mAChR receptors. All obtained binding displacement curves showed the expected sigmoidal shape. * Binding was carried out for 90 min at 37 °C, using membranes from rat heart tissue (M2) and transfected A9Lcells (M1 and M3) and in NG108-15 cells (M4)*

	M1	M2	M3	M4	M5	Source
2	17±5	900±300	290±30	70±20	120±50	This work
	29	610±50	240	330	n.D.	[34]*
4	600±20	47000±19000	7000±2000	1200±200	360±20	This work
telenzepine 2HCl	1.8±0.8	26±5	12±2	29±16	16±9	This work
	1.8	50.3	6.9	17.4	n.D.	[34]*
6	1400±300	10600±1500	8000±3000	2000±400	4100±200	This work

Clearly the rearrangement of pirenzepine and telenzepine causes a tremendous loss of affinity towards all mAChR subtypes. Regarding the affinity constants towards M1 (Figure 4), this loss is even more pronounced in telenzepine (780-fold) compared to pirenzepine (35-fold).

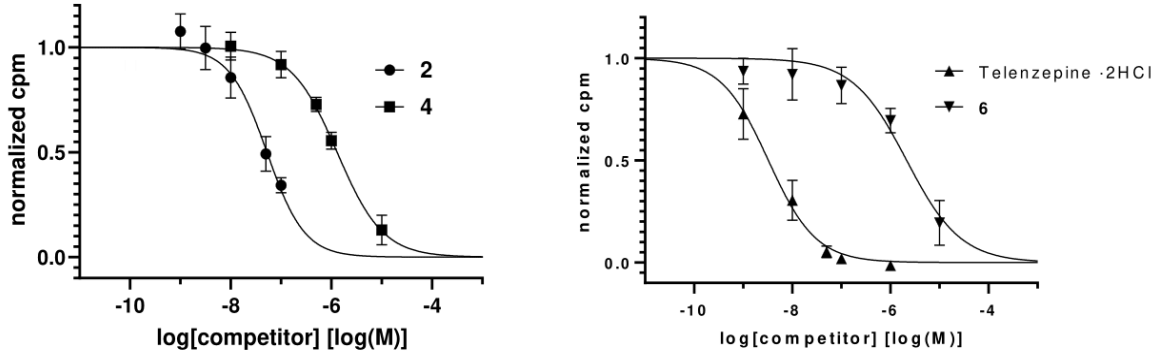


Figure 4: *Competition binding curves using 0.2 nM [^{3}H]NMS on mAChR M1 membranes for compounds* ***2, 4, 6*** *and telenzepine dihydrochloride. Filter bound decay rate is normalized to 1 for binding in absence of competitor and to 0 for nonspecific binding. Error bars indicate the standard deviation of n=3 measurements.*

Literature Research on sources of scientifically used pirenzepine

Pirenzepine dihydrochloride adopts a pivotal role in mAChR research as it is often used experimentally to discriminate mAChR M1 from the other mAChR subtypes. Caused by the different chemical, biological and hence physiological properties, scientific literature which is inadvertently based on **4** instead of pirenzepine needs to be reviewed carefully. According to SciFinder commercial sources[35] pirenzepine dihydrochloride is available as pure substance from 65 different suppliers. To investigate the impact of the pirenzepine production failure, the pirenzepine sources in the literature between the present and the year 2000 were checked (**Figure** 5).

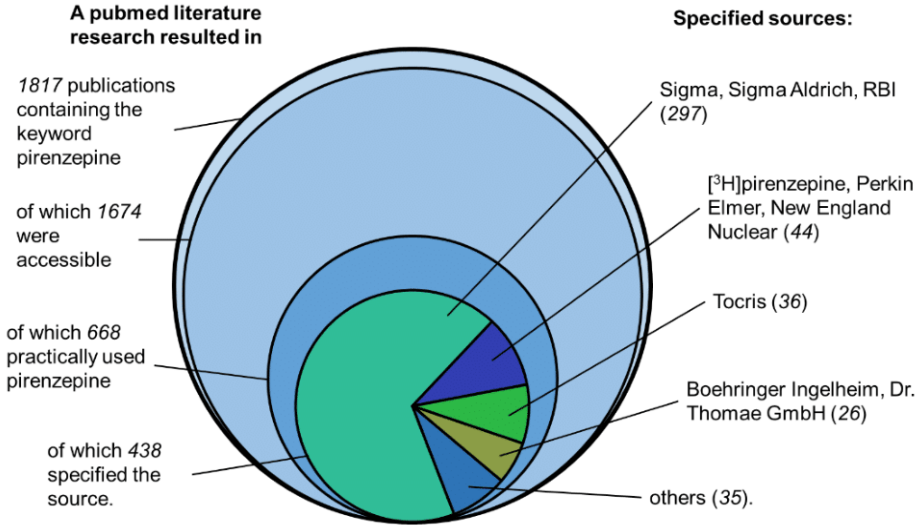


Figure 5: *Graphical illustration of the investigated scientific literature about pirenzepine between January 2000 and June 2020 showing the literature research workflow (left) and the specified sources (right).*

34% of the literature which used pirenzepine did not specify the supplier. Consequently, the impact of the pirenzepine confusion on the scientific data integrity can only be estimated. Based on the fraction of publications which specified a supplier it is reassuring to know that pirenzepine was never obtained from an evidently affected source. In the vast majority of the investigated publications pirenzepine is used for its mAChR M1 antagonistic properties in sophisticated experimental setups. It therefore appears unlikely that the structural identity of pirenzepine would have been questioned in these experiments, given that there are numerous other factors that could cause unexpected experimental results.

Conclusion

We present a case in which a literature-unknown chemical (**4**) was confused with pirenzepine by at least one producer and two fine chemical distributors. Formation of **4** was caused by an acid catalyzed rearrangement during dihydrochloride formation. In comparison to pirenzepine, **4** showed a strongly decreased affinity to mAChRs. It remains unclear, whether more samples of pirenzepine's doppelgänger is still in circulation and if other producers resort to the synthesis description leading to the rearrangement product. Fortunately, none of the pirenzepine-containing drugs tested within this work contained **4**. However, entries in online pharmacies show that the affected producer is or was also producing pirenzepine tablets for the pharmaceutical market.

We strongly advise all users of pirenzepine to confirm the chemical identity of their product with the analytical methods presented within this work. Furthermore, we want to raise general awareness that fine chemicals can enter the supply chain under a wrong label and that a natural suspicion of the declared content is to some degree always justified. To avoid being a victim of chemicals sold under the wrong label, we encourage a critical inspection of the certificate of analysis and recommend close collaboration and constructive discussion with distributors and manufactures to improve the quality on chemical supplies in a more and more globalized world.

Conflict of interest

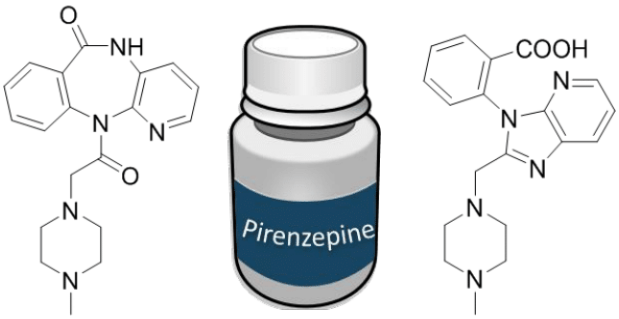
There are no conflicts to declare.

Acknowledgment

We thank Mag. Ronald Fiedler and Mag. Dr. Thomas Nagel from the AKH Wien hospital pharmacy for recording the IR spectra. Our gratitude goes to Dr. Katharina Pallitsch and the Institute of Organic Chemistry, University of Vienna for recording 600 MHz NMR spectra and to Daniel Dobusch for performing the HRMS measurements.

Data of the literature research are available on request.

Table of contents graphic



References

1. Lang N., Collie B., Gocke A., Zhai B., Ullrich P., Moldenhauer C. How the Global Chemical Industry Has Become a Battle of Equals. Available from: https://www.bcg.com/publications/2015/globalization-automotive-how-global-chemical-industry-become-battle-equals.aspx.
2. Jung U., Rothman A., Mahnke T., Roth R. Why Speciality Chemical Distributors Need to Raise Their Game. Available from: https://www.bcg.com/de-at/publications/2018/why-specialty-chemical-distributors-need-to-raise-their-game.aspx.
3. Distributor - ECHA. Available from: https://echa.europa.eu/support/getting-started/distributor [accessed January 01, 2021].
4. Heavey S., Richwine L. U.S., China clash over heparin contaminant's role. *Reuters*. Available from: https://www.reuters.com/article/us-heparin-china-idUSN2142999820080422 [accessed January 01, 2021].
5. Bogdanich W., Hooker J. From China to Panama, a Trail of Poisoned Medicine. *The New York Times*. Available from: https://www.nytimes.com/2007/05/06/world/americas/06poison.html [accessed January 01, 2021].

6. Brunner H., Veriá M., Polterauer P., Grabner G. Effect of pirenzepine, a new gastric acid-inhibiting agent, on exocrine pancreatic secretion in man. *Arzneimittelforschung* 1977;**27**(3):684–7.
7. Carmine AA., Brogden RN. Pirenzepine. *Drugs* 1985;**30**(2):85–126. Doi: 10.2165/00003495-198530020-00001.
8. Kang P. Optical and pharmacological strategies of myopia control: Myopia control. *Clinical and Experimental Optometry* 2018;**101**(3):321–32. Doi: 10.1111/cxo.12666.
9. A 24-Week Study of Topical Pirenzepine or Placebo in Type 2 Diabetic Patients (T2DM) With Peripheral Neuropathy. *U.S. National Library of Medicine*. Available from: https://clinicaltrials.gov/ct2/show/NCT04005287.
10. Hammer R., Berrie CP., Birdsall NJM., Burgen ASV., Hulme EC. Pirenzepine distinguishes between different subclasses of muscarinic receptors. *Nature* 1980;**283**(5742):90–2. Doi: 10.1038/283090a0.
11. Burke RE. The relative selectivity of anticholinergic drugs for the M1 and M2 muscarinic receptor subtypes. *Movement Disorders* 1986;**1**(2):135–44. Doi: 10.1002/mds.870010208.
12. Cilleros-Mañé V., Just-Borràs L., Tomàs M., Garcia N., Tomàs JM., Lanuza MA. The M_2 muscarinic receptor, in association to M_1, regulates the neuromuscular PKA molecular dynamics. *The FASEB Journal* 2020;**34**(4):4934–55. Doi: 10.1096/fj.201902113R.
13. Pirenzepine. *Drugs.Com*. Available from: https://www.drugs.com/international/pirenzepine.html [accessed October 9, 2019].
14. El-Obeild HA., Babhair SA., Al-Badr AA. Pirenzepine Dihydrochloride. *Analytical Profiles of Drug Substances*, vol. 16, Elsevier; 1987, p. 445–506.
15. Pirenzepine. Available from: https://www.drugbank.ca/drugs/DB00670 [accessed January 01, 2021].
16. Schmidt GD-CD., Engelhorn RD., Leitold MD. 11-Substituted 5 11-Dihydro-6h-Pyrido(2 3-B)(1 4)benzodiazepin-6-Ones. DE1795183 (B1), 1972.
17. Eberlein WDCD., Breuer G. Process for the preparation of 5,11-dihydro-11-((4-methyl-1-piperazinyl)-acetyl)-6H-pyrido(2,3-b)(1,4)benzodiazepin-6-one. DE3235795 (A1), 1984.
18. Hulinská H., Polívka Z., Jílek J., Šindelář K., Holubek J., Svátek E., et al. Experimental antiulcer agents: N-substituted 2-(4-methyl-1-piperazinyl)acetamides as pirenzepine models and some related compounds. *Collection of Czechoslovak Chemical Communications* 1988;**53**(8):1820–44. Doi: 10.1135/cccc19881820.
19. Zhang Y. Pirenzepine production method. CN104744457 (A), 2015.
20. Yang Y. Method for synthesizing pirenzepine hydrochloride. CN103044419 (A), 2013.
21. Kovač T., Oklobdžija M., Comisso G., Decorte E., Fajdiga T., Moimas F., et al. New synthesis of 11-acyl-5,11-dihydro-6 *H* -pyrido[2,3-b][1,4]-benzodiazepin-6-ones and related studies: New Synthesis of 11-Acyl-5,11-dihydro-6 *H* -pyrido[2,3-b][1,4]-benzodiazepin-6-ones. *Journal of Heterocyclic Chemistry* 1983;**20**(5):1339–49. Doi: 10.1002/jhet.5570200537.
22. Buděšínský M., Symerský J., Podlaha J., Podlahová J., Polívka Z., Protiva M. Unexpected formation of a 11 *H* -pyrido[2,1- *b*]quinazolin-11-one derivative from 5,11-dihydro-6 *H* -pyrido[2,3- *b*]-1,4-benzodiazepin-6-one. *Journal of Heterocyclic Chemistry* 1989;**26**(5):1229–35. Doi: 10.1002/jhet.5570260505.
23. Mitchell SM., Ullman JL., Teel AL., Watts RJ. pH and temperature effects on the hydrolysis of three β-lactam antibiotics: Ampicillin, cefalotin and cefoxitin. *Science of The Total Environment* 2014;**466–467**:547–55. Doi: 10.1016/j.scitotenv.2013.06.027.
24. Dražić T., Roje M. β-Lactam rearrangements into five-membered heterocycles. *Chem Heterocycl Comp* 2017;**53**(9):953–62. Doi: 10.1007/s10593-017-2156-z.
25. Stockbrügger RW. Clinical Significance of M_1 Receptor Antagonists. *Pharmacology* 1988;**37**(1):54–63. Doi: 10.1159/000138507.
26. Tränkle C., Andresen I., Lambrecht G., Mohr K. M2 Receptor Binding of the Selective Antagonist AF-DX 384: Possible Involvement of the Common Allosteric Site. *Mol Pharmacol* 1998;**53**(2):304–12. Doi: 10.1124/mol.53.2.304.

27. Micheletti R., Montagna E., Giachetti A. AF-DX 116, a cardioselective muscarinic antagonist. *J Pharmacol Exp Ther* 1987;**241**(2):628–34.
28. Doods H., Entzeroth M., Mayer N. Cardioselectivity of AQ-RA 741, a novel tricyclic antimuscarinic drug. *Eur J Pharmacol* 1991;**192**(1):147–52. Doi: 10.1016/0014-2999(91)90081-z.
29. Ozenil M., Pacher K., Balber T., Vraka C., Roller A., Holzer W., et al. Enhanced arecoline derivatives as muscarinic acetylcholine receptor M1 ligands for potential application as PET radiotracers. *European Journal of Medicinal Chemistry* 2020;**204**:112623. Doi: 10.1016/j.ejmech.2020.112623.
30. Bolton P. Hydrolysis of amides. II. Substituent effects in dilute acid and alkali. *Aust J Chem* 1966;**19**(6):1013. Doi: 10.1071/CH9661013.
31. 盐酸哌仑西平片. Available from: https://www.larspring.com/front/product/toProduct?uuid=551ae1c9ea1d4f70b116c4561ccd2d16.
32. 盐酸哌仑西平片. Available from: https://www.yaofangwang.com/medicine-318468.html.
33. Sturm E., Junker A. Determination of telenzepine in human serum by gas chromatography—mass spectrometry. *Journal of Chromatography B: Biomedical Sciences and Applications* 1988;**430**:43–51. Doi: 10.1016/S0378-4347(00)83132-1.
34. Karton Y., Bradbury BJ., Baumgold J., Paek R., Jacobson KA. Functionalized congener approach to muscarinic antagonists: analogs of pirenzepine. *Journal of Medicinal Chemistry* 1991;**34**(7):2133–45. Doi: 10.1021/jm00111a032.
35. SciFinder. Available from: https://scifinder.cas.org [accessed January 01, 2021].

3.4. Pitfalls and solutions of the fully-automated radiosynthesis of [^{11}C]metoclopramide

Verena Pichler,[1] **Marius Ozenil**,[1] Karsten Bamminger,[1,2] Chrysoula Vraka,[1] Marcus Hacker,[1] Oliver Langer,[1,3,4] Wolfgang Wadsak,[1,2]

[1] Division of Nuclear Medicine, Department of Biomedical Imaging and Image-guided Therapy, Medical University of Vienna, Vienna, Austria.
[2] Center for Biomarker Research in Medicine, CBmed GmbH, Graz, Austria.
[3] Preclinical Molecular Imaging, AIT Austrian Institute of Technology GmbH, Seibersdorf, Austria.
[4] Department of Clinical Pharmacology, Medical University of Vienna, Vienna, Austria.

The doctoral candidate performed many of the contributing radiosyntheses and quality controls and contributed to the interpretation of the results as well as to manuscript preparation.

Pichler *et al. EJNMMI Radiopharmacy and Chemistry* (2019) 4:31
https://doi.org/10.1186/s41181-019-0083-2

EJNMMI Radiopharmacy and Chemistry

RESEARCH ARTICLE Open Access

Pitfalls and solutions of the fully-automated radiosynthesis of [^{11}C]metoclopramide

Verena Pichler[1*], Marius Ozenil[1], Karsten Bamminger[1,2], Chrysoula Vraka[1], Marcus Hacker[1], Oliver Langer[1,3,4] and Wolfgang Wadsak[1,2]

* Correspondence: verena.pichler@meduniwien.ac.at
[1]Division of Nuclear Medicine, Department of Biomedical Imaging and Image-guided Therapy, Medical University of Vienna, Vienna, Austria
Full list of author information is available at the end of the article

Abstract

Background: [^{11}C]Metoclopramide is a new radiotracer for investigating the activity of P-glycoprotein at the blood-brain barrier. A highly stable and reproducible radiosynthesis is a prerequisite for clinical studies applying [^{11}C]metoclopramide or other ^{11}C-labelled radiotracers, therefore all potential pitfalls must be identified and monitored to allow a stable process.

Results: Long-term production ($n = 94$ in a time range of approximately 2 years) of [^{11}C]metoclopramide synthesized on two commercially available synthesizers yielded 3.9 ± 2.0 GBq of product with a molar activity of 132 ± 164 GBq/μmol and an overall success rate of 93%. During all successful productions, the product quality was in accordance with the recommendations of the European Pharmacopoeia. The most common pitfalls that were identified for the radiosynthesis included poor turnover into [^{11}C]CH_3OTf, decomposition of the solvent or insufficient semi-preparative HPLC performance.

Conclusion: The study provides long-term insight in the improved, robust and stable preparation of [^{11}C]metoclopramide for human use.

Keywords: [^{11}C]metoclopramide, carbon-11, radiosynthesis, blood-brain-barrier, PET

Background

[^{11}C]Metoclopramide is a novel positron emission tomography (PET) radiotracer, which has been developed to measure the activity of P-glycoprotein (P-gp) at the blood-brain-barrier, an important efflux transporter, which restricts the brain distribution of many different drugs (Bauer et al. 2019; Tournier et al. 2019; Auvity et al. 2018; Pottier et al. 2016). [^{11}C]Metoclopramide is a weak P-gp substrate, which has considerably higher brain uptake under conditions of full P-gp function as compared with previously described avid P-gp substrates for PET (e.g. [^{11}C]verapamil or [^{11}C]*N*-desmethyl-loperamide). Consequently, [^{11}C] metoclopramide may possess a better sensitivity to measure moderate changes in P-gp function at the blood-brain barrier than previously described radiotracers (Bauer et al. 2019). Carbon-11 is an attractive radionuclide for PET imaging as it allows to radiolabel most drug molecules without structural changes. Moreover, its short radioactive half-life (20.4 min) leads to relatively low radiation exposure of study participants and allows for repeated PET scanning within one imaging session (e.g. two consecutive scans without and with pre-treatment with a

Springer Open

© The Author(s). 2019 **Open Access** This article is distributed under the terms of the Creative Commons Attribution 4.0 International License (http://creativecommons.org/licenses/by/4.0/), which permits unrestricted use, distribution, and reproduction in any medium, provided you give appropriate credit to the original author(s) and the source, provide a link to the Creative Commons license, and indicate if changes were made.

P-gp inhibitor). For a successful clinical application, stable and reliable radiosynthesis procedures are therefore a prerequisite.

Here, we present the fully-automated radiosynthesis of [^{11}C]metoclopramide (Fig. 1) conducted with a GE TRACERlab™ FX C Pro or GE TRACERlab™ FX2 C system, respectively. The main pitfalls of the radiosynthesis were identified e.g. decomposition of solvent or insufficient separation on semi-preparative HPLC and appropriate solutions were implemented.

Material and methods

All chemicals were obtained from commercial sources and used as received. The precursor *O*-desmethyl-metoclopramide (GMP grade) as well as the reference compound metoclopramide (4-amino-5-chloro-*N*-[2-(diethylamino)ethyl]-2-methoxy-benzamide) were purchased from ABX (Radeberg, Germany). The Ni catalyst (Shimalilte Ni reduced, 80/100 mesh) was purchased from Shimadzu (Kyoto, Japan). SepPak® C18 plus cartridges for solid-phase extraction were purchased from Waters (Waters® Associates Milford, MA, USA). Low-protein binding Millex GS® 0.22 µm sterile filters were purchased from Millipore® (Bedford, MA, USA). The silver triflate column was prepared according to the recommendation of the module producer General Electric Medical System, Uppsala, Sweden. Silver triflate and carbopack adsorbent C, 80–100 mesh was obtained by Sigma Aldrich and used as received.

Instrumentation

[^{11}C]CO_2 was produced in a GE PETtrace 860 cyclotron (General Electric Medical System, Uppsala, Sweden) via the ^{14}N(p,α)^{11}C nuclear reaction by irradiation of a gas target (aluminium) filled with N_2 + 1% O_2 (Air Liquide, Vienna, Austria). Typical beam currents were 60–65 µA and the irradiation was stopped as soon as the desired activity level was reached (approx. 80–130 GBq [^{11}C]CO_2; corresponding to 30–40 min irradiation time). The synthesis of [^{11}C]metoclopramide starting from [^{11}C]CO_2 (Fig. 1) was performed in two different GE modules (GE Healthcare, Uppsala, Sweden), namely a TRACERlab™ FX C Pro and a TRACERlab™ FX2 C module. For analytical HPLC, an Agilent 1260 system was used, which was equipped with a quaternary pump (G1311B), a multi wavelength UV-detector (G1365D), a column oven (G1316A), a manual injector (G1328C), as well as a radio-detector controlled by GINA Star software (Elysia-Raytest; Straubenhardt, Germany). Osmolality of the formulated radiotracer solution was

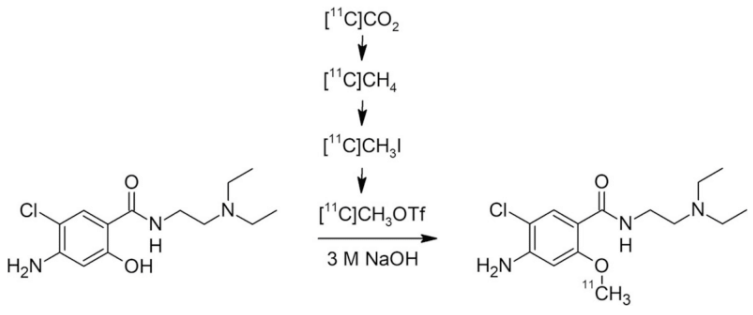


Fig. 1 Scheme for the radiosynthesis of [^{11}C]metoclopramide

measured using a Wescor osmometer Vapro® 5600 (Sanova Medical Systems, Vienna, Austria) and pH was always measured using a WTW inoLab 740 pH meter (WTW, Weilheim, Germany) for every released product. Gas chromatography was performed using a 430-GC system (Bruker Daltonik GmbH, Bremen, Germany) and a capillary column (forte GC Capillary Column ID-BP20; 12 m × 0.22 mm × 0.25 μm) from SGE Analytical Sciences Pty Ltd. (Victoria, Australia). Butanone was analysed with a Bruker Avance III 200 spectrometer (200 MHz for ^{1}H).

Preparation of the synthesizers

The flow charts of the TRACERlab™ FX C Pro and FX2 C are depicted in Fig. 2. All parts involved in the radiosynthesis were first flushed with helium and subsequently checked for tightness by applying a helium flow of 100 mL/min, which has to decrease below 4 mL/min when all lines are tightly sealed. The methyl iodide trap was heated to 200 °C for approximately 20 min and afterwards cooled down to ≤35 °C. The silver triflate column was preheated to 200 °C before start of the synthesis for approximately 15 min. The reaction vessels V1-V3 and the corresponding transfer lines via the reaction vial and HPLC injection loop into the waste were washed twice with water and acetone. Complete removal of all traces of solvent was assured by visual inspection of all connected tubes. The radiotracer formulation part of the module was washed with water and ethanol including the bulb and product collection vial. The preparation procedure was performed similarly for the GE TRACERlab™ FX C Pro and TRACERlab™ FX2 C. A detailed protocol for the module preparation was published recently (Vraka et al. 2019).

The reaction vials were filled with 1 mL water (aqua ad injectabilia; V2), 5 mL sodium chloride 9% (V4), 1.5 mL ethanol (V5) and 10 mL water (aqua ad injectabilia; V6). The bulb was filled with 80 mL of water (aqua ad injectabilia), a C18 Plus Sep-Pak (equilibrated with 10 mL ethanol and 20 mL water) was placed on the Sep-Pak position and 6 mL of phosphate buffered saline (prepared by Vienna General Hospital pharmacy, Austria; 0.021 M phosphate buffer, 0.188 M NaCl, pH 7.7) were placed in the product collection vial. For patient application, a product vial with sterile filter and sterile air ventilation was prepared in a laminar air flow cell and connected to the product tubing. Prior to use, the reaction vessel had been stored at 100 °C for at least 4 h. Immediately before start of the radiosynthesis, 1 mg of *O*-desmethyl-metoclopramide (3.5 μmol) was dissolved in 400 μL butanone and transferred to the reaction vessel. Then 7 μL of 3 M aqueous NaOH solution (21 μmol, 6 equivalents) was added to deprotonate the phenol.

Fully-automated radiosynthesis of [^{11}C]metoclopramide

The synthesis sequence started with a 15–20 min pre-run including heating of the carbon dioxide trap to 400 °C and subsequent cooling to < 50 °C. During the heating process, the trap was continuously flushed with helium (50 mL/min). When 400 °C was reached, 3 min of hydrogen pre-equilibration of the carbon dioxide trap took place. Afterwards the carbon dioxide trap was cooled to < 50 °C and the methane trap was cooled to − 75 °C ending the pre-run with the comment 'ready to receive activity'.

The automatic radiosynthesis was then started by delivering 116 ± 17 GBq of [^{11}C]CO_2 to the carbon dioxide trap and confirmation of the end of delivery. The gas

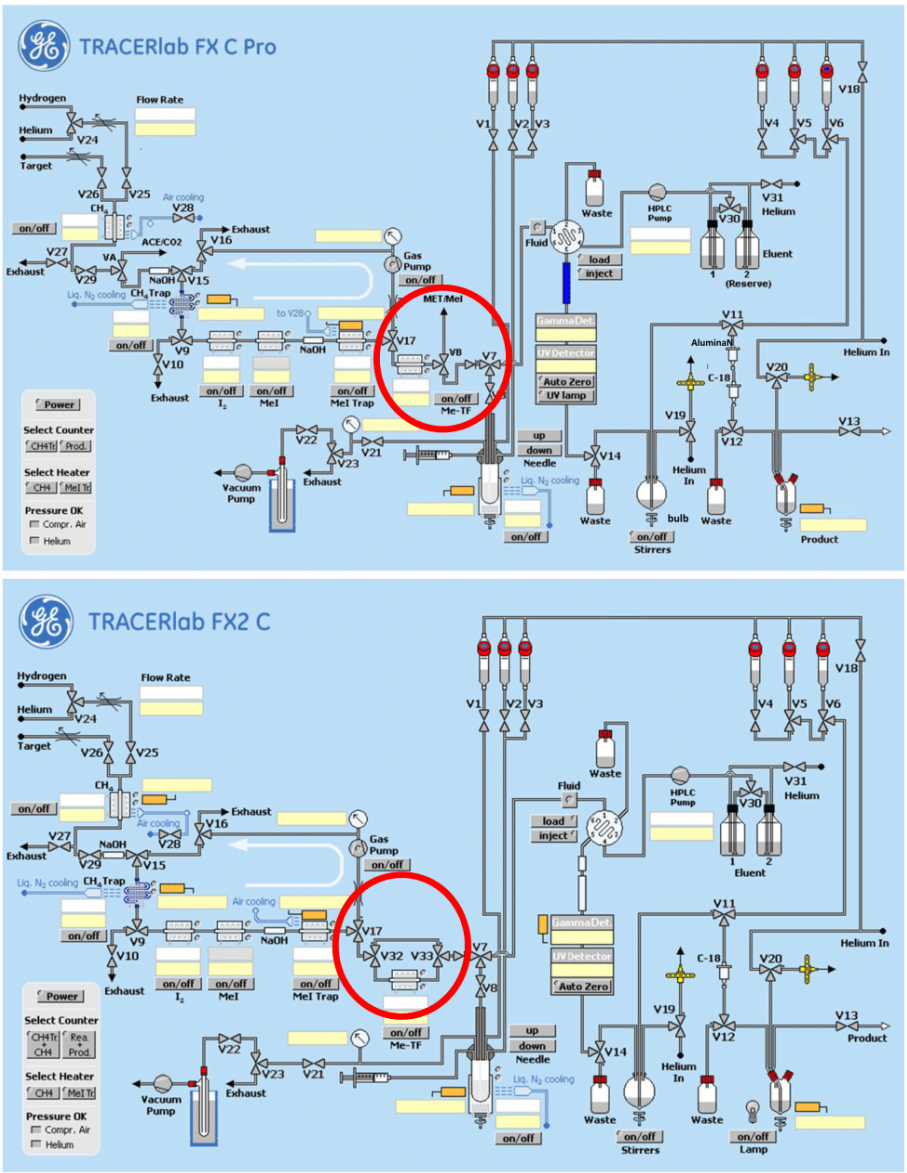


Fig. 2 Flow charts of the used synthesis modules TRACERlab™ FX C Pro and TRACERlab™ FX2 C. The major differences between the set-ups concern the installation of the silver triflate column are highlighted (red circle)

phase transformation of $[^{11}C]CO_2$ via the formation of $[^{11}C]CH_4$ produced approximately 50 GBq of $[^{11}C]CH_3I$ and has been described in detail elsewhere (Vraka et al. 2019; Pichler et al. 2018a; Philippe et al. 2018; Larsen et al. 1997). $[^{11}C]CH_3OTf$ was produced by passing $[^{11}C]CH_3I$ gas through the silver triflate column at 200 °C. After completion of the activity trapping within the reaction mixture, the reaction took place at 110 °C for 2 min. Afterwards the reaction mixture was quenched with water from V2 and transferred to the semi-preparative HPLC via the injection valve. For semi-preparative HPLC, a SUPELCOSIL LC-ABZ+ column (5 µm, 250 mm × 10 mm) from Merck (Darmstadt, Germany) was eluted with freshly prepared 20 mM aqueous

NaH_2PO_4 / acetonitrile (80/20) at a flow rate of 5 mL/min with UV absorption measured at 254 nm (Fig. 3).

In total, 70 syntheses were performed on the TRACERlab™ FX C Pro, of which the first eight syntheses were performed for establishment and evaluation of the automated radiosynthesis and analytical and preparative HPLC establishment. These syntheses were excluded from statistical analysis as the final activity yield was not always measured. Three syntheses failed, caused by insufficient transfer of the activity into the reactor (no formation of $[^{11}C]CH_3I$ or $[^{11}C]CH_3OTf$), insufficient separation or no product formation at all besides other technical issues. Thirty-eight radiosyntheses were performed so far on the GE TRACERlab™ FX2 C, of which six syntheses were performed for validation of the new module (excluded data) and four synthesis failed. Out of these productions (n = 94, excluding test syntheses, 7 fail synthesis), 81 radiosynthesis were released for clinical application, the remaining six productions were released but for other applications. Details on optimization radiosyntheses performed, which were not released for human application but are included in the overall analysis are shown in Table 1. The success rate of $[^{11}C]$metoclopramide produced on TRACERlab™ FX C Pro or GE TRACERlab™ FX2 C was 95 and 88%, respectively. The productions were performed between August 2017 and September 2019. The change of the synthesis module was implemented in December 2018.

Quality control of $[^{11}C]$metoclopramide

The quality control parameters encompassed the parameters pH, osmolality, organic solvent content, radionuclidic purity, radiochemical and chemical purity as well as biological testing of sterility and endotoxins. All tests performed were in accordance with the recommendations of the European Pharmacopoeia for other ^{11}C-radiotracers. The chemical and radiochemical purity was measured by means of RP-HPLC using an X-Bridge BEH Shield RP-18, 4.6 × 50 mm, 2.5 µm, 130 Å (Waters GmbH) column eluted at a flow rate of 1 mL/min with a gradient program (Fig. 4) of the following solvents:

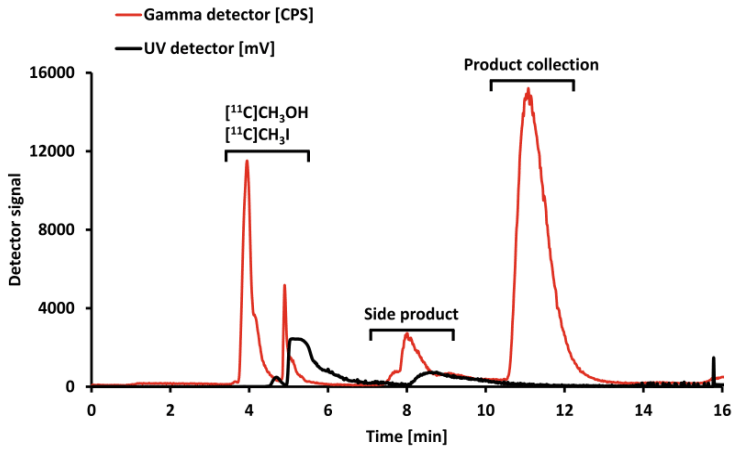


Fig. 3 Typical semi-preparative RP-HPLC chromatogram of a $[^{11}C]$metoclopramide radiosynthesis including the signal of the UV-detector (254 nm, black) and radio-detector (red). The product peak has a retention time of approximately 10.5–12.5 min

Table 1 Overview on evaluation batches and overall yield of [^{11}C]metoclopramide productions with changing reaction conditions

Solvent	Reactive synthon	RCY (% based on [^{11}C]CO_2, decay corrected)	Activity yield [GBq]
Acetone ($n = 3$)	[^{11}C]CH_3OTf	20.7 ± 4.5%	5.4 ± 1.2
Butanone ($n = 3$, evaluation batches)	[^{11}C]CH_3OTf	20.8 ± 3.8%	6.3 ± 1.7
Butanone ($n = 1$)	[^{11}C]CH_3I	no product	0
Butanone ($n = 94$, overall productions)	[^{11}C]CH_3OTf	13.2 ± 6.7	3.9 ± 2.0

solvent A: aqueous acetonitrile (90%), solvent B: water and solvent C: aqueous ammonium phosphate buffer (50 mM), pH 9.3 adjusted with NaOH (Nics et al. 2018). The retention time of the precursor *O*-desmethyl-metoclopramide was between 1 min 20 s to 1 min 50 s and for the product [^{11}C]metoclopramide 2 min 50 s to 3 min 20 s (Fig. 5). The calibration curve was set up at 225 nm for the concentration range 0.1–5 μg/mL (0.1, 0.5, 2, 3.5 and 5 μg/mL standards) including blank measurements all performed in at least three repetitions (Fig. 4).

The retention times were checked prior every radiosynthesis by injection of the respective reference compounds. Both, the semi-preparative as well as the analytical HPLC systems were tested for the retention times of the reactive intermediates methyl iodide, methyl triflate and methanol (from the reaction of methyl triflate with water) as well as [^{11}C]CH_3I, [^{11}C]CH_3OTf, [^{11}C]CO_2 and a mixture of [^{11}C]CH_3OTf with water (for the retention time of [^{11}C]CH_3OH).

Statistical analysis

Yield calculation consisted of the measured activity of the product in GBq corrected for decay divided by the produced starting activity of [^{11}C]CO_2 in GBq and is expressed in % if not stated otherwise (Coenen et al. 2017).

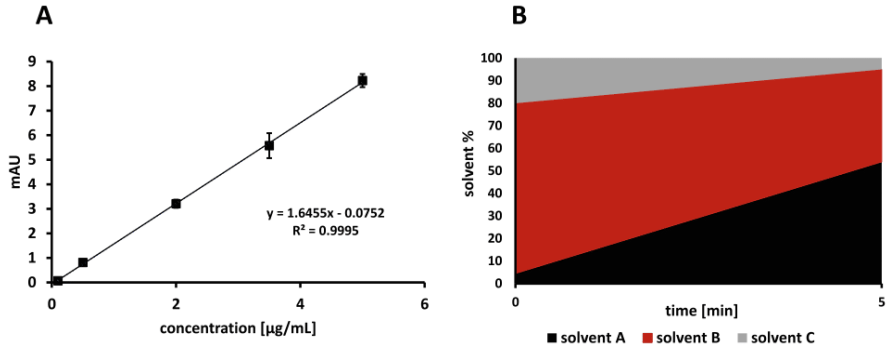


Fig. 4 a Calibration curve of metoclopramide in the range of 0.1–5 μg/mL measured at a wavelength of 225 nm. The limit of detection and limit of quantification were 0.2 μg/mL and 0.7 μg/mL, respectively. **b** Gradient for the analytical RP-HPLC for the quality control of [^{11}C]metoclopramide. The mobile phase consist of solvent A: aqueous acetonitrile (90%), solvent B: water and solvent C: aqueous ammonium phosphate buffer (50 mM), pH 9.3 adjusted with NaOH

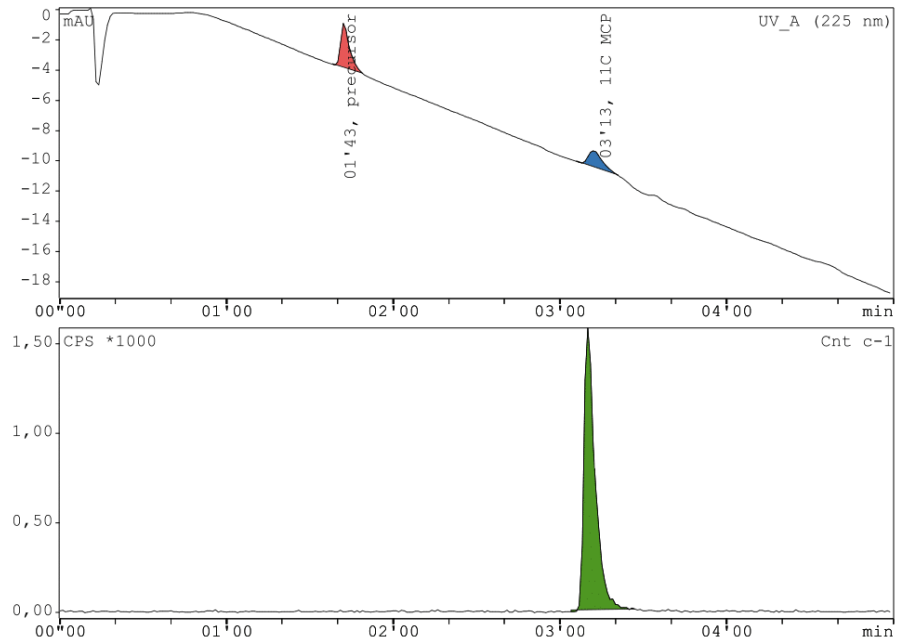


Fig. 5 Exemplary analytical RP-HPLC chromatogram of [^{11}C]metoclopramide formulated for i.v. injection including the signal of the UV-detector (225 nm, upper channel) and radio-detector (lower channel)

If not indicated otherwise, all values are depicted as mean ± standard deviation. All results derived from synthesis or quality control were analysed by means of MS Excel® 2013. Significance was tested with GraphPad Prims 6 by means of t test analysis.

Results and discussion

Automated radiosynthesis optimization for human application

Starting from 116 ± 17 GBq of [^{11}C]CO_2, 39 ± 13 GBq of [^{11}C]CH_3OTf was trapped in 400 µL butanone within the reactor containing *O*-desmethyl-metoclopramide and aqueous sodium hydroxide solution after approximately 15 min. In the original radiosynthesis published by F. Caillé and coworkers (Caillé et al. 2018) the [^{11}C]CH_3OTf was trapped at − 20 °C in acetone, with subsequent heating to 110 °C. This radiosynthesis had to be adjusted in order to minimize mechanical strain caused by heating acetone over the boiling point and to reduce the effort of maintenance of the synthesis modules, although the chemical turnover in acetone and butanone was comparable during the establishment process (see Table 1). For this reason, the solvent acetone was exchanged by butanone, which additionally enabled the omission of the cooling during the [^{11}C]CH_3OTf trapping step due to its higher boiling point. The trapping efficiency of [^{11}C]CH_3OTf in acetone and butanone was approximately 80% (non-decay corrected), in accordance to previously published data (Pichler et al. 2018b). Afterwards, the reaction solution was heated to 110 °C for 2 min, cooled to ≤35 °C and quenched with water. Semi-preparative radio-HPLC (Fig. 3) revealed the presence of the following radioactive peaks: [^{11}C]CH_3I and [^{11}C]CH_3OH (from the reaction of [^{11}C]CH_3OTf and water) at early retention times between 3 and 6 min, followed by a minor unknown side product at 8 min and the desired product fraction at approximately 12 min. In contrast

to a previous study (Caillé et al. 2018) the semi-preparative HPLC column was changed from a Waters Symmetry® C18 7.8 × 300 mm, 7 µm column to a SUPELCOSIL LC-ABZ+ column. After the semi-preparative HPLC purification (Fig. 3), 3.9 ± 2.0 GBq of product was isolated, which corresponded to a radiochemical yield of 13 ± 7% (based on the starting activity of $[^{11}C]CO_2$, decay-corrected) or 23 ± 11% (based on trapped $[^{11}C]CH_3I$, decay-corrected).

Molar activity and quality control

The molar activity of the final formulated product was 132 ± 164 GBq/µmol (range: 5–659 GBq/µmol). The molar activity was calculated according to the recently published nomenclature and harmonization guidelines (Coenen et al. 2017). The calibration curve as well as the limits of quantification and detection were determined according to ICH (International Council for Harmonisation) guidelines (see Fig. 4) (Balaram et al. 2011). If the concentration of metoclopramide was below the limit of detection (LOD), the value was set to the LOD of 0.2 µg/mL for molar activity calculation. Hence, the molar activity was presumably even better than stated in 11 out of 94 production runs, due to hitting the detection limits of the analytical method.

The quality control parameters are listed in Table 2. The parameter radiochemical purity, radionuclidic purity (γ spectrum), half-life, residual solvents as well as the physiological parameters pH and osmolality were measured before release of the product. Sterility and endotoxin testing were performed after decay of the radioactivity. All parameters were in accordance with the recommendations of the European Pharmacopoeia as applied for other ^{11}C-radiotracers (European Directorate for the Quality of Medicines (EDQM) 2016).

Differences and similarities of TRACERlab™ FX C Pro and TRACERlab™ FX2 C

In general, the productions with the TRACERlab™ FX C Pro afforded significantly lower molar activities (62 ± 80 GBq/µmol) than the newly installed TRACERlab™ FX2 C (299 ± 184 GBq/µmol). This considerable difference in molar activity can presumably be explained by the long usage of the TRACERlab™ FX C Pro leading to carbon deposits. A detailed analysis of potential sources of carbon load in synthesizers has been

Table 2 Quality control parameters for all released batches ($n = 81$) of $[^{11}C]$metoclopramide according to the recommendations of the European Pharmacopoeia for ^{11}C-radiotracers

Quality control parameter	Release criteria	Quality control
Radiochemical purity	> 95%	99 ± 1%
Molar activity	no release criteria	132 ± 164 GBq/µmol
Half-life	20.3 ± 2.0 min	19.4 ± 0.8 min
Radionuclidic purity (y-line)	430–520 keV	505 ± 15 keV
Residual solvents	< 410 ppm per solvent	< 410 ppm butanone
		< 410 ppm acetonitrile
	< 10% ethanol	< 10% ethanol
pH	4.5–8.5	7.5 ± 0.2
Osmolality	200–400 mosm/kg	316 ± 37 mosm/kg
Sterility	pass	pass
Endotoxins	Pass	pass

published by our group recently (Pichler et al. 2018b). The final radioactivity amount of [^{11}C]metoclopramide at the end of synthesis was slightly higher for the TRACERlab™ FX C Pro than for the TRACERlab™ FX2 C (4.2 ± 1.9 GBq versus 3.4 ± 2.2 GBq, not significant).

The synthetic program of [^{11}C]metoclopramide of the TRACERlab™ FX C Pro had to be adjusted for the TRACERlab™ FX2 C to implement the synthesis of [^{11}C]metoclopramide. The main difference between the modules is the changed installation of the silver triflate column (Fig. 2). For the TRACERlab™ FX C Pro, the silver triflate column has to be inserted before the synthesis in a horizontal position. Here, the main disadvantage lies in the recurrent manual removal and therefore opening of the column which may lead to the introduction of humidity. On the other hand, the exchange of the connecting tubes is easy and fast. For the TRACERlab™ FX2 C, the silver triflate column has a smaller column diameter, and the column is inserted in a vertical position. Here, the silver triflate column can be automatically by-passed and therefore the main disadvantage of the TRACERlab™ FX C Pro was overcome. However, a disadvantage of the TRACERlab™ FX2 C is the inaccessibility of the connecting tubing between the [^{11}C]CH_3I trap and the silver triflate column. Additionally, the heating and cooling of the silver triflate column has to take place in a mode where the valves are closed and therefore the column may be pressurized.

Analysis of pitfalls of the [^{11}C] metoclopramide production

Overall synthesis success rate was 93% combined for both modules (n = 94). The identified problems are depicted in Fig. 6. The first step with potential failure was the [^{11}C]CH_3I production, for which in some cases no conversion of [^{11}C]CH_4 into [^{11}]CH_3I was observed. A higher failure rate was due to insufficient transformation of [^{11}C]CH_3I into the more reactive intermediate [^{11}C]CH_3OTf. In these cases activity was either trapped on the silver triflate column or the activity was successfully transferred to the reactor, but no reaction took place due to insufficient amounts of [^{11}C]CH_3OTf. During the semi-preparative HPLC purification step two possible failure scenarios occurred: firstly, there was a poor separation between the side product and the [^{11}C]metoclopramide fraction leading to an impure product and subsequently inhibiting product release. Secondly,

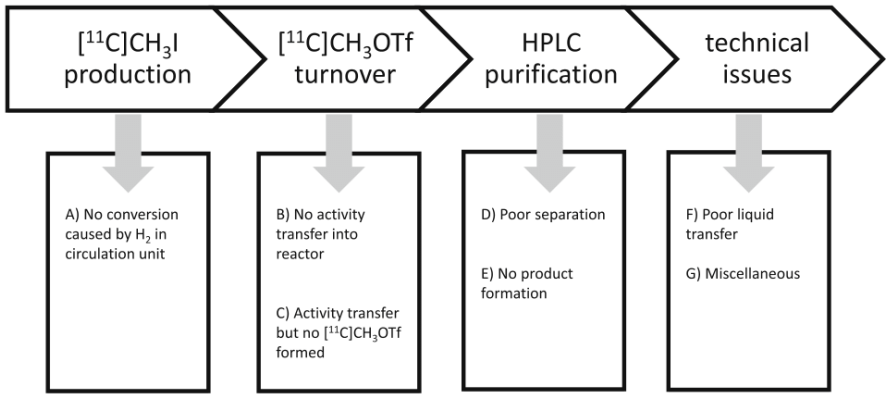


Fig. 6 Scheme of the pitfalls of [^{11}C]metoclopramide synthesis

there was no product formation at all, which may be attributed to insufficient conversion of [^{11}C]CH_3I into [^{11}C]CH_3OTf or resulting from traces of decomposed butanone. A test synthesis using [^{11}C]CH_3I as reactive synthon proved the necessity of [^{11}C]CH_3OTf for the preparation of [^{11}C]metoclopramide (see Table 1). All other synthesis failures were attributable to technical issues like clogging of tubings or valves.

Pitfalls of [^{11}C]CH_3I production

In general, the gas-phase [^{11}C]CH_3I production was very stable and reproducible as described before (Pichler et al. 2018b). However, a potential source of failure in the [^{11}C]CH_3I production could be identified in the course of the evaluation of [^{11}C]metoclopramide. In these cases, the characteristic pattern of the re-circulation of [^{11}C]CH_4 and trapping of [^{11}C]CH_3I was not observed. Instead, the radioactivity was passing through the [^{11}C]CH_3I trap without any trapping (see Fig. 7). Hence, this failure in [^{11}C]CH_3I production was therefore visible within the first few seconds of the re-circulation process. Once the failure in trapping was noticed, the circulation unit could be flushed with helium and the synthesis could be immediately re-started, as the precursor solution was not affected. In these rare cases, the second run was always successful.

The cause for this failure could be confirmed and the erroneous circulation pattern could be reproduced when the whole circuit unit was flushed with hydrogen (100 mL/min for 2–3 min) instead of helium prior to the [^{11}C]CH_3I production. The introduction of hydrogen into the unit is only explicable, if a valve is leaking or a faulty circuit happens during the conditioning of the CO_2 trap. Other (non-commercial) gas-phase [^{11}C]CH_3I production units are not trapping the formed [^{11}C]CH_4 on a cooled methane trap (personal communication, see also methane trap in Fig. 2) and therefore the produced [^{11}C]CH_4 is not separated from remaining [^{11}C]CO_2 and unreacted H_2. As the production of [^{11}C]CH_3I in these production units is working properly, we assume that this problem may only occur in presence of high amounts of hydrogen.

Validation of [^{11}C]CH_3OTf production

Overall, the [^{11}C]CH_3OTf production was more prone to failure than the [^{11}C]CH_3I production and was the main source of synthesis failure. With the set-up of the

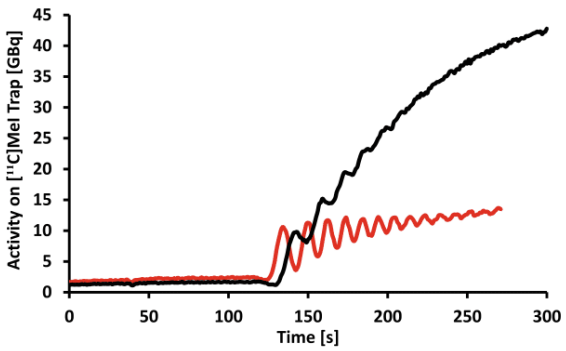


Fig. 7 Progression of the turnover of [^{11}C]CH_4 to [^{11}C]CH_3I and trapping of the activity on the methyl iodide trap, for a successful reaction (black) and failed reaction caused by presence of hydrogen (red) in the circulation unit of the GE TRACERlab™ FX C Pro synthesizer

TRACERlab™ FX2 C module, two different unwanted scenarios were observed. In the first scenario, the [^{11}C]CH_3I was either almost completely trapped on the silver triflate column or insufficiently transferred from the silver triflate column into the reactor. In the second scenario, a very good transfer of the radioactivity into the reactor was observed, but there was no conversion of [^{11}C]CH_3I into [^{11}C]CH_3OTf. The trapping of the [^{11}C]CH_3I on the silver triflate column primarily occurred in our facility, when the silver triflate column was exposed to humidity. However, the main source of failure was the insufficient transformation of [^{11}C]CH_3I into [^{11}C]CH_3OTf. Consequently, the silver triflate column must be checked and replaced regularly in order to guarantee a stable process. The exchange of the silver triflate column was performed every 15th–20th synthesis for the GE TRACERlab™ FX C Pro. The successful transformation of [^{11}C]CH_3I into [^{11}C]CH_3OTf was indirectly detected by analytical HPLC analysis of the crude reaction mixture. Although [^{11}C]CH_3I reacts with water of the mobile phase to [^{11}C]CH_3OH, a certain amount of non-reacted [^{11}C]CH_3I was detectable (see Fig. 8). [^{11}C]CH_3OTf, on the other hand, reacts very quickly with water, so that no

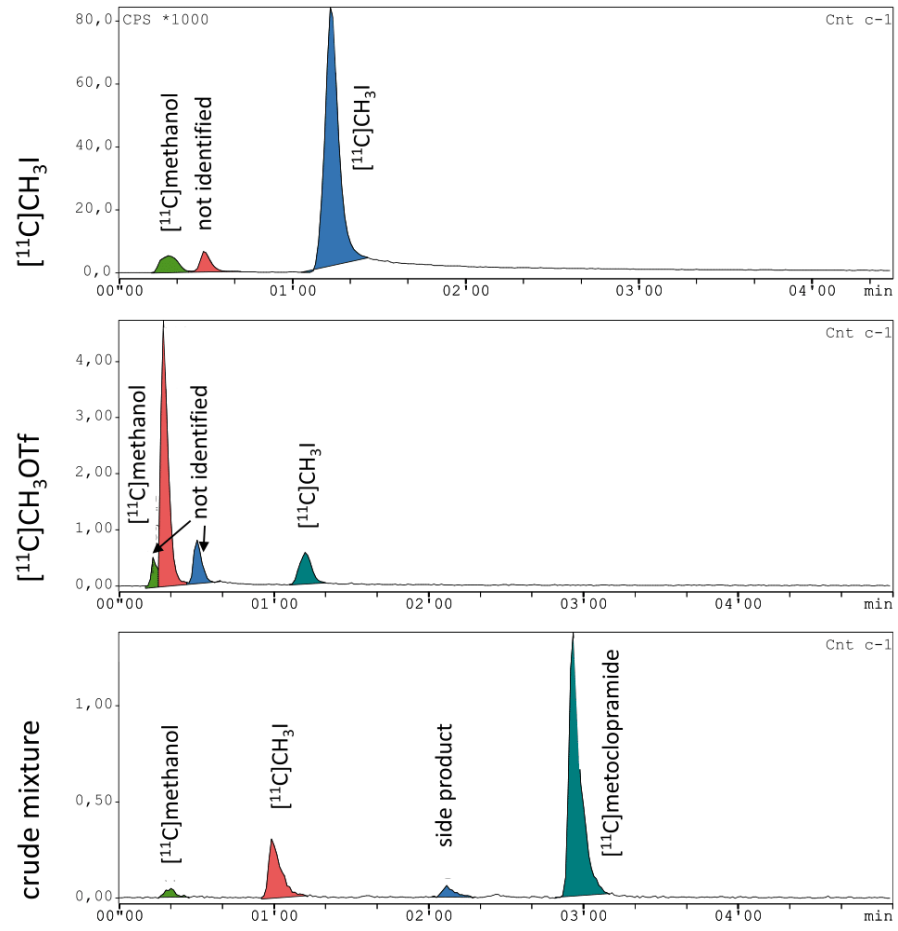


Fig. 8 Radio-HPLC analysis of [^{11}C]CH_3I, [^{11}C]CH_3OTf and crude reaction mixture. The individual peaks were identified by co-injection of commercially available unlabelled reference compounds. The analyzed [^{11}C]CH_3OTf batch contained approximately 13% of [^{11}C]CH_3I due to incomplete conversion of [^{11}C]CH_3I into [^{11}C]CH_3OTf. [^{11}C] methanol originates from the reaction of [^{11}C]CH_3OTf with water. A similar phenomenon was seen for the crude reaction mixture

[^{11}C]CH_3OTf peak is detectable but a pronounced [^{11}C]CH_3OH peak. For failure analysis after the synthesis, the injection of the crude reaction mixture into analytical HPLC allows the following conclusions: (i) a detectable [^{11}C]CH_3I peak indicated an insufficient conversion to [^{11}C]CH_3OTf, which considerably lowers the radiochemical yield; (ii) if only the [^{11}C]CH_3OH peak was present, the reaction of [^{11}C]CH_3I to [^{11}C]CH_3OTf took place, so that other factors, like insufficiently inert atmosphere, among others, were responsible for low product conversion.

Separation efficiency of semi-preparative HPLC and other technical issues

A poor semi-preparative chromatogram was present, when either there was an insufficient separation of product and side product or there was no product formation at all. For an efficient purification of [^{11}C] metoclopramide it was necessary to prepare the mobile phase freshly at least once per week. Otherwise the tailing of the [^{11}C]metoclopramide peak enhanced (Fig. 9), as well as the amount of the side peak at around 8 min appeared to increase. Analysis of the collected semi-preparative HPLC product fraction by analytical HPLC showed that the collected peak consist of both, side product and [^{11}C]metoclopramide. Exchange of the HPLC solvent restored the separation and reduced the peak at approximately 8 min.

A reduced or no formation of the product was either due to poor [^{11}C]CH_3OTf formation but also caused by decomposition of the butanone after long time usage (Fig. 9). Acetone is known to undergo aldol reactions when stored on molecular sieves (JoVE Science Education Database 2019). However, GC and ^{1}H-NMR did not show any aldol reaction product in amounts higher than 0.01% (GC analysis) or at all (^{1}H-NMR) in butanone, which was stored over molecular sieves for more than 6 months. Still, the olfactory differences between the bottle of butanone stored over molecular sieves and a bottle of butanone without molecular sieves suggests that butanone underwent molecular sieve-catalyzed reactions. This small amount of formed aldol product might still be enough to interfere with the radiolabeling via [^{11}C]CH_3OTf. Therefore, a regular exchange of butanone at least every 3 months is recommended.

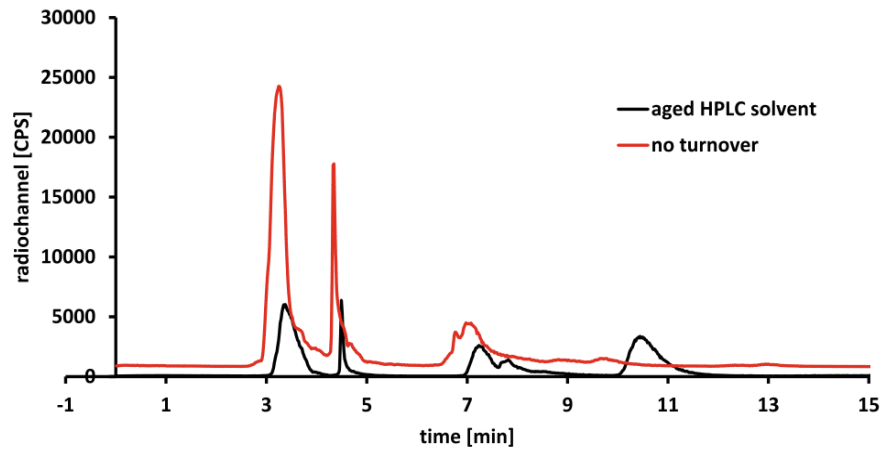


Fig. 9 Insufficient semi-preparative RP-HPLC chromatograms caused by aged HPLC solvent (black) or decomposed butanone (red)

Conclusion

[^{11}C]Metoclopramide was reliably synthesized on both, a GE TRACERlab™ FX C Pro and GE TRACERlab™ FX2 C synthesis module, for more than 100 synthesis in good yields and high molar activities. The quality of the final product was in accordance with the recommendations of the European Pharmacopoeia for other ^{11}C-radiotracers. The main technical problems were identified, and individual solutions were developed in order to keep synthesis failures at a minimum.

Abbreviations

PET: positron emission tomography; P-gp: P-glycoprotein; RP-HPLC: reversed phase-high performance liquid chromatography

Acknowledgements

The authors thank A. Krcal and T. Zenz for their continuous technical support, F. Caillé (Service Hospitalier Frédéric Joliot, Orsay, France) for advice regarding the set-up of the radiosynthesis and K. Pallitsch for the preparation of silver triflate on carbon. Moreover, the Medical Imaging Cluster at the Medical University of Vienna is acknowledged for supporting this study.

Authors' contributions

VP, MO and CV conducted the radiosynthesis and quality controls. VP, MO and KB interpreted the results. VP, MO and OL wrote the manuscript. WW and MH contributed to the design of the experiments and contributed to the writing of the manuscript. All authors read and approved the final manuscript.

Funding

This work was supported by the Austrian Science Fund (FWF) (grant KLI 694-B30, to O. Langer).

Availability of data and materials

Please contact corresponding author for data request.

Ethics approval and consent to participate

This article does not contain any studies with human participants or animals performed by any of the authors.

Consent for publication

Not applicable.

Competing interests

All authors declare that they have no financial conflict or competing interests to disclose.

Author details

[1]Division of Nuclear Medicine, Department of Biomedical Imaging and Image-guided Therapy, Medical University of Vienna, Vienna, Austria. [2]Center for Biomarker Research in Medicine, CBmed GmbH, Graz, Austria. [3]Preclinical Molecular Imaging, AIT Austrian Institute of Technology GmbH, Seibersdorf, Austria. [4]Department of Clinical Pharmacology, Medical University of Vienna, Vienna, Austria.

Received: 18 October 2019 Accepted: 4 December 2019
Published online: 18 December 2019

References

Auvity S, Caillé F, Marie S, Wimberley C, Bauer M, Langer O, et al. P-glycoprotein (ABCB1) inhibits the influx and increases the efflux of 11 C-metoclopramide across the blood–brain barrier: a PET study on nonhuman Primates. J Nucl Med. 2018; 59(10):1609–15.

Balaram G, Munjal P, Dhagash AP. Validation of analytical procedures: methodology ICH-Q2B. Int J Pharm Innov. 2011;2249–1031(1):45–50.

Bauer M, Tournier N, Langer O. Imaging P-glycoprotein function at the blood–brain barrier as a determinant of the variability in response to central nervous system drugs. Clin Pharmacol Ther. 2019;105(5):1061–4.

Caillé F, Goutal S, Marie S, Auvity S, Cisternino S, Kuhnast B, et al. Positron emission tomography imaging reveals an importance of Saturable liver uptake transport for the pharmacokinetics of metoclopramide. Contrast Media Mol Imaging. 2018;2018:7310146.

Coenen HH, Gee AD, Adam M, Antoni G, Cutler CS, Fujibayashi Y, et al. Consensus nomenclature rules for radiopharmaceutical chemistry – setting the record straight. Nucl Med Biol. 2017;55:v–xi.

European Directorate for the Quality of Medicines (EDQM). General Monograph 0125 - radiopharmaceutical preparations in european pharmacopoeia. Strasbourg: Council of Europe; 2016.

JoVE Science Education Database. Organic chemistry preparing anhydrous reagents and equipment. Cambridge: JoVE; 2019.

Larsen P, Ulin J, Dahlstrøm K, Jensen M. Synthesis of [11C] iodomethane by iodination of [11C]methane. Appl Radiat Isot. 1997;48(2):153–7.

Nics L, Steiner B, Klebermass E-M, Philippe C, Mitterhauser M, Hacker M, et al. Speed matters to raise molar radioactivity: fast HPLC shortens the quality control of C-11 PET-tracers. Nucl Med Biol. 2018;57:28–33.

Philippe C, Mairinger S, Pichler V, Stanek J, Nics L, Mitterhauser M, et al. Comparison of fully-automated radiosyntheses of [11C] erlotinib for preclinical and clinical use starting from in target produced [11C]CO2 or [11C]CH4. EJNMMI Radiopharm Chem. 2018;3:1–9.
Pichler V, Vraka C, Berroterán-Infante N, Krcal A, Eidherr H, Traub-Weidinger T, et al. L-[S-methyl-11C] methionine – an example of radiosynthetic optimization. Appl Radiat Isot. 2018a;141(May):107–11.
Pichler V, Zenz T, Philippe C, Vraka C, Berrotéran-Infante N, Pfaff S, et al. Molar activity – the keystone in 11C-radiochemistry: an explorative study using the gas phase method. Nucl Med Biol. 2018b;67:21–6.
Pottier G, Marie S, Goutal S, Auvity S, Peyronneau M-A, Stute S, et al. Imaging the impact of the P-glycoprotein (ABCB1) function on the brain kinetics of metoclopramide. J Nucl Med. 2016;57(2):309–14.
Tournier N, Bauer M, Pichler V, Nics L, Klebermass EM, Bamminger K, et al. Impact of P-glycoprotein function on the brain kinetics of the weak substrate 11C-metoclopramide assessed with PET imaging in humans. J Nucl Med. 2019;60(7):985–91.
Vraka C, Pichler V, Pfaff S, Balber T, Hacker M, Mitterhauser M, et al. Technical aspect of the automated synthesis and real-time kinetic evaluation of [^{11}C]SNAP-7941. J Vis Exp. 2019;146:1–10.

Publisher's Note

Springer Nature remains neutral with regard to jurisdictional claims in published maps and institutional affiliations.

Submit your manuscript to a SpringerOpen journal and benefit from:

► Convenient online submission
► Rigorous peer review
► Open access: articles freely available online
► High visibility within the field
► Retaining the copyright to your article

Submit your next manuscript at ► springeropen.com

3.5. Molar activity – The keystone in ^{11}C-radiochemistry: An explorative study using the gas phase method

Verena Pichler,[1] Thomas Zenz,[1] Cécile Philippe,[1] Chrysoula Vraka,[1] Neydher Berrotéran-Infante,[1] Sarah Pfaff,[1] Lukas Nics,[1] **Marius Ozenil**,[1] Oliver Langer,[1,2,3] Matthäus Willeit,[4] Tatjana Traub-Weidinger,[1] Rupert Lanzenberger,[4] Markus Mitterhauser,[1,5] Marcus Hacker,[1] Wolfgang Wadsak[1,6]

[1] Department of Biomedical Imaging and Image-guided Therapy, Division of Nuclear Medicine, Medical University of Vienna, Vienna, Austria
[2] Department of Clinical Pharmacology, Medical University of Vienna, Vienna, Austria
[3] Center for Health and Bioresources, AIT Austrian Institute of Technology GmbH, Seibersdorf, Austria
[4] Department of Psychiatry and Psychotherapy, Division of General Psychiatry, Medical University of Vienna, Vienna, Austria
[5] Ludwig-Boltzmann-Institute Applied Diagnostics, Vienna, Austria
[6] CBmed GmbH - Center for Biomarker Research in Medicine, Graz, Austria

The doctoral candidate performed several of the contributing radiosyntheses and quality controls and contributed to the interpretation of the results as well as to manuscript preparation.

Nuclear Medicine and Biology 67 (2018) 21–26

Contents lists available at ScienceDirect

Nuclear Medicine and Biology

journal homepage: www.elsevier.com/locate/nucmedbio

Molar activity – The keystone in ^{11}C-radiochemistry: An explorative study using the gas phase method

Verena Pichler [a,*], Thomas Zenz [a], Cécile Philippe [a], Chrysoula Vraka [a], Neydher Berrotéran-Infante [a], Sarah Pfaff [a], Lukas Nics [a], Marius Ozenil [a], Oliver Langer [a,b,c], Matthäus Willeit [d], Tatjana Traub-Weidinger [a], Rupert Lanzenberger [d], Markus Mitterhauser [a,e], Marcus Hacker [a], Wolfgang Wadsak [a,f]

[a] Department of Biomedical Imaging and Image-guided Therapy, Division of Nuclear Medicine, Medical University of Vienna, Vienna, Austria
[b] Department of Clinical Pharmacology, Medical University of Vienna, Vienna, Austria
[c] Center for Health and Bioresources, AIT Austrian Institute of Technology GmbH, Seibersdorf, Austria
[d] Department of Psychiatry and Psychotherapy, Division of General Psychiatry, Medical University of Vienna, Vienna, Austria
[e] Ludwig-Boltzmann-Institute Applied Diagnostics, Vienna, Austria
[f] CBmed GmbH - Center for Biomarker Research in Medicine, Graz, Austria

ARTICLE INFO

Article history:
Received 10 July 2018
Received in revised form 28 September 2018
Accepted 29 September 2018

Keywords:
Molar activity
Specific activity
Carbon-11
Automated synthesis

ABSTRACT

Introduction: Radiochemists/radiopharmacists, involved in the preparation of radiopharmaceuticals are regularly confronted with the requirement of continuous high quality productions in their day-to-day business. One of these requirements is high specific or molar activity of the radiotracer in order to avoid *e.g.* receptor saturation and pharmacological or even toxic effects of the applied tracer for positron emission tomography. In the case of ^{11}C-labeled radiotracers, the reasons for low molar activity are manifold and often the search for potential ^{12}C-contaminations is time-consuming.
Methods: In this study, diverse ^{12}C-contaminations were analyzed and quantified, which occurred during >450 syntheses of six PET tracers using [^{11}C]CO_2 or [^{11}C]CH_3I generated *via* the gas phase method in a commercially available synthesizer. Additionally, non-radioactive syntheses were performed in order to identify the origins of carbon-12.
Results: The manifold contributions to low molar activity can be attributed to three main categories, namely technical parameters (*e.g.* quality of target gases, reagents or tubings), inter/intralaboratory parameters (*e.g.* maintenance interval, burden of the module, *etc.*) and interoperator parameters (*e.g.* handling of the module).
Conclusion: Our study provides a better understanding of different factors contributing to the overall carbon load of a synthesis module, which facilitates maintenance of high molar activity of carbon-11-labeled radiopharmaceuticals.

© 2018 Elsevier Inc. All rights reserved.

1. Introduction

^{11}C-labeled radiotracers for application in positron emission tomography (PET) play an important role in neuroimaging, especially for *in vivo* analysis of receptor expression and disease-induced alterations thereof in the brain. The concept of molar activity is especially relevant for potential receptor occupancy and saturation, as well as to avoid undesired pharmacological effects. In small-animal PET measurement, it is *e.g.* stated that the receptor saturation should be below 5%, and reasonably, an exceptionally high molar activity is necessary [1]. As a result, the radioactivity as well as the moles of the substance are determined for these PET-tracers and their ratio is called the molar activity. Just recently, Coenen et al. started a movement for standardization of radiopharmaceutical nomenclature und definitions. Accordingly, the term molar activity (A_m) is used for 'the measured radioactivity per mole of compound measured in Bq/mol or GBq/μmol'. Besides, the measured activity per gram of compound in Bq/g or GBq/g is designated as specific activity (A_S) [2].

It is obvious, that time is an important factor in radiochemistry, as the molar activity is continuously decreasing over time due to radioactive decay. Time has a higher impact on short-lived radionuclides (such as carbon-11) compared to longer-lived ones (like fluorine-18). Furthermore, ^{11}C-chemistry displays another characteristic making the molar activity even more crucial compared to productions of PET tracers with a different radiolabel. Most ^{11}C-tracer productions start with [^{11}C]CO_2 and, unfortunately, the non-radioactive contaminant CO_2 is ubiquitous in surrounding air, whereas it is rather unlikely that *e.g.* cyclotron produced fluorine-18 is, besides other sources, contaminated with high amounts of naturally occurring fluorine-19 *per se*.

* Corresponding author at: Waehringer Guertel 18-20, 1090 Vienna, Austria.
E-mail address: verena.pichler@meduniwien.ac.at (V. Pichler).

https://doi.org/10.1016/j.nucmedbio.2018.09.003
0969-8051/© 2018 Elsevier Inc. All rights reserved.

Carbon-11, a cyclotron generated nuclide, is produced either by irradiation of N_2/O_2 or N_2/H_2 gas mixtures. In most cases, the generated [^{11}C]CO_2 (or [^{11}C]CH_4) is further processed to receive the most important synthon [^{11}C]CH_3I. Reasonably, the molar activity for syntheses starting from [^{11}C]CH_4 is generally higher than for those starting from [^{11}C]CO_2 [3]. The processing of [^{11}C]CO_2 to [^{11}C]CH_3I is performed either *via* the 'wet' method with $LiAlH_4$ and HI, or *via* a gas phase reaction using H_2 and I_2. Potential carbon-12 sources were extensively discussed for the 'wet' method [4,5] as well as for the single pass I_2 method [6]. However, less information is available for the synthesis of [^{11}C]CH_3I through the gas phase iodination reaction of commercially available modules such as GE TRACERlab FX C [7] or Synthra MeIplus. This fact is astonishing considering that most of ^{11}C-syntheses are performed during routine production or clinical trials, and the production has to be performed on a weekly or even daily base. Therefore, a constant aim is to keep the molar activity high and predictable. Every inexplicable decrease is the fear of a radiochemist specialized on ^{11}C-tracer preparation and also of technicians involved.

The aim of our investigations was the identification and evaluation of potential carbon-11 sources within the [^{11}C]CH_3I production unit of the GE TRACERlab FX C Pro. These investigations were based on six ^{11}C-labeled PET tracers, which were produced on a weekly to nearly daily base within our facility over the course of 1.5 years. Due to the clinical demand for high radiochemical yields, often 2–3 applications have to be possible with one radiochemical production. Hence, all syntheses were performed using the [^{11}C]CO_2 target. Additionally, we established a protocol to minimize potential risks for poor/decreased molar activities as well as to optimize the maintenance interval for the equipment in order to guarantee high and reproducible quality within our daily routine production of 2–3 ^{11}C-tracer preparations per day on the same synthesizer.

2. Experimental

2.1. Material and reagents

All chemicals and solvents were obtained from commercial sources with analytical grade and used without further purification. Iodine (sublimated grade for analysis; ACS, Pharm.Eur.) was purchased from Merck (Darmstadt, Germany; product number: 1.04761.0100). The nickel catalyst (Shimalilte Ni reduced, 80/100 mesh) was purchased from Shimadzu (Kyoto, Japan) and was mixed with a molecular sieve (4 Å, 80/100 mesh, purchased from Grace, Columbia, USA). The [^{11}C]CH_3I trap consisted of Porapak Q (50–80 mesh, Waters, Vienna, Austria). Silver triflate impregnated carbon was prepared by dissolving 1 g of silver trifluoromethanesulfonate (Sigma Aldrich, Vienna, Austria) in 20 mL acetonitrile (for DNA synthesis, ≤10 ppm H_2O, Merck, Darmstadt, Germany). To this solution, 3 g of Graphpac-GC (80/100 mesh, Alltech, Deerfield, Illinois, USA) was added and the suspension was stirred in the dark for about 30 min. The solvent was removed under reduced pressure and the obtained powder was further dried in the dark for 2 h (rotary evaporator). The three ascarite II traps (ascarite®, approx. 20–30 mesh, Sigma Aldrich, Vienna, Austria) were used to avoid contaminations with moisture within the methyl iodide production unit.

2.2. General method for the in-target [^{11}C]CO_2 production and delivery to the hot cell

[^{11}C]CO_2 was produced by means of a GE PETtrace 860 cyclotron (General Electric Healthcare, Uppsala, Sweden) and a GE [^{11}C]CO_2 high pressure target *via* the $^{14}N(p,\alpha)^{11}C$ reaction by a high purity gas mixture of N_2 6.0 and 1% O_2 5.5 (Air Liquide, Vienna, Austria). Alphagaz™ 2 helium 6.0 (≥99.9999%, Air Liquide, Vienna Austria) and Alphagaz™ 2 hydrogen 6.0 (99.9999%, Air Liquide, Vienna Austria) was used as inert gas and reduction reagent, respectively. The target consisted of an aluminium alloy and target foils made of Havar (alloy of cobalt). Depending on the experimental schedules irradiation times and beam currents were varied. However, standard settings were an irradiation time of 30 min and beam current of 65 μA yielding approximately 120 GBq of [^{11}C]CO_2. Moreover, delivery time from target to the Hot Cells/TRACERlab FX C Pro synthesizer was 4 min, including an automatic, additional refill/delivery cycle to assure complete emptying of the target. Subsequently, the delivered [^{11}C]CO_2 was trapped on a molecular sieve at room temperature and either released by heating to 400 °C for Grignard reactions ([^{11}C]-(+)-PHNO, [*carbonyl*-^{11}C] WAY100635) or further processed according to Larsen et al. [8] by means of the in-built methylation process in the GE TRACERlab FX C Pro synthesizer (General Electric Healthcare, Uppsala, Sweden) (Fig. 1).

2.3. Maintenance interval for the GE TRACERlab FX C Pro

The maintenance interval recommended by the commercial supplier of the GE TRACERlab FX C Pro for the most common tasks was adapted to serve the needs of our facility. The adaptions are listed in Table 1.

2.4. Preparation of the GE TRACERlab FX C Pro for [^{11}C]CH_3I based productions

Module preparation started with flushing of the "[^{11}C]CH_3I preparation unit" with helium (20–50 mL/min) (*via* V24, V25, V29, VA, V15, V9, V17, V16) as well as flushing the lines to the reactor (*via* VB, V7 and V8) for around 1 min. Subsequently, the same pathways were checked for leakages with a helium flow of 100 mL/min. In order to guarantee tightness the flow had to decrease below 4 mL/min.

Heating to 200 °C under a continuous helium flow (50 mL/min) of the [^{11}C]CH_3I trap – and, if applied, the silver triflate column – was performed to remove traces of chemical contaminants from the previous synthesis. During that time, V1–V3 were washed two to three times with water followed by acetone *via* the reactor as well as the load and inject positions of the HPLC valve. The reactor as well as the lines from V1–V3 and the line to the injection valve were dried with a continuous helium stream *via* V18. V4, V5 and V6 were washed with either ethanol or water *via* the product vial or V11 and V12. The HPLC lines were washed with HPLC solvent *via* V14 into the waste bottle as well as into the bulb. The bulb line was washed with water and HPLC solvent *via* V11 and V12.

All lines associated with the reactor were afterwards checked for presence of solvent residues, which have to be fully removed.

15 min before the start of the synthesis, a pre-run sequence was started, consisting of a heating step of the [^{11}C]CO_2 trap ([^{11}C]CH_4 production unit) to 400 °C with a helium stream of 50 mL/min *via* V27 (2 min). The [^{11}C]CO_2 trap was pre-flushed with hydrogen gas (3 min) still at 400 °C and subsequently cooled down to at least 50 °C. Cooling of the CH_4 trap to −78 °C with liquid nitrogen was started before release of radioactivity from the target.

2.5. General procedure for the conversion of [^{11}C]CO_2 to [^{11}C]CH_3I

[^{11}C]CO_2 was trapped at room temperature on a molecular sieve including nickel as catalyst. Afterwards, the [^{11}C]CO_2 trap was flushed with helium (50 mL/min) and subsequently filled with hydrogen (120 mL/min). V27 was closed prior to V25 and the [^{11}C]CO_2 trap was heated to 400 °C. The formed [^{11}C]CH_4 was released with a helium stream *via* V10 (exhaust exit) and trapped on the [^{11}C]CH_4 trap, which was cooled to −75 °C. V10 was closed, V9 opened and [^{11}C]CH_4 was released into the circulation unit by heating the trap slowly to 80 °C. Inside the circulation unit, the [^{11}C]CH_4 was converted to [^{11}C]CH_3I, whereas an optimal result was achieved by around 10–11 circulations within approximately 3 min. Around 10% of the radioactivity were usually trapped on the [^{11}C]CH_3I trap within the first circulation and approximately 35–50% of the starting activity were trapped as [^{11}C]CH_3I after the circulation process had ended. Afterwards V16 (exhaust exit) was

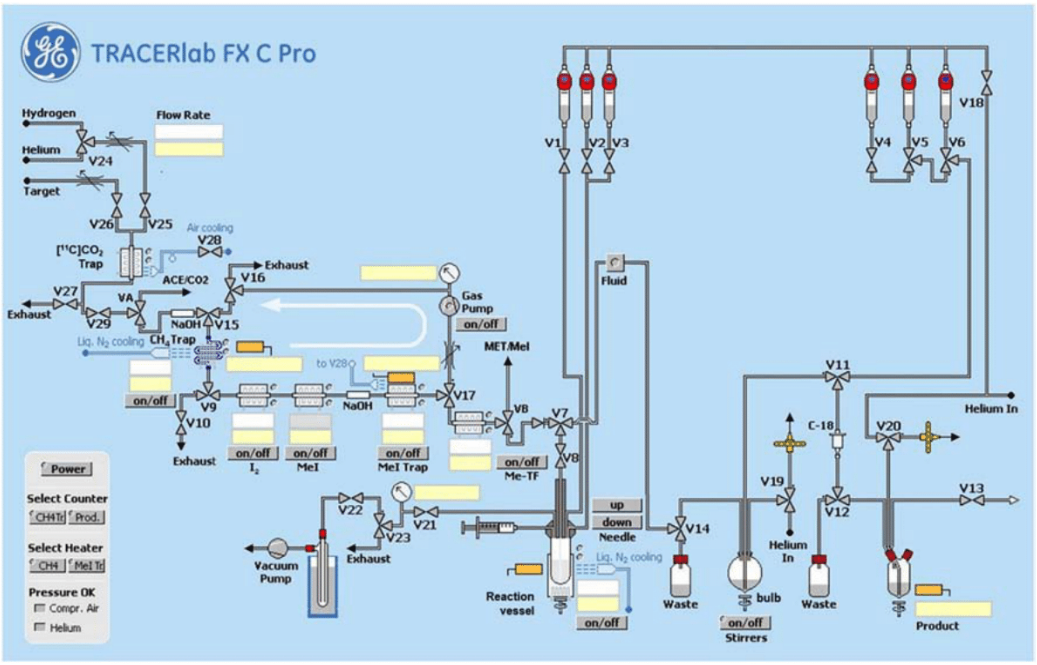


Fig. 1. Scheme of the [^{11}C]CH_3I production unit of the GE TRACERlab FX C Pro.

opened and the trap was heated to 90 °C to remove potential byproducts. Afterwards V16 was closed, the trap was further heated to 190 °C and the radioactivity was released into the reaction vessel *via* V17, VB (silver triflate column or bypass), V7 and V8. Around 75–90% of [^{11}C]CH_3I/[^{11}C]CH_3OTf was trapped inside of the reactor, highly depending on the employed trapping solvent.

2.6. General procedure for [^{11}C]CO_2 release for Grignard reactions

In general, Grignard reactions can be directly conducted using [^{11}C]CO_2 from the cyclotron. In our facility, firstly [^{11}C]CO_2 was trapped on the [^{11}C]CO_2 trap prior to the actual reaction start, in order to allow a controlled [^{11}C]CO_2 release into a plastic reaction loop, previously coated with the respective Grignard reagent. In advance, the cyclotron target was flushed twice with target gas.

Accordingly, the [^{11}C]CO_2 trap was heated for 5–10 min to 400 °C with a helium stream (20 mL/min) *via* V27 to remove potential CO_2 traces and subsequently cooled to room temperature. It is important to avoid accidental flushing of this trap with hydrogen gas to prevent the chemical reaction to [^{11}C]CH_4. Then, the cyclotron produced [^{11}C]CO_2 was trapped. The trap was successively heated to 300 °C with a gentle helium stream (5–10 mL/min) *via* the exhaust valve V27. When a temperature of 300 °C was reached, it was further increased to 400 °C, while V27 was closed, and V29 and VA were opened for release of the activity to the loop.

2.7. Tracer production

Four tracers were produced by methylation reactions, using [^{11}C]CH_3I or [^{11}C]CH_3OTf, respectively, and were therefore dependent on a good performance of the [^{11}C]CH_3I production unit: [^{11}C]DASB (n = 158), [^{11}C]harmine (n = 109), [^{11}C]PIB (n = 61) and [^{11}C]erlotinib (n = 49). The synthesis procedures were performed as described previously [9–12]. Two tracers were produced *via* Grignard reactions. A detailed description of the synthesis of [^{11}C]-(+)-PHNO (n = 49) as well as [*carbonyl*-^{11}C]WAY100635 (n = 31) was published elsewhere [13,14]. For analysis of the trapping efficiency of different solvents, additional data from productions for [^{11}C]methionine (n = 14) [15] and [^{11}C]tariquidar (n = 10) [16] were added.

2.8. Analytical procedure for the quantification of molar activity

For analysis of the molar activities, an Agilent 1260 system (Agilent Technologies GmbH, Santa Clara, CA, USA) equipped with a quaternary pump (G1311B), a multi wavelength UV-detector (G1365D), a manual injector (G1328C), a NaI (Tl) detector from Berthold Technologies (Bad Wildbad, Germany) and GINA Star controlling software (Elysia-Raytest; Straubenhardt, Germany) was used. The column was an X-Bridge BEH Shield RP-18, 4.6 × 50 mm, 2.5 µm, 130 Å (Waters, Austria). All details for the different mobile phases, limits of detection and quantification were presented recently [17].

Table 1
Recommended *versus* established maintenance interval for the most common tasks of module servicing in our facility.

Maintenance tasks	Recommended interval	Our interval
Leak test	Every 5th synthesis	Every synthesis
1st iodine trap	Every 5th synthesis	Once per week (approx. 7–10th synthesis)
2nd iodine trap	n.a.	Every 30th synthesis
Water traps	Every 20th synthesis	Every 15–20th synthesis
Iodine refill	Every 20th synthesis	Every 25th synthesis
Change of CH_3I trapping material	Every 20th synthesis	Dependent on synthesis performance (every 150–200th syntheses)
Change CO_2 trap/CH_4 oven material	Every 100th synthesis	Dependent on synthesis performance (every 200–400th syntheses)
Change CO_2 cooling trap material	n.a.	Dependent on synthesis performance (~1000th syntheses)

2.9. Partial runs for the analysis of potential contamination with ubiquitous CO_2

The identification of potential sources of non-radioactive carbon dioxide was performed by analysis of partial runs (*i.e.* simulated preparations interrupted after specific steps).

(1) For analysis of the precursor quality, the [^{11}C]DASB radiolabeling precursor (MASB) was solved in 0.4 mL DMSO and an HPLC run was performed in order to determine the amount of DASB contained in the precursor.
(2) For identification of potential carbon-12 contamination originating from the target (including target gas, tubings and distribution ways, but not from the irradiation process), the target was flushed twice with target gas without previous irradiation. The potential carbon-12 dioxide contamination was trapped in the CO_2 trap. The circulation process was performed as described before and the produced CH_3I was released into a solution of 1 mg MASB in 0.4 mL DMSO. Afterwards the reaction mixture was quenched with 1 mL of water and the amount of the formed DASB was analyzed.
(3) For identification of potential carbon-12 contamination resulting from the module or inert gas source: the [^{11}C]CO_2 trap was flushed with a stream of helium (50 mL/min) and the circulation process was performed as described before. The trapping and analysis of DASB was performed as described for (2).

2.10. Statistical analysis of molar activity for a set of PET tracers

The molar activities of the aforementioned six PET tracers were analyzed over a course of approximately 1.5 years with around 10–15 carbon-11 productions per week. Production records were statistically analyzed by Microsoft Excel 2010 and *t*-test was performed with Graph Pad Prism 6 (GraphPad Software, La Jolla, CA, USA). Moving average analysis was executed by trend line analysis also in Microsoft Excel 2010.

All calculation for molar activities and yields within the different processes were performed at the same time point (end of syntheses or end of the respective process) but non-decay corrected to depict the situation during a synthesis.

Box plot analysis (Fig. 3) shows the overall range of values (minimal to maximal value), the range between the 25th to 75th percentile as box and the median value is shown as intermediate line of the box. All data for Fig. 5 are expressed as mean ± SD, whereas in Figs. 2, 4, and 6 every point represents a single experiment/event to enable trend analysis.

3. Results and discussion

The molar activities of six PET-tracers, [^{11}C]DASB, [^{11}C]harmine, [^{11}C]PIB, [^{11}C]erlotinib, [^{11}C]-(+)-PHNO and [*carbonyl*-^{11}C]WAY100635, was monitored over the course of 1.5 years with a high turnover of around 10–15 carbon-11 productions per week produced on the same GE TRACERlab FX C Pro system (Fig. 2). Moving average analysis showed a continuous trend with a peak in molar activity around every 3 months (approx. 150 syntheses). Within our production scheme, the main reason for a fast drop in molar activity was found to be the filling level of the target gas bottle (major effect) or the inert gas bottle (helium bottle, minor effect).

On the other hand, the molar activity was highly dependent on the quality of the starting materials (different production lots of commercial suppliers, time of solvent usage, *etc.*). Therefore the average molar activity was also PET-tracer dependent. The highest A_m at end of synthesis (non-decay corrected) was achieved for [^{11}C]harmine (146 ± 108 GBq/μmol), [^{11}C]DASB (133 ± 110 GBq/μmol), as well as the Grignard reaction based tracers [^{11}C]-(+)-PHNO (132 ± 92 GBq/μmol) and [*carbonyl*-^{11}C]WAY100635 (137 ± 101 GBq/μmol), whereas [^{11}C]erlotinib (101 ± 57 GBq/μmol) and [^{11}C]PIB (103 ± 61 GBq/μmol) showed the lowest values.

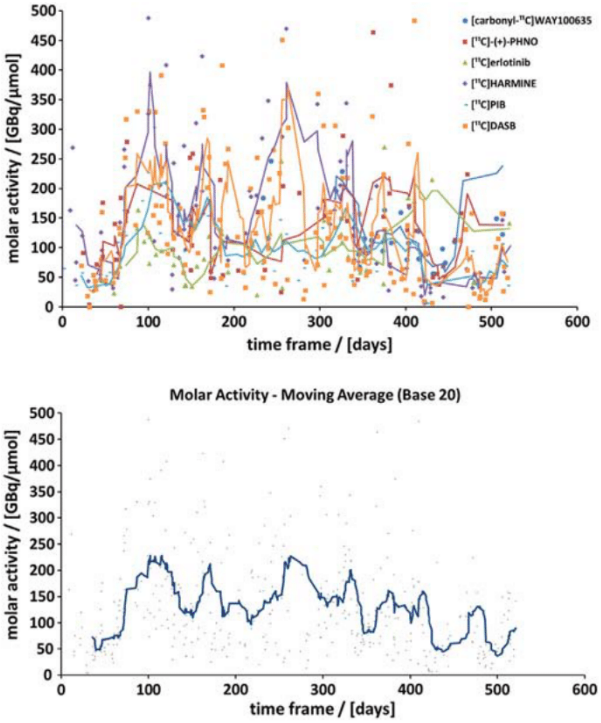


Fig. 2. Top: Overview on molar activities of an overall of 457 syntheses of the following PET-tracers: [*carbonyl*-^{11}C]WAY-100635 (n = 31), [^{11}C]-(+)-PHNO (n = 49), [^{11}C]erlotinib (n = 49), [^{11}C]harmine (n = 109), [^{11}C]PIB (n = 61) and [^{11}C]DASB (n = 158). The lines are the moving average analysis (base 4) for the respective radiotracer to visualize the trend over the time. Bottom: Moving average analysis over all molar activities with a period of 20 to show the fluctuation within approximately a month independent on the respective radiotracer.

Interestingly, we observed a slight trend to lower molar activities throughout the day when using the synthesizer repeatedly for ^{11}C-tracer preparations. In general, the first production resulted in higher molar activity than the successive ones. This trend is explicable either by residues from previous runs, which could not be removed by the cleaning procedure, or it is potentially a sum of effects caused by the type of tracer in combination with effects caused by the producer. However, a more extensive evaluation is necessary to fully explain this trend — performing three consecutive syntheses with the same tracer and the same producer. Unfortunately, we are not able to perform such experiments at the moment due to logistical restrictions in connection with the clinical routine schedule.

However rare, excessive or wrong use of the module by the producer can dramatically influence the performance. Intra- and interoperator variabilities were also clearly seen (Fig. 3).

When a reduction in molar activities was observed, it was essential to clearly distinguish between a drop (a) only for [^{11}C]CH_3I based tracers, (b) only for Grignard-reaction based tracers or (c) for both. In our facility, the main reasons for a decreasing molar activity only for [^{11}C]CH_3I based tracers were identified as (organic) contamination of the ascarite traps or molecular sieves, damaged tubing or clogging of valves. As the transformation of [^{11}C]CO_2 to [^{11}C]CH_3I was found to show a linear trend with around 37 ± 4% absolute yield of [^{11}C]CH_3I (Fig. 4) every drastic discrepancy indicated a beginning systematic disturbance of this process.

Once a poor performance (with unaltered turnover of [^{11}C]CO_2 to [^{11}C]CH_3I) was observed, it was mandatory to change all ascarite traps in order to gain sufficient molar activities again. Moreover, it was found that a few syntheses were necessary for regeneration of the system (*i.e.* additional methylation runs without tracer preparation).

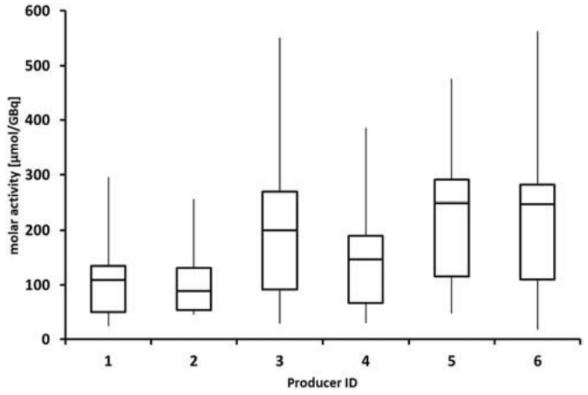


Fig. 3. Inter- and intraoperator variabilities in molar activities shown for [^{11}C]harmine. Box plot analysis includes the minimum to maximum value (upper and lower whisker), the range of the 25th to 75th percentile (box) as well as the median value (intermediate line of the box). In overall 86 syntheses were included in the analysis with the following assignment to the producers: producer 1 (n = 10); producer 2 (n = 12), producer 3 (n = 29), producer 4 (n = 7), producer 5 (n = 16), and producer 6 (n = 12). 23 syntheses were excluded as no assignment to a single producer was possible (productions in pairs due to teaching aspects) or when only ≤5 syntheses per producer were available.

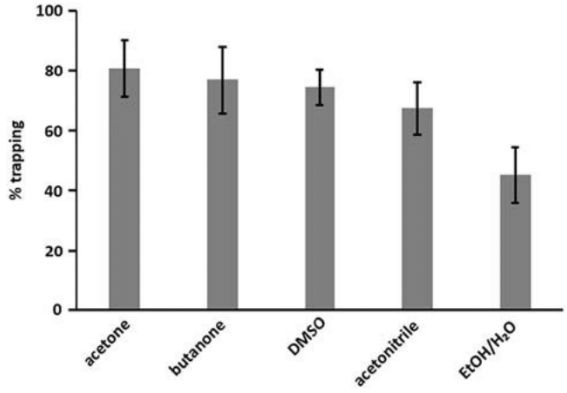


Fig. 5. Trapping efficiency of [^{11}C]CH_3I or [^{11}C]CH_3OTf, respectively, in five solvents, namely acetone ([^{11}C]tariquidar, n = 10), butanone ([^{11}C]PIB, n = 48), DMSO ([^{11}C]DASB and [^{11}C]harmine, n = 31), acetonitrile ([^{11}C]erlotinib, n = 49) and a mixture of ethanol/water ([^{11}C]methionine, n = 14) at room temperature. Values are expressed as mean ± SD.

When additionally to the drop in molar activity the radiochemical yield in [^{11}C]CH_3I decreased to less than approximately 30% it was mainly caused by partial clogging of the gas pump valve, which was recognizable by a reduction in the number of the cycles during the transformation of [^{11}C]CH_4 to [^{11}C]CH_3I *via* valves V9, V17, V16 and V15.

Although the reaction solvent did not influence the molar activity of the respective tracer, a distinct difference in the trapping efficiency and consequently on the yield was observable (Fig. 5). The most effective solvents for trapping [^{11}C]CH_3I or [^{11}C]CH_3OTf at room temperature were polar, aprotic solvents, like DMSO, acetone, and butanone, with a nearly quantitative recovery of the activity. The least effective ones were polar, protic solvents, such as a mixture of ethanol and water, which additionally were able to act as nucleophile themselves and, therefore, potentially produce side products, *e.g.* [^{11}C]methanol or [*methyl*-^{11}C]methylethylether.

As Grignard reactions, as used for *e.g.* the synthesis of [^{11}C]-(+)-PHNO, do not proceed *via* [^{11}C]CH_3I, a drop in molar activity solely for this kind of reactions was mainly caused by impurities of the used reagents. This problem was often caused by repeated usage of critical reagents (*e.g.* CO_2 enrichment in these containers). In most cases a significant increase of the molar activity was achieved by using a fresh batch of the applied chemical reagent.

However, when a drop in both, [^{11}C]CO_2 and [^{11}C]CH_3I based reactions, occurred, the main carbon source was either a contamination of the [^{11}C]CO_2 trap or within the cyclotron target. As mentioned before, this increased carbon load was mainly brought about by a low fill level of the target gas bottle.

For identification of the origin of organic contamination, we performed three successive syntheses, in which two partial runs and a full run were conducted on the same day. For molar activity measurement, the [^{11}C]DASB production scheme was used. The partial runs included the identification of the amount of DASB within the starting material, the contribution to the carbon load by the module and the cyclotron target, as well as measurement of the carbon load solely originating from the module.

The amount of DASB within the starting material was negligible for the following calculations. The results for the carbon load were opposed to the produced DASB. The correlation between the identified carbon load of the sum of the contributions of module and cyclotron and the obtained molar activity is depicted in Fig. 6. Here, it is obvious that small changes in the carbon-load influence the molar activity more drastically in the high molar activity range than in the low one. Thus, high fluctuations are more likely and common at high molar activities.

The experimental work-up using different partial runs was successfully applied to identify and eliminate carbon contaminations faster within our synthetic protocol and production routine. Hence, we recommend following this procedure in the set-up and during continuous monitoring of automated radiosyntheses of ^{11}C-tracers.

In summary, three clearly recognizable parameters for performance of carbon-11 syntheses in terms of molar activity were identified: technical, inter/intralaboratory and interoperator parameters (Fig. 7).

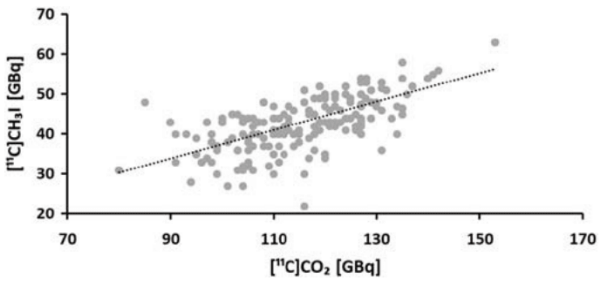


Fig. 4. Absolute yield of [^{11}C]CH_3I in relation to the starting activity of [^{11}C]CO_2 (n = 262). The linear regression analysis (dotted line) highlights the increasing trend (y = 0.3558x + 1.9012; R2 = 0.449).

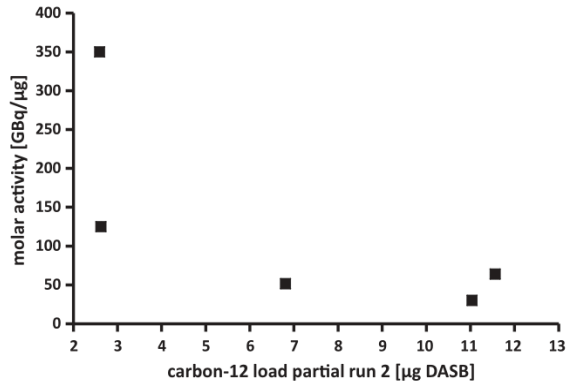


Fig. 6. Relationship between the ^{12}C-load (absolute amount of produced DASB) of the sum of contributions from synthesizer and cyclotron processes and molar activity of [^{11}C]DASB measured on the same day.

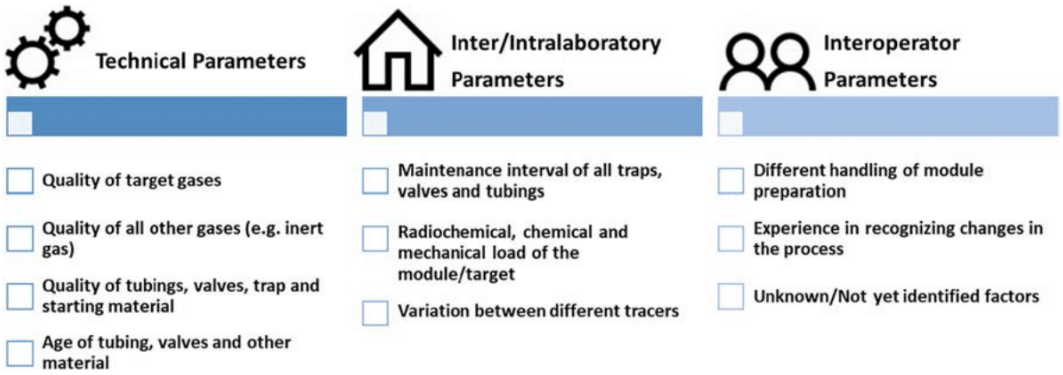


Fig. 7. Identified parameters influencing the molar activity of the six analyzed radiotracers.

The technical parameters included mostly external factors, such as the quality of the target and inert gas, the quality of the reagents and consumables, which were dependent on the commercial supplier and therefore often difficult to control.

Easier to adapt and modify were the inter-/intralaboratory parameters as, for instance, the maintenance intervals had to be changed to generate continuous high performance and to keep the carbon load within the module at a low level.

The trickiest part was the determination of interoperator parameters, such as varying module preparation procedures and monitoring of the synthetic process. Only extensive validation, (re-) training of the personnel and clear and concise standard operational procedures lead to satisfactory and consistent molar activities.

4. Conclusion

The aim of this extensive study was to identify carbon-12 contaminations within the synthetic procedure which influence the molar activities of six examined carbon-11 based PET tracers. The identified parameters were manifold and could be summarized into technical, inter/intralaboratory and interoperator parameters. For this purpose, both a retrospective analysis of >450 synthesis data and dedicated experiments (including partial synthetic runs as well as full radiochemical runs) were conducted in order to facilitate the identification process of the responsible parts within the synthesizer for reduced molar activities. Addressing the identified parameters before set-up and monitoring them during operation guarantees stable quality of ^{11}C-tracer preparations with constant molar activities.

Acknowledgement

We thank Andreas Krcal for his technical support and help with the maintenance of the GE TRACERlab FX C Pro module and Katharina Pallitsch for preparing silver triflate.

Disclosure statement

The authors declare that they have no conflict of interest.

This article does not contain any studies with human participants or animals performed by any of the authors.

References

[1] Lancelot S, Zimmer L. Small-animal positron emission tomography as a tool for neuropharmacology. Trends Pharmacol Sci 2010;31(9):411–7.
[2] Coenen HH, Gee AD, Adam M, Antoni G, Cutler CS, Fujibayashi Y, et al. Consensus nomenclature rules for radiopharmaceutical chemistry – setting the record straight. Nucl Med Biol 2017:55:v-xi.
[3] Andersson J, Truong P, Halldin C. In-target produced [^{11}C]methane: increased specific radioactivity. Appl Radiat Isot 2009;67(1):106–10.
[4] Iwata R, Ido T, Ujiie A, Takahashi T, Ishiwata K, Hatano K, et al. Comparative study of specific activity of [^{11}C]methyl iodide: a search for the source of carrier carbon. Int J Rad Appl Instrum A 1988;39(1):1–7.
[5] Gómez-Vallejo V, Llop J. Specific activity of [^{11}C]CH_3I synthesized by the "wet" method: main sources of non-radioactive carbon. Appl Radiat Isot 2009;67(1):111–4.
[6] Zhang M-R, Suzuki K. Sources of carbon which decrease the specific activity of [^{11}C]CH_3I synthesized by the single pass I2 method. Appl Radiat Isot 2005;62(3):447–50.
[7] Kniess T, Rode K, Wuest F. Practical experiences with the synthesis of [^{11}C]CH_3I through gas phase iodination reaction using a TRACERlabFXC synthesis module. Appl Radiat Isot 2008;66(4):482–8.
[8] Larsen P, Ulin J, Dahlstrøm K, Jensen M. Synthesis of [^{11}C]iodomethane by iodination of [^{11}C]methane. Appl Radiat Isot 1997;48(2):153–7.
[9] Haeusler D, Mien LK, Nics L, Ungersboeck J, Philippe C, Lanzenberger RR, et al. Simple and rapid preparation of [^{11}C]DASB with high quality and reliability for routine applications. Appl Radiat Isot 2009;67(9):1654–60.
[10] Philippe C, Haeusler D, Mitterhauser M, Ungersboeck J, Viernstein H, Dudczak R, et al. Optimization of the radiosynthesis of the Alzheimer tracer 2-(4-N-[^{11}C]methylaminophenyl)-6-hydroxybenzothiazole ([^{11}C]PIB). Appl Radiat Isot 2011;69(9):1212–7.
[11] Philippe C, Zeilinger M, Mitterhauser M, Dumanic M, Lanzenberger R, Hacker M, et al. Parameter evaluation and fully-automated radiosynthesis of [^{11}C]harmine for imaging of MAO-A for clinical trials. Appl Radiat Isot 2015;97:182–7.
[12] Philippe C, Mairinger S, Pichler V, Stanek J, Nics L, Mitterhauser M, et al. Comparison of fully-automated radiosyntheses of [^{11}C]erlotinib for preclinical and clinical use starting from in target produced [^{11}C]CO_2 or [^{11}C]CH_4. EJNMMI Radiopharm Chem 2018;3:8.
[13] Rami-Mark C, Ungersboeck J, Haeusler D, Nics L, Philippe C, Mitterhauser M, et al. Reliable set-up for in-loop 11C-carboxylations using Grignard reactions for the preparation of [carbonyl-^{11}C]WAY-100635 and [^{11}C]-(+)-PHNO. Appl Radiat Isot 2013;82:75–80.
[14] Wadsak W, Mien L-K, Ettlinger DE, Lanzenberger R, Haeusler D, Dudczak R, et al. Simple and fully automated preparation of [carbonyl-^{11}C]WAY-100635. Radiochim Acta 2007;95(7):417–22.
[15] Mitterhauser M, Wadsak W, Krcal A, Schmaljohann J, Eidherr H, Schmid A, et al. New aspects on the preparation of [^{11}C]Methionine – a simple and fast online approach without preparative HPLC. Appl Radiat Isot 2005;62:441–5.
[16] Bauer F, Kuntner C, Bankstahl JP, Wanek T, Bankstahl M, Stanek J, et al. Synthesis and in vivo evaluation of [^{11}C]tariquidar, a positron emission tomography radiotracer based on a third-generation P-glycoprotein inhibitor. Bioorg Med Chem 2010;18(15):5489–97.
[17] Nics L, Steiner B, Klebermass E-M, Philippe C, Mitterhauser M, Hacker M, et al. Speed matters to raise molar radioactivity: fast HPLC shortens the quality control of C-11 PET-tracers. Nucl Med Biol 2018;57:28–33.

3.6. The Radiopharmaceutical Chemistry of Carbon-11: Tracers and Applications

Verena Pichler,[1] Neydher Berroterán-Infante,[1] **Marius Ozenil**,[1] Sarah Pfaff,[1] Cécile Philippe,[1] Wolfgang Wadsak[1]

[1] Department of Biomedical Imaging and Image-guided Therapy, Division of Nuclear Medicine, Medical University of Vienna, Vienna, Austria

The doctoral candidate wrote this book chapter together with the listed coauthors, focusing on the subchapter “Application of Other Carbon-11 Precursors in Tracer Preparation”.

The Radiopharmaceutical Chemistry of Carbon-11: Tracers and Applications

Verena Pichler, Neydher Berroterán-Infante, Marius Ozenil, Sarah Pfaff, Cécile Philippe, and Wolfgang Wadsak

Introduction

In this chapter, several different aspects of carbon-11 radiochemistry are discussed, including general and technical considerations surrounding setup for ^{11}C-radiosyntheses and specific radiolabeling routes for the preparation of representative ^{11}C-labeled radiotracers. The optimization of equipment and labeling procedures—especially with respect to time—is a must when dealing with the short-lived radionuclide carbon-11. Time reduction in all processes (including quality control) is of the utmost importance, though both accuracy and reproducibility must be maintained. The synthetic possibilities for ^{11}C-labeled radiotracers resemble a multicolored bouquet of flowers, with methods ranging from gas-phase reactions to in-loop syntheses and from straightforward ^{11}C-methylations to tricky multistep Grignard reactions. A variety of synthons—including [^{11}C]CH_3I, [^{11}C]HCN, [^{11}C]CS_2, and [^{11}C]CO—are used to prepare a multitude of radiotracers incorporating a ^{11}C-radiolabel at desired positions in the target molecule without altering its physicochemical and biological properties. Although several critical limitations are placed upon ^{11}C-radiochemists—including time constraints as well as the need for sufficient yields and molar activities—you will find plenty of examples within this chapter of instances in which scientists have overcome these obstacles and were able to set up feasible synthetic routes that demonstrate the beauty of ^{11}C-radiochemistry.

V. Pichler · N. Berroterán-Infante · M. Ozenil · S. Pfaff
C. Philippe · W. Wadsak (✉)
Department of Biomedical Imaging and Image-guided Therapy, Division of Nuclear Medicine, Medical University of Vienna, Vienna, Austria
e-mail: wolfgang.wadsak@meduniwien.ac.at

Technical Aspects of Carbon-11: Commercially Available Synthesizers and Optimization

General Considerations for Radiotracer Production and the Setup of Synthesizers

The routine production of ^{11}C-labeled radiotracers requires equipment that ensures the safety of the attending radiochemists. This suite of equipment typically involves a lead-shielded working space, so-called hot cells, an active gas compression system for storing exhaust air in tanks during the decay process and radiation monitoring systems. The heart of every ^{11}C-radiochemistry laboratory is the semi-automated or fully automated synthesizer, in which the actual chemical conversion of the precursor to the radiolabeled product takes place.

Carbon-11 synthesis modules—like any other synthesizer in radiochemistry—should comply with a set of specific properties in order to fulfill the demands of routine production with a high degree of reproducibility [1]. As a result, the modules must facilitate or allow for the following:

- The possibility for the automation of all processes
- The reproducibility of robust processes
- Modifications for challenging syntheses (*e.g.* in-loop reactions)
- Constant quality of the radiolabeled product in terms of molar activity and radiochemical yield
- The production of multiple doses per day
- Reduced maintenance efforts

Independent of the manufacturer, versatile synthesis modules for carbon-11 radiochemistry must have a minimum configuration featuring four major parts (for an overview, see Fig. 1). The first part consists of an instrument for the production of [^{11}C]methyl iodide ([^{11}C]iodomethane)—with or without an extension to prepare [^{11}C]methyl triflate—either via the "wet" method (see the section on "'Wet' Production

© Springer Nature Switzerland AG 2019
J. S. Lewis et al. (eds.), *Radiopharmaceutical Chemistry*, https://doi.org/10.1007/978-3-319-98947-1_12

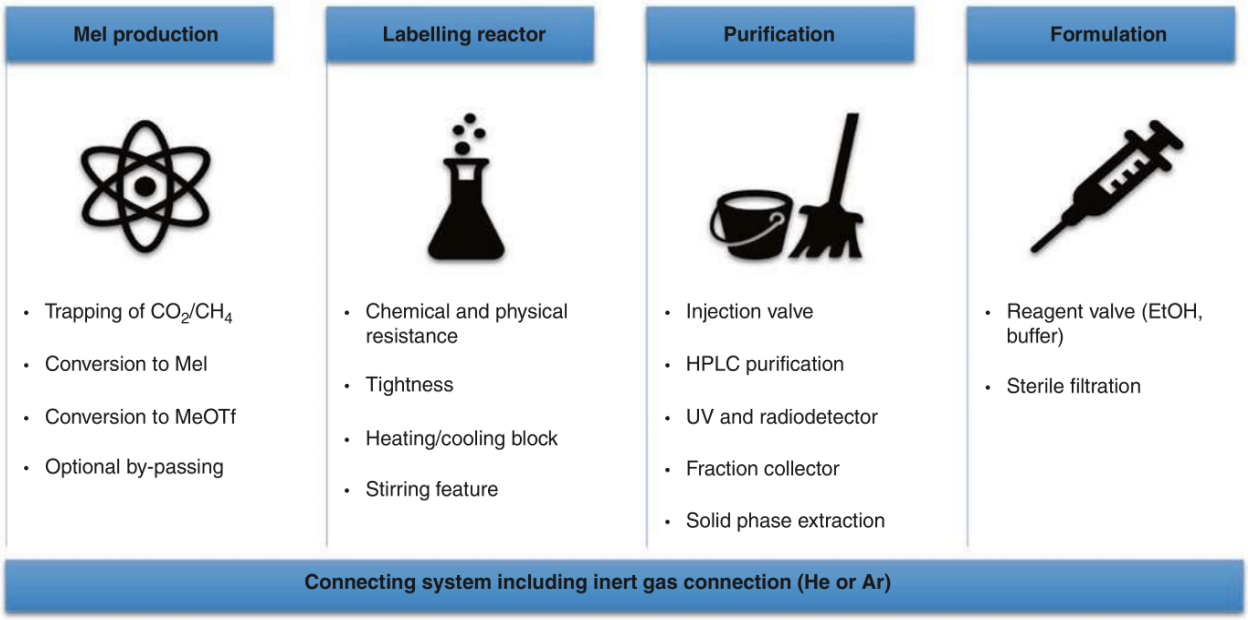


Fig. 1 Overview of the four necessary procedures for a successful radiosynthesis

of [^{11}C]CH_3I") or the "gas-phase" method (see the section on "'Gas-Phase' Production of [^{11}C]CH_3I"). The next part is composed of the reaction and reagent vessels necessary for conducting the radiolabeling procedure, including a heating/cooling block. This part has to be connected via an injection valve to the third component: a purification system including an HPLC for the separation of precursors, possible by-products, and the radiotracer of interest (see the section on "Purification and Separation") and often also a solid-phase extraction (SPE) system or a rotary evaporator to get rid of residual solvents used during HPLC. For clinical purposes, a fourth component is built in to facilitate the formulation of the radiolabeled compound in a manner suitable for intravenous injections. All four of these parts are connected via tubes and externally controllable valves, and the transportation of all gaseous or liquid/dissolved precursors, intermediates, and products is realized via an inert gas flow (mainly helium or argon).

Reactors and Reagent Vessels

The reaction vessel—which contains the dissolved non-radiolabeled organic precursor—is directly connected to the [^{11}C]CO_2/[^{11}C]methyl iodide production unit (Fig. 2; see Part 2). In addition, exhaust tubing should be present to prevent overpressure and to ensure a constant gas flow during the delivery of the radioactive precursor. In most cases, there is at least one additional segment of tubing for the addition of reagents or solvents to quench the reaction. The tubing for the addition of the radioactive intermediate—*e.g.* [^{11}C]methyl iodide—reaches down to the bottom of the reaction vessel to facilitate the ideal trapping of the radioactivity. In some cases, the height of the position of this inlet tubing can be adjustable. All other tubes are positioned in the upper part of the vessel to prevent an inadvertent backflow of the reaction mixture. Furthermore, this component also includes a heating/cooling block that enables diverse reaction conditions as well as a stirring unit.

The first step of the radiolabeling reaction is the trapping of the radioactive precursor/intermediate in the solution containing the nonradioactive precursor. Subsequently, the reaction vessel is closed for the entirety of the reaction time, and the reaction mixture is heated to the desired temperature. The tightness of the reactor is a key factor for successful radiosyntheses, as this reduces the possibility of losing radioactivity due to evaporation. After the completion of the reaction, the mixture is cooled to room temperature, and the reaction is quenched (*e.g.* by addition of HPLC solvent or water). As time efficiency is crucial when working with such a short-lived radionuclide, an efficient heating/cooling system can save precious time.

It is important to mention—though perhaps obvious—that all tubes and vessels must be chemically resistant and need to display a high degree of stability over a wide range of temperatures. As many ^{11}C-based radiotracers are highly lipophilic—especially those designed to permeate the blood-brain barrier, such as [^{11}C]PIB or [^{11}C]DASB—the reactor should preferably be made of either glass or plastic with a polar surface in order to avoid non-specific binding between

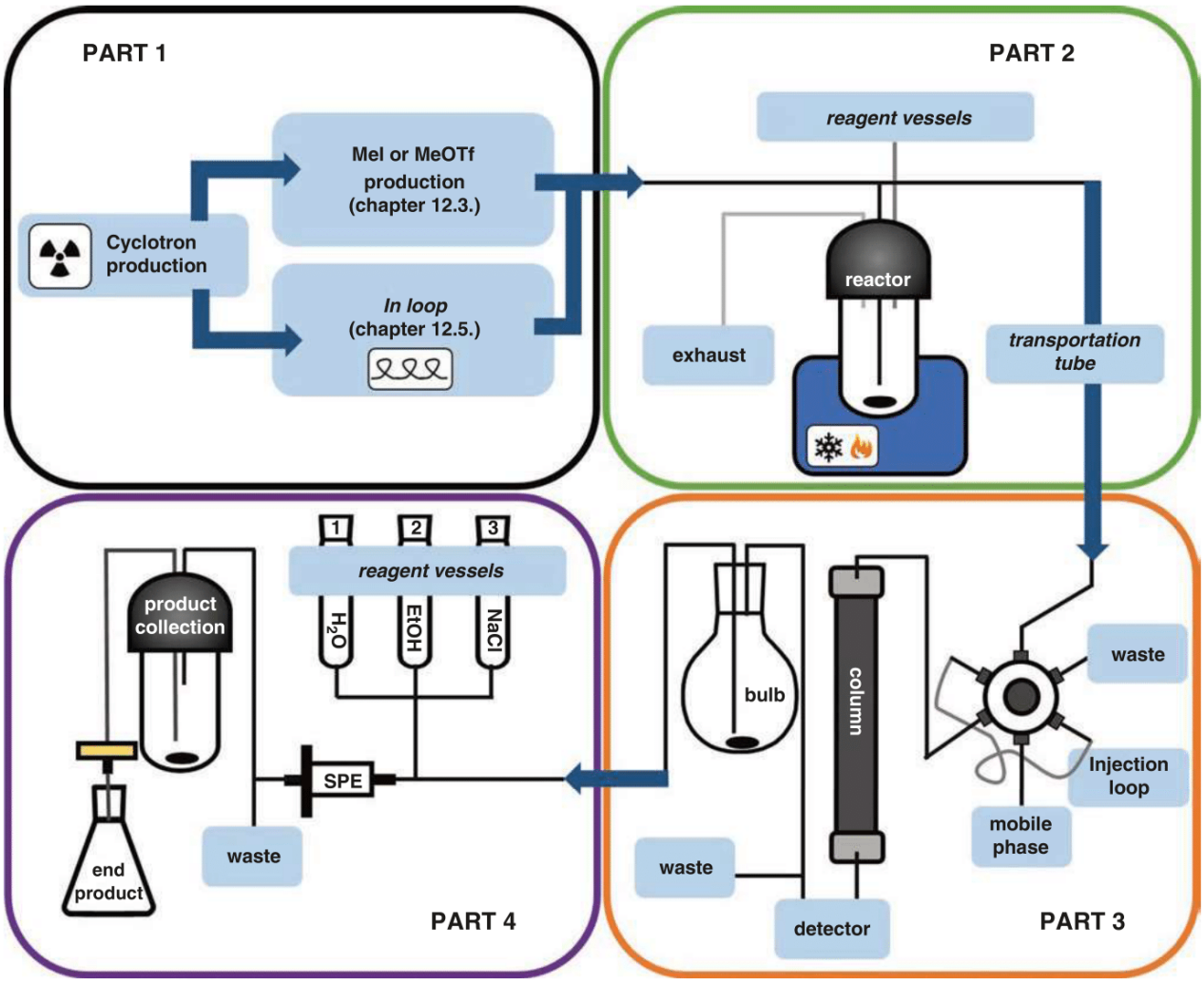


Fig. 2 The four essential parts of carbon-11 radiosynthetic modules

the tracer and the surfaces of the instrument. Moisture- and air-sensitive reactions often require modifications to the module array in order to increase turnover and yield. One potential modification of the module involves using a loop instead of a vessel-based reactor as a platform for either conversion steps or whole radiosyntheses. For example, radiochemical Grignard reactions are often performed "in-loop," bypassing the [^{11}C]methyl iodide production unit (see the section on "Grignard Reactions in Carbon-11 Radiochemistry (In-Loop)").

Purification and Separation

One characteristic of carbon-11 radiochemistry is that vast excesses of non-radioactive precursor typically remain even after the creation of a new radiotracer. Hence, the majority of carbon-11 syntheses require a purification process to separate the ^{11}C-labeled compound from unreacted precursor, side products, and organic solvents from the conversion process (see Fig. 2, Part 3).

To this end, the crude reaction mixture is typically transferred to an HPLC system, including an injection valve, a column, a UV/Vis and radioactivity detectors, and an apparatus enabling the collection of the peak of interest. The collected product peak still contains organic solvents from the mobile phase—*e.g.* acetonitrile or methanol—which must be removed prior to the formulation of the radiotracer for patients. In order to remove these solvents, the collected product is first diluted with large amounts of water. This solution is then transferred to a reversed-phase C_{18} cartridge for purification via SPE. The dilution step is necessary in order to reduce the amount of nonpolar solvents, as the presence of these solvents can reduce the efficiency of the cartridge. Depending on the physicochemical parameters of the product, the use of other cartridges—including those

containing ion-exchange resins—or even combinations thereof can be advantageous as well.

The last part of the module consists of additional reagent vessels, a product collection vial, and a final segment of tubing including a sterile filter for the filling of the final product vial under aseptic conditions (see Fig. 2, Part 4). These reagent vessels are connected to the SPE cartridge with the retained product, and the cartridge is washed with water to remove the final traces of organic solvents. Then, the purified product is recovered from the SPE cartridge via elution with a small amount of an organic solvent that is well tolerated in living organisms (such as ethanol) into the product collection vial where formulation takes place.

Formulation

Following synthesis and purification, the radiolabeled product must be prepared for intravenous administration to patients [2], as a so-called *parenteral preparation*. Parenteral preparations are sterile aqueous preparations that may include excipients for the adjustment of osmolality and pH. In the final steps described in the section on "Purification and Separation," the radiotracer is washed out of the SPE cartridge with ethanol and directly into the product collection vial already containing a buffered solution for the adjustment of pH and osmolality (*e.g.* phosphate-buffered saline). Depending on the specifications within the applicable pharmacopeia, up to 10% v/v ethanol is allowed in injections. Last but not least, the cartridge is rinsed with physiological sodium chloride solution (0.9% w/v) to ensure the complete transfer of the product from the SPE cartridge and through the lines. The well-stirred solution is then transferred from the product collection vial in the production hot cell into the final sterile product vial in the filling hot cell, where it is sterile filtered under aseptic conditions (*i.e.* laminar airflow) and subsequently ready to use.

Optimizing Possibilities Within the Synthesizer

Careful handling and maintenance significantly extend the lifetime of every module. Before starting a synthesis, the synthesizer should be checked, and all tubings and vessels must be washed and dried. Checking the system thoroughly for leakages reduces the loss of radioactivity during syntheses and is mandatory when dealing with gaseous reagents such as [^{11}C]CO_2, [^{11}C]CH_4, and [^{11}C]methyl iodide. The cleaning of all necessary tubing and connections within the module removes residues or particles from prior syntheses and thus reduces the likelihood of synthesis failures due to blockages within the tubes and valves. The exclusion and elimination of humidity is not only essential for highly moisture-sensitive reactions like Grignard reactions but can also increase radiochemical yields by preventing the hydrolysis of reagents. For example, [^{11}C]methyl iodide can be hydrolyzed to form the unwanted byproduct [^{11}C]methanol.

The optimization of yields is an essential practice for every radiochemist. In this regard, a particularly useful strategy—especially when working with short-lived radionuclides—lies in minimizing reaction, purification, and transfer times. For carbon-11 and its 20-min physical half-life, reducing the total synthesis time by just 3 min will result in a 10% increase in the yield of the reaction! Shortening the connecting tubes and miniaturizing reactor vessels can lead not only to reduced transportation times but also to reductions in the amount of product lost within the tubes and on vessel walls.

In addition, the consistent performance of radiotracer production ensures high molar/specific activity [3]. In general, every CO_2 source within the early components of the synthesizer can significantly affect molar activity. The main sources for nonradioactive CO_2 are the target gas itself and the connection tube between the target and the synthesizer. Therefore, the quality of the target gas as well as that of the inert gas used for transportation is the most important factor when it comes to low molar activity. Additional CO_2 contamination can also be caused by leaks in the system as well as poor quality traps for humidity or CO_2, especially traps based on molecular sieves or charcoal. Furthermore, one should also pay careful attention to the absence of CO_2 in the hydrogen gas used for the reduction of [^{11}C]CO_2 to [^{11}C]CH_4. In the end, it becomes clear that comprehensive and constant monitoring of the module is the best way to detect alterations or deteriorations within the system as early as possible and thus to reduce the probability of poor quality productions or even failed syntheses.

Post-target Production: From [^{11}C]CO_2 to [^{11}C]CH_3I

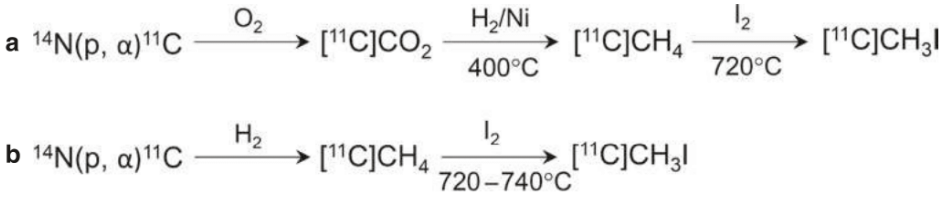
General Aspects of [^{11}C]CH_3I Production

^{11}C-based methylations are used to introduce a [^{11}C]CH_3-moiety into a molecule. They are—by far—the most widely used method for the ^{11}C-labeling of organic molecules. The most commonly used methylation agent is [^{11}C]methyl iodide ([^{11}C]CH_3I; [^{11}C]iodomethane), which can be produced either via the so-called "wet" method (Fig. 3) or the gas-phase method (Fig. 4; see also Chap. 11 "Carbon-11-Labeled Precursors for Labeling").

Fig. 3 "Wet" method for the preparation of [^{11}C]methyl iodide



Fig. 4 "Gas-phase" method for the preparation of [^{11}C] methyl iodide. (**a**) Starting from cyclotron-produced [^{11}C] carbon dioxide and (**b**) starting from cyclotron-produced [^{11}C]methane



"Wet" Production of [^{11}C]CH$_3$I

The "wet" chemistry method for the production of [^{11}C]methyl iodide [4] consists of the reduction of [^{11}C]carbon dioxide ([^{11}C]CO_2) to [^{11}C]methanol ([^{11}C]CH_3OH) via reduction with lithium aluminum hydride ($LiAlH_4$) and subsequent reaction with hydroiodic acid (HI). More specifically, [^{11}C]CO_2 is produced in the cyclotron via the ^{14}N(p,α)^{11}C-reaction and is then trapped in a solution of $LiAlH_4$ in tetrahydrofuran (THF). Thereby [^{11}C]CO_2 is reduced to [^{11}C]CH_3OH. After the evaporation of the THF, HI is slowly added to the precipitate, and the reaction mixture is heated to 90 °C. The resultant [^{11}C]CH_3I can then be distilled using an ascarite/phosphorus pentoxide trap into the solution containing the organic molecule to be ^{11}C-methylated. This trap is needed to remove excess HI (via ascarite) and to eliminate traces of water (via phosphorus pentoxide), both of which are essential for good methylation yields. This method is not without its drawbacks, of course. For example, the use of $LiAlH_4$ can be associated with low molar activities, and HI can degrade tubing and valves.

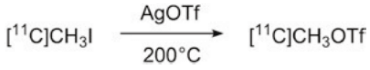
Tricks of the Trade To minimize contamination with atmospheric carbon, all sensitive tubes and vials should be flushed with inert gas (such as helium or argon) whenever possible.

"Gas-Phase" Production of [^{11}C]CH$_3$I

Although the "wet" chemistry method is very reliable in terms of radiochemical yields, the "gas-phase" method [5] is more commonly used for the production of [^{11}C]methyl iodide today. This approach is simpler than the "wet" chemistry method and results in higher molar activities due to its avoidance of the use of $LiAlH_4$ (a source of CO_2).

As in the "wet" method, the "gas-phase" method begins when [^{11}C]CO_2 is produced in the cyclotron. This [^{11}C]CO_2 is commonly trapped on a molecular sieve (4 Å) and converted to [^{11}C]CH_4 in the presence of Ni catalyst and hydrogen at 400 °C (Fig. 5). Afterward, [^{11}C]CH_4 is reacted with elemental iodine (I_2) at 720–740 °C to produce [^{11}C]CH_3I. Since the efficiency of the conversion of [^{11}C]CH_4 to [^{11}C]CH_3I is only 20–30%, this process might be repeated a couple of times. Indeed, there are several different technical solutions for this repetition. For example, a pump can be used to pass [^{11}C]CH_4 several times through the iodine column in a circulating process to increase the conversion yield. In this approach, a trap has to be installed to collect [^{11}C]CH_3I produced during the reaction. Following the reaction, [^{11}C]CH_3I can be released from the trap via heating and transferred to the reactor using a gentle gas flow (*e.g.* He, 5 mL/min).

Fig. 5 Synthesis of [^{11}C]methyl triflate



Tricks of the Trade In order to achieve high molar activities of [^{11}C]CH_3I, it is essential to continually flush all sensitive tubes and vials with an inert gas such as helium or argon. Furthermore, both the [^{11}C]CO_2 trap and the [^{11}C]CH_3I trap must be heated to 400 °C and 190 °C, respectively, immediately prior to the start of synthesis for a couple of minutes in order to remove moisture and atmospheric carbon. During the heating process, the inert gas should constantly flow (20–50 mL/min) through the traps. Before starting the synthesis, the traps have to be cooled down to room temperature again in order to enable efficient trapping.

Transformation of [^{11}C]CH$_3$I to [^{11}C]CH$_3$OTf

[^{11}C]Methyl triflate ([^{11}C]CH_3OTf) is a much more reactive reagent for ^{11}C-methylations and, therefore, is used for the ^{11}C-methylation of nucleophiles with low reactivity (Fig. 6). [^{11}C]Methyl triflate can be produced easily via the passage of [^{11}C]CH_3I through a heated (200 °C) column loaded with graphitized carbon impregnated with silver triflate (AgOTf) [6].

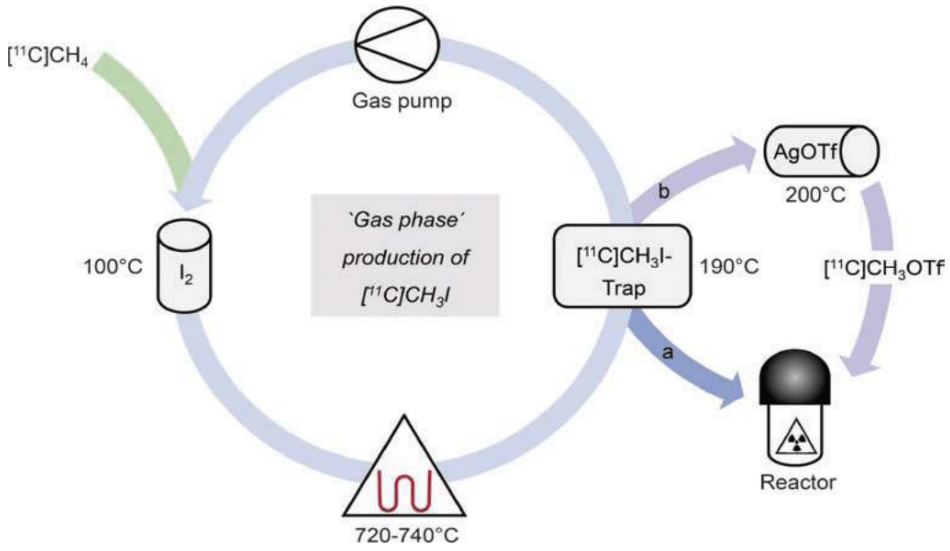


Fig. 6 "Gas-phase" production of [^{11}C]methyl iodide. (a) Direct delivery of [^{11}C]CH_3I into the reactor and (b) online passage of [^{11}C]CH_3I through AgOTf for conversion into [^{11}C]CH_3OTf

Tricks of the Trade The silver triflate (AgOTf)-impregnated graphitized carbon is extremely sensitive to moisture. If it comes into contact with humid air or other sources of moisture, the conversion of [^{11}C]CH_3I into [^{11}C]CH_3OTf will no longer occur, and the AgOTf-impregnated graphitized carbon has to be exchanged. Furthermore, the carbon substrate is sensitive to light and therefore has to be stored in the dark (the column in which this reagent is used has to be "light-proof" as well). After filling the column with the AgOTf-impregnated graphitized carbon, the column must be heated to 200 °C for 2 h under a continuous flow of inert gas (50–100 mL/min) to remove any contamination. The filled column can be reused for multiple syntheses but has to be kept closed under an inert atmosphere or needs to be heated up to 200 °C for 15–20 min under a continuous flow of inert gas (50–100 mL/min) before every synthesis.

A Comparison of the [^{11}C]-Methylation of Amines, Acids/Alcohols, and Thiols

Amines, acids, alcohols, and thiols can all be labeled with [^{11}C]CH_3 moieties. To this end, the functional group in question is reacted with [^{11}C]CH_3I/[^{11}C]CH_3OTf via nucleophilic substitution to create a secondary or tertiary amine, ester, ether, or thioether. ^{11}C-Methylations are quite simple and fast. Indeed, the reaction can often be performed by transferring [^{11}C]CH_3I or [^{11}C]CH_3OTf into a solution containing the precursor and quickly heating (<5 min) up this reaction solution. Solvents like DMSO, acetone, 2-butanone, or acetonitrile are commonly used depending on the temperature and polarity required for the reaction. For the methylation of hydroxyl and carboxyl groups, the addition of a base (*e.g.* NaOH or TBAH) is needed to deprotonate the functional group. In contrast, amines and thiols can be methylated without prior deprotonation. Examples of ^{11}C-methylations are provided in the sections on "Applications of Carbon-11 Tracers Produced Using [^{11}C]MeI" and "[^{11}C]CO_2 Fixation and Its Application."

Tricks of the Trade The precursor for methylation should be dissolved shortly before starting the synthesis. It is best to add the base directly into the solution of the precursor. In addition, one should always remember that heating and cooling might take significant extra time. As a result, gains in radioactive yield created by performing reactions at elevated temperatures may be offset by corresponding losses in yield due to decay.

Applications of Carbon-11 Tracers Produced Using [^{11}C]MeI

As previously mentioned in the section on "Post-target Production: From [^{11}C]CO_2 to [^{11}C]CH_3I", ^{11}C-methylations are the most common type of ^{11}C-labeling reactions. As a result, they have contributed to the development of a variety of important radiotracers with different applications.

^{11}C-Amino Acids

Due to the essential role of amino acids in all kinds of biological processes, several PET tracers based on amino acid scaffolds have been developed and have proved to be a versatile research tools. A variety of ^{11}C-labeling reactions—*e.g.*

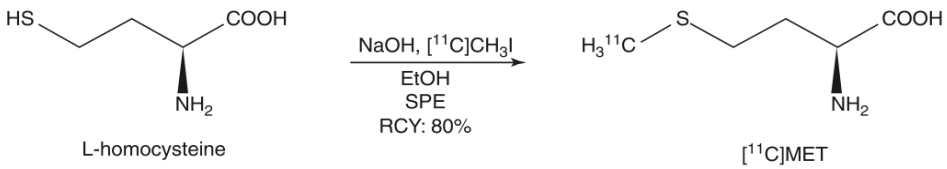


Fig. 7 Radiochemical synthesis of [^{11}C]MET

alkylations, carboxylations, and cyanations—can provide standard and non-standard amino acids which share the (bio) chemical properties of their nonradioactive counterparts. This latter point is particularly important, since ^{18}F-labeled amino acids have been proposed as more practical alternatives to ^{11}C-labeled amino acids. However, the introduction of fluorine atoms can significantly change the chemical properties of an amino acid [7].

L-[Methyl-^{11}C]Methionine The high uptake of [^{18}F] FDG in healthy brain tissues has been described as a major limitation for its use in the imaging of brain tumors. Radiolabeled amino acids such as L-[*methyl*-^{11}C]methionine were proposed as a way to circumvent this issue, since their uptake in a healthy brain is low. Moreover, the upregulation of type L-amino acid carriers in several brain tumors can lead to the increased accumulation of L-[*methyl*-^{11}C]methionine [8]. Although several ^{11}C-labeled amino acids have been used in neuro-oncology, L-[*methyl*-^{11}C]methionine is indisputably the most often employed due to its fast, convenient, and high-yield radiochemical synthesis which enables scans for two to three consecutive patients with the same production batch. While various methods have been described to synthesize L-[*methyl*-^{11}C]methionine, in our hands the most practical way utilizes L-homocysteine as the precursor (in EtOH and activated with 0.1 M NaOH) and [^{11}C]CH_3I as methylation agent (Fig. 7).

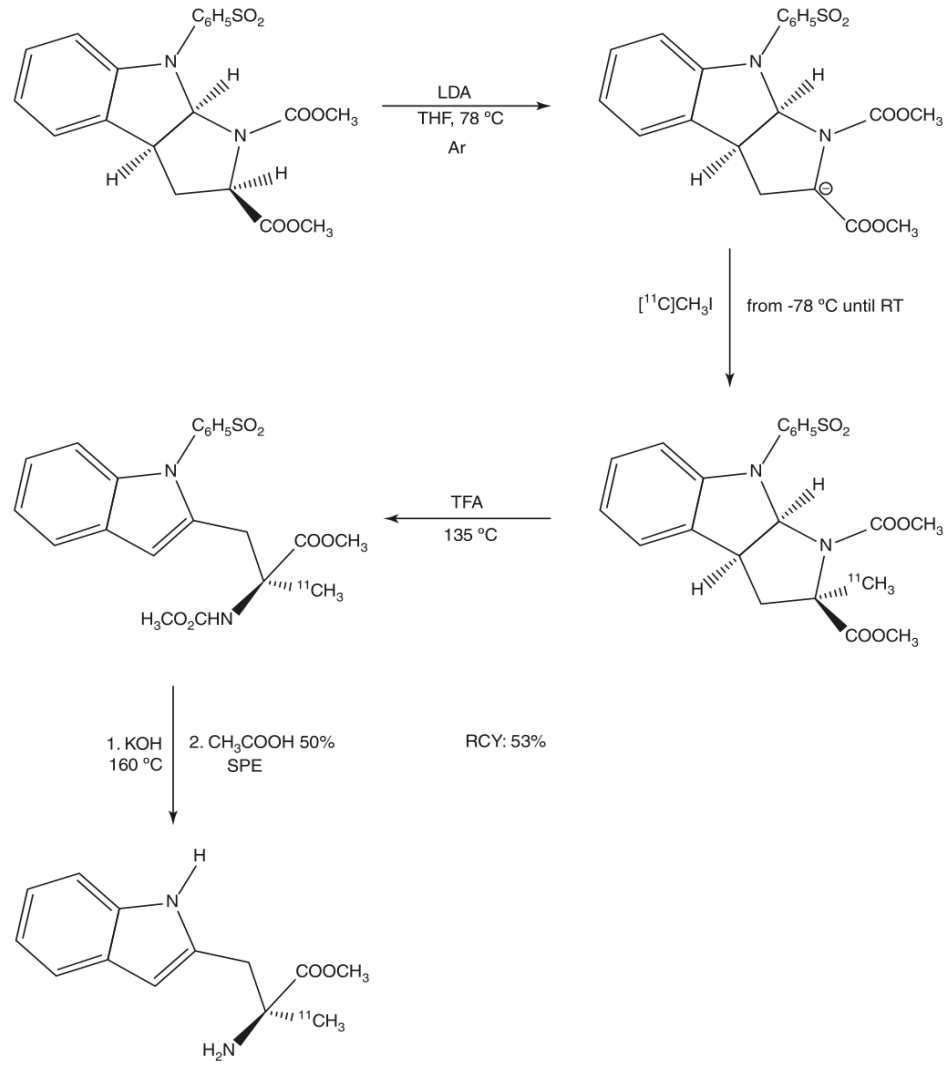
Alpha-[^{11}C]Methyl-L-Tryptophan ([^{11}C]AMT) Serotonergic neurotransmission is known to be relevant in different pathways of the brain, such as mood, sleep, feeding, and sexual behavior. Moreover, its dysregulation has been related to numerous neurologic and psychiatric disorders, including depression, affective diseases, and epilepsy. Therefore, the *in vivo* measurement of the rate of serotonin synthesis can provide a reliable view of ongoing serotonergic processes [9]. [^{11}C]AMT is the methylated form of the amino acid tryptophan—a precursor of serotonin (also known as 5-HT)—which is further enzymatically converted to α-[^{11}C]methyl-serotonin ([^{11}C]AM-5HT) in the brain. Unlike native 5-HT, [^{11}C]AM-5HT is not further metabolized by the enzyme monoamine oxidase A and therefore accumulates in serotonergic nerve terminals, a phenomenon which facilitates the evaluation of the synthesis rate of 5-HT [10]. More recently, [^{11}C]AMT has also been used in PET imaging of different tumors, such as breast, brain, and lung cancers [11]. The radiosynthesis [12] of [^{11}C]AMT is quite complex and highly sensitive to traces of moisture (Fig. 8). To wit, the synthesis requires the fresh preparation of lithium diisopropylamide (LDA) at −78 °C as well as the use of gastight syringes for the addition of liquids. LDA serves as a strong base to yield the activated enolate precursor under argon atmosphere that further reacts with [^{11}C]CH_3I. After the ^{11}C-methylation reaction, an acid-catalyzed decyclization steps the basic hydrolysis of the protecting groups, and finally SPE purification provides the desired product: [^{11}C]AMT.

^{11}C-Amino Acid Derivatives

[^{11}C]Choline Prostate carcinomas are the most common type of cancer in men, with particularly high rates of disease in 60–70-year-old men [13]. Although [^{18}F]FDG is by far the most used tracer in oncology, its utility in the diagnosis and staging of prostate cancer is limited due to several factors, including the uptake of the radiotracer in the adjacent urinary bladder, inflammatory conditions, and scar tissue. Therefore, radiotracers such as [^{11}C]choline and its ^{18}F-analogues were developed to target the biosynthesis of cellular membrane (phospholipids), since this process is known to be increased in prostate cancer cells. [^{11}C]Choline is also utilized similarly to L-[*methyl*-^{11}C]methionine in the diagnosis of brain tumors. The radiosynthesis of [^{11}C]choline has been amply described, and excellent yields are always obtained in short synthesis times (Fig. 9). For instance, the reaction takes place smoothly when using a solution of dimethylaminoethanol in DMF as the precursor and [^{11}C]CH_3I as the labeling agent. Purification by means of SPE (without HPLC) is sufficient, since a cation exchange resin can be used due to the cationic nature of the product.

^{11}C-Labeled Neuroimaging Tracers

Neuroimaging is one of the main applications of PET. In fact, the brain was the initial focus of PET imaging when the technology was first introduced, and over the years, numerous PET tracers have been developed to visualize brain functions and characterize neurological and psychiatric disorders. From a chemical point of view, methylated amines are a frequent structural motif in drugs designed for the central



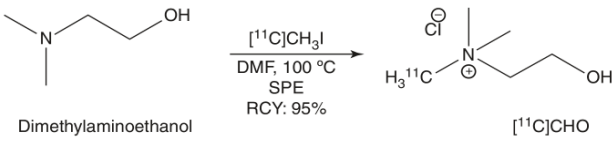


Fig. 8 Radiochemical synthesis of [^{11}C]AMT

Fig. 9 Radiochemical synthesis of [^{11}C]CHO

nervous system [14]. This has fueled the development of corresponding radiotracers via amine-directed ^{11}C-methylations, although tracers have been developed via the ^{11}C-methylations of alcohols, amides, and thiols as well. Moreover, the metabolic fate of these ^{11}C-methylated tracers usually follows a pathway that involves demethylation, thus producing radioactive metabolites that are more polar and have a lower molecular weight than the parent radiotracer and which often possess low uptake in the brain.

[^{11}C]Pittsburgh Compound B ([^{11}C]PiB) Alzheimer's disease (AD) is a type of dementia characterized by significant loss of neurons and deficiencies in neurotransmitter systems. It accounts for the majority of dementia cases, and its prevalence is estimated to quadruple over the next 50 years [15]. The occurrence of symptoms similar to those present in other types of dementia (*e.g.* mild cognitive impairment) impedes the accurate diagnosis of this disease. Autopsies, however, have revealed that the deposition of β-amyloid (in conjunction with the aggregation of tau protein) is an important hallmark of AD. Therefore, PET imaging of these β-amyloid deposits, also known as plaques, has been described as an effective technique to confront this problem. To this end, [^{11}C]PiB—a thioflavin T analogue—was developed as a tracer to visualize such plaques. It is until now the most applied tracer for the *in vivo* visualization of amyloid plaques, although a couple of ^{18}F-labeled analogues have

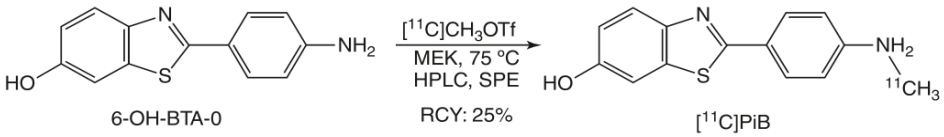


Fig. 10 Radiochemical synthesis of [^{11}C]PiB

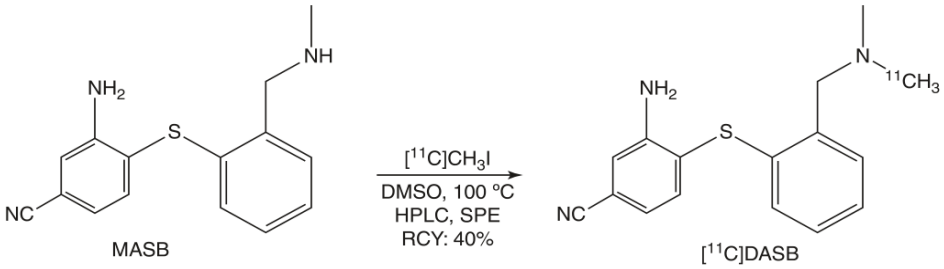


Fig. 11 Radiochemical synthesis of [^{11}C]DASB

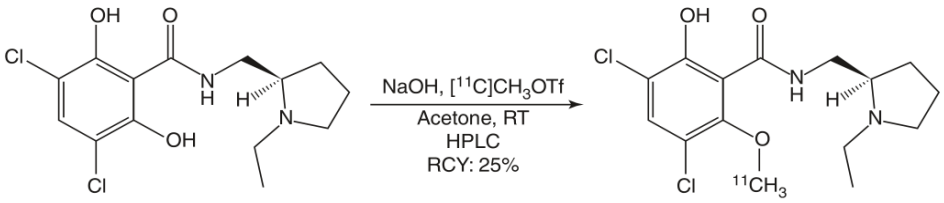


Fig. 12 Radiochemical synthesis of [^{11}C]raclopride

been developed as well. The radiochemical synthesis of [^{11}C]PiB (Fig. 10) initially employed [^{11}C]CH_3I as the labeling agent but was later optimized using [^{11}C]CH_3OTf [16]. In light of the lower nucleophilicity of anilines, the higher reactivity of [^{11}C]CH_3OTf proves beneficial, ultimately creating a simple and efficient strategy for radiolabeling. As usual, purification via HPLC and SPE after the labeling reaction yields the product [^{11}C]PiB.

[^{11}C]3-Amino-4-(2-Dimethylaminomethylphenylsulfanyl)Benzonitrile ([^{11}C]DASB) The serotonin transporter (5-HTT) is a protein located in the plasma membrane of serotonergic neurons which regulates 5-HT concentrations from the synaptic cleft through reuptake into the presynaptic neuron. The *in vivo* assessment of 5-HTT expression and density—although sometimes intricate—can enable enhanced analysis of neuropsychiatric disorders. Dysregulation of 5-HTT has been reported in several conditions, especially depression. Moreover, parallel investigations have suggested the involvement of the 5-HTT polymorphisms in such conditions. Therefore, 5-HTT has been proposed as a target for drugs known as selective serotonin reuptake inhibitors (SSRIs). Although several compounds have been nominated as potential PET radiotracers for 5-HTT, [^{11}C]DASB is widely acknowledged as the gold standard tracer for PET studies of the 5-HTT due to its high affinity and selectivity for its target, high brain uptake, and fast binding equilibrium. The synthesis of [^{11}C]DASB (Fig. 11) occurs in a straightforward manner after the trapping of [^{11}C]CH_3I in a solution containing the precursor—3-amino-4-(2-methylaminomethylphenylsulfanyl)-benzonitrile (MASB)—in DMSO. Afterward, the product is purified using HPLC and SPE [17].

[^{11}C]3,5-Dichloro-N-[[(2S)-1-Ethylpyrrolidin-2-yl] Methyl]-2-Hydroxy-6-Methoxy Benzamide ([Methoxy-^{11}C]Raclopride) The neurotransmitter dopamine exerts its functions through five G-protein-coupled receptors—D_1 and D_5 (both D_1-type receptors) as well as D_2, D_3, and D_4 (all three D_2-type receptors)—which possess a broad distribution in the brain and also in the peripheral nervous system. Moreover, the involvement of the dopamine receptor system in a variety of diseases has been reported, including movement disorders such as Parkinson's and Huntington's diseases. In particular, the role of the D_2/D_3 receptors in these conditions has been investigated with [*methoxy*-^{11}C]raclopride (Fig. 12) by evaluating the density of these postsynaptic receptors in the striatum. [*Methoxy*-^{11}C]Raclopride is a benzamide derivative and a highly selective D_2/D_3 receptor antagonist which possesses a moderate affinity toward these receptors. The synthesis of [*methoxy*-^{11}C]raclopride has been reported using both [^{11}C]CH_3I and [^{11}C]CH_3OTf, though the latter has shown to produce higher radiochemical yields. To this end, a solution of desmethyl-raclopride in acetone or 2-butanone together with 5 M sodium hydroxide is commonly used as precursor solution and kept at low temperatures (15–20 °C) during the trapping of [^{11}C]CH_3OTf. After the labeling reaction, the product is purified via HPLC. By using the

appropriate conditions for this purification, the fraction containing the product can be directly filtered into the product vial without further treatment (*i.e.* no SPE necessary).

[^{11}C]Harmine ([^{11}C]HAR) The degradation of monoamine neurotransmitters (*e.g.* 5-HT, dopamine, or norepinephrine) plays a key role in the regulation of neurotransmission. A type of enzymes known as monoamine oxidases (MAO)—and more specifically the enzyme MAO-A—is responsible for the degradation of the neurotransmitters mentioned above. MAO-A is primarily found in catecholaminergic neurons, and its dysregulation has been correlated with several behavioral and neuronal disease states, including panic, bipolar affective, and major depressive disorders. Besides its expression in the brain, MAO-A is also located in cardiac muscle cells, where it has been identified as a major source of reactive oxygen species (ROS) that can affect function and viability of the myocardium. The *in vivo* measurement of the density of MAO-A has been achieved with a couple of PET ligands, including the β-carboline derivative [^{11}C]HAR, which is a reversible inhibitor of MAO-A that displays high affinity and selectivity for the enzyme. The radiosynthesis of [^{11}C]HAR requires a base for the formation of the phenoxide anion (Fig. 13) that subsequently reacts with [^{11}C]CH_3I [18]. Therefore, a solution of the precursor harmol in DMSO must be freshly prepared for each radiosynthesis prior to the addition of 5 M sodium hydroxide. The resulting solution should be light yellow; a green-colored solution should not be obtained.

[^{11}C]CO_2 Fixation and Its Application

Introduction to [^{11}C]CO_2 Fixation Chemistry

The application of [^{11}C]CO_2 as a starting material for ^{11}C-radiosyntheses is attractive for accessing functional groups with high oxidation states such as carboxylic acids, ureas, and carbamates (Fig. 14). From a chemical point of view, the direct incorporation of [^{11}C]CO_2 into radiotracers is quite challenging, as carbon dioxide is unreactive, and thus

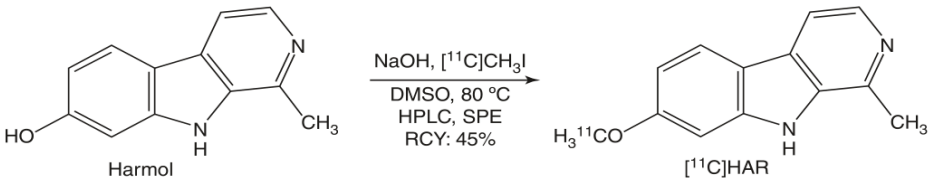


Fig. 13 Radiochemical synthesis of [^{11}C]HAR

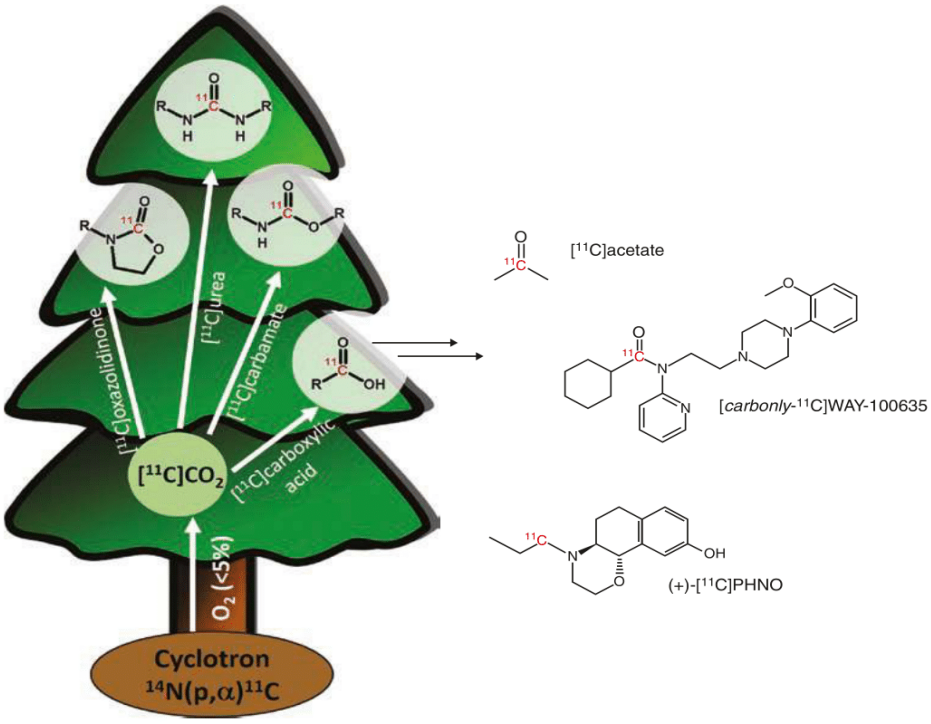


Fig. 14 Reaction pathways to [^{11}C]CO_2 fixation products yielding in high oxidation state functional groups

highly reactive nucleophiles or catalysts must be used to facilitate the effective fixation of [^{11}C]CO_2 [19].

A successful synthetic procedure for the fixation of [^{11}C]CO_2 uses organometallic reagents such as Grignard reagents, organolithiums, or silanamines. The functional groups formed through these reactions are mostly carboxylic acids and derivatives thereof such as carboxyamides. In general, these very reactive reagents are moisture sensitive and unstable, which makes automation cumbersome and reproducibility difficult (for a discussion of Grignard reactions, see the section on "Grignard Reactions in Carbon-11 Radiochemistry (In-Loop)." In contrast, transition metal-mediated carboxylation reactions involving organoboron and organozinc reagents are superior in terms of the stability of the reagents.

The spectrum of CO_2 fixation agents has recently expanded, especially due to the growing field of "green" chemistry and approaches involving guanidines and amidines. These strategies facilitate the formation of functional groups with even higher oxidation states than carboxylic acid derivatives, including ureas, carbamates, and oxazolidinones [20].

Grignard Reactions in Carbon-11 Radiochemistry (In-Loop)

Grignard reactions involve organometallic compounds—alkyl or aryl magnesium halides—which work as nucleophiles, attacking electrophilic carbons and leading to the formation of carbon-carbon bonds. In radiochemistry, [^{11}C]CO_2 typically serves as the electrophilic reagent for these reactions. Grignard reactions can be performed rapidly and quantitatively. These traits, along with the direct availability of [^{11}C]CO_2 from cyclotrons, make this approach highly attractive for the production of PET radiotracers. One of the most popular PET tracers, [^{11}C]acetate, was developed by Pike *et al.* more than 35 years ago and is produced via a Grignard reaction using [^{11}C]CO_2 [21]. Since then, the most common radioactive carboxylation reactions have been the syntheses of [^{11}C]acetate and [^{11}C]palmitate. Grignard reactions have also been applied to the production of [*carbonyl*-^{11}C]WAY100635 and (+)-[^{11}C]PHNO, two important radiotracers in neuroimaging. The syntheses of both were described by Mark *et al.* using a loop for the Grignard reaction [22].

Moisture Sensitivity, Solvents, and Preparation

Grignard reagents are extremely sensitive to moisture, and any contact with water results in the formation of magnesium hydroxides that precipitate in organic solvents. Therefore, the synthesis module in which the Grignard reaction takes place must be moisture-free. It is not possible to keep the whole hot cell under inert atmosphere, but the operator should avoid any water contamination inside the cell while preparing the synthesizer. The optimal strategy for cleaning and preparing a synthesizer prior to Grignard reactions is comprised of three washing steps. First, the system is washed with water to remove all hydrophilic impurities. Afterward, acetone is used as a cleaning agent to eliminate any water residue. Finally, an additional wash is performed with a nonpolar organic solvent, typically the same substance used for performing the reaction. The last washing is critical, as acetone itself contains an electrophilic carbon (a ketone) that is susceptible to attack by Grignard reagent. In addition, all lines must be properly dried with an inert gas, typically helium or argon. Grignard reactions require dry and aprotic solvents such as diethylether or tetrahydrofuran (THF). Furthermore, it is important to consider that these solvents may contain stabilizing agents that can hinder the synthesis or lead to the formation of by-products. Hence, the use of freshly distilled solvents is recommended, as they are free of any stabilizers and completely dry. Moreover, the organometallic reagent must be used within a short period of time to obtain good molar activities. The reason is clear: the ubiquitous presence of CO_2. The diffusion of air (containing atmospheric CO_2) through the septum of the storage bottle may take place, leading to the incorporation of this CO_2—rather than [^{11}C]CO_2—into the Grignard reagent even at room temperature or during storage.

Technical Considerations: Reaction Vessels Versus In-Loop Syntheses for Grignard Reactions

Grignard reactions can be performed in every vial or vessel that enables reactions under inert atmosphere. Two approaches are commonly used for Grignard-based radiosyntheses. The first is the "classical" vessel-based method using a reactor. The second approach, in contrast, uses a polymeric loop as the site of the reaction. Both approaches have advantages and disadvantages. As a result, preparations of [^{11}C]acetate, for example, using both methods have been published [23, 24]. For reactions in a conventional reactor, the metal halide precursor is dissolved in an aprotic and dry solvent, and [^{11}C]CO_2 is bubbled through the precursor solution. Subsequently, the reaction is quenched and the solvents are evaporated. Thereafter, the product is purified by a distillation step, leaving metal-hydroxyl impurities inside the reactor vessel and transferring the clean product to a product vial. On the one hand, this purification method is relatively elegant and efficient for one-step reactions. On the other hand, the distillation step is time-consuming and requires a tight system that is both temperature- and pressure-stable. Therefore, this approach is not practical for radiosyntheses involving multistep reactions during which the decay of carbon-11 plays a dominant role in the determination of yield.

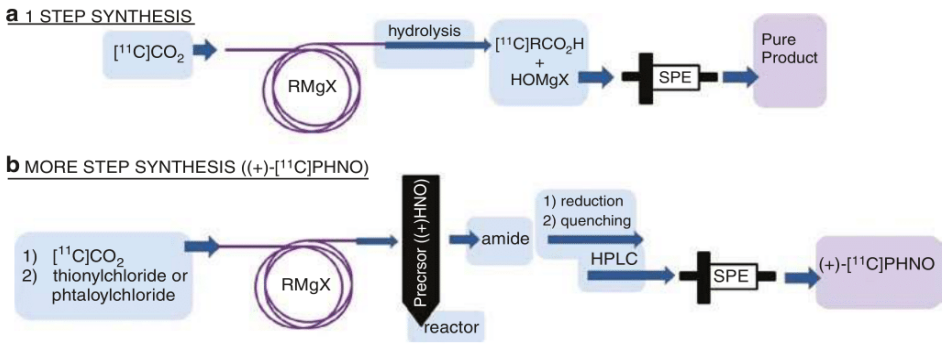


Fig. 15 Scheme of in-loop syntheses for (**a**) a one-step reaction and (**b**) a multistep synthesis of (+)-[^{11}C]PHNO

The alternative method is the "in-loop" synthesis (Fig. 15). In this case, the inner surface of a polymer loop is coated with the Grignard solution by pushing it through the loop with a flow of an inert gas. Subsequently, [^{11}C]CO_2 is passed through the impregnated loop, and it reacts with the organometallic reagent. When performing a one-step reaction that forms a carboxylic acid salt, the crude mixture can then be purified using an HPLC system. In case of multistep reactions (e.g., (+)-[^{11}C]PHNO and [*carbonyl*-^{11}C]WAY-100635), the intermediate species remain in the loop and are eluted into a reaction vessel during the subsequent step. Perhaps not surprisingly, the length and material of the loop must be tested and optimized for each application. The loop material must exhibit low non-specific binding and resistance to both the Grignard reagent and its solvent. The in-loop reaction boasts high conversion rates due to reaction of the reagents on the large surface area of the loops. Accordingly, one significant advantage of the in-loop method is the possibility of fast conversion reactions without the need for cooling or heating. Additionally, plastic tubes are usually available in each laboratory, so in-loop syntheses are easily accessible for anyone and offer a plethora of synthesis possibilities. However, the crude reaction mixture of multistep "in-loop" reactions must be purified via distillation or the use of SPE cartridges in a manner similar to that used for vial-based systems.

Other Applications: Neuroimaging Using (+)-[^{11}C]PHNO and [Carbonyl-^{11}C]WAY-100635

In neuroimaging, radiotracers that specifically target receptors or transporters with high (subtype) selectivity are used. In this respect, (+)-[^{11}C]PHNO and [*carbonyl*-^{11}C]WAY-100635 are applied to target dopamine D_2/D_3 receptors ((+)-[^{11}C]PHNO) or serotonin-1A receptors ([*carbonyl*-^{11}C]WAY-100635), respectively, for the visualization of physiological processes in the brain or mental disorders like schizophrenia or depression. The production of these radiotracers requires multistep syntheses, after which by-products are removed. Both syntheses start with the Grignard reaction followed by the conversion of the carboxyl group to the respective carboxylic acid chloride using thionyl chloride. The crude mixture is transferred to a reactor containing the dissolved precursor—(+)HNO or WAY-100634, respectively—by pushing the thionyl chloride/THF solution through the loop. While the reaction of [*carbonyl*-^{11}C]WAY-100635 is stopped after a heating step, the synthesis of (+)-[^{11}C]PHNO requires an additional step in which $LiAlH_4$ is used to reduce the acyl intermediate to the alkyl product [25–27]. The purification of both compounds takes place via semi-preparative HPLC, and SPE is subsequently used to remove the organic solvents used during chromatography (as described in the section on "Technical Aspects of Carbon-11: Commercially Available Synthesizers and Optimization"). To conclude, Grignard reactions are a versatile tool for the incorporation of carbon-11 into radiotracers and have become well-established in the clinic. Moreover, the advent of in-loop syntheses has made them even more accessible for multistep reactions in radiochemistry.

Tricks of the Trade Careful attention should be dedicated to the removal of all traces of water/moisture from all equipment used with reactive Grignard species. Ideally, single-use materials should be employed for these steps. Stabilizers (*e.g.* xylene) in reagents and solvents should also always be avoided, as they might lead to the formation of by-products.

Application of Other Carbon-11 Precursors in Tracer Preparation

Overview of Other Methodologies for the Production of ^{11}C-Labeled Radiotracers

The vast majority of carbon-11 tracers are produced via reaction with electrophilic methylating agents such as [^{11}C]CH_3I or [^{11}C]CH_3OTf. In the section on "[^{11}C]CO_2 Fixation and Its Application," we have seen that the reaction between

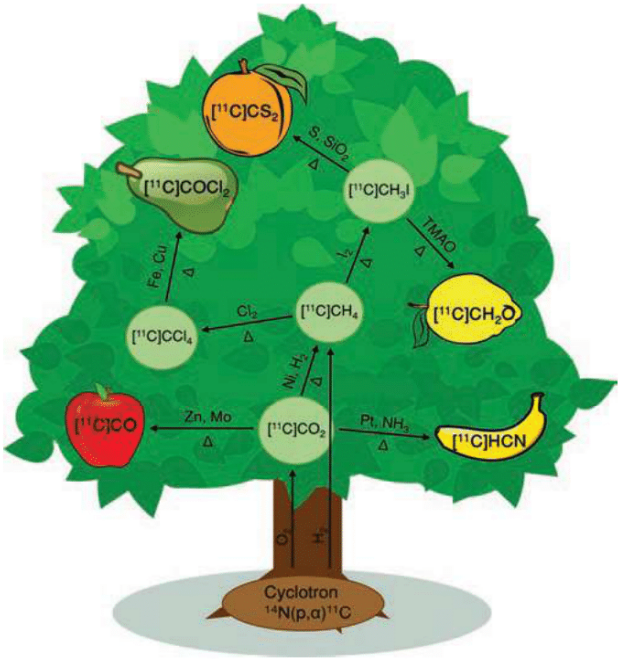


Fig. 16 Reaction pathways to less-common carbon-11 precursors

Grignard reagents and $[^{11}C]CO_2$ has also become a well-established route to ^{11}C-based radiotracers. Considering the breadth of carbon chemistry, it is surprising that ^{11}C-labeled radiotracers are almost exclusively synthesized from a small variety of radiolabeled precursors. This imbalance between what is *possible* and what is *feasible* can be attributed to the high degree of automation and time constraints associated with ^{11}C-based radiosyntheses. However, unconventional carbon-11 precursors are nonetheless important tools that can both open up synthetic pathways to otherwise inaccessible radiotracers and enable the labeling of a higher number of positions within a molecule. An assortment of such rarely used carbon-11 precursors is shown in Fig. 16 as lower- and higher-hanging fruits [28].

Carbonylation

The term "carbonylation" refers to the introduction of carbon monoxide into organic or inorganic molecules. $[^{11}C]CO$ can be straightforwardly and rapidly (<5 min) obtained via the reduction of $[^{11}C]CO_2$ over zinc or molybdenum in high radiochemical yields. However, compared to the other carbon-11 precursors discussed in this chapter, $[^{11}C]CO$ is quite unreactive. One strategy to increase the reactivity of $[^{11}C]CO$ is to apply pressures of 350+ bar within an autoclave system in order to increase its solubility and shift the reaction equilibrium toward nongaseous products. Obviously, however, this high-pressure process comes with disadvantages such as high-maintenance intervals and complexity. In response to the drawbacks of high-pressure processes, lower-pressure methods have been developed. Generally, ^{11}C-carbonylations are typically performed using transition metal-mediated cross-couplings between nucleophilic and electrophilic reagents, thereby enabling the synthesis of a variety of carbonyl-labeled moieties (*e.g.* esters, amides, hydrazines, acrylamides, and carbamates). Not surprisingly, the ligand system of the transition metal strongly affects the efficiency of $[^{11}C]CO$ trapping and therefore the radiochemical yield [29]. One example of ^{11}C-carbonylation is the synthesis of [*carbonyl*-^{11}C]raclopride, which is labeled at a metabolically more stable position than the better known [*methoxy*-^{11}C] raclopride (Fig. 17).

Reactive C=O Species: [^{11}C]Formaldehyde and [^{11}C]Phosgene

Formaldehyde is a well-studied and multifaceted reagent which can be used for a myriad of reactions. As early as 1972, $[^{11}C]$formaldehyde ($[^{11}C]HCHO$) was prepared via the ferric-molybdenum oxide-catalyzed oxidation of $[^{11}C]$methanol. However, the specialized equipment required for this procedure hampered the application of this approach in most carbon-11 laboratories. Recently, $[^{11}C]$formaldehyde has been prepared in a one-pot synthesis by treating $[^{11}C]CH_3I$ with trimethylamine *N*-oxide (TMAO), a strategy which has greatly widened the scope of its application and led to a series of novel radiotracers [30]. Examples of radiosyntheses performed with $[^{11}C]$formaldehyde include reductive aminations, ring closure reactions, and electrophilic aromatic substitution. Depending on the substrate, a reductive amination approach can have several advantages compared to conventional $[^{11}C]CH_3I$-based methylations, including insensitivity to moisture, reduced cross-reactivity with other nucleophiles, and avoidance of alkaline reaction conditions. This, in turn, helps radiochemists eschew protecting groups when using this strategy, as illustrated by the conversion of serotonin to *N*-$[^{11}C]$methylserotonin (see Fig. 17) [31].

Considering its high reactivity and the high number of functional groups that it could theoretically label, $[^{11}C]$phosgene ($[^{11}C]COCl_2$) is a very promising carbon-11 precursor. However, the use of $[^{11}C]COCl_2$ has remained limited to a small number of groups due to its cumbersome synthesis. Typical procedures for the synthesis of $[^{11}C]$phosgene involve the chlorination of $[^{11}C]CH_4$ to form $[^{11}C]CCl_4$, which is then oxidized at high temperature in the presence of iron or copper catalysts without the intentional addition of oxygen. In another synthetic route which has increased the reliability of the synthesis of $[^{11}C]$phosgene, the ^{11}C-labeled synthon is formed in the pretreatment tube of a commercially

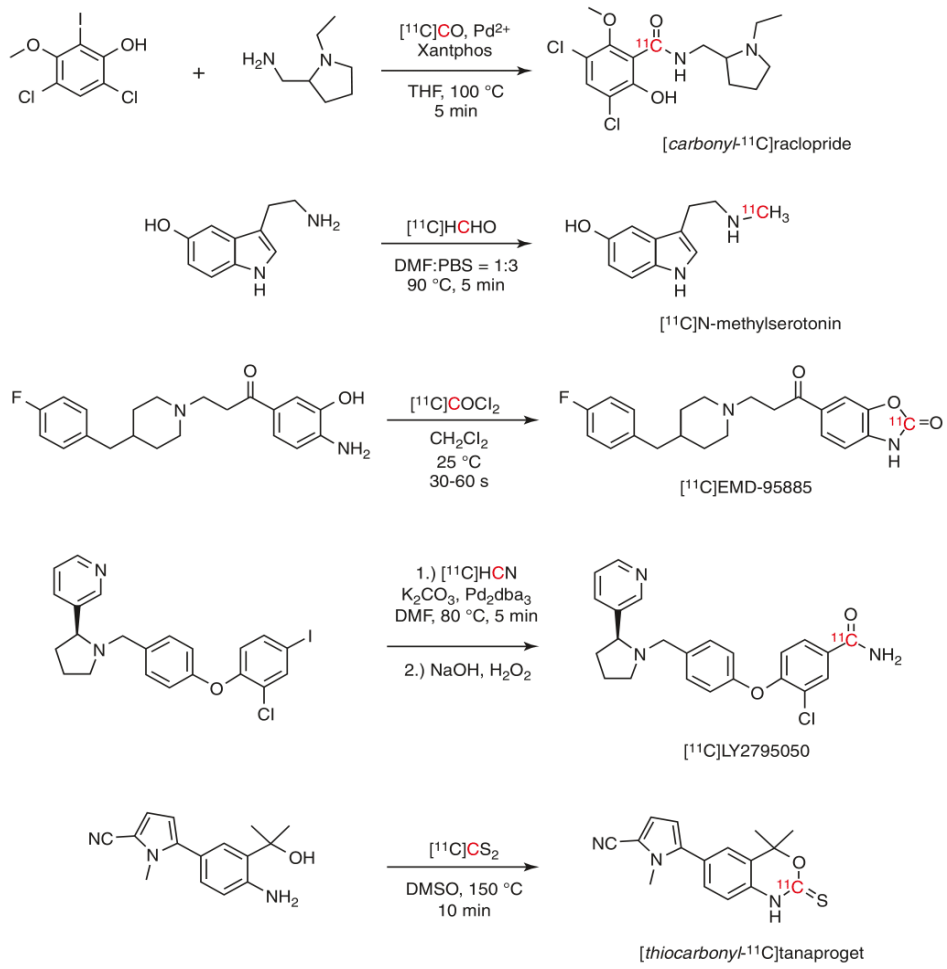


Fig. 17 Representative reactions of the carbon-11 precursors discussed in this chapter

available CCl_4 gas detection system. A variety of structures are accessible using [^{11}C]phosgene-based radiolabeling reactions, including amides, carbamates, ureas, and uric acids [32]. Indeed, the high reactivity of [^{11}C]phosgene is exemplified by the almost instantaneous formation of [^{11}C]EMD-95885 (see Fig. 17) [33].

[^{11}C]Hydrogen Cyanide ([^{11}C]HCN)

Due to the cataclysmic combination of toxicity with volatility, even experienced synthetic chemists try to avoid using hydrogen cyanide. Radiochemists, however, can work with [^{11}C]HCN as carbon-11 precursor without fear, since the amount used lies far below that which is dangerous. [^{11}C]HCN can be prepared by reacting [^{11}C]CH_4 with NH_3 over a platinum catalyst at 950 °C [34]. [^{11}C]HCN is then typically reacted with nitriles bearing aromatic halides or aryl-boronic acids under transition metal-catalyzed conditions. Furthermore, aryl nitriles can be obtained via nucleophilic aromatic substitution with activated arenes. Alpha-amino acids can be synthesized via the nucleophilic ring opening of activated aziridines or the Strecker reaction from aldehydes or ketones. Radiolabeling with [^{11}C]HCN offers more than just a one-step reaction to nitriles, since amides, carboxylic acids, and amines can be readily generated from subsequent reactions. For example, in the synthesis of [^{11}C]LY2795050, the radiolabeled nitrile is hydrolyzed to a primary amide (see Fig. 17) [35]. However, it is important to note that HCN readily adsorbs on stainless steel, and thus inert tubing (*e.g.* Teflon™) must be used in order to avoid the loss of [^{11}C]HCN in transport lines.

[^{11}C]Carbon Disulfide ([^{11}C]CS_2)

Compared to CO_2, carbon disulfide (CS_2) has weaker double bonds and thus increased reactivity. CS_2 is a liquid under standard conditions and is readily condensed and trapped in solution, making it a relatively easy-to-handle carbon-11

precursor. [^{11}C]CS_2 can be obtained by passing [^{11}C]CH_3I over a column containing elemental sulfur and sand at 500 °C. [^{11}C]Dithiocarbamate salts can be formed by reacting [^{11}C]CS_2 at room temperature with a variety of primary amines. Upon heating these salts, they release H_2S and further react to form symmetrical [^{11}C]thiocarbonyl-labeled thioureas. In the presence of electrophilic alkylating agents, thioureas can furthermore be S-alkylated, thereby opening up access to a wide variety of target structures. The three-step reaction from [^{11}C]CS_2 to *S*-alkylated thioureas can be performed in a one-pot setup which is rapid enough for carbon-11 chemistry and results in high radiochemical yields and purities. [^{11}C]Carbon disulfide can also be used for ring closure reactions between amines and alcohols, as illustrated by the synthesis of [*thiocarbonyl*-^{11}C]tanaproget (see Fig. 17) [36].

Technical Advantages: Solid Support, Online, or Other Approaches

The chemical behavior of most carbon-11 precursors (*e.g.* [^{11}C]CH_3I) is best studied (and understood) in solution. Therefore, it appears logical that the majority of ^{11}C-labeling reactions are conducted in the solution phase as well. Indeed, vial-based "in-solution" reactions are predominantly used in carbon-11 chemistry, but reactions on solid supports—such as "on-cartridge" or "in-loop" reactions (see the section on "[^{11}C]CO_2 Fixation and Its Application")—have been developed as well. Syntheses using solid supports offer several advantages that are especially important in carbon-11 chemistry, such as decreased reaction times, higher degrees of automation, and enhanced reliability. This is illustrated by the "on-cartridge" synthesis of [*N-methyl*-^{11}C]choline, in which the precursor 2-dimethylaminoethanol is loaded onto a C_{18} cartridge prior to synthesis. [^{11}C]CH_3I is then distilled across the C_{18} cartridge, and a cationic exchange cartridge is sufficient for the subsequent purification of the product, enabling an overall synthesis time of 12 min from the end of bombardment (EOB) [37].

The Bottom Line

- Speed up! Time is crucial when dealing with carbon-11. All processes from EOB to product release after quality control need to be optimized for minimal time consumption in order to obtain sufficient yields and high molar activities.
- The most important reaction pathway for ^{11}C-radiochemistry is ^{11}C-methylation, and the most important synthon is [^{11}C]methyl iodide ([^{11}C]CH_3I). For higher reactivity, [^{11}C]methyl triflate ([^{11}C]CH_3OTf) can be prepared directly from [^{11}C]CH_3I.
- The use of other ^{11}C-labeled synthons opens additional routes for ^{11}C-radiolabeling in different positions and makes it possible to incorporate carbon-11 into some molecules for which [^{11}C]CH_3I and [^{11}C]CH_3OTf are unsuitable. Along these lines, [^{11}C]CO_2, [^{11}C]CS_2, [^{11}C]$COCl_2$, [^{11}C]HCHO, [^{11}C]CO, or [^{11}C]HCN is used.
- Grignard reactions are attractive due to their ability to incorporate [^{11}C]CO_2, but they are extremely moisture-sensitive and require the use of aggressive chemicals. This makes the automation of these ^{11}C-radiosyntheses very challenging.
- The most widely applied ^{11}C-radiotracer is the amino acid L-[*methyl*-^{11}C]methionine. Clinically, it is mainly used to assess brain tumors.
- ^{11}C-Labeled compounds play a particularly important role in neuroimaging and studying specific processes of nerve cells. Important radiotracers in this respect are [^{11}C]raclopride, [^{11}C]DASB, and [^{11}C]PiB (among many others).

References

1. Shao X, Hoareau R, Runkle AC, Tluczek LJM, Hockley BG, Henderson BD, et al. Highlighting the versatility of the Tracerlab synthesis modules. Part 2: fully automated production of [11C]-labeled radiopharmaceuticals using a Tracerlab FX C-pro. J Label Compd Radiopharm. 2011;54(14):819–38.
2. European Directorate for the Quality of Medicines (EDQM). Parenteral Preparations. In: European Pharmacopoeia, 9th Edition. Strasbourg: Council of Europe; 2015. pp. 871–3.
3. Gómez-Vallejo V, Llop J. Specific activity of [11C]CH3I synthesized by the "wet" method: main sources of non-radioactive carbon. Appl Radiat Isotop. 2009;67(1):111–4.
4. Långström B, Lundqvist H. The preparation of 11C-methyl iodide and its use in the synthesis of 11C-methyl-L-methionine. Int J Appl Radiat Isot. 1976;27(7):357–63.
5. Larsen P, Ulin J, Dahlstrom K, Jensen M. Synthesis of [11C] iodomethane by iodination of [11C]methane. Appl Radiat Isotop. 1997;48(2):153–7.
6. Jewett DM. A simple synthesis of [11C]methyl triflate. Int J Radiat Appl Instrum A. 1992;43(11):1383–5.
7. Ermert J, Coenen HH. Methods for 11C- and 18F-labelling of amino acids and derivatives for positron emission tomography imaging. J Label Compd Radiopharm. 2013;56(3–4):225–36.
8. Crippa F, Alessi A, Serafini GL. PET with radiolabeled aminoacid. Q J Nucl Med Mol Imaging. 2012;56(2):151–62.
9. Visser AKD, van Waarde A, Willemsen ATM, Bosker FJ, Luiten PGM, den Boer JA, et al. Measuring serotonin synthesis: from conventional methods to PET tracers and their (pre)clinical implications. Eur J Nucl Med Mol Imaging. 2011;38(3):576–91.
10. Diksic M, Nagahiro S, Sourkes TL, Yamamoto YL. A new method to measure brain serotonin synthesis in vivo. I. Theory and basic data for a biological model. J Cereb Blood Flow Metab. 1990;10(1):1–12.
11. Huang X, Xiao X, Gillies RJ, Tian H. Design and automated production of 11C-alpha-methyl-l-tryptophan (11C-AMT). Nucl Med Biol. 2016;43(5):303–8.
12. Chakraborty PK, Mangner TJ, Chugani DC, Muzik O, Chugani HT. A high-yield and simplified procedure for the synthesis of α-[11C]methyl-l-tryptophan. Nucl Med Biol. 1996;23(8):1005–8.

13. Reske SN, Blumstein NM, Neumaier B, Gottfried H-W, Finsterbusch F, Kocot D, et al. Imaging prostate cancer with 11C-choline PET/CT. J Nucl Med. 2006;47(8):1249–54.
14. Engkvist O, Wrede P, Rester U. Prediction of CNS activity of compound libraries using substructure analysis. J Chem Inf Comput Sci. 2003 Jan 1;43(1):155–60.
15. Cohen AD, Klunk WE. Early detection of Alzheimer's disease using PiB and FDG PET. Neurobiol Dis. 2014;72(Pt A):117–22.
16. Philippe C, Haeusler D, Mitterhauser M, Ungersboeck J, Viernstein H, Dudczak R, et al. Optimization of the radiosynthesis of the Alzheimer tracer 2-(4-N[11C]methylaminophenyl)-6-hydroxybenzothiazole ([11C]PIB). Appl Radiat Isot. 2011;69(9):1212–7.
17. Haeusler D, Mien L-K, Nics L, Ungersboeck J, Philippe C, Lanzenberger RR, et al. Simple and rapid preparation of [11C] DASB with high quality and reliability for routine applications. Appl Radiat Isot. 2009;67(9):1654–60.
18. Philippe C, Zeilinger M, Mitterhauser M, Dumanic M, Lanzenberger R, Hacker M, et al. Parameter evaluation and fully-automated radiosynthesis of [11C]harmine for imaging of MAO-A for clinical trials. Appl Radiat Isot. 2015;97:182–7.
19. Rotstein BH, Liang SH, Holland JP, Collier TL, Hooker JM, Wilson AA, Vasdev N. 11CO2 fixation: a renaissance in PET radiochemistry. Chem Commun (Camb). 2013;49(59):5621–9.
20. Mossine AV, Brooks AF, Jackson IM, Quesada CA, Sherman P, Cole EL, et al. Synthesis of diverse 11C-labelled PET radiotracers via direct incorporation of [11C]CO2. Bioconjug Chem. 2016;27(5):1382–9.
21. Pike VW, Eakins MN, Allan RM, Selwyn AP. Preparation of [1−11C]acetate—an agent for the study of myocardial metabolism by positron emission tomography. Int J Appl Radiat Isot. 1982;33(7):505–12.
22. Rami-Mark C, Unbergsboek J, Haeusler D, Nics L, Philippe C, Mitterhauser M, et al. Reliable set-up for in-loop 11C-carboxylations using Grignard reactions for the preparation of [carbonyl-11C]WAY-100635 and [11C]-(+)-PHNO. Appl Radiat Isot. 2013;82:75–80.
23. Mitterhauser M, Wadsak W, Krcal A, Schmaljohann J, Bartosch E, Eidherr H, et al. New aspects on the preparation of [11C]acetate—a simple and fast approach via distillation. Appl Radiat Isot. 2004;61(6):1147–50.
24. Soloviev D, Tamburella C. Captive solvent [11C]acetate synthesis in GMP conditions. Appl Radiat Isot. 2006;64(9):995–1000.
25. Plisson C, Huiban M, Pampols-Maso S, Singleton G, Hill SP, Passchier J. Automated preparation of the dopamine D2/3 receptor agonist ligand [11C]-(+)-PHNO for human PET imaging studies. Appl Radiat Isot. 2012;70(2):380–7.
26. Wilson AA, McCormick P, Kapur S, Willeit M, Garcia A, Hussey D, et al. Radiosynthesis and evaluation of [11 C]-(+)-4-Propyl-3,4,4a,5,6,10b-hexahydro-2 H -naphtho[1,2- b][1,4]oxazin-9-ol as a potential radiotracer for in vivo imaging of the dopamine D2 high-affinity state with positron emission tomography. J Med Chem. 2005;48(12):4153–60.
27. Oya S, Joseph SK, Carberry P, Divgi CR, Koren AO. Preparation of [11C]-(+)-PHNO using an automated synthesizer coupled with a stand-alone system for making [11C]propionyl chloride. J Label Compd Radiopharm. 2013;56:466.
28. Dahl K, Halldin C, Schou M. New methodologies for the preparation of carbon-11 labeled radiopharmaceuticals. Clin Transl Imaging. 2017;5(3):275–89.
29. Kealey S, Gee A, Miller PW. Transition metal mediated [11C] carbonylation reactions: recent advances and applications. J Label Compd Radiopharm. 2014;57(4):195–201.
30. Hooker JM, Schönberger M, Schieferstein H, Fowler JS. A simple, rapid method for the preparation of [11C]formaldehyde. Angew Chem Int Ed Engl. 2008;47(32):5989–92.
31. Wu C, Li R, Dearborn D, Wang Y. Reductive amination with [11C] formaldehyde: a versatile approach to radiomethylation of amines. Int J Org Chem. 2012;2(3):202–23.
32. Ogawa M, Takada Y, Suzuki H, Nemoto K, Fukumura T. Simple and effective method for producing [11C]phosgene using an environmental CCl4 gas detection tube. Nucl Med Biol. 2010;37(1):73–6.
33. Roger G, Dollé F, de Bruin B, Liu X, Besret L, Bramoullé Y, et al. Radiosynthesis and pharmacological evaluation of [11C]EMD-95885: a high affinity ligand for NR2B-containing NMDA receptors. Bioorg Med Chem. 2004;12(12):3229–37.
34. Scott PJH. Radiochemical syntheses. Volume 2: further radiopharmaceuticals for positron emission tomography and new strategies for their production. Hoboken: John Wiley & Sons; 2015.
35. Ma L, Placzek MS, Hooker JM, Vasdev N, Liang SH. [11C] Cyanation of arylboronic acids in aqueous solutions. Chem Commun (Camb). 2017;53(49):6597–600.
36. Haywood T, Kealey S, Sánchez-Cabezas S, Hall JJ, Allott L, Smith G, et al. Carbon-11 radiolabelling of organosulfur compounds: 11C synthesis of the progesterone receptor agonist tanaproget. Chem Eur J. 2015;21:9034–8.
37. Pascali C, Bogni A, Iwata R, Cambiè M, Bombardieri E. [11C] Methylation on a C18 Sep-Pak cartridge: a convenient way to produce [N-methyl-11C]choline. J Labelled Comp Radiopharm. 2000;43:195–203.

4. Conclusion and outlook

The research described within this dissertation contributed to the progress of molecular imaging using PET tracers at stages from compound design, development and preclinical evaluation (chapter 3.1 and 3.2), over improvements on radiosynthesis of an established PET tracer (chapter 3.4 and 3.5), all the way to retrospective evaluation of synthesis and quality data from clinically established radiotracers (chapter 3.5). The radiopharmaceutical chemistry of carbon-11 was highlighted in a book chapter (chapter 3.6).

Based on the structure of arecoline, 18 novel small molecules targeting the mAChRs were synthesized and chemically characterized. For every compound, the affinity toward the five mAChR subtypes was assessed in a competitive radioligand binding assay. This revealed a steep structure-activity-relationship for changes at the position of the *O*-methyl group as well as for changes in the arecaidine structure, with observed differences in affinity of more than ten thousand-fold. The arecaidine backbone was proven to be a rewarding structural feature for straightforward and robust carbon-11 labeling on the *N*-methyl group with several different residues on the *O*-methyl moiety. Derivatives containing a diphenylmethyl moiety showed a promising affinity toward mAChR M1, favorable metabolic properties and no detectable binding to the off-target acetylcholinesterase. Thus, binding properties of their carbon-11 labeled counterparts were investigated thoroughly. However, the amount of nonspecific binding anticipated by several different methods was judged as inadequate for further development as PET tracer. Lipophilicity is seen as the major contributor to nonspecific binding. The synthesized set of compounds showed a correlation between mAChR affinity and lipophilicity, which can be explained by the strong contribution of hydrophobic interactions in the orthosteric mAChR ligand binding. The set of hydrobenzoin esters of arecaidine aimed to evade this correlation by including polar interactions to amino acid residues which were not targeted by the previous set of compounds. *In silico* models supported this strategy and consistently depicted the different experimental binding affinity of the enantiomers. Radiolabeling and thorough preclinical evaluation of this next generation compounds is still pending. An overview of the novel small molecules targeting the mAChRs, which were developed during this work (chapter 3.1 and 3.2), is presented in Figure 9.

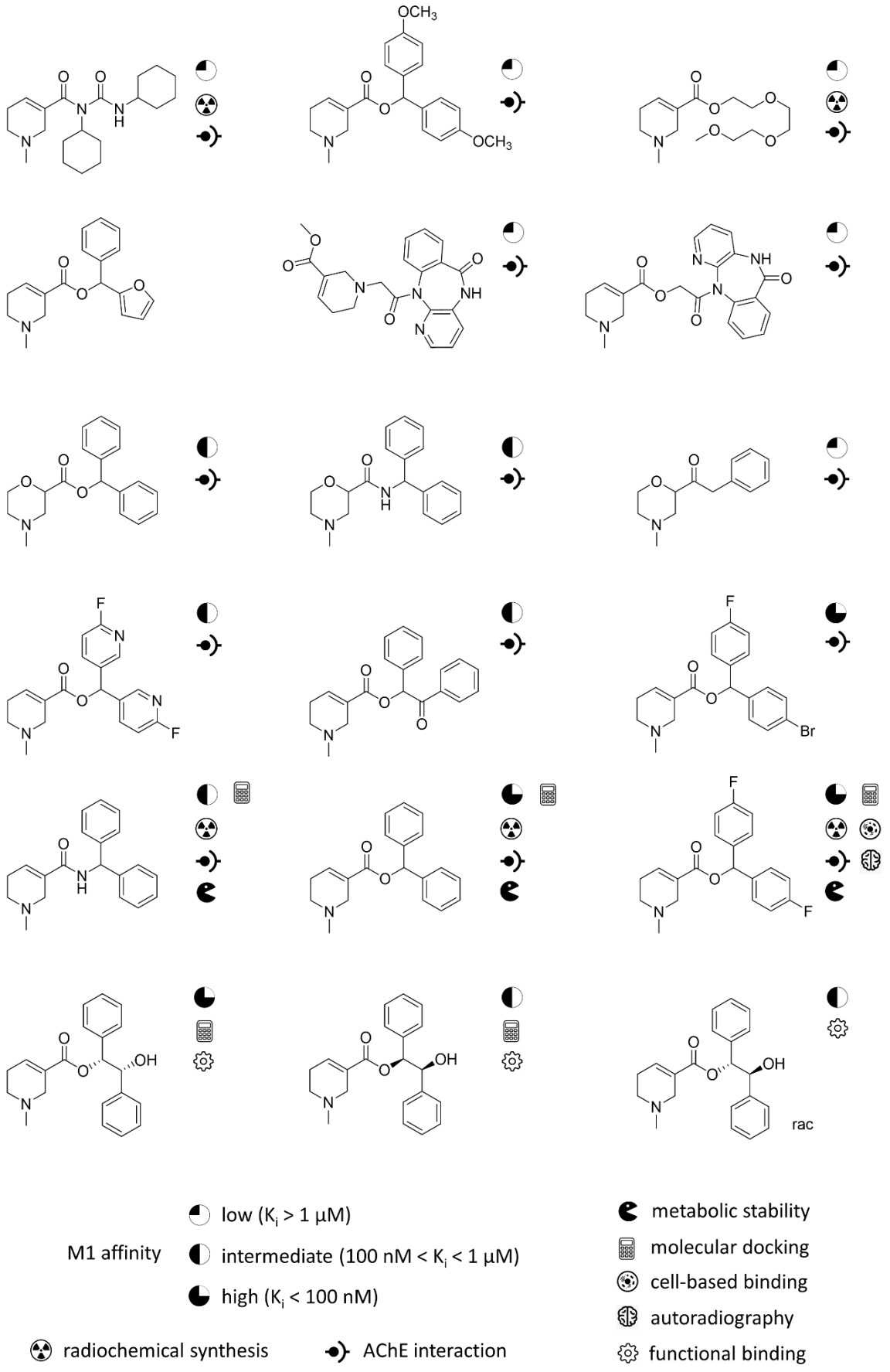


Figure 9: Novel small molecules targeting the mAChRs: Ideograms indicate the methods applied for the preclinical evaluation of the respective compound.

Due to the similarities in the orthosteric binding pockets of mAChR M1-M5, development of "highly" subtype selective drugs remains a challenging task. Subtype selectivity is a pivotal characteristic of newly developed mAChR ligands. Nevertheless, in research articles it is often described with tempting yet undefined adjectives like "pronounced", "strong", "superior". Combining the relations of five K_i values to each other is an unfulfillable task, which is why these values should be looked at all together, to allow for a clear picture of the subtype selectivity.
Assuming that the expression levels of the different mAChR subtypes in the different areas in human brain were known, one could estimate the required subtype selectivity to image a given brain area. However, caused by the lack of truly subtypes selective mAChR ligands, only limited information on the expression levels of the different subtypes in human brain is available. Consequently, it is hard to state which levels of *in vitro* subtype selectivity have to be reached to justify further development as therapeutic or diagnostic. Still, this basic rule holds true: The higher the difference in K_i values, the better. Previous developments of mAChR radiotracers have taught us that subtype selectivity *in vitro* does not necessarily correlate with *in vivo* observations. In the light of that, it makes no sense to view *in vitro* mAChR subtype selectivity as an absolute criterion that should at least be x-fold but rather as a general predictive characteristic to evaluate candidates in the drug development process.
Until recently allosteric mAChR ligands with sufficient affinity (K_i in the low nanomolar range) were not available.[38] Recent advances in crystallography of the mAChR enabled rationalized development of allosteric mAChR ligands, which eventually led to allosteric ligands with sufficient affinity for PET tracer development (M_4R-1023[95] and MK-6884[96]). With respect to subtype-selectivity allosteric ligands appear to be a promising game-changer for mAChR PET tracer development. As of now, no human studies with these compounds have been reported.

While working on the radiolabeling of [^{11}C]pirenzepine, a rearrangement product of pirenzepine, which was unwittingly sold as pirenzepine, was discovered (chapter 3.3). Supported by pirenzepine's approvement as drug and its high relevance in biological assays for the discrimination of M1 over the other mAChR subtypes, the cause and consequence of the formation of this product were investigated. The rearrangement was shown to occur under hot, acidic, aqueous conditions and is comprised of a lactam hydrolysis followed by a nucleophilic addition and elimination. Rearrangement products of pirenzepine and telenzepine exhibited a tremendous loss in mAChR affinity, which will compromise experimental data obtained by their unwitting use. The affected chemical suppliers were informed about this case and withdrew the affected products from the market. An inclusion of the discovered rearrangement product to the monograph of pirenzepine in the European Pharmacopoeia will be pursued.

5. Literature references

(1) Jawerth, N. Radiation and Radionuclides in Medicine - A Brief Overview of Nuclear Medicine and Radiotherapy. *IAEA Bull.* **2014**, *4* (55), 5–7.

(2) Yeong, C.-H.; Cheng, M.; Ng, K.-H. Therapeutic Radionuclides in Nuclear Medicine: Current and Future Prospects. *J. Zhejiang Univ. Sci. B* **2014**, *15* (10), 845–863. https://doi.org/10.1631/jzus.B1400131.

(3) Novartis to Buy French Cancer Specialist AAA for $3.9 Billion. *Reuters*. October 30, 2017.

(4) Mankoff, D. Why Nuclear Imaging and Radiotherapy? In *Radiopharmaceutical Chemistry*; Lewis, J. S., Windhorst, A. D., Zeglis, B. M., Eds.; Springer International Publishing: Cham, 2019; pp 3–10. https://doi.org/10.1007/978-3-319-98947-1_1.

(5) Zanzonico, P. An Overview of Nuclear Imaging. In *Radiopharmaceutical Chemistry*; Lewis, J. S., Windhorst, A. D., Zeglis, B. M., Eds.; Springer International Publishing: Cham, 2019; pp 101–117. https://doi.org/10.1007/978-3-319-98947-1_6.

(6) National Academies of Sciences. *Opportunities and Approaches for Supplying Molybdenum-99 and Associated Medical Isotopes to Global Markets: Proceedings of a Symposium*; 2018. https://doi.org/10.17226/24909.

(7) Ashraf, M. A.; Goyal, A. Fludeoxyglucose (18F). In *StatPearls*; StatPearls Publishing: Treasure Island (FL), 2020.

(8) Hess, S.; Blomberg, B. A.; Rakheja, R.; Friedman, K.; Kwee, T. C.; Høilund-Carlsen, P. F.; Alavi, A. A Brief Overview of Novel Approaches to FDG PET Imaging and Quantification. *Clin. Transl. Imaging* **2014**, *2* (3), 187–198. https://doi.org/10.1007/s40336-014-0062-2.

(9) Bender, D.; Munk, O. L.; Feng, H.-Q.; Keiding, S. Metabolites of 18F-FDG and 3-O-11C-Methylglucose in Pig Liver. *J. Nucl. Med.* **2001**, *42* (11), 1673–1678.

(10) Zhang, Y.; Hong, H.; Cai, W. PET Tracers Based on Zirconium-89. *Curr. Radiopharm.* **2011**, *4* (2), 131–139. https://doi.org/10.2174/1874471011104020131.

(11) Rösch, F. The Basics of Nuclear Chemistry and Radiochemistry: An Introduction to Nuclear Transformations and Radioactive Emissions. In *Radiopharmaceutical Chemistry*; Lewis, J. S., Windhorst, A. D., Zeglis, B. M., Eds.; Springer International Publishing: Cham, 2019; pp 27–61. https://doi.org/10.1007/978-3-319-98947-1_3.

(12) Levin, C. S.; Hoffman, E. J. Calculation of Positron Range and Its Effect on the Fundamental Limit of Positron Emission Tomography System Spatial Resolution. *Phys. Med. Biol.* **1999**, *44* (3), 781–799. https://doi.org/10.1088/0031-9155/44/3/019.

(13) Maddahi, J.; Packard, R. R. S. Cardiac PET Perfusion Tracers: Current Status and Future Directions. *Semin. Nucl. Med.* **2014**, *44* (5), 333–343. https://doi.org/10.1053/j.semnuclmed.2014.06.011.

(14) Brandt, M.; Cardinale, J.; Aulsebrook, M. L.; Gasser, G.; Mindt, T. L. An Overview of PET Radiochemistry, Part 2: Radiometals. *J. Nucl. Med.* **2018**, *59* (10), 1500–1506. https://doi.org/10.2967/jnumed.117.190801.

(15) Radford, L. L.; Lapi, S. E. Methods for the Production of Radionuclides for Medicine. In *Radiopharmaceutical Chemistry*; Lewis, J. S., Windhorst, A. D., Zeglis, B. M., Eds.; Springer International Publishing: Cham, 2019; pp 63–83. https://doi.org/10.1007/978-3-319-98947-1_4.

(16) Dash, A.; Chakravarty, R. Radionuclide Generators: The Prospect of Availing PET Radiotracers to Meet Current Clinical Needs and Future Research Demands. *Am. J. Nucl. Med. Mol. Imaging* **2019**, *9* (1), 30–66.

(17) Internationale Atomenergie-Organisation. *Cyclotron Produced Radionuclides: Principles and Practice*; Vienna, 2008.

(18) Conti, M.; Eriksson, L. Physics of Pure and Non-Pure Positron Emitters for PET: A Review and a Discussion. *EJNMMI Phys.* **2016**, *3*, 8. https://doi.org/10.1186/s40658-016-0144-5.

(19) Wooten, A. L.; Madrid, E.; Schweitzer, G. D.; Lawrence, L. A.; Mebrahtu, E.; Lewis, B. C.; Lapi, S. E. Routine Production of 89Zr Using an Automated Module. *Appl. Sci.* **2013**, *3* (3), 593–613. https://doi.org/10.3390/app3030593.

(20) Leskinen-Kallio, S.; Någren, K.; Lehikoinen, P.; Ruotsalainen, U.; Teräs, M.; Joensuu, H. Carbon-11-Methionine and PET Is an Effective Method To Image Head and Neck Cancer. *J. Nucl. Med.* **1992**, *33* (5), 691–695.

(21) Korsakov, M. V.; Krasikova, R. N.; Fedorova, O. S. Production of High Yield [13N] Ammonia by Proton Irradiation from Pressurized Aqueous Solutions. *J. Radioanal. Nucl. Chem. Artic.* **1996**, *204* (2), 231–239. https://doi.org/10.1007/BF02060311.

(22) Maaniitty, T.; Knuuti, J.; Saraste, A. 15O-Water PET MPI: Current Status and Future Perspectives. *Semin. Nucl. Med.* **2020**, *50* (3), 238–247. https://doi.org/10.1053/j.semnuclmed.2020.02.011.

(23) Zhu, W.; Cheng, Y.; Wang, X.; Yao, S.; Jia, R.; Xu, J.; Bai, C.; Zhao, H.; Huo, L. Head-to-Head Comparison of 68Ga-DOTA-JR11 and 68Ga-DOTATATE PET/CT in Patients with Metastatic, Well-Differentiated

Neuroendocrine Tumors: A Prospective Study. *J. Nucl. Med.* **2019**, jnumed.119.235093. https://doi.org/10.2967/jnumed.119.235093.

(24) Chatal, J.-F.; Rouzet, F.; Haddad, F.; Bourdeau, C.; Mathieu, C.; Le Guludec, D. Story of Rubidium-82 and Advantages for Myocardial Perfusion PET Imaging. *Front. Med.* **2015**, *2* (65). https://doi.org/10.3389/fmed.2015.00065.

(25) Laforest, R.; Lapi, S. E.; Oyama, R.; Bose, R.; Tabchy, A.; Marquez-Nostra, B. V.; Burkemper, J.; Wright, B. D.; Frye, J.; Frye, S.; Siegel, B. A.; Dehdashti, F. [89Zr]Trastuzumab: Evaluation of Radiation Dosimetry, Safety, and Optimal Imaging Parameters in Women with HER2-Positive Breast Cancer. *Mol. Imaging Biol.* **2016**, *18* (6), 952–959. https://doi.org/10.1007/s11307-016-0951-z.

(26) Pfaff, S.; Philippe, C.; Nics, L.; Berroterán-Infante, N.; Pallitsch, K.; Rami-Mark, C.; Weidenauer, A.; Sauerzopf, U.; Willeit, M.; Mitterhauser, M.; Hacker, M.; Wadsak, W.; Pichler, V. Toward the Optimization of (+)-[^{11} C]PHNO Synthesis: Time Reduction and Process Validation. *Contrast Media Mol. Imaging* **2019**, *2019*, 1–13. https://doi.org/10.1155/2019/4292596.

(27) Pichler, V.; Berroterán-Infante, N.; Ozenil, M.; Pfaff, S.; Philippe, C.; Wadsak, W. The Radiopharmaceutical Chemistry of Carbon-11: Tracers and Applications. In *Radiopharmaceutical Chemistry*; Lewis, J. S., Windhorst, A. D., Zeglis, B. M., Eds.; Springer International Publishing: Cham, 2019; pp 221–236. https://doi.org/10.1007/978-3-319-98947-1_12.

(28) Larsen, P.; Ulin, J.; Dahlstrøm, K.; Jensen, M. Synthesis of [11C]Iodomethane by Iodination of [11C]Methane. *Appl. Radiat. Isot.* **1997**, *48* (2), 153–157. https://doi.org/10.1016/S0969-8043(96)00177-7.

(29) Antoni, G. The Radiopharmaceutical Chemistry of Carbon-11: Basic Principles. In *Radiopharmaceutical Chemistry*; Lewis, J. S., Windhorst, A. D., Zeglis, B. M., Eds.; Springer International Publishing: Cham, 2019; pp 207–220. https://doi.org/10.1007/978-3-319-98947-1_11.

(30) Rabinovici, G. D.; Furst, A. J.; O'Neil, J. P.; Racine, C. A.; Mormino, E. C.; Baker, S. L.; Chetty, S.; Patel, P.; Pagliaro, T. A.; Klunk, W. E.; Mathis, C. A.; Rosen, H. J.; Miller, B. L.; Jagust, W. J. 11C-PIB PET Imaging in Alzheimer Disease and Frontotemporal Lobar Degeneration. *Neurology* **2007**, *68* (15), 1205–1212. https://doi.org/10.1212/01.wnl.0000259035.98480.ed.

(31) Hirvonen, J.; Aalto, S.; Lumme, V.; Nagren, K.; Kajander, J.; Vilkman, H.; Hagelberg, N.; Oikonen, V.; Hietala, J. Measurement of Striatal and Thalamic Dopamine D2 Receptor Binding with 11C-Raclopride: *Nucl. Med. Commun.* **2003**, *24* (12), 1207–1214. https://doi.org/10.1097/00006231-200312000-00002.

(32) Kim, J. S.; Ichise, M.; Sangare, J.; Innis, R. B. PET Imaging of Serotonin Transporters with [11C]DASB: Test-Retest Reproducibility Using a Multilinear Reference Tissue Parametric Imaging Method. *J. Nucl. Med. Off. Publ. Soc. Nucl. Med.* **2006**, *47* (2), 208–214.

(33) Gee, A. D.; Bongarzone, S.; Wilson, A. A. Small Molecules as Radiopharmaceutical Vectors. In *Radiopharmaceutical Chemistry*; Lewis, J. S., Windhorst, A. D., Zeglis, B. M., Eds.; Springer International Publishing: Cham, 2019; pp 119–136. https://doi.org/10.1007/978-3-319-98947-1_7.

(34) Eckelman, W. C.; Kilbourn, M. R.; Mathis, C. A. Discussion of Targeting Proteins in Vivo: In Vitro Guidelines. *Nucl. Med. Biol.* **2006**, *33* (4), 449–451. https://doi.org/10.1016/j.nucmedbio.2006.03.008.

(35) Pichler, V.; Berroterán-Infante, N.; Philippe, C.; Vraka, C.; Klebermass, E.-M.; Balber, T.; Pfaff, S.; Nics, L.; Mitterhauser, M.; Wadsak, W. An Overview of PET Radiochemistry, Part 1: The Covalent Labels ^{18} F, ^{11} C, and ^{13} N. *J. Nucl. Med.* **2018**, *59* (9), 1350–1354. https://doi.org/10.2967/jnumed.117.190793.

(36) Vraka, C.; Nics, L.; Wagner, K.-H.; Hacker, M.; Wadsak, W.; Mitterhauser, M. Log P , a Yesterday's Value? *Nucl. Med. Biol.* **2017**, *50*, 1–10. https://doi.org/10.1016/j.nucmedbio.2017.03.003.

(37) van Assema, D. M. E.; Lubberink, M.; Boellaard, R.; Schuit, R. C.; Windhorst, A. D.; Scheltens, P.; Lammertsma, A. A.; van Berckel, B. N. M. P-Glycoprotein Function at the Blood–Brain Barrier: Effects of Age and Gender. *Mol. Imaging Biol.* **2012**, *14* (6), 771–776. https://doi.org/10.1007/s11307-012-0556-0.

(38) Kruse, A. C.; Kobilka, B. K.; Gautam, D.; Sexton, P. M.; Christopoulos, A.; Wess, J. Muscarinic Acetylcholine Receptors: Novel Opportunities for Drug Development. *Nat. Rev. Drug Discov.* **2014**, *13* (7), 549–560. https://doi.org/10.1038/nrd4295.

(39) Vuckovic, Z.; Gentry, P. R.; Berizzi, A. E.; Hirata, K.; Varghese, S.; Thompson, G.; van der Westhuizen, E. T.; Burger, W. A. C.; Rahmani, R.; Valant, C.; Langmead, C. J.; Lindsley, C. W.; Baell, J. B.; Tobin, A. B.; Sexton, P. M.; Christopoulos, A.; Thal, D. M. Crystal Structure of the M $_5$ Muscarinic Acetylcholine Receptor. *Proc. Natl. Acad. Sci.* **2019**, *116* (51), 26001–26007. https://doi.org/10.1073/pnas.1914446116.

(40) Abrams, P.; Andersson, K.-E.; Buccafusco, J. J.; Chapple, C.; de Groat, W. C.; Fryer, A. D.; Kay, G.; Laties, A.; Nathanson, N. M.; Pasricha, P. J.; Wein, A. J. Muscarinic Receptors: Their Distribution and Function in Body Systems, and the Implications for Treating Overactive Bladder. *Br. J. Pharmacol.* **2006**, *148* (5), 565–578. https://doi.org/10.1038/sj.bjp.0706780.

(41) Thal, D. M.; Sun, B.; Feng, D.; Nawaratne, V.; Leach, K.; Felder, C. C.; Bures, M. G.; Evans, D. A.; Weis, W. I.; Bachhawat, P.; Kobilka, T. S.; Sexton, P. M.; Kobilka, B. K.; Christopoulos, A. Crystal Structures of the M1 and M4 Muscarinic Acetylcholine Receptors. *Nature* **2016**, *531* (7594), 335–340. https://doi.org/10.1038/nature17188.

(42) Bolden, C.; Cusack, B.; Richelson, E. Antagonism by Antimuscarinic and Neuroleptic Compounds at the Five Cloned Human Muscarinic Cholinergic Receptors Expressed in Chinese Hamster Ovary Cells. *J. Pharmacol. Exp. Ther.* **1992**, *260* (2), 576–580.

(43) Maslinski, W.; Grabczewska, E.; Bartfai, T.; Ryzewski, J.; Larsen, S.; Wilgocki, M.; Wold, S. Muscarinic Antagonist Binding to Intact Rat Thymocytes. *Acta Chem. Scand.* **1990**, *44*, 147–151. https://doi.org/10.3891/acta.chem.scand.44-0147.

(44) Nelson, C. P.; Nahorski, S. R.; Challiss, R. A. J. Constitutive Activity and Inverse Agonism at the M_2 Muscarinic Acetylcholine Receptor. *J. Pharmacol. Exp. Ther.* **2006**, *316* (1), 279–288. https://doi.org/10.1124/jpet.105.094383.

(45) Jakubik, J.; El-Fakahany, E. E. Current Advances in Allosteric Modulation of Muscarinic Receptors. *Biomolecules* **2020**, *10* (2), 325. https://doi.org/10.3390/biom10020325.

(46) Ma, L.; Seager, M. A.; Wittmann, M.; Jacobson, M.; Bickel, D.; Burno, M.; Jones, K.; Graufelds, V. K.; Xu, G.; Pearson, M.; McCampbell, A.; Gaspar, R.; Shughrue, P.; Danziger, A.; Regan, C.; Flick, R.; Pascarella, D.; Garson, S.; Doran, S.; Kreatsoulas, C.; Veng, L.; Lindsley, C. W.; Shipe, W.; Kuduk, S.; Sur, C.; Kinney, G.; Seabrook, G. R.; Ray, W. J. Selective Activation of the M_1 Muscarinic Acetylcholine Receptor Achieved by Allosteric Potentiation. *Proc. Natl. Acad. Sci.* **2009**, *106* (37), 15950–15955. https://doi.org/10.1073/pnas.0900903106.

(47) Steinfeld, T.; Mammen, M.; Smith, J. A. M.; Wilson, R. D.; Jasper, J. R. A Novel Multivalent Ligand That Bridges the Allosteric and Orthosteric Binding Sites of the M_2 Muscarinic Receptor. *Mol. Pharmacol.* **2007**, *72* (2), 291–302. https://doi.org/10.1124/mol.106.033746.

(48) Sehnal, D.; Rose, A.; Koca, J.; Burley, S.; Velankar, S. Mol*: Towards a Common Library and Tools for Web Molecular Graphics. *Workshop Mol. Graph. Vis. Anal. Mol. Data* **2018**, 29–33. https://doi.org/10.2312/MOLVA.20181103.

(49) Liu, Y.-J.; Peng, W.; Hu, M.-B.; Xu, M.; Wu, C.-J. The Pharmacology, Toxicology and Potential Applications of Arecoline: A Review. *Pharm. Biol.* **2016**, *54* (11), 2753–2760. https://doi.org/10.3109/13880209.2016.1160251.

(50) Food and Agriculture Organization of the United Nations http://www.fao.org/home/en/ (accessed Nov 18, 2020).

(51) Garg, A.; Chaturvedi, P. A Review of the Systemic Adverse Effects of Areca Nut or Betel Nut. *Indian J. Med. Paediatr. Oncol.* **2014**, *35* (1), 3. https://doi.org/10.4103/0971-5851.133702.

(52) Wolf-Pflugmann, M.; Lambrecht, G.; Wess, J.; Mutschler, E. Synthesis and Muscarinic Activity of a Series of Tertiary and Quaternary N-Substituted Guvacine Esters Structurally Related to Arecoline and Arecaidine Propargyl Ester. *Arzneimittelforschung.* **1989**, *39* (5), 539–544.

(53) Carron, M.; Veronese, S. Atropine Sulfate for Treatment of Bradycardia in a Patient with Morbid Obesity: What May Happen When You Least Expect It. *Case Rep.* **2015**, bcr2014207596–bcr2014207596. https://doi.org/10.1136/bcr-2014-207596.

(54) Shah, J.; Jiang, A.; Fekete, Z. Anisocoria Secondary to Inadvertent Contact with Scopolamine Patch. *BMJ Case Rep.* **2017**, bcr-2017-221677. https://doi.org/10.1136/bcr-2017-221677.

(55) Tytgat, G. N. Hyoscine Butylbromide: A Review of Its Use in the Treatment of Abdominal??Cramping and Pain. *Drugs* **2007**, *67* (9), 1343–1357. https://doi.org/10.2165/00003495-200767090-00007.

(56) Kaessner, F.; Hodder, R.; Bateman, E. D. A Review of Ipratropium Bromide/Fenoterol Hydrobromide (Berodual??) Delivered Via Respimat Soft Mist Inhaler in Patients with Asthma and Chronic Obstructive Pulmonary Disease: *Drugs* **2004**, *64* (15), 1671–1682. https://doi.org/10.2165/00003495-200464150-00005.

(57) Porro, B.; Dal Monte, P. R.; Petrillo, M.; Piccari, G.; D'Imperio, N.; Daniotti, S. Pirenzepine versus Cimetidine in Duodenal Ulcer. *Digestion* **1982**, *23* (2), 110–115. https://doi.org/10.1159/000198696.

(58) Tourtellotte, W. W.; Potvin, A. R.; Syndulko, K.; Hirsch, S. B.; Gilden, E. R.; Potvin, J. H.; Hansch, E. C. Parkinson's Disease: Cogentinr with Sinemetr, a Better Response. *Prog. Neuropsychopharmacol. Biol. Psychiatry* **1982**, *6* (1), 51–55. https://doi.org/10.1016/S0364-7722(82)80107-0.

(59) Kelleher, C. A Review of Solifenacin in the Treatment of Urinary Incontinence. *Ther. Clin. Risk Manag.* **2008**, *Volume 4*, 117–128. https://doi.org/10.2147/TCRM.S1274.

(60) Xiang, Z.; Thompson, A. D.; Jones, C. K.; Lindsley, C. W.; Conn, P. J. Roles of the M1 Muscarinic Acetylcholine Receptor Subtype in the Regulation of Basal Ganglia Function and Implications for the Treatment of Parkinson's Disease. *J. Pharmacol. Exp. Ther.* **2012**, *340* (3), 595–603. https://doi.org/10.1124/jpet.111.187856.

(61) Langmead, C. J.; Watson, J.; Reavill, C. Muscarinic Acetylcholine Receptors as CNS Drug Targets. *Pharmacol. Ther.* **2008**, *117* (2), 232–243. https://doi.org/10.1016/j.pharmthera.2007.09.009.

(62) Jiang, S.; Li, Y.; Zhang, C.; Zhao, Y.; Bu, G.; Xu, H.; Zhang, Y.-W. M1 Muscarinic Acetylcholine Receptor in Alzheimer's Disease. *Neurosci. Bull.* **2014**, *30* (2), 295–307. https://doi.org/10.1007/s12264-013-1406-z.

(63) Shekhar, A.; Potter, W. Z.; Lightfoot, J.; Lienemann, J.; Dubé, S.; Mallinckrodt, C.; Bymaster, F. P.; McKinzie, D. L.; Felder, C. C. Selective Muscarinic Receptor Agonist Xanomeline as a Novel Treatment Approach

for Schizophrenia. *Am. J. Psychiatry* **2008**, *165* (8), 1033–1039. https://doi.org/10.1176/appi.ajp.2008.06091591.

(64) Barak, S.; Weiner, I. The M1/M4 Preferring Agonist Xanomeline Reverses Amphetamine-, MK801- and Scopolamine-Induced Abnormalities of Latent Inhibition: Putative Efficacy against Positive, Negative and Cognitive Symptoms in Schizophrenia. *Int. J. Neuropsychopharmacol.* **2011**, *14* (9), 1233–1246. https://doi.org/10.1017/S1461145710001549.

(65) Eckelman, W.; Reba, R.; Rzeszotarski, W.; Gibson, R.; Hill, T.; Holman, B.; Budinger, T.; Conklin, J.; Eng, R.; Grissom, M. External Imaging of Cerebral Muscarinic Acetylcholine Receptors. *Science* **1984**, *223* (4633), 291–293. https://doi.org/10.1126/science.6608148.

(66) Raedler, T. J.; Knable, M. B.; Jones, D. W.; Urbina, R. A.; Gorey, J. G.; Lee, K. S.; Egan, M. F.; Coppola, R.; Weinberger, D. R. In Vivo Determination of Muscarinic Acetylcholine Receptor Availability in Schizophrenia. *Am. J. Psychiatry* **2003**, *160* (1), 118–127. https://doi.org/10.1176/appi.ajp.160.1.118.

(67) Raedler, T. J. Comparison of the In-Vivo Muscarinic Cholinergic Receptor Availability in Patients Treated with Clozapine and Olanzapine. *Int. J. Neuropsychopharmacol.* **2007**, *10* (02), 275. https://doi.org/10.1017/S1461145706006584.

(68) Eckelman, W. C. Imaging of Muscarinic Receptors in the Central Nervous System. *Curr. Pharm. Des.* **2006**, *12* (30), 3901–3913. https://doi.org/10.2174/138161206778559678.

(69) Toyohara, J.; Sakata, M.; Ishiwata, K. Human Brain Imaging of Acetylcholine Receptors. In *Imaging of the Human Brain in Health and Disease*; Elsevier, 2014; pp 113–160. https://doi.org/10.1016/B978-0-12-418677-4.00006-3.

(70) Prenant, C.; Barre, L.; Crouzel, C. Synthesis of [11C]-3-Quinuclidinylbenzilate (QNB). *J. Label. Compd. Radiopharm.* **1989**, *27* (11), 1257–1265. https://doi.org/10.1002/jlcr.2580271104.

(71) Frey, K. A.; Koeppe, R. A.; Mulholland, G. K.; Jewett, D.; Hichwa, R.; Ehrenkaufer, R. L. E.; Carey, J. E.; Wieland, D. M.; Kuhl, D. E.; Agranoff, B. W. In Vivo Muscarinic Cholingeric Receptor Imaging in Human Brain with [11C]Scopolamine and Positron Emission Tomography. *J. Cereb. Blood Flow Metab.* **1992**, *12* (1), 147–154. https://doi.org/10.1038/jcbfm.1992.18.

(72) Dewey, S. L.; Macgregor, R. R.; Brodie, J. D.; Bendriem, B.; King, P. T.; Volkow, N. D.; Schlyer, D. J.; Fowler, J. S.; Wolf, A. P.; Gatley, S. J.; Hitzemann, R. Mapping Muscarinic Receptors in Human and Baboon Brain Using [N-11C-Methyl]-Benztropine. *Synapse* **1990**, *5* (3), 213–223. https://doi.org/10.1002/syn.890050307.

(73) Koeppe, R. A.; Frey, K. A.; Mulholland, G. K.; Kilbourn, M. R.; Buck, A.; Lee, K. S.; Kuhl, D. E. [^{11}C]Tropanyl Benzilate—Binding to Muscarinic Cholinergic Receptors: Methodology and Kinetic Modeling Alternatives. *J. Cereb. Blood Flow Metab.* **1994**, *14* (1), 85–99. https://doi.org/10.1038/jcbfm.1994.13.

(74) Suhara, T.; Inoue, O.; Kobayashi, K.; Suzuki, K.; Tateno, Y. Age-Related Changes in Human Muscarinic Acetylcholine Receptors Measured by Positron Emission Tomography. *Neurosci. Lett.* **1993**, *149* (2), 225–228. https://doi.org/10.1016/0304-3940(93)90777-I.

(75) Quirion, R. Cholinergic Markers in Alzheimer Disease and the Autoregulation of Acetylcholine Release. *J. Psychiatry Neurosci. JPN* **1993**, *18* (5), 226–234.

(76) Seeman, P.; Madras, B. *Imaging of the Human Brain in Health and Disease*; Elsevier, 2013.

(77) Nishiyama, S.; Sato, K.; Harada, N.; Kakiuchi, T.; Tsukada, H. Development and Evaluation of Muscarinic Cholinergic Receptor Ligands N-[11c]Ethyl-4-Piperidyl Benzilate and n-[11c]Propyl-4-Piperidyl Benzilate: A Pet Study in Comparison with n-[11c]Methyl-4-Piperidyl Benzilate in the Conscious Monkey Brain. *Nucl. Med. Biol.* **2000**, *27* (8), 733–740. https://doi.org/10.1016/S0969-8051(00)00167-0.

(78) Tsukada, H.; Takahashi, K.; Miura, S.; Nishiyama, S.; Kakiuchi, T.; Ohba, H.; Sato, K.; Hatazawa, J.; Okudera, T. Evaluation of Novel PET Ligands (+)N-[11C]Methyl-3-Piperidyl Benzilate ([11C](+)3-MPB) and Its Stereoisomer [11C](-)3-MPB for Muscarinic Cholinergic Receptors in the Conscious Monkey Brain: A PET Study in Comparison with [11C]4-MPB. *Synapse* **2001**, *39* (2), 182–192. https://doi.org/10.1002/1098-2396(200102)39:2<182::AID-SYN10>3.0.CO;2-Q.

(79) Yamamoto, S.; Ouchi, Y.; Nakatsuka, D.; Tahara, T.; Mizuno, K.; Tajima, S.; Onoe, H.; Yoshikawa, E.; Tsukada, H.; Iwase, M.; Yamaguti, K.; Kuratsune, H.; Watanabe, Y. Reduction of [11C](+)3-MPB Binding in Brain of Chronic Fatigue Syndrome with Serum Autoantibody against Muscarinic Cholinergic Receptor. *PLoS ONE* **2012**, *7* (12), e51515. https://doi.org/10.1371/journal.pone.0051515.

(80) Flier, J. S.; Underhill, L. H.; Goyal, R. K. Muscarinic Receptor Subtypes. *N. Engl. J. Med.* **1989**, *321* (15), 1022–1029. https://doi.org/10.1056/NEJM198910123211506.

(81) Elhusseiny, A.; Cohen, Z.; Olivier, A.; Stanimirović, D. B.; Hamel, E. Functional Acetylcholine Muscarinic Receptor Subtypes in Human Brain Microcirculation: Identification and Cellular Localization. *J. Cereb. Blood Flow Metab.* **1999**, *19* (7), 794–802. https://doi.org/10.1097/00004647-199907000-00010.

(82) Jagoda, E. M.; Kiesewetter, D. O.; Shimoji, K.; Ravasi, L.; Yamada, M.; Gomeza, J.; Wess, J.; Eckelman, W. C. Regional Brain Uptake of the Muscarinic Ligand, [18F]FP-TZTP, Is Greatly Decreased in M2 Receptor Knockout Mice but Not in M1, M3 and M4 Receptor Knockout Mice. *Neuropharmacology* **2003**, *44* (5), 653–661. https://doi.org/10.1016/S0028-3908(03)00050-9.

(83) Podruchny, T. A.; Connolly, C.; Bokde, A.; Herscovitch, P.; Eckelman, W. C.; Kiesewetter, D. O.; Sunderland, T.; Carson, R. E.; Cohen, R. M. In Vivo Muscarinic 2 Receptor Imaging in Cognitively Normal Young and Older Volunteers. *Synapse* **2003**, *48* (1), 39–44. https://doi.org/10.1002/syn.10165.

(84) Ravasi, L.; Kiesewetter, D. O.; Shimoji, K.; Lucignani, G.; Eckelman, W. C. Why Does the Agonist [18F]FP-TZTP Bind Preferentially to the M2 Muscarinic Receptor? *Eur. J. Nucl. Med. Mol. Imaging* **2006**, *33* (3), 292–300. https://doi.org/10.1007/s00259-005-1966-x.

(85) Mirza, N. R.; Peters, D.; Sparks, R. G. Xanomeline and the Antipsychotic Potential of Muscarinic Receptor Subtype Selective Agonists. *CNS Drug Rev.* **2006**, *9* (2), 159–186. https://doi.org/10.1111/j.1527-3458.2003.tb00247.x.

(86) Farde, L.; Suhara, T.; Halldin, C.; Nybäck, H.; Nakashima, Y.; Swahn, C.-G.; Karlsson, P.; Ginovart, N.; Bymaster, F.; Shannon, H.; Foged, C.; Suzdak, P. D.; Sauerberg, P. PET Study of the M_1-Agonists [^{11}C]Xanomeline and [^{11}C]Butylthio-TZTP in Monkey and Man. *Dement. Geriatr. Cogn. Disord.* **1996**, *7* (4), 187–195. https://doi.org/10.1159/000106877.

(87) Ridler, K.; Cunningham, V.; Huiban, M.; Martarello, L.; Pampols-Maso, S.; Passchier, J.; Gunn, R. N.; Searle, G.; Abi-Dargham, A.; Slifstein, M.; Watson, J.; Laruelle, M.; Rabiner, E. A. An Evaluation of the Brain Distribution of [11 C]GSK1034702, a Muscarinic-1 (M 1) Positive Allosteric Modulator in the Living Human Brain Using Positron Emission Tomography. *EJNMMI Res.* **2014**, *4* (1), 66. https://doi.org/10.1186/s13550-014-0066-y.

(88) Mogg, A. J.; Eessalu, T.; Johnson, M.; Wright, R.; Sanger, H. E.; Xiou, H.; Crabtree, M.; Smith, A.; Colvin, E.; Schober, D.; Gehlert, D.; Jesudason, C.; Goldsmith, P.; Johnson, M. P.; Felder, C. C.; Barth, V. N.; Broad, L. M. *In Vitro* Pharmacological Characterization and *in Vivo* Validation of LSN3172176 a Novel M1 Selective Muscarinic Receptor Agonist Tracer Molecule for Positron Emission Tomography (PET). *J. Pharmacol. Exp. Ther.* **2018**, jpet.117.246454. https://doi.org/10.1124/jpet.117.246454.

(89) Bradley, S. J.; Molloy, C.; Bundgaard, C.; Mogg, A. J.; Thompson, K. J.; Dwomoh, L.; Sanger, H. E.; Crabtree, M. D.; Brooke, S. M.; Sexton, P. M.; Felder, C. C.; Christopoulos, A.; Broad, L. M.; Tobin, A. B.; Langmead, C. J. Bitopic Binding Mode of an M $_1$ Muscarinic Acetylcholine Receptor Agonist Associated with Adverse Clinical Trial Outcomes. *Mol. Pharmacol.* **2018**, *93* (6), 645–656. https://doi.org/10.1124/mol.118.111872.

(90) Buiter, H. J. C.; Leysen, J. E.; Schuit, R. C.; Fisher, A.; Lammertsma, A. A.; Windhorst, A. D. Radiosynthesis and Biological Evaluation of the M1 Muscarinic Acetylcholine Receptor Agonist Ligand [11C]AF150(S). *J. Label. Compd. Radiopharm.* **2012**, *55* (7), 264–273. https://doi.org/10.1002/jlcr.2932.

(91) Buiter, H. J.; Windhorst, A. D.; Huisman, M. C.; Yaqub, M.; Knol, D. L.; Fisher, A.; Lammertsma, A. A.; Leysen, J. E. [11C]AF150(S), an Agonist PET Ligand for M1 Muscarinic Acetylcholine Receptors. *EJNMMI Res.* **2013**, *3*, 19. https://doi.org/10.1186/2191-219X-3-19.

(92) Malmquist, J.; Varnäs, K.; Svedberg, M.; Vallée, F.; Albert, J. S.; Finnema, S. J.; Schou, M. Discovery of a Novel Muscarinic Receptor PET Radioligand with Rapid Kinetics in the Monkey Brain. *ACS Chem. Neurosci.* **2017**, *9* (2), 224–229. https://doi.org/10.1021/acschemneuro.7b00340.

(93) Nabulsi, N. B.; Holden, D.; Zheng, M.-Q.; Bois, F.; Lin, S.-F.; Najafzadeh, S.; Gao, H.; Ropchan, J.; Lara-Jaime, T.; Labaree, D.; Shirali, A.; Slieker, L.; Jesudason, C.; Barth, V.; Navarro, A.; Kant, N.; Carson, R. E.; Huang, Y. Evaluation of ^{11} C-LSN3172176 as a Novel PET Tracer for Imaging M $_1$ Muscarinic Acetylcholine Receptors in Nonhuman Primates. *J. Nucl. Med.* **2019**, *60* (8), 1147–1153. https://doi.org/10.2967/jnumed.118.222034.

(94) Wood, M. R.; Noetzel, M. J.; Melancon, B. J.; Poslusney, M. S.; Nance, K. D.; Hurtado, M. A.; Luscombe, V. B.; Weiner, R. L.; Rodriguez, A. L.; Lamsal, A.; Chang, S.; Bubser, M.; Blobaum, A. L.; Engers, D. W.; Niswender, C. M.; Jones, C. K.; Brandon, N. J.; Wood, M. W.; Duggan, M. E.; Conn, P. J.; Bridges, T. M.; Lindsley, C. W. Discovery of VU0467485/AZ13713945: An M $_4$ PAM Evaluated as a Preclinical Candidate for the Treatment of Schizophrenia. *ACS Med. Chem. Lett.* **2017**, *8* (2), 233–238. https://doi.org/10.1021/acsmedchemlett.6b00461.

(95) Deng, X.; Hatori, A.; Chen, Z.; Kumata, K.; Shao, T.; Zhang, X.; Yamasaki, T.; Hu, K.; Yu, Q.; Ma, L.; Wang, G.; Wang, L.; Shao, Y.; Josephson, L.; Sun, S.; Zhang, M.; Liang, S. Synthesis and Preliminary Evaluation of ^{11} C-Labeled VU0467485/AZ13713945 and Its Analogues for Imaging Muscarinic Acetylcholine Receptor Subtype 4. *ChemMedChem* **2019**, *14* (3), 303–309. https://doi.org/10.1002/cmdc.201800710.

(96) Tong, L.; Li, W.; Lo, M. M.-C.; Gao, X.; Wai, J. M.-C.; Rudd, M.; Tellers, D.; Joshi, A.; Zeng, Z.; Miller, P.; Salinas, C.; Riffel, K.; Haley, H.; Purcell, M.; Holahan, M.; Gantert, L.; Schubert, J. W.; Jones, K.; Mulhearn, J.; Egbertson, M.; Meng, Z.; Hanney, B.; Gomez, R.; Harrison, S. T.; McQuade, P.; Bueters, T.;

Uslaner, J.; Morrow, J.; Thomson, F.; Kong, J.; Liao, J.; Selyutin, O.; Bao, J.; Hastings, N. B.; Agrawal, S.; Magliaro, B. C.; Monsma, F. J.; Smith, M. D.; Risso, S.; Hesk, D.; Hostetler, E.; Mazzola, R. Discovery of [^{11} C]MK-6884: A Positron Emission Tomography (PET) Imaging Agent for the Study of M4Muscarinic Receptor Positive Allosteric Modulators (PAMs) in Neurodegenerative Diseases. *J. Med. Chem.* **2020**, *63* (5), 2411–2425. https://doi.org/10.1021/acs.jmedchem.9b01406.

(97) [11C]MK-6884 Positron Emission Tomography (PET) Tracer Validation Trial (MK-6884-001) - Tabular View - ClinicalTrials.gov https://clinicaltrials.gov/ct2/show/record/NCT02621606 (accessed Apr 29, 2020).

(98) Third International Symposium on Radiopharmaceutical Chemistry. *J. Label. Compd. Radiopharm.* **1981**, *18* (1–2), 79–158. https://doi.org/10.1002/jlcr.2580180103.

(99) Vora, M. M.; Finn, R. D.; Boothe, T. E.; Liskwosky, D. R.; Potter, L. T. [N-Methyl-11C]-Scopolamine: Synthesis and Distribution in Rat Brain. *J. Label. Compd. Radiopharm.* **1983**, *20* (11), 1229–1236. https://doi.org/10.1002/jlcr.2580201103.

(100) Dewey, S.L.; MacGregor, R.R.; Bendriem, B.; Fowler, J.S.; King, P.T.; Schlyer, D.J.; Wolf, A.P.; Volkow, N.D.; Christman, D.R.; Brodie, J.D.; Hitzemann, R. [11C]-Benztropine as a Possible Muscarinic Cholinergic Receptor Ligand for Use in PET. *J Nucl Med* **1989**, *30*, 741–748.

(101) Mulholland, G.K.; Jewett, D.M.; Otto, C.A.; Kilbourn, M. R.; Sherman, P.S.; Koeppe, R.A.; Wieland, D.M.; Frey, K.A.; Kuhl, D.E. Synthesis and Preliminary Evaluation of [C-11]-(+)-2-Tropanyl Benzilate (C-11TRB) as a Iigand for the Muscarinic Receptor. *J Nucl Med* **1988**, *29*, 932–940.

(102) Mulholland, G.K.; Jewett, D.M.; Otto, C.A.; Kilbourn, M. R.; Sherman, P.S.; Kuhl, D.E. Synthesis and Regional Brain Distribution of [C-11]N-Methyl-4- Piperidyl Benzilate ([C-11]NMPB) in the Rat. *J Nucl Med* **1988**, *29*, 768.

(103) Halldin, C.; Müller, L.; Foged, C.; Sauerberg, P.; Karlsson, P.; Hall, H.; Farde, L. Preparation of Three Carbon-11 Labelled Novel Functional M1 Selective Muscarinic Agonists. *J Nucl Med* **1993**, *7* (34).

(104) Kiesewetter, D. O.; Lee, J.; Lang, L.; Park, S. G.; Paik, C. H.; Eckelman, W. C. Preparation of 18F-Labeled Muscarinic Agonist with M2 Selectivity. *J. Med. Chem.* **1995**, *38* (1), 5–8. https://doi.org/10.1021/jm00001a002.

(105) Takahashi, K.; Murakami, M.; Miura, S.; Iida, H.; Kanno, I.; Uemura, K. Synthesis and Autoradiographic Localization of Muscarinic Cholinergic Antagonist (+)N-[11C]Methyl-3-Piperidyl Benzilate as a Potent Radioligand for Positron Emission Tomography. *Appl. Radiat. Isot.* **1999**, *50* (3), 521–525. https://doi.org/10.1016/S0969-8043(97)10155-5.

(106) Huiban, M.; Pampols-Maso, S.; Passchier, J. Fully Automated Synthesis of the M1 Receptor Agonist [11C]GSK1034702 for Clinical Use on an Eckert & Ziegler Modular Lab System. *Appl. Radiat. Isot.* **2011**, *69* (10), 1390–1394. https://doi.org/10.1016/j.apradiso.2011.05.007.

(107) Nabulsi, N.; Holden, D.; Zheng, M.-Q.; Slieker, L.; Barth, V.; Lin, S.; Kant, N.; Jesudason, C.; Labaree, D.; Shirali, A. Evaluation of a Novel, Selective M1 Muscarinic Acetylcholine Receptor Ligand 11C-LSN3172176 in Non-Human Primates. *J. Nucl. Med.* **2017**, *58* (supplement 1), 275–275.

(108) Varastet, M.; Brouillet, E.; Chavoix, C.; Prenant, C.; Crouzel, C.; Stulzaft, O.; Bottlaender, M.; Cayla, J.; Mazière, B.; Mazière, M. In Vivo Visualization of Central Muscarinic Receptors Using [11C]Quinuclidinyl Benzilate and Positron Emission Tomography in Baboons. *Eur. J. Pharmacol.* **1992**, *213* (2), 275–284. https://doi.org/10.1016/0014-2999(92)90692-W.

(109) Caldwell, J. H.; Link, J. M. Imaging Left Ventricular Muscarinic Receptor Heterogeneity: A Tool to Evaluate Individuals at Risk for Sudden Death? *Circ. Cardiovasc. Imaging* **2009**, *2* (5), 353–355. https://doi.org/10.1161/CIRCIMAGING.109.900621.

(110) Delforge, J.; Le Guludec, D.; Syrota, A.; Bendriem, B.; Crouzel, C.; Slama, M.; Merlet, P. Quantification of Myocardial Muscarinic Receptors with PET in Humans. *J. Nucl. Med. Off. Publ. Soc. Nucl. Med.* **1993**, *34* (6), 981–991.

(111) Reardon, S. Whole-Body PET Scanner Produces 3D Images in Seconds. *Nature* **2019**, *570* (7761), 285–286. https://doi.org/10.1038/d41586-019-01833-z.

(112) Shah, N.; Khurana, S.; Cheng, K.; Raufman, J.-P. Muscarinic Receptors and Ligands in Cancer. *Am. J. Physiol. - Cell Physiol.* **2009**, *296* (2), C221–C232. https://doi.org/10.1152/ajpcell.00514.2008.

(113) Wu, J.; Zhou, J.; Yao, L.; Lang, Y.; Liang, Y.; Chen, L.; Zhang, J.; Wang, F.; Wang, Y.; Chen, H.; Ma, J. High Expression of M3 Muscarinic Acetylcholine Receptor Is a Novel Biomarker of Poor Prognostic in Patients with Non-Small Cell Lung Cancer. *Tumour Biol. J. Int. Soc. Oncodevelopmental Biol. Med.* **2013**, *34* (6), 3939–3944. https://doi.org/10.1007/s13277-013-0982-x.

6. List of figures and tables

Figure 1: Principle of a PET scan. 2
Figure 2: Main cellular metabolism of 2-[^{18}F]FDG trapping. 3
Figure 3: Reaction pathways to carbon-11 synthons. Own work, also published.[27] 6
Figure 4: Graphical illustration of the mAChR M1 crystal structure PDB:5CXV[41] using Mol*.[48] The approximal location of the orthosteric binding site and the allosteric binding sites are highlighted. The receptor structure contains the co-crystallized orthosteric antagonist tiotropium, which is displayed in 'ball and stick' style. In the side view the protein is displayed as cartoon and in the top view it is displayed as Gaussian surface. 10
Figure 5: Top left: kiosk selling fruits of *Areca catechu* in Myanmar (own photograph), top right: user of Areca catechu with red-stained teeth (reproduced with permission of Gunda Wörlein, https://indojunkie.com/), bottom left: fruits of *Areca catechu* hanging in a kiosk in Myanmar (own photograph), bottom right: peeled fruit of *Areca catechu* (own photograph). 11
Figure 6: Structures of arecoline and some well-known orthosteric mAChR ligands. 12
Figure 7: Structures and binding properties of mAChR ligands previously evaluated as imaging probes. Emphasis is given on more recent developments. First synthesis: (*R*,*S*)-[^{125}I]IQNB[98], [*carbonyl*-^{11}C]QNB[70], [^{11}C]scopolamine[99], [^{11}C]benztropine[100], [^{11}C]TRB[101], [^{11}C]NMPB[102], [^{11}C]xanomeline[103], [^{18}F]FP-TZTP[104], (+)-[^{11}C]3-MPB[105], [^{11}C]GSK1034702[106], [^{11}C]AF150(S),[90] (*S*,*R*)-[^{11}C]1-methylpiperidin-3-yl)2-cyclopentyl-2-hydroxy-2-phenylacetate[92], [^{11}C]LSN3172176[107], [^{11}C]M_4R-1023[95], [^{11}C]MK-6884[96]. First in man/animal: (*R*,*S*)-[^{125}I]IQNB[65], [*carbonyl*-^{11}C]QNB[108], [^{11}C]scopolamine[71], [^{11}C]benztropine[72], [^{11}C]TRB[73], [^{11}C]NMPB[74], [^{11}C]xanomeline[86], [^{18}F]FP-TZTP[83], (+)-[^{11}C]3-MPB[79], [^{11}C]GSK1034702[87], [^{11}C]AF150(S),[91] (*S*,*R*)-[^{11}C]1-methylpiperidin-3-yl)2-cyclopentyl-2-hydroxy-2-phenylacetate[92], [^{11}C]LSN3172176[107], [^{11}C]M_4R-1023[95], [^{11}C]MK-6884[96] 17
Figure 8: General influence of affinity and lipophilicity on imaging properties in mAChR PET tracer development. 18
Figure 9: Novel small molecules targeting the mAChRs: Ideograms indicate the methods applied for the preclinical evaluation of the respective compound. 104

Table 1: Properties of common PET nuclides.[17–19] 5
Table 2: Design and test criteria for the discovery and development of small molecule radiotracers. 7
Table 3: Binding parameters of well-known mAChR ligands given in nM. Data of scopolamine is given as K_i values from a competitive radioligand binding assay using [^{3}H]NMS. Values of BQCA are given as inflection point of ACh efficacy potentiation as measured by calcium mobilization. 9

7. Supporting information

On the following pages the supporting information of the works 1.-3. is depicted in the same order as in the main texts (chapter 3).

Supporting Information

Enhanced arecoline derivatives as muscarinic acetylcholine receptor M1 ligands for potential application as PET-radiotracers

Marius Ozenil,[1] Katharina Pacher,[1] Theresa Balber,[1] Chrysoula Vraka,[1] Alexander Roller,[2] Wolfgang Holzer,[3] Helmut Spreitzer,[3] Markus Mitterhauser,[1,4] Wolfgang Wadsak,[1,5] Marcus Hacker,[1] Verena Pichler[1,*]

[1] *Department of Biomedical Imaging and Image-guided Therapy, Division of Nuclear Medicine, Medical University of Vienna*
[2] *X-ray Structure Analysis Centre, Faculty of Chemistry, University of Vienna*
[3] *Department of Pharmaceutical Chemistry, Faculty of Life Sciences, University of Vienna*
[4] *Ludwig Boltzmann Institute Applied Diagnostics, Vienna*
[5] *CBmed GmbH - Center for Biomarker Research in Medicine, Graz*

*corresponding author: Verena Pichler

Table of contents

Further syntheses 2
Radiolabeling of [^{11}C]pirenzepine 4
Chiral separation of **3e** 6
Determination of [^{3}H]NMS K_D towards M1-M5 7
EeAChE affinity and metabolism 7
Metabolic stability 8
Metabolite identification 9
Plasma stability 9
NMR spectra 11
X-ray Analysis 25

Further syntheses

Precursor **2k** features two potential nucleophilic sites that could react with [^{11}C]CH_3I: a secondary amine of the arecoline and a secondary urea nitrogen. Base-free conditions as they were employed in the radiosynthesis should strongly favor the methylation of the secondary amine. However, in order to ensure that both methylated regioisomers do not coincidentally exhibit the same retention time in the used radio-HPLC system, **11** is a necessary reference compound.

1k in dry DMF and dry DMSO with an excess of CH_3I did not show reactivity. Addition of base (1.5 eq Cs_2CO_3 or NaH) resulted in Fmoc deprotection. Consequently, the *N*-Boc-protected analogue **9** was used for subsequent synthesis trials. Once again base free conditions with excess of CH_3I did not yield the methylated product and urea cleavage happened upon addition of base (1.5 eq Cs_2CO_3 or NaH).

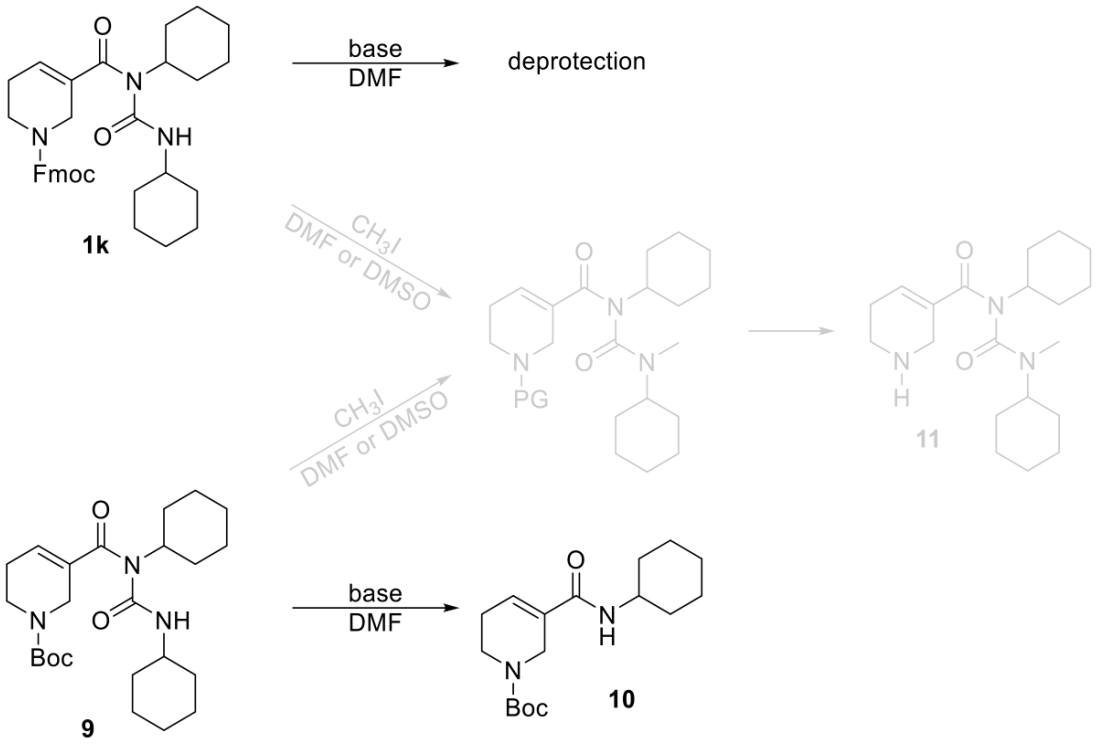


Figure S1: Synthesis overview: attempted synthesis of **11** and urea clavage of **9** to **10**.

***tert*-butyl 5-{[3-cyclohexyl(cyclohexylcarbamoyl)amino]carbonyl}-1,2,3,6-tetrahydro pyridine-1-carboxylate (9).** DCC (49.9 mg, 0.242 mmol) was added to a solution of *N*-Boc-guvacine (50.0 mg, 0.220 mmol) in dry DMF (1 mL). After stirring for 1 h DMF was evaporated. The residue was extracted with EE (5 mL) and purified by preparative TLC (PE:EE = 3:1; silica gel 40 F254 20x20 cm, 0.25 mm; R_f = 0.55-0.85; developed 3x). The product was obtained as white, crystalline solid (28.9 mg, 30 %).

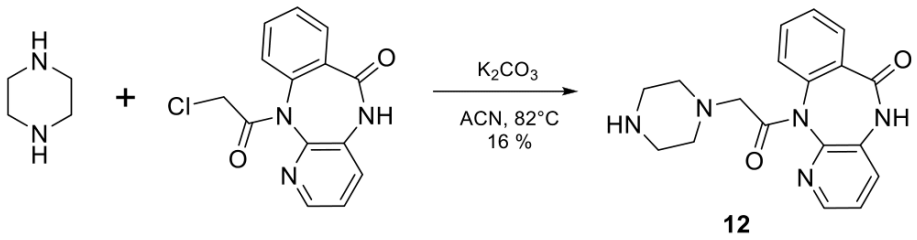
^{1}H-NMR (200MHz, $CDCl_3$) δ 6.25 (brs, 2H), 4.12 (brs, 2H), 4.10-3.94 (m, 1H), 3.60 (brs, 1H), 3.49 (t, J=5.7Hz, 2H), 2.20 (brs, 2H), 2.00-1.53 (m, 12H), 1.47 (s, 9H), 1.40-1.04 (m, 8H). HRMS (ESI) calcd for $C_{24}H_{39}N_3NaO_4$ (M + Na^+) 456.2833, found 456.2839

tert-butyl 5-(cyclohexylcarbamoyl)-1,2,3,6-tetrahydropyridine-1-carboxylate (10). NaH (1.7 mg of a 60 % emulsion in mineral oil, 0.0415 mmol) was added to a stirred solution of **9** (15 mg, 0.0346 mmol) dry DMF (1 mL) at rt. After 30 min CH_3I was added (6.5 µL, 0.104 mmol). After 18 h the reaction mixture was diluted with water (10 mL) and extracted with Et_2O (3x15 mL). The organic phase was washed with water (10 mL) and purified by preparative TLC (PE:EE = 3:1; silica gel 40 F254 with concentration zone 20x20 cm, 0.10 mm; R_f = 0.20-0.28). The product was obtained as colorless oil (5.3 mg, 50 %).

^{1}H-NMR (400MHz, $CDCl_3$) δ 6.57 (brs, 1H, H-4), 5.52 (brs, 1H, NH), 4.15-4.10 (m, 2H, H-6), 3.86-3.78 (m, 1H, Cy H-1), 3.47 (t, J=5.6Hz, 2H, H-2), 2.29-2.21 (m, 2H, H-3), 1.98-1.88 (m, 2H, Cy H-2), 1.76-1.67 (m, 2H, Cy H-3,5), 1.67-1.57 (m, 1H, Cy H-4), 1.47 (s, 9H, CH_3), 1.45-1.30 (m, 2H, Cy H-3,5), 1.23-1.05 (m, 3H, Cy H-2,4,6). ^{13}C-NMR (100MHz, $CDCl_3$) δ 171.8 (CONH), 154.8 (OCON), 131.0-129.0 (C-4), 80.0 ($OC(CH_3)_4$), 48.2 (Cy C-1), 42.7 (C-6), 39.5 (C-2), 33.1 (Cy C-2,6), 28.4 (CH_3), 25.5 (Cy C-4), 25.0 (C-3), 24.8 (Cy C-3,5). ^{15}N-NMR (41MHz, $CDCl_3$) δ -256.6 (CONH). (one quaternary carbon could not be detected) According to TLC product spot is immediately formed after addition of base and remains constant over time. Consequently, a reaction time of around 10 min is likely sufficient and also addition of CH_3I can be omitted.

Considering the unreactivity of an excess of CH_3I towards **1k** and **9** under the otherwise same reaction conditions as applied in the radiolabeling, it appears very unlikely that the urea-*N*-methylated regioisomer is formed during radiolabeling.

A precursor (**12**) for the synthesis of [^{11}C]pirenzepine was synthesized from piperazine (99°%, Alfa Aesar) and 11-(chloroacetyl)-5,11-dihydro-6*H*-pyrido[2,3-*b*][1,4]benzodiazepin-6-one (99 %, abcr) as illustrated in Figure S2.



12

Figure S2: Synthesis of the precursor for the radiolabeling of [^{11}C]pirenzepine.

11-(2-(piperazin-1-yl)acetyl)-5,11-dihydro-6*H*-benzo[*e*]pyrido[3,2-*b*][1,4]diazepin-6-one (12). A solution of piperazine (120 mg, 1.39 mmol) in ACN (2 mL) was added dropwise to a

stirred suspension of 11-(chloroacetyl)-5,11-dihydro-6*H*-pyrido[2,3-*b*][1,4]benzodiazepin-6-one (200 mg, 0.70 mmol) and K_2CO_3 (144 mg, 1.04 mmol) in ACN (3mL). The reaction mixture was refluxed for 30 min, allowed to cool to room temperature and poured on H_2O (5 mL). Extraction with DCM (2x10 mL) followed by precipitation with hexane afforded the product as white solid (37 mg, 16 %).

^{1}H-NMR (400MHz, $CDCl_3$) δ 8.27 (brs, 1H, Ar H-2), 7.97 (d, *J*=7.7Hz, 1H, Ar H-7), 7.63 (m, 2H, Ar H-9,10), 7.54 (dd, *J*=7.9Hz, *J*=1.6Hz, 1H, Ar H-4), 7.43 (m, 1H, Ar H-8), 7.29 (dd, *J*=7.9Hz, *J*=4.7Hz, 1H, Ar H-3), 3.65 (m, 1H, $COCH_2$), 3.14 (m, 1H, $COCH_2$), 2.69 (m, 2H, H-3,5), 2.57 (m, 2H, H-3,5), 2.37 (m, 2H, H-2,6), 2.08 (m, 2H, H-2,6). ^{13}C-NMR (100MHz, $CDCl_3$) δ 167.8 (NHCO), 147.7 (Ar C-11a), 144.6 (Ar C-2), 140.6 (Ar C-10a), 133.3 (Ar C-9), 131.2 (Ar C-7), 130.7 (Ar C-4a), 129.5 (Ar C-4), 128.6 (Ar C-10), 128.1 (Ar C-8), 123.7 (Ar C-3), 61.9 ($COCH_2N$), 54.1 (C-2,6), 45.6 (C-3,5).* HRMS (ESI) calcd for $C_{18}H_{20}N_5O_2$ ($M + H^+$) 338.1612, found 338.1613.

*the quaternary carbons Ar C-6a and $NCOCH_2$ could not be found

Radiolabeling of [^{11}C]pirenzepine.

[^{11}C]pirenzepine was produced as positive control for autoradiography. The synthesis was performed using the same materials and methods as described in the main text, with following changes and details: 1 mg precursor (**12**) was dissolved in 0.5 mL DMSO. [^{11}C]Pirenzepine was purified using a µBondapak™ C18 7.8x300 mm Prep Column (Waters) with 50 mM $NH_4H_2PO_4$ buffer pH 9.3 : ACN = 80 : 20 at flow of 7.5 mL/min. Interestingly, under these chromatographic conditions [^{11}C]pirenzepine is less retained by the stationary phase compared to **12** (Figure S3). Whereas, usually the methylated product has a higher retention time compared to its *N*-desmethyl precursor (Figure S4). For the quality control of [^{11}C]pirenzepine an XSelect™ (HSS T3, 3.5 µm, 100 x 4.6 mm) column with 25 mM $NH_4H_2PO_4$ buffer pH 9.3 : ACN = 75 : 25 at flow of 1 mL/min was used ($k_{prec.}$ = 1.68, $k_{prod.}$ = 2.33, LOQ = 1.3 µg/mL). Five batches of [^{11}C]pirenzepine were prepared (yield = 3.7 ± 1.0 GBq, RCY = 12.3 ± 3.8 %, A_m at EOS = 137 ± 94 GBq/µmol).

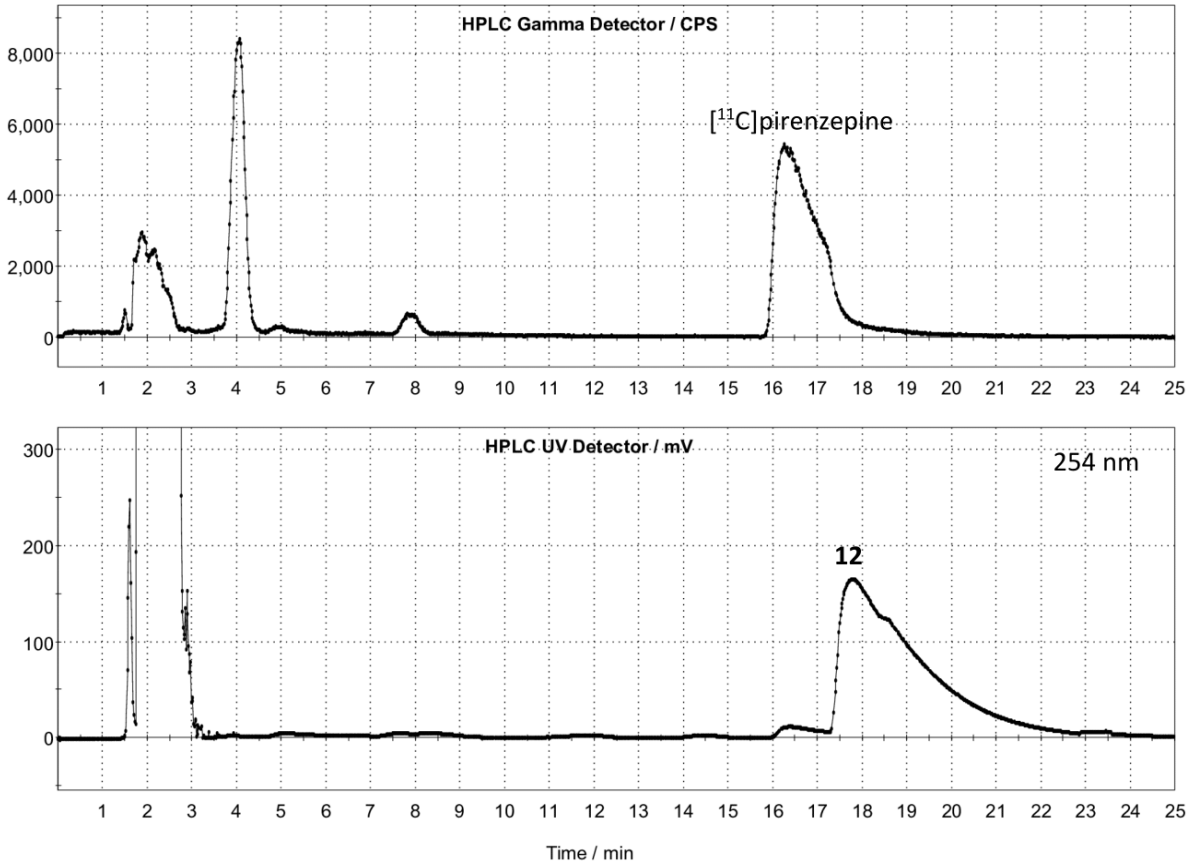


Figure S3: Exemplary preparative chromatograms of the purification of [^{11}C]pirenzepine. Precursor (**12**) and [^{11}C]pirenzepine exhibit strong tailing. However, [^{11}C]pirenzepine elutes earlier, which prevents the precursor (**12**) from smearing into the product fraction. The product fraction was collected from 15.9 min to 17.2 min.

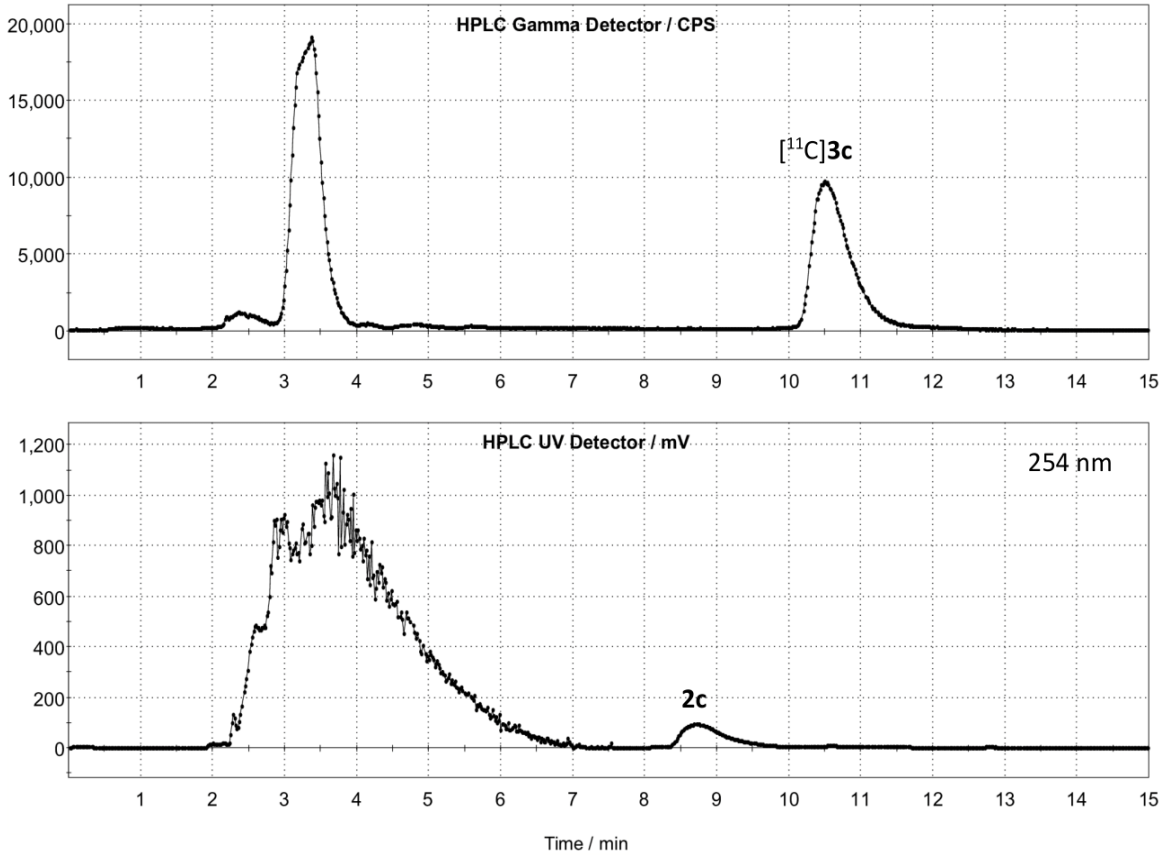
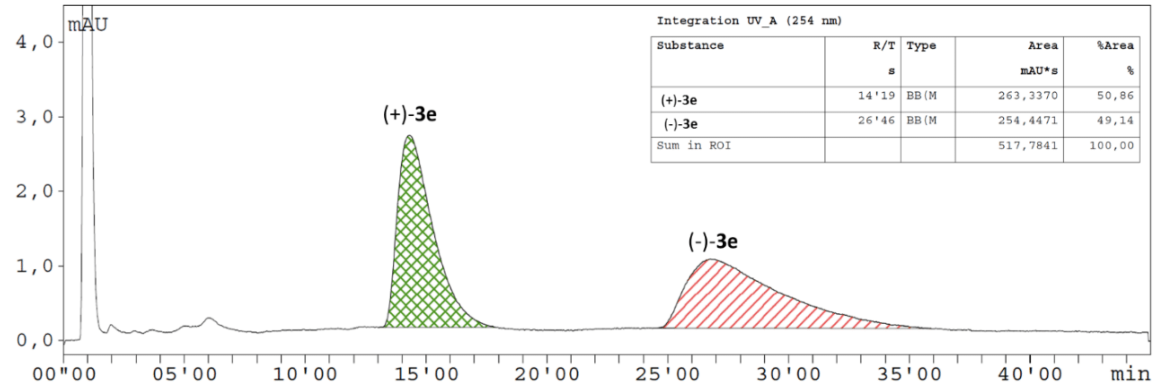


Figure S4: Exemplary preparative chromatograms of the purification of [^{11}C]**3c**. The product fraction was collected from 10.2 min to 11.2 min.

Chiral separation of 3e



Substance	R/T s	Type	Area mAU*s	%Area %
(+)-3e	14'19	BB(M	263,3370	50,86
(-)-3e	26'46	BB(M	254,4471	49,14
Sum in ROI			517,7841	100,00

Figure S5: UV-HPLC chromatogram of 2 µL 1 mg/mL solution of racemic **3e** on a chiral column (AGP 0.3 cm; Ø×5 cm 5 µM) using 12% 2-propanol in 10 mM NH_4Ac pH 5.8 at a flow of 0.5 mL/min.

Determination of [^{3}H]NMS K_D towards M1-M5

Equilibrium dissociation constants (K_D) of [^{3}H]NMS were determined *via* a direct radioligand binding assay. For every subtype a saturation binding curve with specific binding at six different concentrations was experimentally determined. Specific binding was delineated from total binding minus non-specific binding. Total binding was determined by incubating 5 µL DMSO, 50 µL radioligand solution and 445 µL membrane suspension for 1.5 h at 20 °C. For the determination of non-specific binding 5 µL 100 µM scopolamine in DMSO was used instead of pure DMSO. Bound and unbound ligand were separated using the filtration method as explained in the main text. Concentrations were chosen around the expected K_D and to reach saturation. The binding curve was fitted with Equation S1 and the determined K_D values are shown in Table S1.

$$SB = \frac{B_{max} \cdot c_{[^3H]NMS}}{K_D + c_{[^3H]NMS}}$$

Equation S1: Saturation function for specific binding. SB: specific binding [cpm], B_{max}: maximum specific binding [cpm], $c_{[^3H]NMS}$: radioligand concentration [nM], K_D: equilibrium dissociation constant [nM].

Table S1: Equilibrium dissociation constants (K_D) given in nM for mAChR receptor subtypes M1-M5. K_D values of this work are comparable to literature. The shown sources also determined the K_D *via* saturation binding on membrane preparations of CHO cells transfected with human mAChRs. Presented are means ± standard deviation from three independent measurements performed in triplicates.

	M1	M2	M3	M4	M5
this work	0.18±0.06	0.24±0.07	0.23+0.10	0.10±0.04	0.35±0.16
Lit[i]	0.17	0.15	0.16	0.07	-
Lit[ii]	0.25	0.32	0.23	0.20	0.26
Lit[iii]	0.051	0.29	0.086	0.056	0.20

EeAChE affinity and metabolism

Before starting the Ellman's assay the required enzyme concentration was evaluated. The enzyme was diluted using a mixture of 20 mM NaH_2PO_4 and 20 mM Na_2HPO_4 in a 4:6 ratio at pH 8.0 (3.75 µL enzyme solution (1 mg/mL) in 996 µL buffer). The resulting enzyme solution was then diluted with a 50 mM NaH_2PO_4 buffer (pH = 8.0), which gave the concentration used (250 µL in 13.5 mL buffer). These solutions were tested in combination with the highest concentration of ATI (3 mM) and with DTNB (0.5 mM). The kinetic was observed using a photometer. As the enzyme solution with the final concentration of 0.0682 µg/mL did not show a plateau over a 10 minute time period, this concentration was used for the Ellman's Assay.

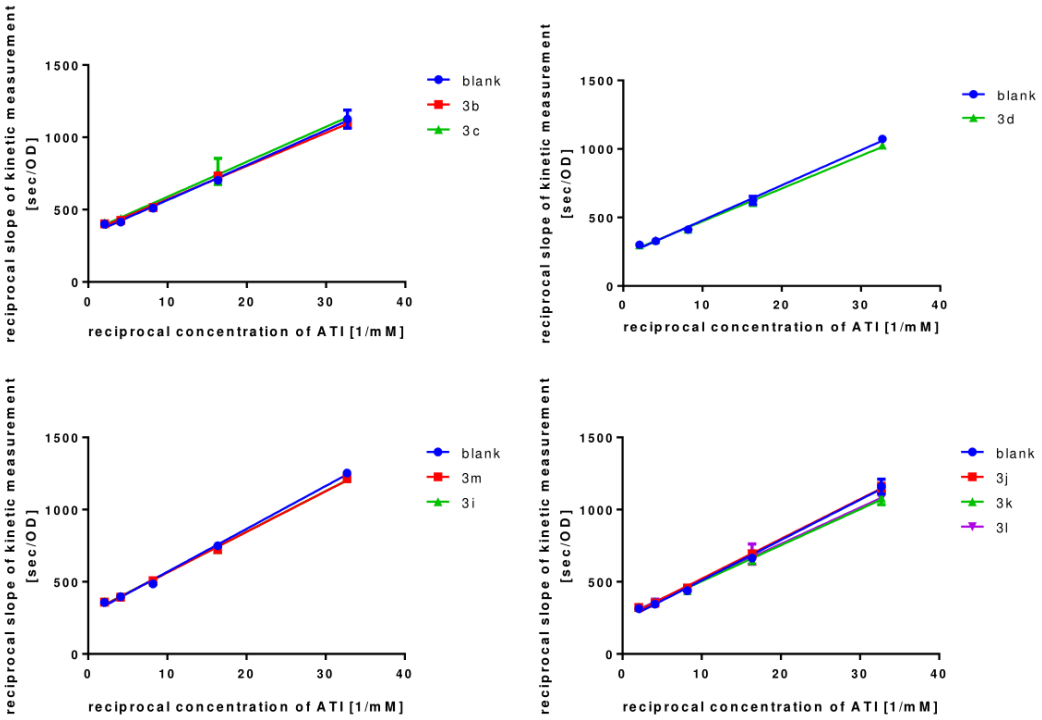


Figure S6: reciprocal slope of kinetic measurement plotted against the reciprocal substrate.

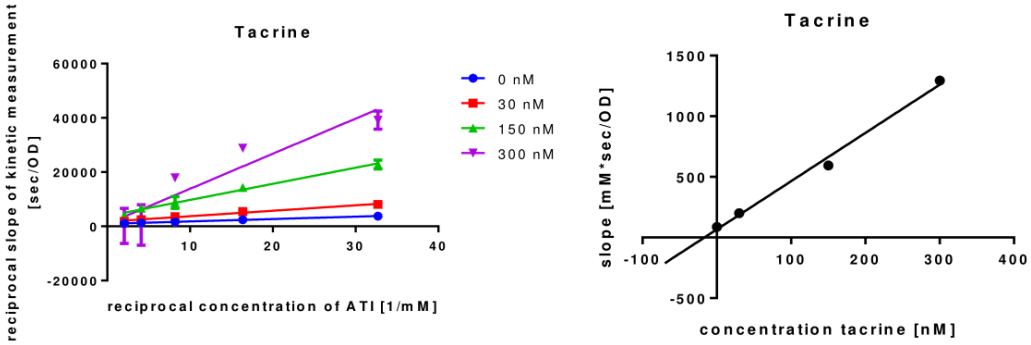


Figure S7: left: reciprocal slope of kinetic measurement plotted against the reciprocal substrate concentration; **right:** slope of the linear regression lines from the double reciprocal plot plotted against the tacrine concentration. The K_i of tacrine was obtained from the negative abscissa intercept in this plot.

Metabolic stability

Table S2: Retention times in the HPLC methods for metabolic stability.

retention time [min] in method	[^{11}C]arecaidine	[^{11}C]arecaidine ethyl ester	parent compound
[^{11}C]**3b**	2.2	8.3	16.2
[^{11}C]**3c**	2.1	8.1	14.1
[^{11}C]**3i**	2.2	8.6	14.8

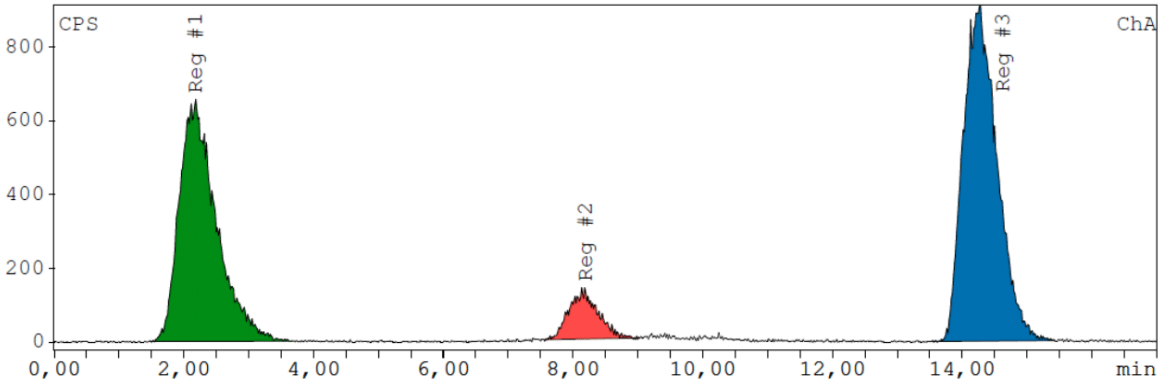


Figure S8: HPLC radio channel of a [^{11}C]**3c** 40 min timepoint measurement showing [^{11}C]arecaidine (green), [^{11}C]arecaidine ethyl ester (red), [^{11}C]**3c** (blue).

Metabolite identification

15 µL microsomes were preincubated in 257 µL PBS, 15 µL solution A and 3 µL solution B by gently shaking at 37 °C for 10 min. 10 µL of **3b** (10 mg/mL in EtOH) was added and 50 µL samples were taken at 0, 10, 20, 40 and 60 min. The samples were immediately quenched with 50 µL ACN:MeOH = 1:1, centrifuged at 21500 g for 5 min and 50 µL of the supernatant was purified with the same HPLC conditions used for the assessment of the metabolic stability of [^{11}C]**3b**. However, NH_4Ac was used as buffer substance instead of $NH_4H_2PO_4$ to allow for compatibility with direct HRMS measurements. A UV peak at the retention time of the observed less polar radiometabolite emerged and grew over time. It was collected from the 60 min time point and HRMS analysis revealed an exclusive peak at 170.1177 m/z, indicating the formation of arecaidine ethyl ester.

Plasma stability

12 µL formulated [^{11}C]**3c** was incubated with 1 mL plasma by gently shaking at 37 °C and 200 µL samples were taken at 0, 30 and 60 min. The samples were immediately quenched with 200 µL ACN:MeOH = 1:1, centrifuged at 21500 g for 5 min and 50-200 µL of the supernatant was analyzed with the same HPLC conditions used for the assessment of the metabolic stability of [^{11}C]**3c**. Peak areas of appearing radiometabolites were decay corrected for their retention times and related to the total peak area.

Interactions of [^{11}C]3c with CHO-M1 cells

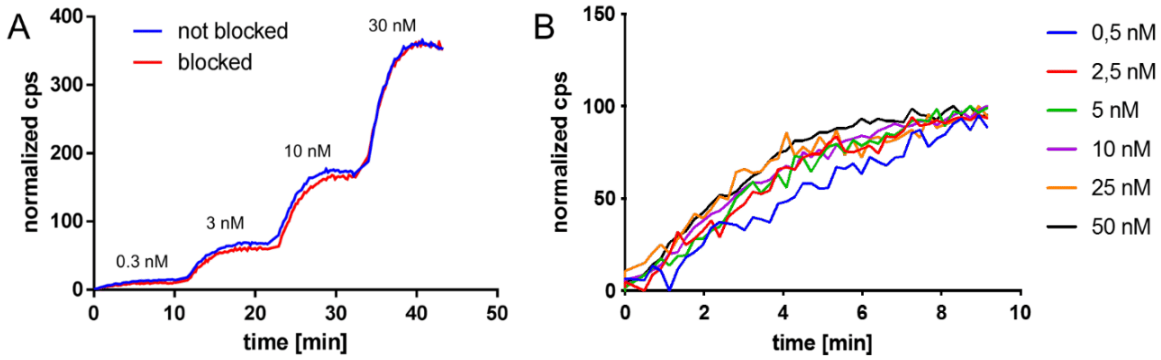


Figure S9: *Binding curves of [^{11}C]**3c** on CHO-M1 cells. Count rates are corrected for decay and normalized. A: No effect on the kinetic of [^{11}C]**3c** binding on CHO-M1 cells was observed by preblocking with 10 µM scopolamine. B: Binding curvature in dependence of [^{11}C]**3c** concentration.*

NMR spectra

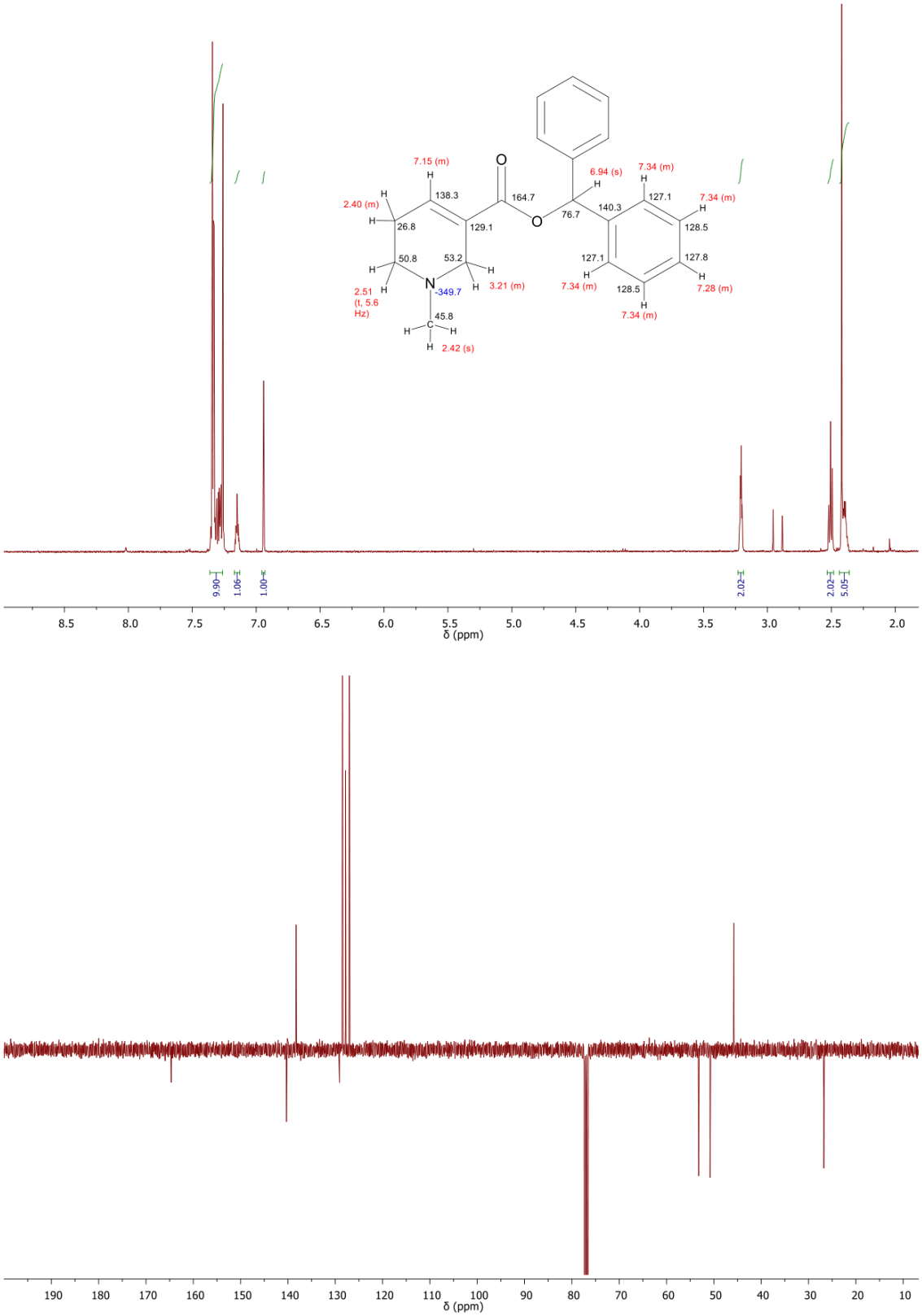


Figure S10: ^{1}H and ^{13}C NMR spectra of **3b** including assignment of signals.

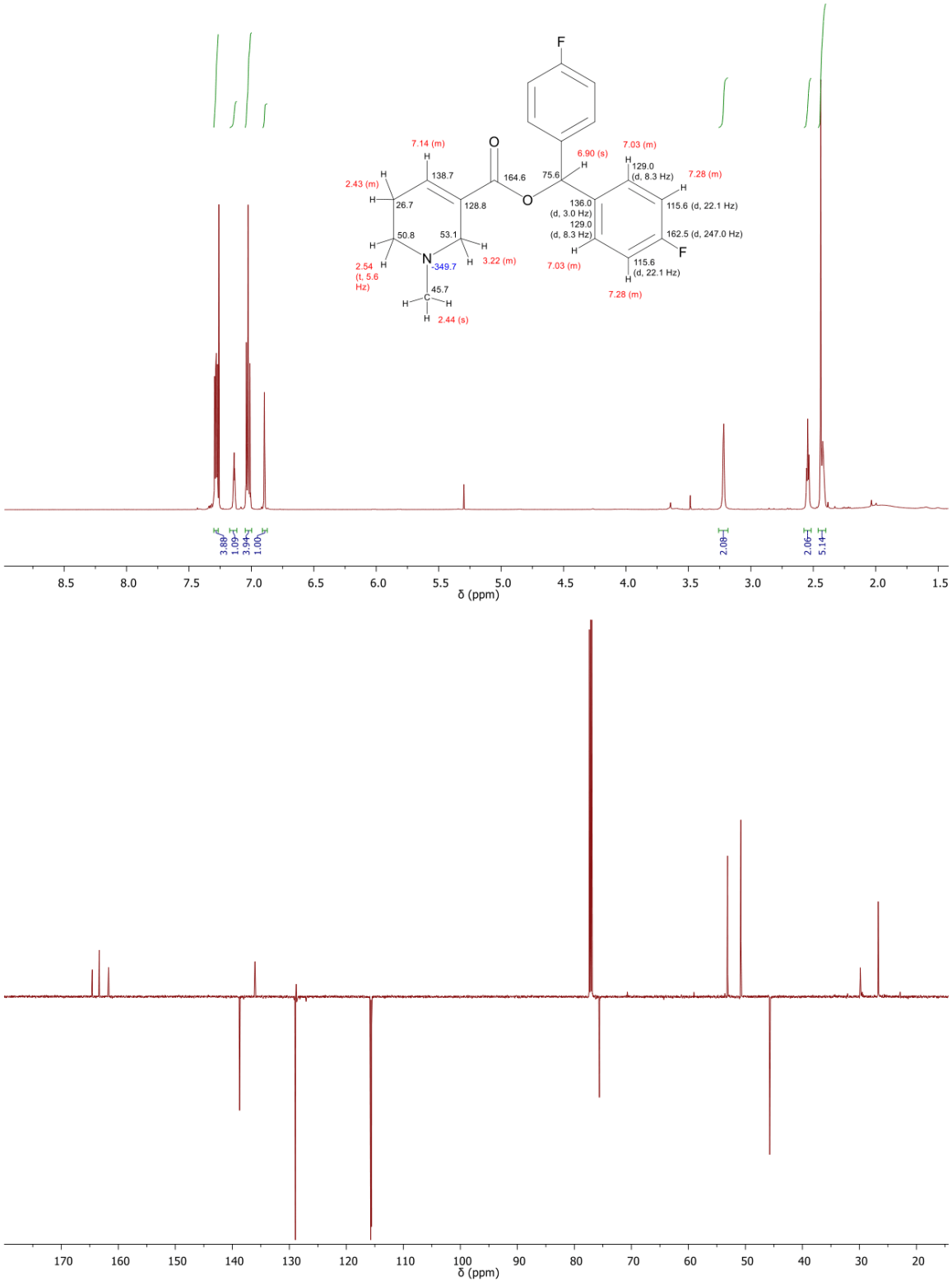


Figure S11: ^{1}H and ^{13}C NMR spectra of **3c** including assignment of signals.

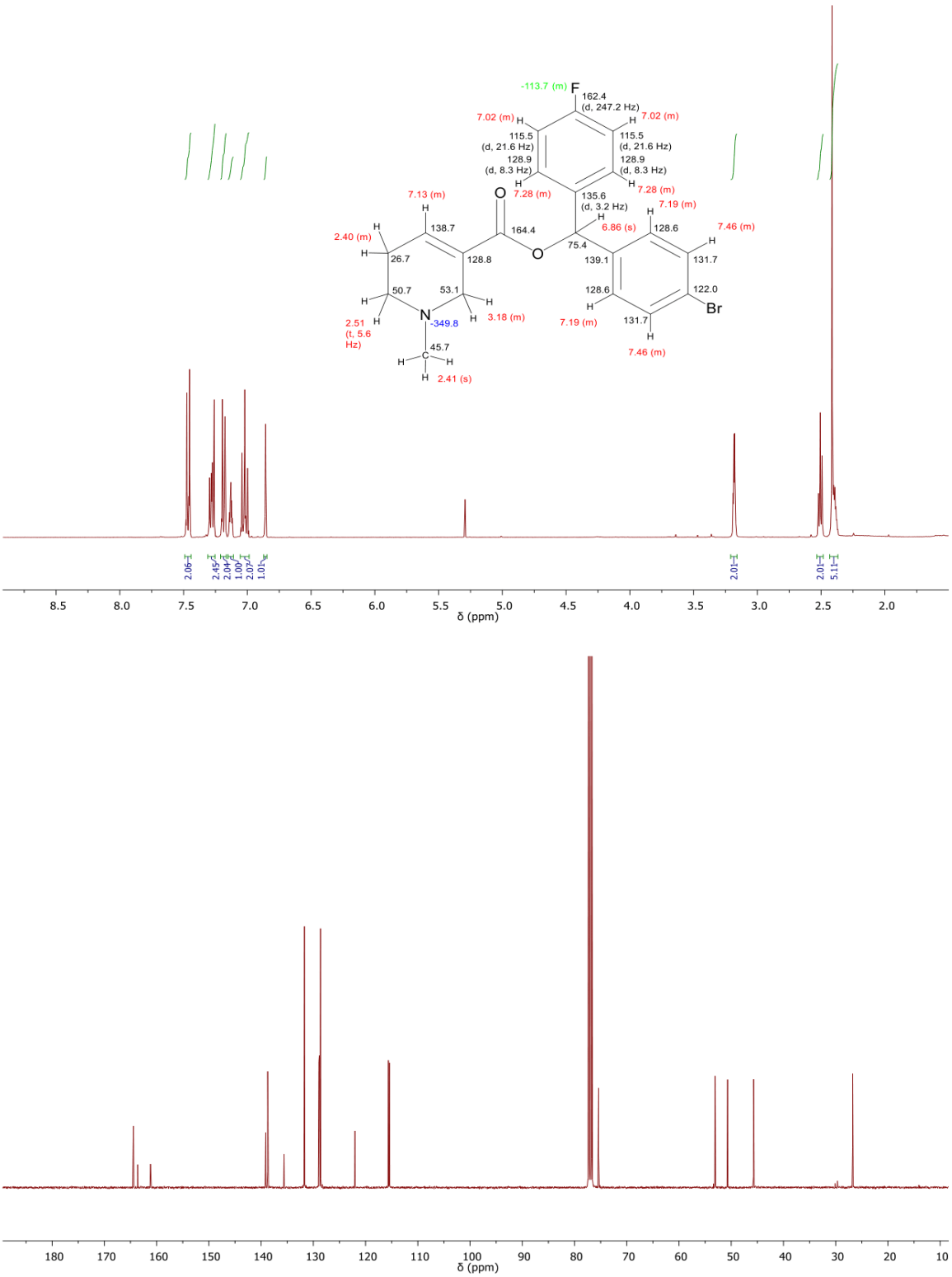


Figure S12: ^{1}H and ^{13}C NMR spectra of **3e** including assignment of signals.

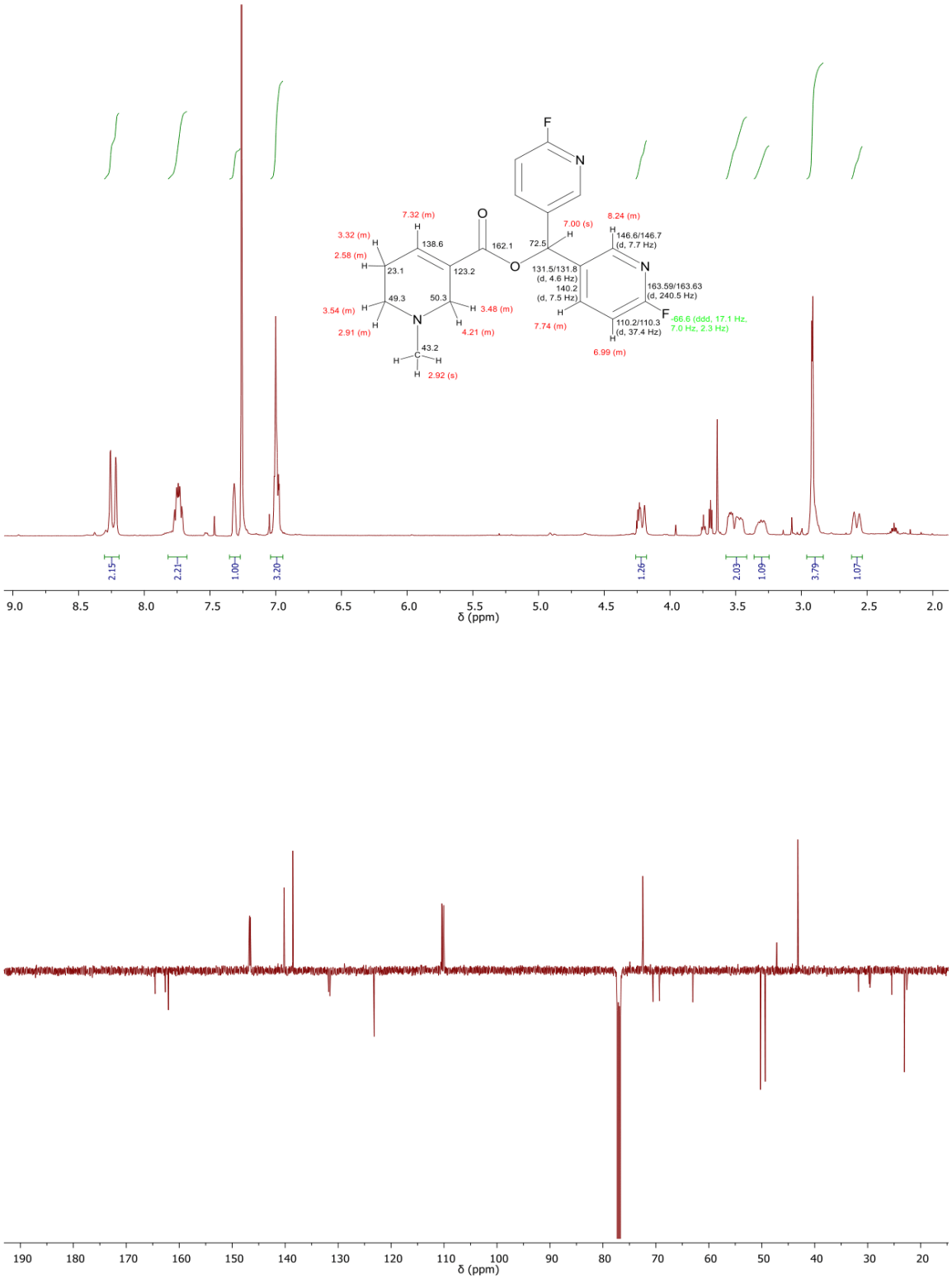


Figure S13: ^{1}H and ^{13}C NMR spectra of **3f** including assignment of signals.

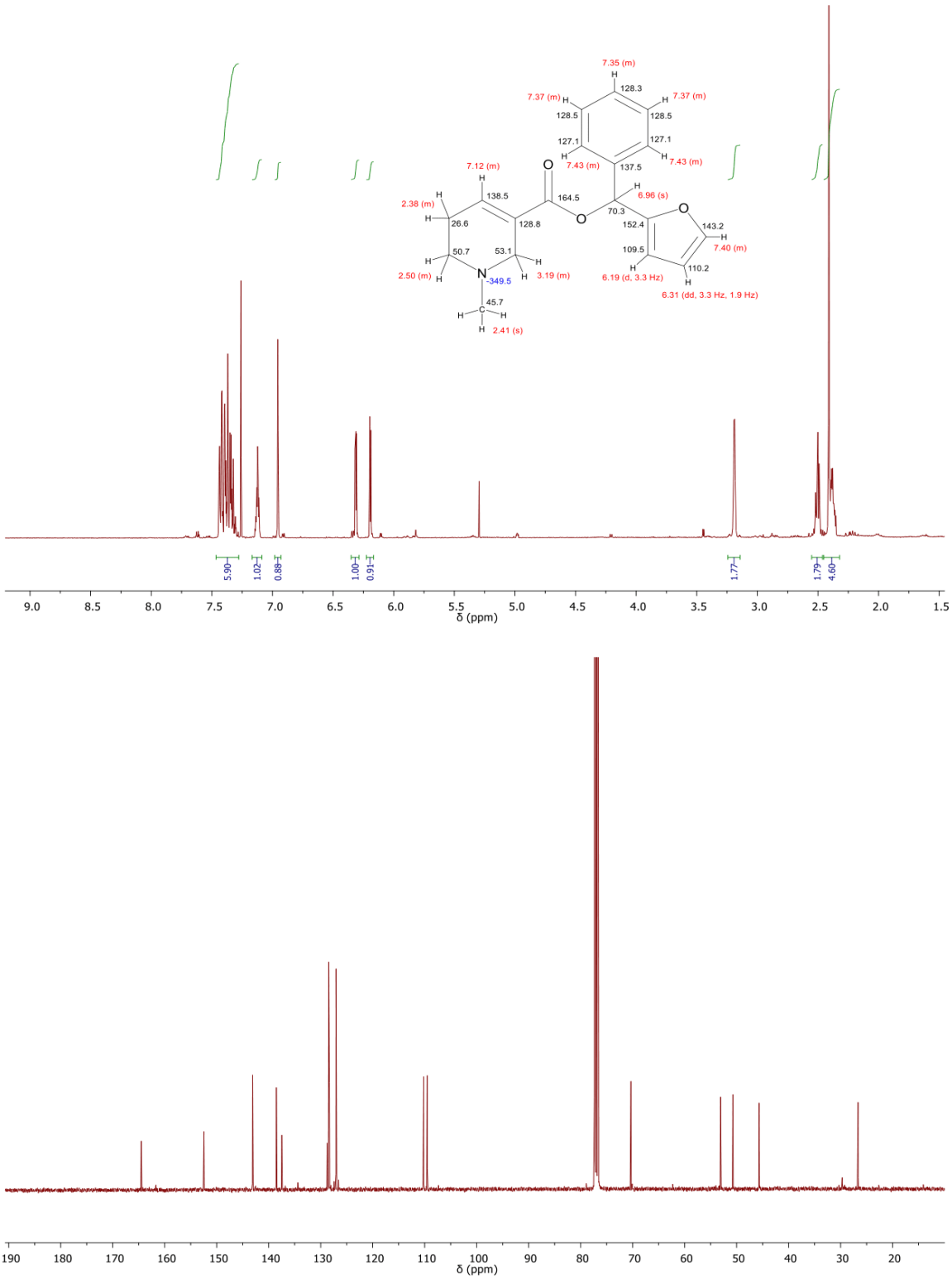


Figure S14: ^{1}H and ^{13}C NMR spectra of **3g** including assignment of signals.

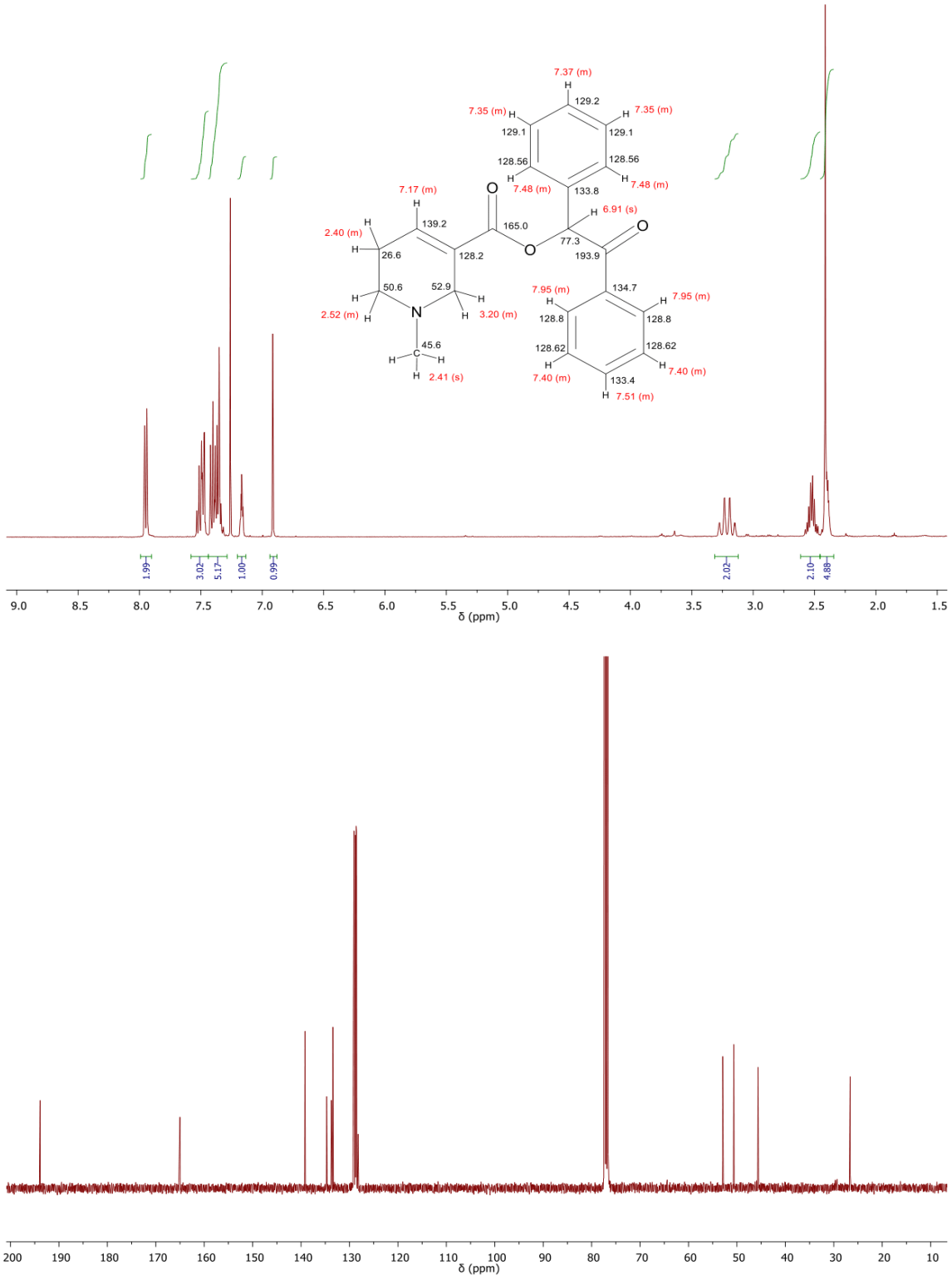


Figure S15: ^{1}H and ^{13}C NMR spectra of **3h** including assignment of signals.

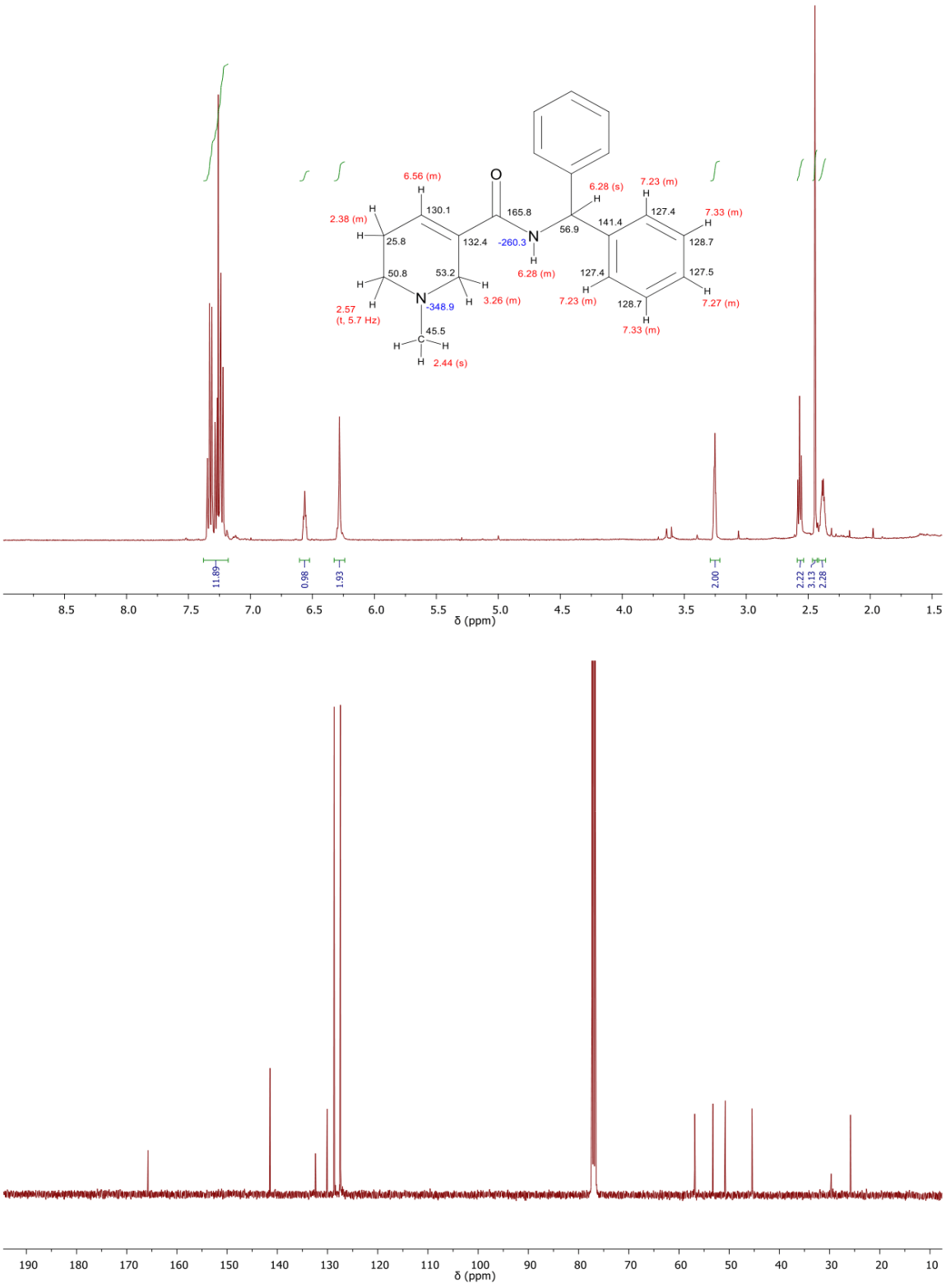


Figure S16: ^{1}H and ^{13}C NMR spectra of **3i** including assignment of signals.

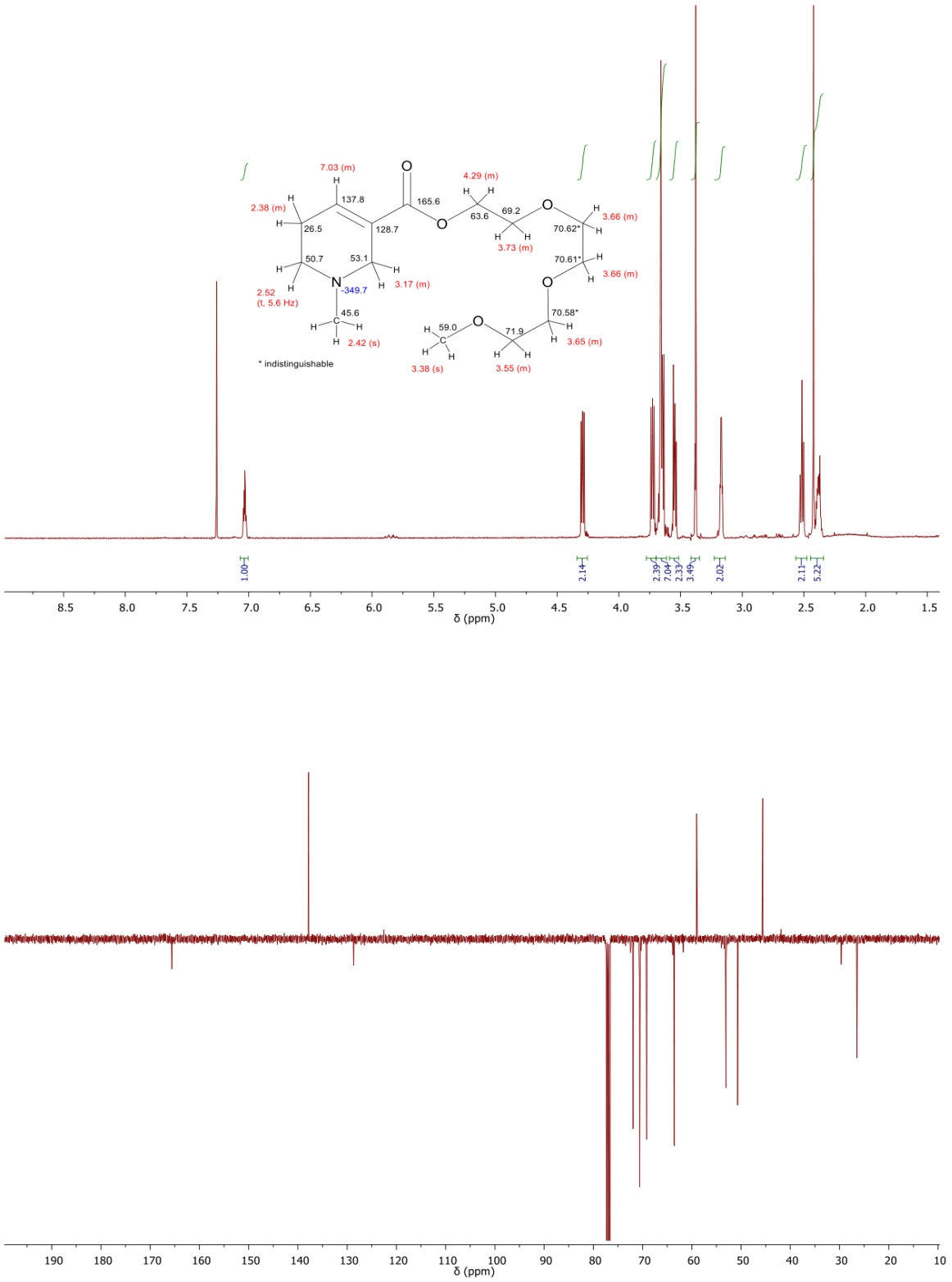


Figure S17: ^{1}H and ^{13}C NMR spectra of **3j** including assignment of signals.

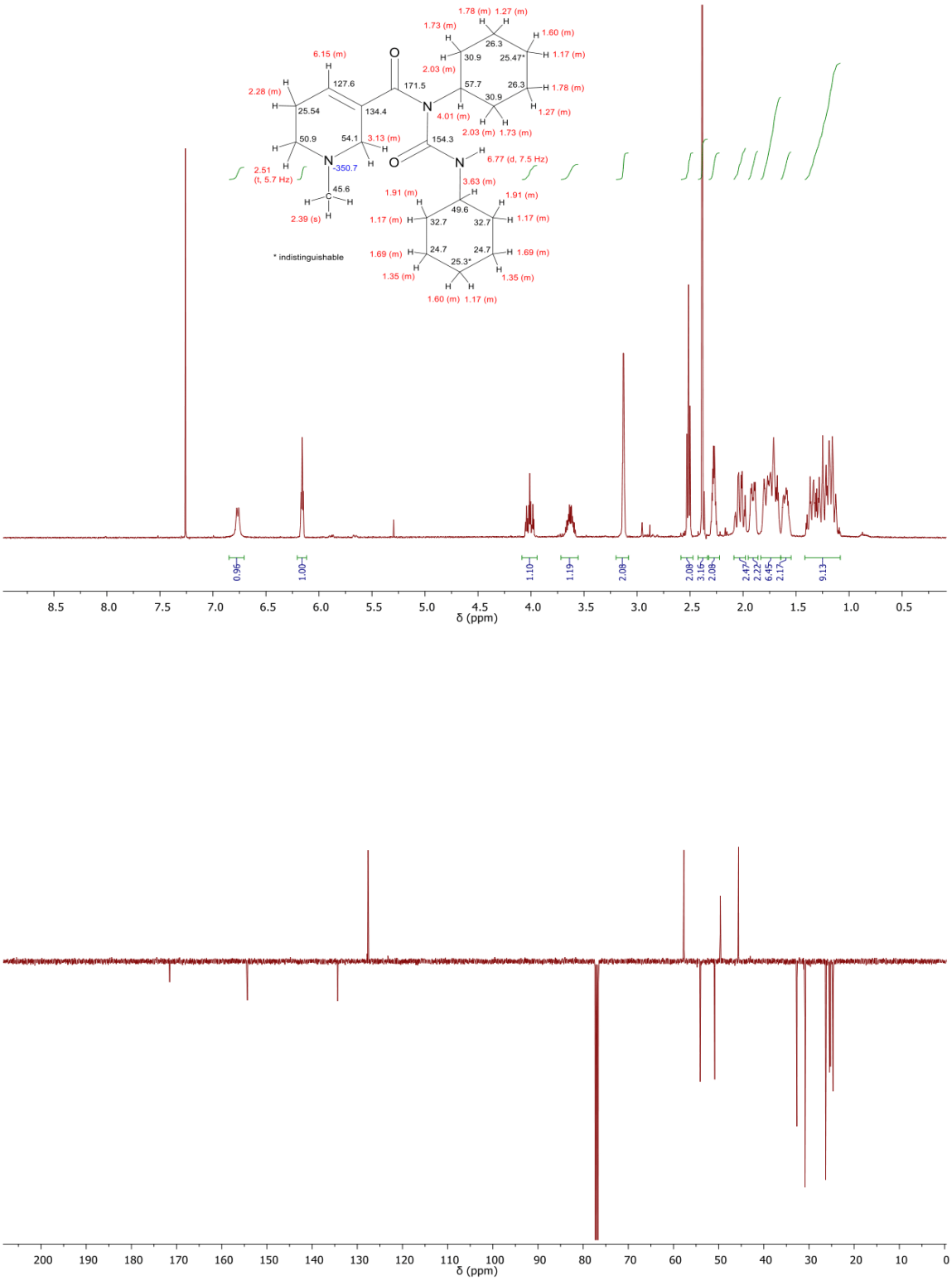


Figure S18: ^{1}H and ^{13}C NMR spectra of **3k** including assignment of signals.

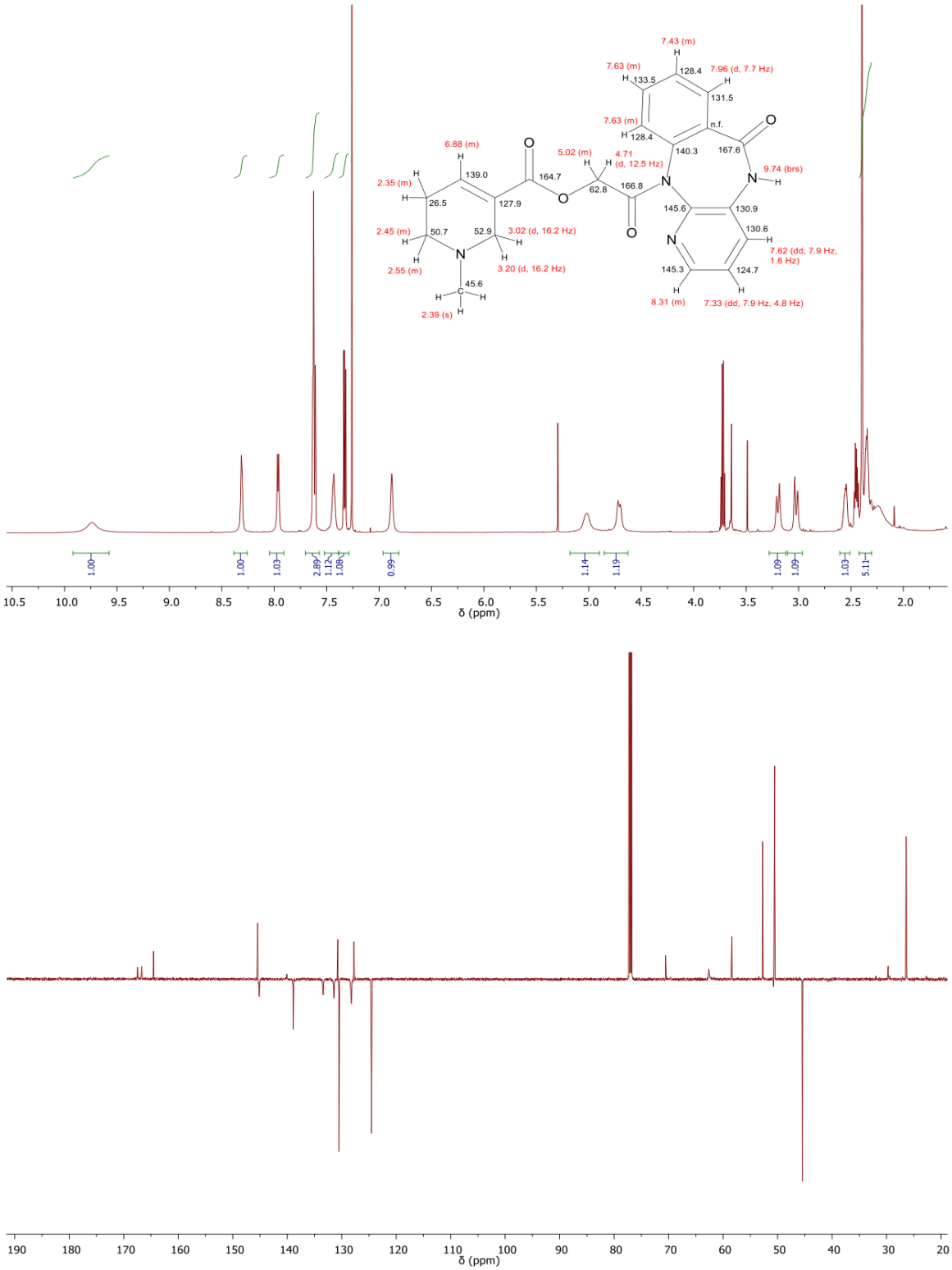


Figure S19: ^{1}H and ^{13}C NMR spectra of **3l** including assignment of signals.

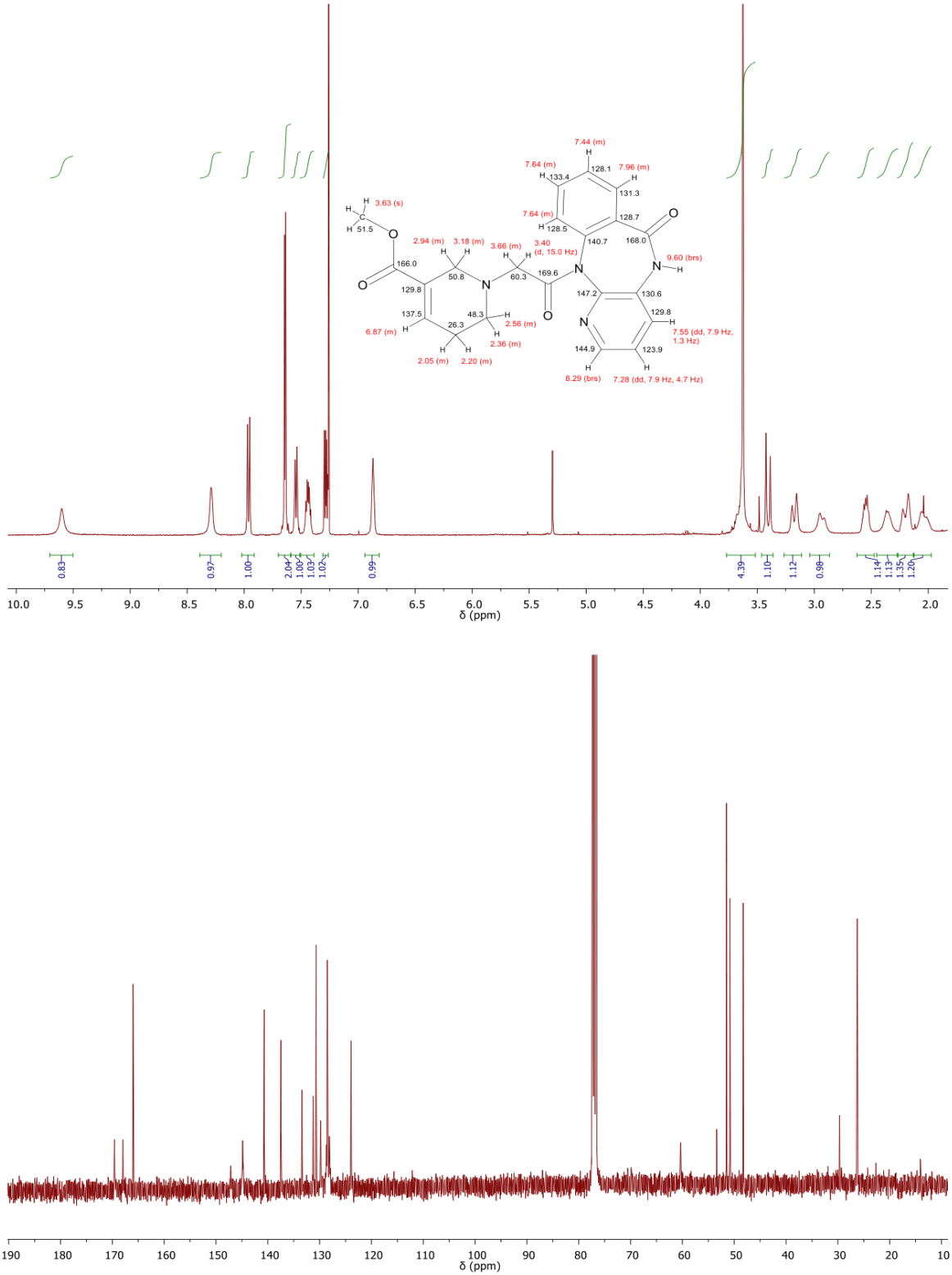


Figure S20: ^{1}H and ^{13}C NMR spectra of **3m** including assignment of signals.

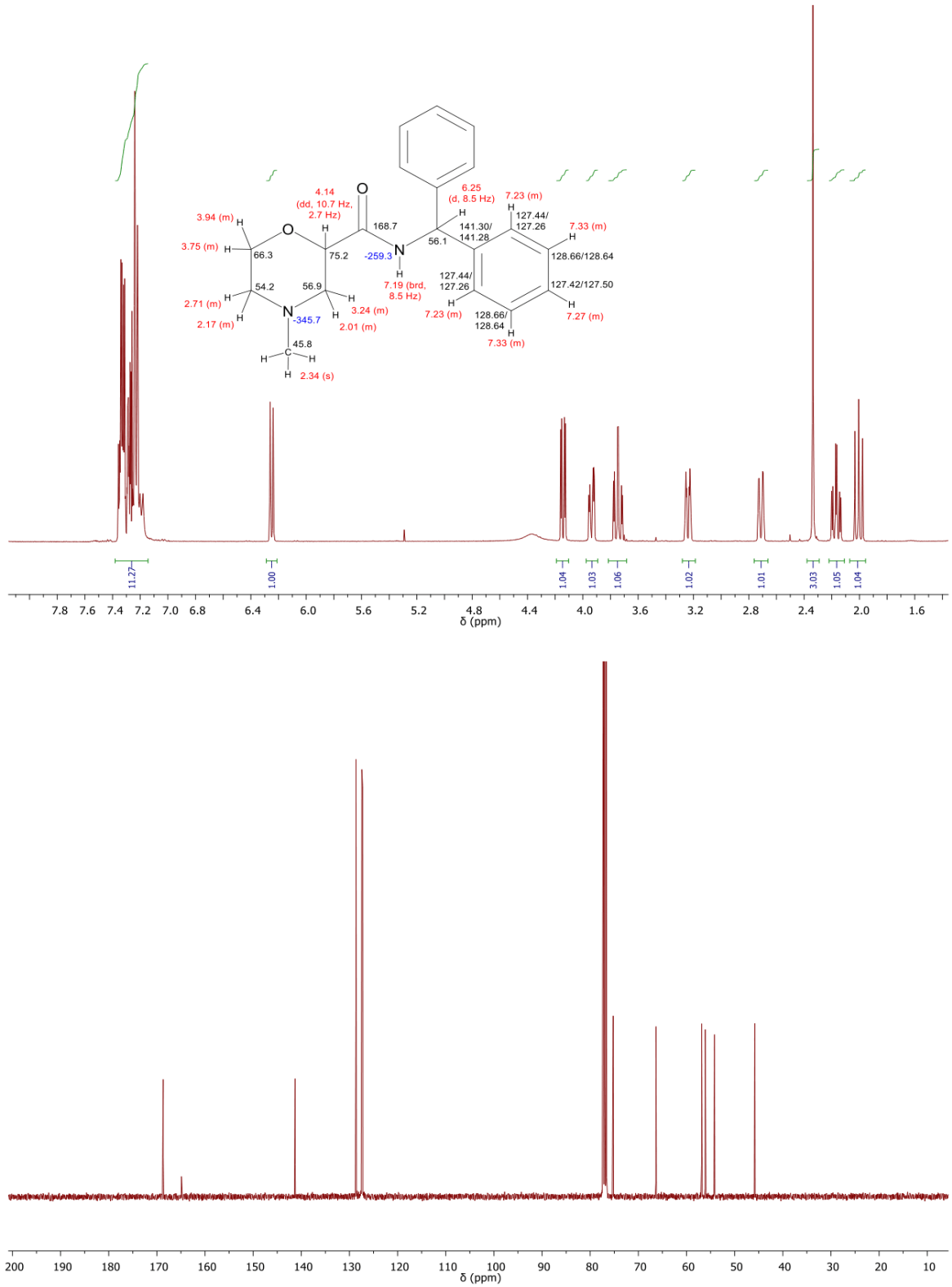


Figure S21: ^{1}H and ^{13}C NMR spectra of **6** including assignment of signals.

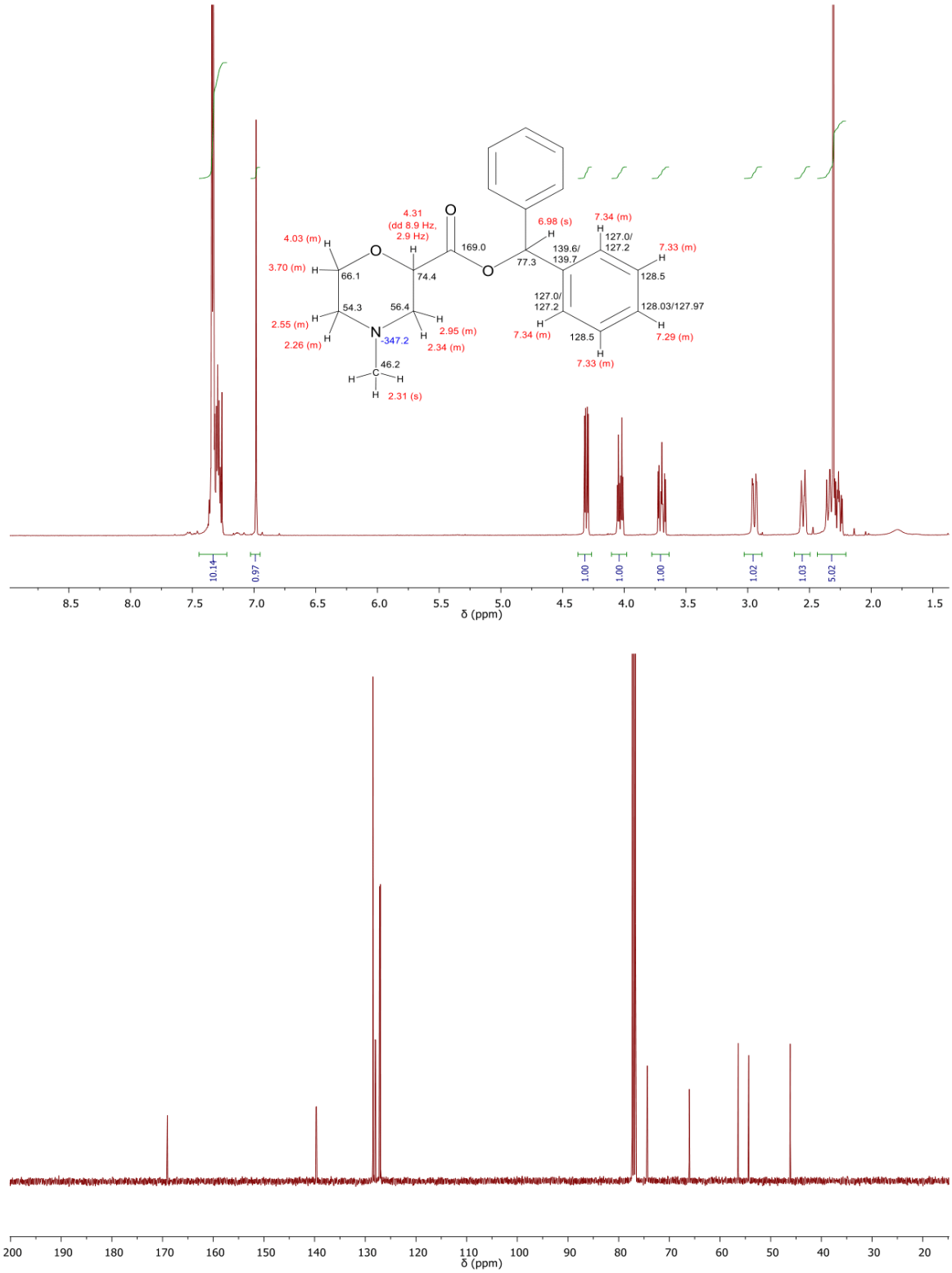


Figure S22: ^{1}H and ^{13}C NMR spectra of **7** including assignment of signals.

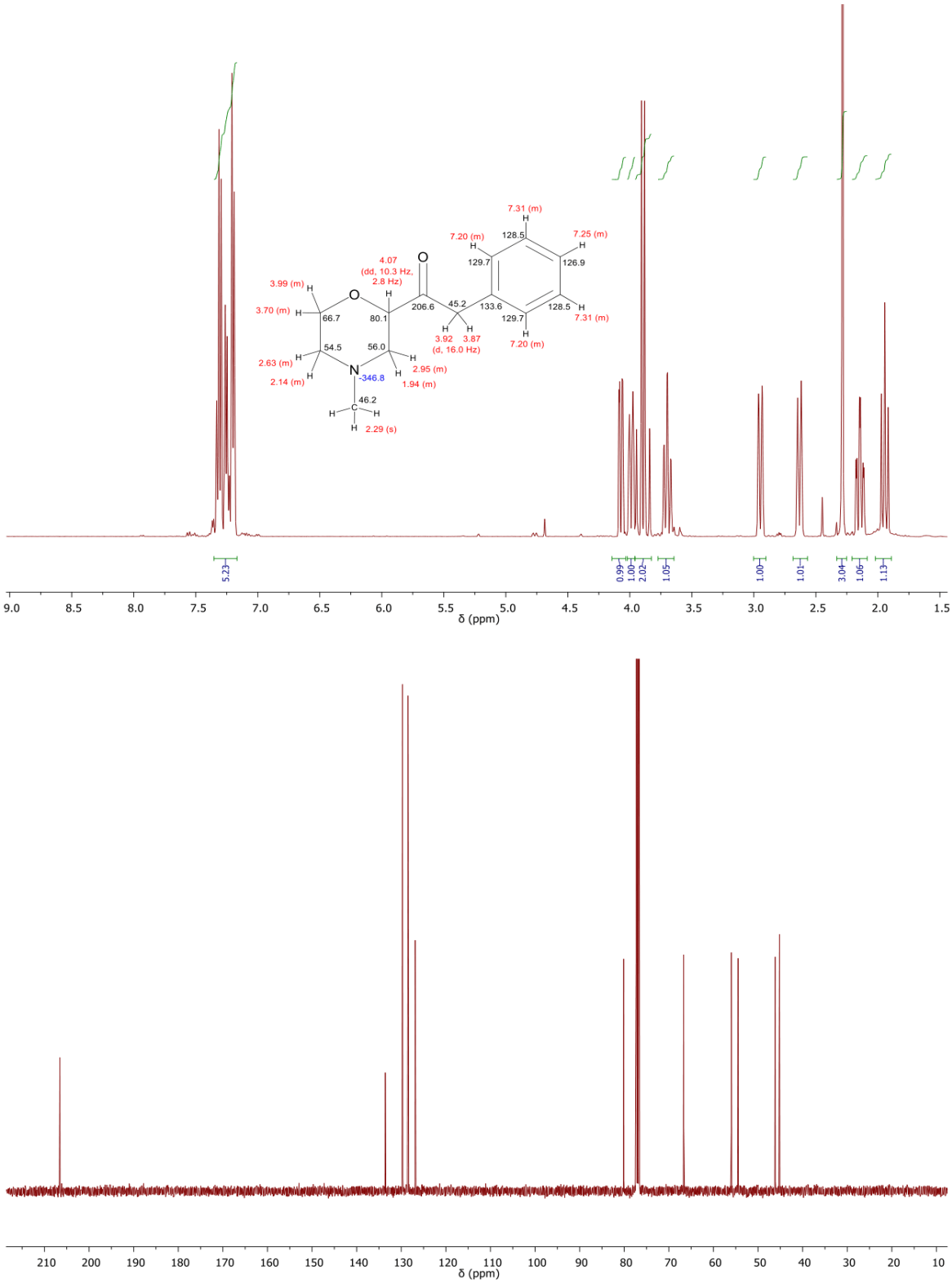


Figure S23: ^{1}H and ^{13}C NMR spectra of **3b** including assignment of signals.

X-ray Analysis

The X-ray intensity data were measured on Bruker D8 Venture diffractometer equipped with multilayer monochromator, Mo and Cu K/a INCOATEC micro focus sealed tube and Oxford cooling system. The structure was solved by *direct methods*. Non-hydrogen atoms were refined with *anisotropic displacement parameters*. Hydrogen atoms were inserted at calculated positions and refined with riding model. The following software was used: *Bruker SAINT software package*[iv] using a narrow-frame algorithm for frame integration, *SADABS*[v] for absorption correction, *OLEX2*[vi] for structure solution, refinement, molecular diagrams and graphical user-interface, *Shelxle*[vii] for refinement and graphical user-interface *SHELXS-2015*[viii] for structure solution, *SHELXL-2015*[ix] for refinement, *Platon*[x] for symmetry check. Experimental data and CCDC-Codes Experimental data and CCDC-Code (Available online: http://www.ccdc.cam.ac.uk/conts/retrieving.html) can be found in Table S3. Crystal data, data collection parameters, and structure refinement details are given in Table S4 - Table S7. Crystal structure and packing view is visualized in Figure S24 - Figure S27.

Table S3: Experimental parameter and CCDC-Code.

Sample	Machine	Source	Temp.	Detector Distance	Time/ Frame	#Frames	Frame width	CCDC
	Bruker		[K]	[mm]	[s]		[°]	
3k	D8	Cu	100	34	15	2553	0.5	1866258
5	D8	Mo	150	30	5	501	1.000	1977571

***N*-cyclohexyl-*N*-(cyclohexylcarbamoyl)-1-methyl-1,2,5,6-tetrahydropyridine-3-carboxamide** for **3k** " Eur. J. Med. Chem.".

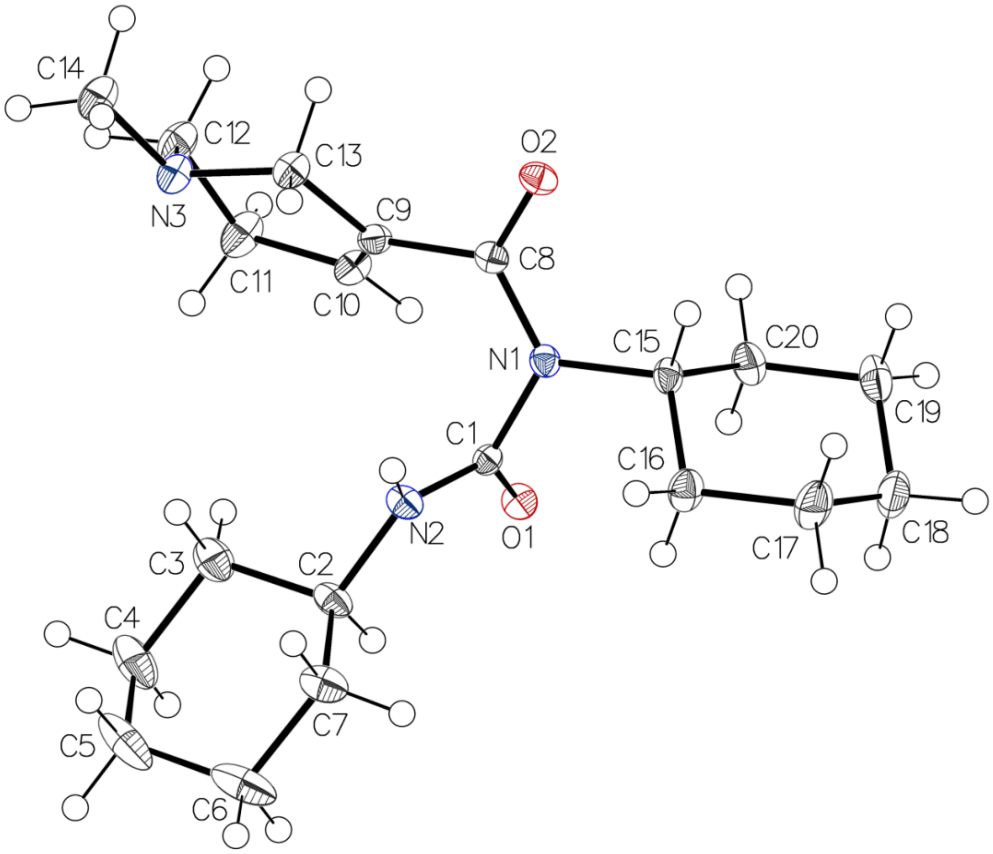


Figure S24: Asymmetric Unit of **3k**, drawn with 50% displacement ellipsoid. The bond precision for C-C single bonds is 0.0022Å.

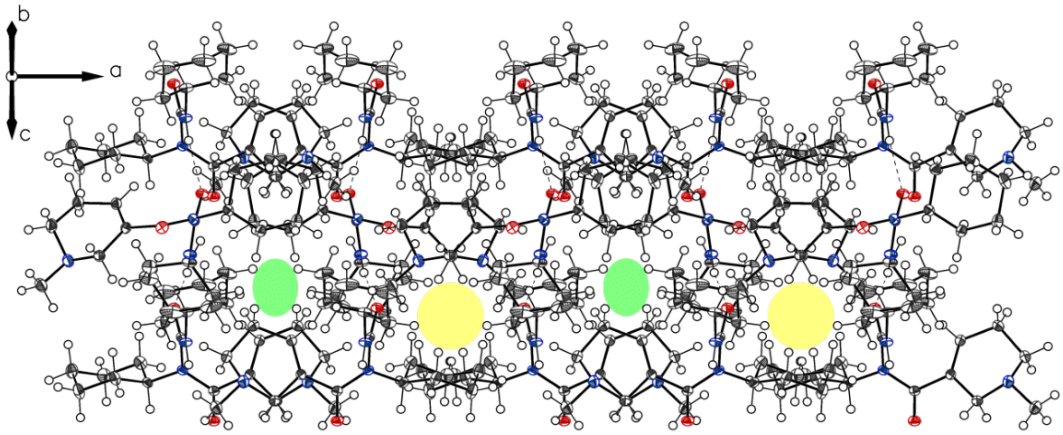


Figure S25: Packing of **3k**, two free tube volumes with diameters around 2-2.5 Å characterize the packing. Both tubes are formed by hydrogen spheres. Also a moderate intermolecular hydrogen bond ($N_2H\ldots O_1$) is characterizing the packing.

Table S4: Sample and crystal data of **3k**.

Chemical formula	C20H33N3O2	**Crystal system**	orthorhombic	
Formula weight [g/mol]	347.49	**Space group**	*Pna21*	
Temperature [K]	100	**Z**	4	
Measurement method	\f and \w scans	**Volume [Å^3]**	1973.81(9)	
Radiation (Wavelength [Å])	CuKα (λ = 1.54178)	**Unit cell dimensions [Å] and [°]**	12.6877(3)	90
Crystal size / [mm^3]	0.61 × 0.19 × 0.182		16.3698(4)	90
Crystal habit	clear colourless needle		9.5034(3)	90
Density (calculated) / [g/cm^3]	1.169	**Absorption coefficient / [mm^{-1}]**	0.597	
Abs. correction Tmin	0.6345	**Abs. correction Tmax**	0.7536	
Abs. correction type	multiscan	**F(000) [e$^-$]**	760	

Table S5: Data collection and structure refinement of **3k**.

Index ranges	-15 ≤ h ≤ 15, -20 ≤ k ≤ 20, -10 ≤ l ≤ 11	**Theta range for data collection [°]**	10.764 to 144.162	
Reflections number	18703	**Data / restraints / parameters**	3575/1/227	
Refinement method	Least squares	**Final R indices**	all data	R1 = 0.0271, wR2 = 0.0728
Function minimized	Σ w(F_o^2 - F_c^2)^2		I>2σ(I)	R1 = 0.0270, wR2 = 0.0727
Goodness-of-fit on F^2	1.055	**Weighting scheme**	w=1/[$\sigma^2(F_o^2)$+(0.0399P)^2+0.2962P]	
Largest diff. peak and hole [e Å^{-3}]	0.20/-0.14		where P=(F_o^2+2F_c^2)/3	

2-carboxy-4-methylmorpholin-4-ium bromide for **5** “Eur. J. Med. Chem.”

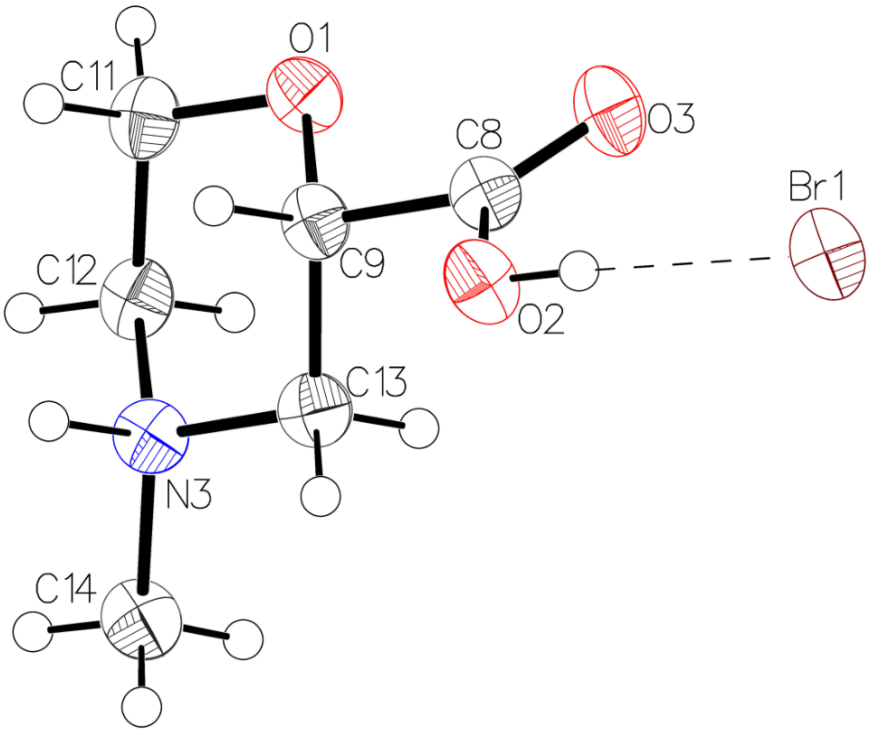


Figure S26: Asymmetric Unit of **5**, drawn with 50% displacement ellipsoid. The bond precision for C-C single bonds is 0.0100Å.

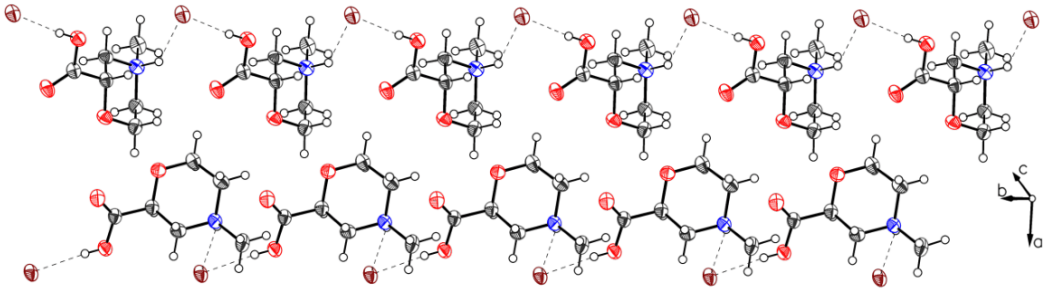


Figure S27: Packing of **5**.

Table S6: Sample and crystal data of **5.**

Chemical formula	C6H12BrNO3	**Crystal system**	monoclinic	
Formula weight [g/mol]	226.08	**Space group**	*P21/n*	
Temperature [K]	100	**Z**	4	
Measurement method	\f and \w scans	**Volume [Å^3]**	873.81(8)	
Radiation (Wavelength [Å])	MoKα (λ = 0.71073)	**Unit cell dimensions [Å] and [°]**	11.1252(6)	90
Crystal size / [mm^3]	1 × 0.5 × 0.1		7.1215(4)	114.093(2)
Crystal habit	clear colourless block		12.0815(6)	90
Density (calculated) / [g/cm^3]	1.718	**Absorption coefficient / [mm^{-1}]**	4.666	
Abs. correction Tmin	0.4573	**Abs. correction Tmax**	0.7461	
Abs. correction type	multiscan	**F(000) [e$^-$]**	456	

Table S7: Data collection and structure refinement of **5.**

Index ranges	-15 ≤ h ≤ 15, -10 ≤ k ≤ 10, -17 ≤ l ≤ 17	**Theta range for data collection [°]**	4.198 to 61.224	
Reflections number	22129	**Data / restraints / parameters**	2656/0/106	
Refinement method	Least squares	**Final R indices**	all data	R1 = 0.0397, wR2 = 0.1043
Function minimized	Σ w(F_o^2 - F_c^2)^2		I>2σ(I)	R1 = 0.0368, wR2 = 0.1021
Goodness-of-fit on F^2	1.078	**Weighting scheme**	w=1/[σ2(Fo2)+(0.0679P)2 +0.5591P]	
Largest diff. peak and hole [e Å^{-3}]	1.97/-1.33		where P=(F_o^2+2F_c^2)/3	

[i] ValiScreen® GPCR Cell Line human Muscarinic Acetylcholine Receptor, Technical Data Sheet; Perkin Elmer: Waltham, MA, 2009.
[ii] Jakubík J., Randáková A., El-Fakahany E. E., Doležal V. Divergence of allosteric effects of rapacuronium on binding and function of muscarinic receptors. *BMC Pharmacology*, **2009**, *9*:15.
[iii] Vogel, H. G. Drug Discovery and Evaluation: Pharmacological Assays 3rd edition, Springer: Berlin Heidelberg New York, 2008; p 513.
[iv] Bruker SAINT v8.37A Copyright © 2005-2016 Bruker AXS
[v] Sheldrick, G. M. (1996). *SADABS.* University of Göttingen, Germany.
[vi] Dolomanov, O.V., Bourhis, L.J., Gildea, R.J, Howard, J.A.K. & Puschmann, H. , OLEX2, (2009), J. Appl. Cryst. 42, 339-341.
[vii] C. B. Huebschle, G. M. Sheldrick and B. Dittrich, ShelXle: a Qt graphical user interface for SHELXL, J. Appl. Cryst., 44, (2011) 1281-1284.
[viii] Sheldrick, G. M. (1996). *SHELXS.* University of Göttingen, Germany.
[ix] Sheldrick, G. M. (1996). *SHELXL.* University of Göttingen, Germany.
[x] Spek, A. L. (2009). *Acta Cryst.* D65, 148-155.

pharmaceuticals

MDPI

Supporting Information

Synthesis, Biological, and Computational Evaluation of Antagonistic, Chiral Hydrobenzoin Esters of Arecaidine Targeting mAChR M1

Marius Ozenil [1], Jonas Aronow [1], Daniela Piljak [1], Chrysoula Vraka [1], Wolfgang Holzer [2], Helmut Spreitzer [2], Wolfgang Wadsak [1,3], Marcus Hacker [1] and Verena Pichler [2,*]

[1] Department of Biomedical Imaging and Image-guided Therapy, Division of Nuclear Medicine, Medical University of Vienna, 1090 Vienna, Austria; marius.ozenil@meduniwien.ac.at (M.O.); jonas.aronow@meduniwien.ac.at (J.A.); daniela.piljak@gmx.at (D.P.); chrysoula.vraka@meduniwien.ac.at (C.V.); wolfgang.wadsak@meduniwien.ac.at (W.W.); marcus.hacker@meduniwien.ac.at (M.H.)

[2] Department of Pharmaceutical Chemistry, Faculty of Life Sciences, University of Vienna, 1090 Vienna, Austria; wolfgang.holzer@univie.ac.at (W.H.); helmut.spreitzer@univie.ac.at (H.S.)

[3] CBmed GmbH - Center for Biomarker Research in Medicine, 8036 Graz, Austria

* Correspondence: verena.pichler@univie.ac.at; Tel.: +43-1-4277-55624

Content:

Exemplary competitive binding curves on human mAChR M1 (Figure S1)
UV-HPLC chromatograms (Figure S2, Figure S3)
NMR spectra (Figure S4, Figure S5, Figure S6)

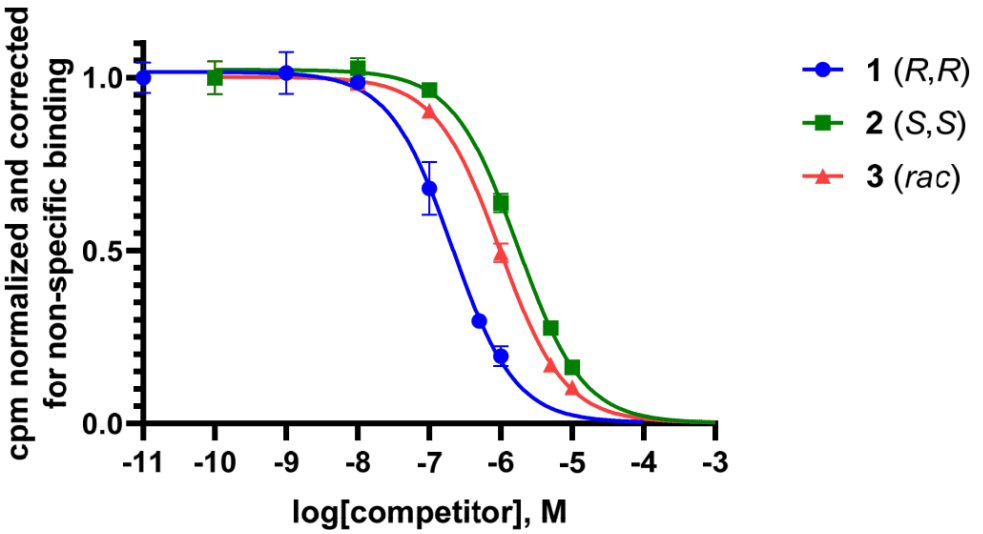


Figure 1. Exemplary competitive binding curves of **1**, **2**, and **3** on human mAChR M1 expressed on cell membranes of stably transfected CHO cells using [*N*-methyl-^{3}H]scopolamine methyl chloride. Values at 10^{-11} M and 10^{-10} M represent full binding in absence of competitor.

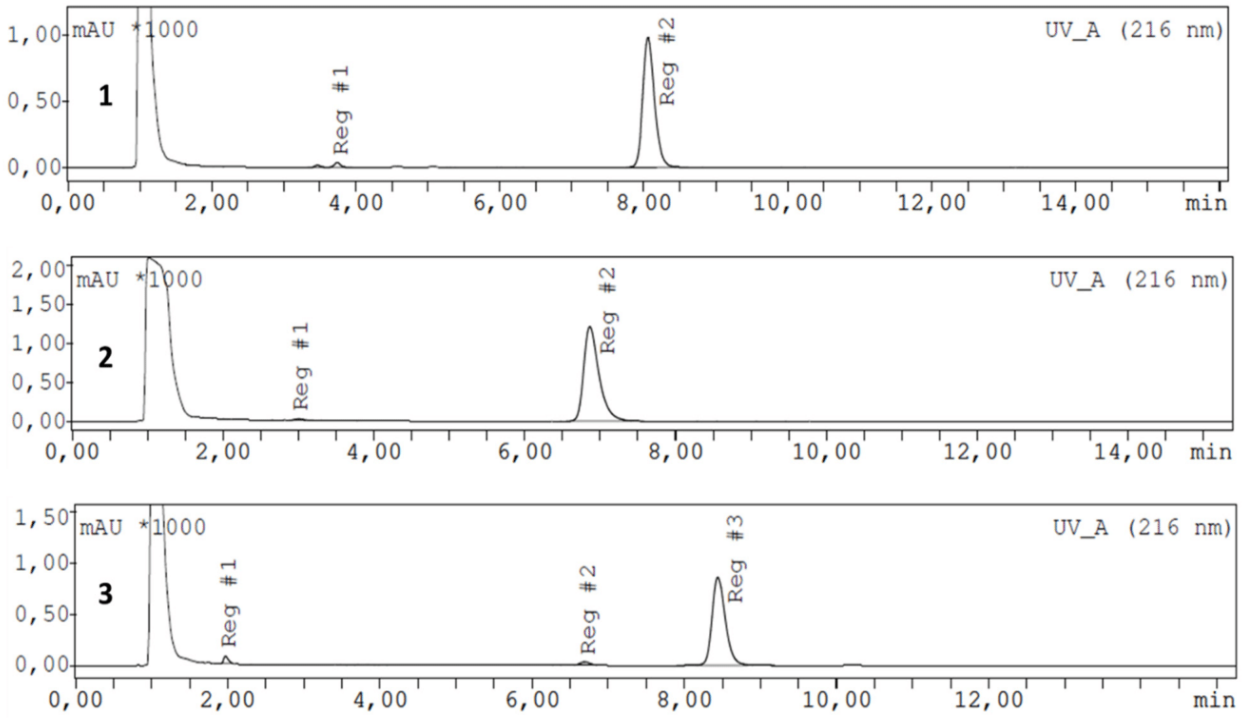


Figure 2. Isocratic HPLC chromatograms of compounds **1–3**. 35–40% ACN in 25 mM $NH_4H_2PO_4$ buffer pH 9.3 at a flow of 1 mL/min.

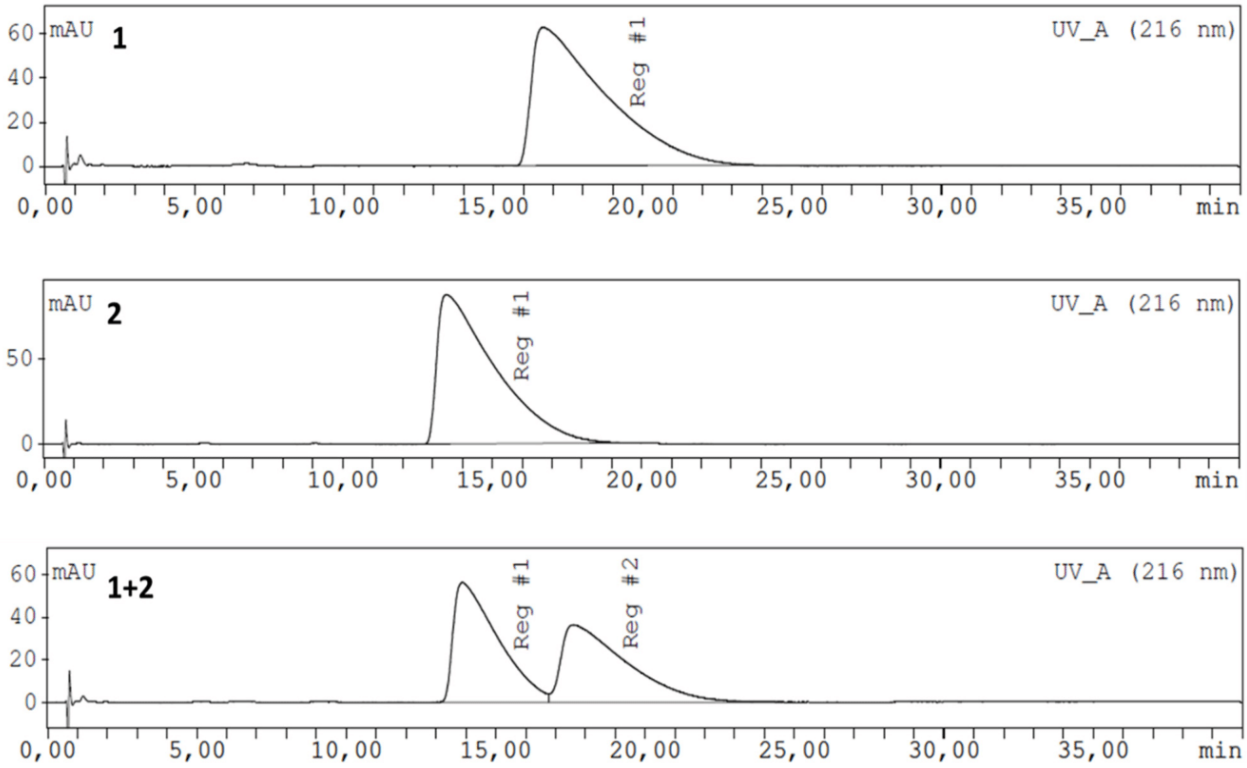


Figure 3. Chiral chromatography using a an AGP 0.3 cmØ × 5 cm 5 µM column operated with 2% IPA in 10 mM NH_4Ac pH 5.8 at a flow of 0.5 mL/min.

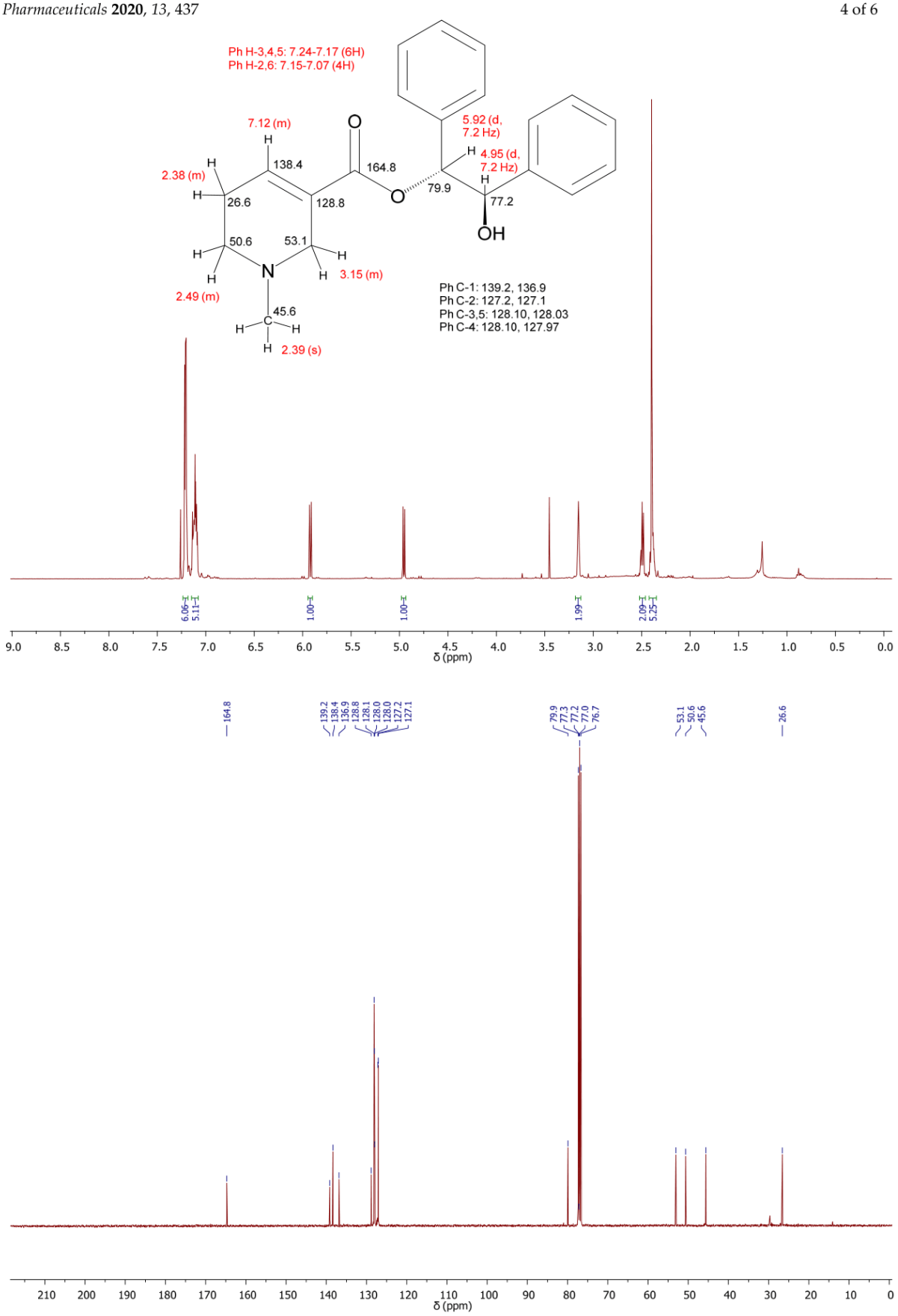


Figure 4. ^{1}H- and ^{13}C-NMR spectrum of **1**.

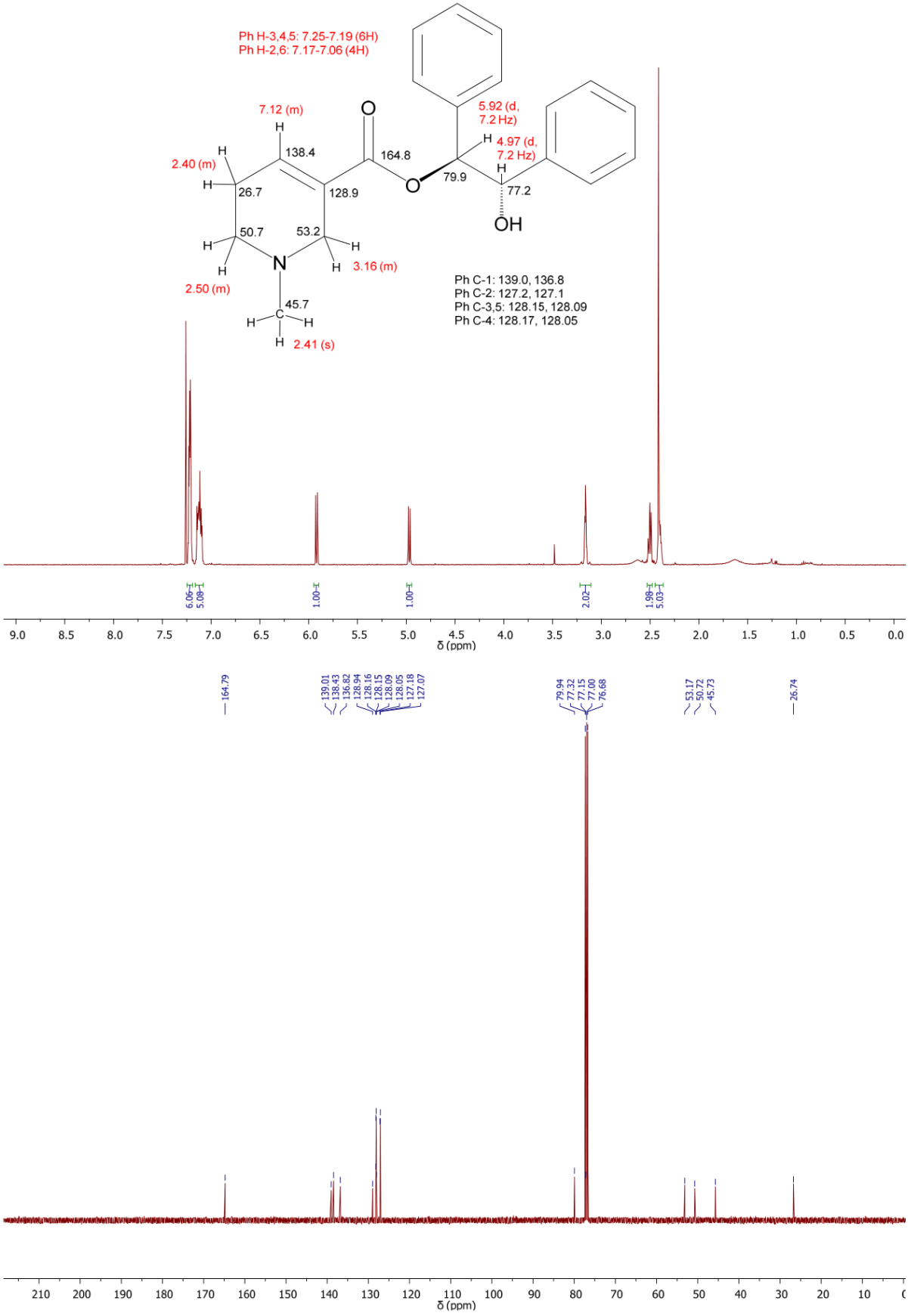


Figure 5. ^{1}H- and ^{13}C-NMR spectrum of **2**.

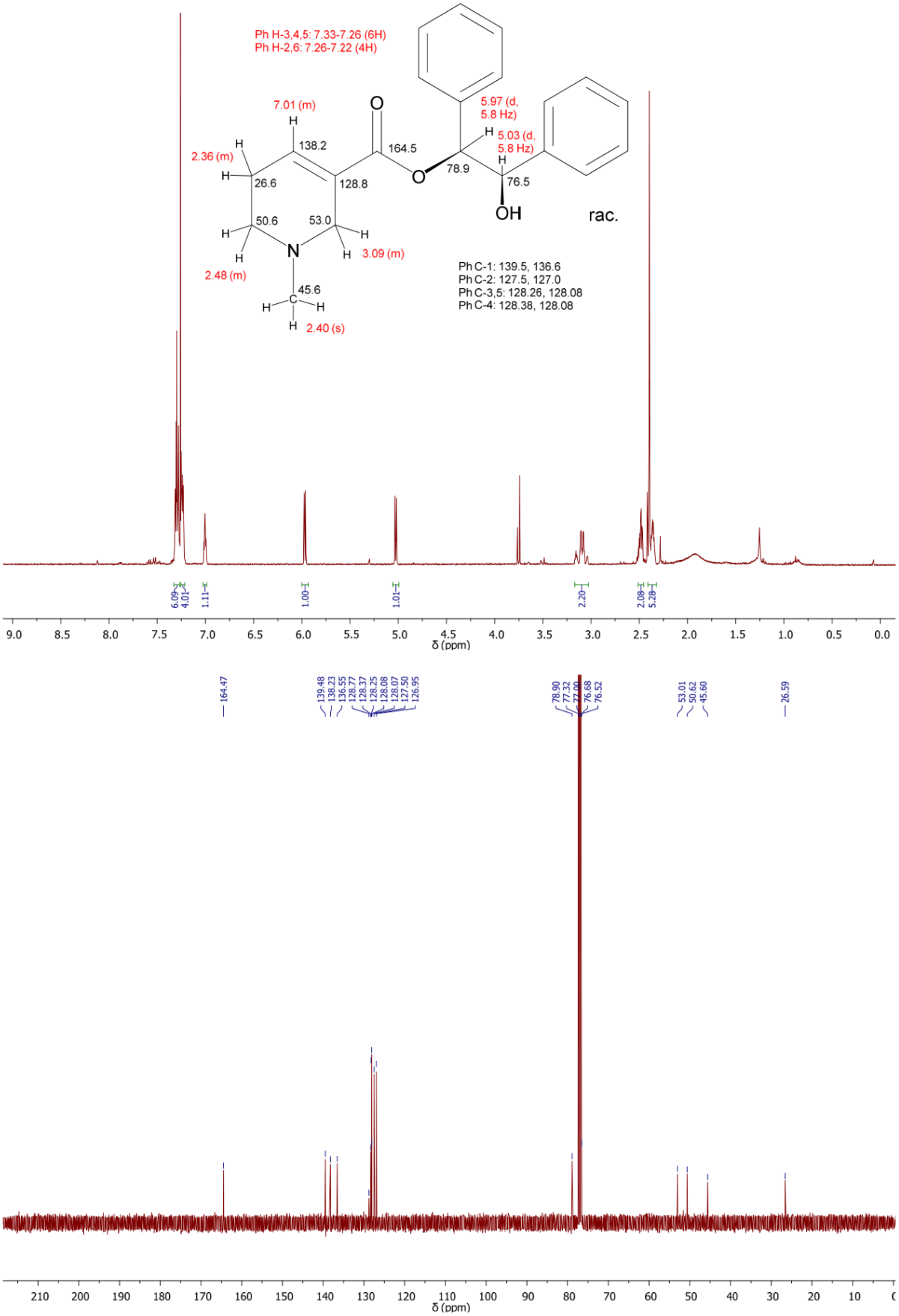


Figure 6. ^{1}H- and ^{13}C-NMR spectrum of **3**.

Supporting Information

Pirenzepine's doppelgänger: Momentous rearrangement of the most prominent muscarinic M1 antagonist

Marius Ozenil,[1] Lukas Skos,[1] Alexander Roller,[2] Natalie Gajic,[2] Wolfgang Holzer,[3] Helmut Spreitzer,[3] Sonja Platzer-Ozenil, Chrysoula Vraka,[1] Marcus Hacker,[1] Wolfgang Wadsak,[1,4] Verena Pichler[3,*]

[1] Department of Biomedical Imaging and Image-guided Therapy, Division of Nuclear Medicine, Medical University of Vienna

[2] X-ray Structure Analysis Centre, Faculty of Chemistry, University of Vienna

[3] Department of Pharmaceutical Chemistry, Faculty of Life Sciences, University of Vienna

[4] CBmed GmbH - Center for Biomarker Research in Medicine, Graz

*corresponding author

Table of contents

Table of contents 2
Materials 2
Instrumentation 3
Analytical differentiation between 2 and 4 4
Synthesis 8
Kinetics 11
Rearrangement using HCl in [^{18}O]H_2O 11
Rearrangement in simulated gastric fluid 11
Determination of affinities toward mAChR M1-M5 11
Cytotoxicity toward CHO Cell Line 12
References 13

Materials

11-(Chloroacetyl)-5,11-dihydro-6*H*-pyrido[2,3-*b*][1,4]benzodiazepin-6-one (abcr), 1-methylpiperazine (alfa aesar), Telenzepine dihydrochloride (Sigma Aldrich, T122), scopolamine hydrobromide (Sigma Aldrich), [^{18}O]H_2O (98 atom %, Hyox-18, Rotem), hydrochloric acid (HCl, 37%, Merck), pepsin (from porcine gastric mucosa, 3200-4500 units/mg protein, Sigma Aldrich), [*N*-methyl-^{3}H]scopolamine methyl chloride ([^{3}H]NMS, 2.964 TBq/µmol, 37 MBq, in 1 mL ethanol), poly(ethyleneimine) (PEI, 50% in H_2O, Fluka), phosphate buffered saline (PBS, pH 7.4, Gibco, Life Technologies Limited), acetonitrile (ACN, for HPLC, ≥99.9%, Sigma Aldrich),dichloromethane (DCM, EMPROVE® ESSENTIAL, Merck), dimethylsulfoxide (DMSO, ≥99.9%, Sigma Aldrich) and methanol (MeOH, for HPLC, ≥99.9%, Sigmal Aldrich) were used without further purification.

Table S1: *Obtained samples of fine chemical batches.*

#	company name	ordering number	lot number or batch
1	abcam	ab120153	APN10196-3-4
2	abcr	AB349569	1313238
3	AK Scientific	O383	080223G
4	EDQM Ref standard	Y0000038	batch 1
5	Glentham Life Sciences	GP0823	658NXR
6	Henan Allgreen Chemical	not reported	not reported
7	Hycultec	HY-17037	25525
8	Sigma Aldrich	P7412	079K1733V
9	TCI	P2457	XLZNG-SG

Table S2: *Obtained pharmaceuticals.*

company name	trade name	manufacturing	lot number or batch
Boehringer Ingelheim	Gastrozepin 50 mg, 50 Tabletten	Boehringer Ingelheim Ellas S.A., Greece	844033
Boehringer Ingelheim	Гастроцепін таблетки 25 мг, 50 таблеток	Boehringer Ingelheim Ellas S.A., Greece	744487
Boehringer Ingelheim	ガストロゼピン錠 100錠（10錠×10）	Nippon Boehringer Ingelheim, Japan	889001

Hikma	Gastrozepin 50 mg, 100 Tabletten	Delpharm Brétigny, France	G001
日医工株式会社 (Nichi-Iko)	ピレンゼピン塩酸塩錠25mg 100錠（10錠×10·PTP）	not specified in leaflet	CC2001
エスエス製業 (SSP Co. Ltd)	ガストール	SSP Pharmaceutical Co., Japan	01037E

Instrumentation

NMR samples were measured in $CDCl_3$ (≥ 99.8%, stabilized with silver foil, Sigma Aldrich) or D_2O (99.9%, Sigma Aldrich) at 25 °C. Chemical shifts are given referenced to the solvent signal of ^1H in $CDCl_3$ (δ 7.26 ppm), ^1H in D_2O (δ 4.79 ppm) and ^{13}C (δ 77.0 ppm) in $CDCl_3$. ^{15}N signals are given referenced to liquid NH_3. Combination of standard NMR techniques, such as COSY, NOESY, APT, HSQC and HMBC, allowed for unambiguous assignment of NMR signals, unless stated otherwise. NMR experiments were performed with a Bruker Avance III 400 or Bruker Avance III 600 spectrometer. ESI-TOF HRMS spectra were recorded with a Bruker maXis 4G instrument. IR spectra were recorded on a Shimadzu IRAffinity-1S FTIR spectrometer. Melting points were determined at a 2°C/min ramp with a DigiMelt SRS MPA160. MMFF94 energy was determined using LigandScout 4.4.3.

HPLC analyses were performed using a XSelect HSS T3 column (3.5 µm, 100 x 4.6 mm) on an Agilent 1200 series quaternary pump and degasser equipped with an Agilent 1100 series autosampler and UV detector (upgraded to G1315B DAD). Injection volume was set to 20 µL and UV detection wavelength to 216 nm. Linear gradient programs using 25 mM $(NH_4)H_2PO_4$ pH 9.3 buffer, acetonitrile (ACN) and an initial 3 min equilibration phase were applied for the analysis of **2, 4**, telenzepine and **6** (Table S3). For qualitative analysis of commercial pirenzepine samples the samples were injected at a concentration of 100 µg/mL. Pirenzepine containing tablets were suspended in water to yield the same concentration and insoluble additives were removed by centrifugation and/or filtration prior HPLC analysis.

Table S3: *HPLC parameters of the methods for the analysis of pirenzepine, telenzepine and their rearrangement products. LOD = limit of detection, LOL = limit of linearity*[i]

compound	t_R [min]	LOD [µg/mL]	LOL [µg/mL]	gradient
2	6.7	0.30	>50	0 min: 15% ACN, 3 min: 15% ACN, 9 min: 60% ACN, 9.01 min: 15% ACN.
4	3.0	0.41	>100	
Telenzepine	7.3	0.74	>50	0 min: 12% ACN, 8 min: 45% ACN, 8.25 min: 10% ACN.
6	5.1	0.38	>50	

Stably transfected CHO-K1 cells containing human muscarinic receptors M1-M5 were purchased from Missouri University of Science and Technology cDNA Resource Center (Cell Catalog#: CEM1000000, CEM2000000, CEM3000000, CEM4000000, CEM5000000) and maintained in Ham's F12 Nutrient Mixture (Gibco, Life Technologies Limited) supplemented with 10% FBS (Gibco, Life Technologies Limited) and 250 µg/mL Geneticin® (G418, Thermo Fisher) at 37 °C and 5% CO_2 in a cell incubator. Cells were passaged using Gibco Trypsin-EDTA (0.05%). A solution of P2714-1BTL, Sigma-Aldrich in 10 mL water was used as protease inhibitor cocktail. Count rate of the filter pieces was measured using 2 mL Ultima Gold (high flashpoint LSC cocktail, PerkinElmer) in CPM mode on a 300 SL Automatic TDCR liquid scintillation counter (HIDEX).

The X-ray intensity data were measured on Bruker D8 Venture diffractometer equipped with multilayer monochromator, Mo K/α INCOATEC micro focus sealed tube and Oxford cooling system. The structures were solved by *Direct Methods, Charge Flipping and Intrinsic Phasing*. Non-hydrogen atoms were refined with *anisotropic displacement parameters*. Hydrogen atoms were inserted at calculated positions and refined with riding model. The following software was used: *Bruker SAINT software package*[ii] using a narrow-frame algorithm for frame integration, *SADABS*[iii] for absorption correction, *OLEX2*[iv] for structure solution, refinement, molecular diagrams and graphical user-interface, *Shelxle*[v] for refinement and graphical user-interface *SHELXS-2015*[vi] for structure solution, *SHELXL-2015*[vii] for refinement, *Platon*[viii] for symmetry check. Experimental data and CCDC-Codes Experimental data (Available online: http://www.ccdc.cam.ac.uk/conts/retrieving.html) can be found in **Table S4**. Crystal data, data collection parameters,

and structure refinement details are given in **Table S5** to**Table S10**. Asymmetric Unit visualized in **Figure S5** to **Figure S7**.

Table S4: *Experimental parameter and CCDC-Code.*

Sample	Machine	Source	Temp.	Detector Distance	Time/ Frame	#Frames	Frame width	CCDC
	Bruker		[K]	[mm]	[s]		[°]	
4	D8	Mo	100	35	8	612	0.600	2010631
5	D8	Mo	100	35	8	3808	0.700	2010632
6	D8	Mo	100	40	10	1040	0.500	2010633

Analytical differentiation between 2 and 4

Pirenzepine dihydrochloride obtained from the EDQM **(2).**

^{1}H-NMR (400MHz, D_2O) δ 8.34 (m, 1H, Ar H-2), 7.85-7.46 (m, 6H, Ar H-3,4,7-10), 4.32 (d, 0.65H, *J*=16.7Hz, $COCH_2N)^{\Delta}$, 4.23 (d, 0.35H, *J*=16.6Hz, $COCH_2N$)*, 3.88 (d, 0.65H, *J*=16.7Hz, $COCH_2N)^{\Delta}$, 3.86 (d, 0.35H, *J*=16.6Hz, $COCH_2N$)*, 3.95-3.10 (m, 8H, H-2,3,5,6), 2.98 (s, 1.95H, $CH_3)^{\Delta}$, 2.96 (s, 1.05H, CH_3)*. ^{13}C-NMR (100MHz, D_2O) δ 169.1 $(NHCO)^{\Delta}$, 168.9 (NHCO)*, 167.3 (NCO)*, 166.7 $(NCO)^{\Delta}$, 146.5 (Ar C-2) $^{\Delta}$, 146.4 (Ar C-2)*, 144.2 (Ar C-11a)*, 143.6 (Ar C-11a)$^{\Delta}$, 139.1 (Ar C-10a)$^{\Delta}$, 138.0 (Ar C-10a)*, 135.9 (Ar C 3°)*, 135.2 (Ar C 3°)$^{\Delta}$, 133.3 (Ar C 3°)*, 133.2 (Ar C 3°)$^{\Delta}$, 132.2 (Ar C 3°)*, 131.8 (Ar C 3°)$^{\Delta}$, 131.4 (Ar C 3°)*, 131.2 (Ar C-4a)$^{\Delta}$, 130.9 (Ar C-4a)*, 130.4 (Ar C 3°)$^{\Delta}$, 129.4 (Ar C-6a)*, 128.4 (Ar C-6a)$^{\Delta}$, 128.0 (Ar C 3°)$^{\Delta}$, 127.5 (Ar C 3°)*, 127.1 (Ar C 3°)$^{\Delta}$, 126.6 (Ar C 3°)*, 57.8 $(COCH_2N)^{\Delta}$, 57.5 ($COCH_2N$)*, 51.6 (C-3,5)*, 51.5 (C-3,5)$^{\Delta}$, 50.1 (C-2,6), 43.4 (CH_3). ^{15}N-NMR (41MHz, D_2O) δ 292.6 (Ar N-1), 143.7 (Ar N-11), 133.3 (Ar N-5), 40.2 (N-4). HRMS (ESI) calcd for $C_{19}H_{22}N_5O_2$ ($M + H^+$) 352.1768, found 352.1773. m.p. 235 °C decomp.

NMR at 20°C in D_2O allows for the resolution of the interconverting exocyclic amide bond conformations.[2]ix Signals marked with '$^{\Delta}$' correspond to the more populated conformation, whereas '*' marks signals of the less populated conformation. In case signals of both conformations coincide, no mark is given. Most tertiary aromatic carbons could not be allocated unambiguously and are therefore labelled 'Ar C 3°'.

Pirenzepine dihydrochloride which actually contained the constitutional isomer **2-(2-((4-methylpiperazin-1-yl)methyl)-3*H*-imidazo[4,5-*b*]pyridin-3-yl)benzoic acid dihydrochloride (4).**

^{1}H-NMR (400MHz, D_2O) δ 8.51 (dd, 1H, *J*=5.0Hz, *J*=1.3Hz, Ar H-5), 8.43 (dd, 1H, *J*=8.3Hz, *J*=1.3Hz, Ar H-7), 8.37 (dd, 1H, *J*=7.7Hz, *J*=1.7Hz, Ph H-6), 7.99 (m, 1H, Ph H-4), 7.93 (m, 1H, Ph H-5), 7.73 (m, 1H, Ph H-3), 7.72 (dd, 1H, *J*=8.3Hz, *J*=5.0Hz, Ar H-6), 4.11 (s, 2H, $ArCH_2N$), 3.48 (m, 2H, H-3,5), 3.04 (m, 2H, H-3,5), 2.93 (m, 2H, H-2,6), 2.89 (s, 3H, CH_3), 2.72 (m, 2H, H-2,6). ^{13}C-NMR (100MHz, D_2O) δ 168.1 (COOH), 153.0 (Ar C-2), 147.2 (Ar C-5), 146.5 (Ar C-3a), 135.5 (Ph C-4), 133.3 (Ph C-6), 132.7 (Ph C-5), 131.2 (Ph C-2), 130.2 (Ph C-3), 129.1 (Ph C-1), 127.3 (Ar C-7a), 127.2 (Ar C-7), 122.7 (Ar C-6), 53.7 (C-3,5), 52.3 ($ArCH_2N$), 50.3 (C-2,6), 50.0 (C-2,6), 43.4 (CH_3). ^{15}N-NMR (41MHz, D_2O) δ 255.9 (Ar N-4), 180.7 (Ar N-1), 167.5 (Ar N-3), 41.6 (N-4), 36.7 (N-1). HRMS (ESI) calcd for $C_{19}H_{22}N_5O_2$ ($M + H^+$) 352.1768, found 352.1773. m.p. 185 °C decomp.

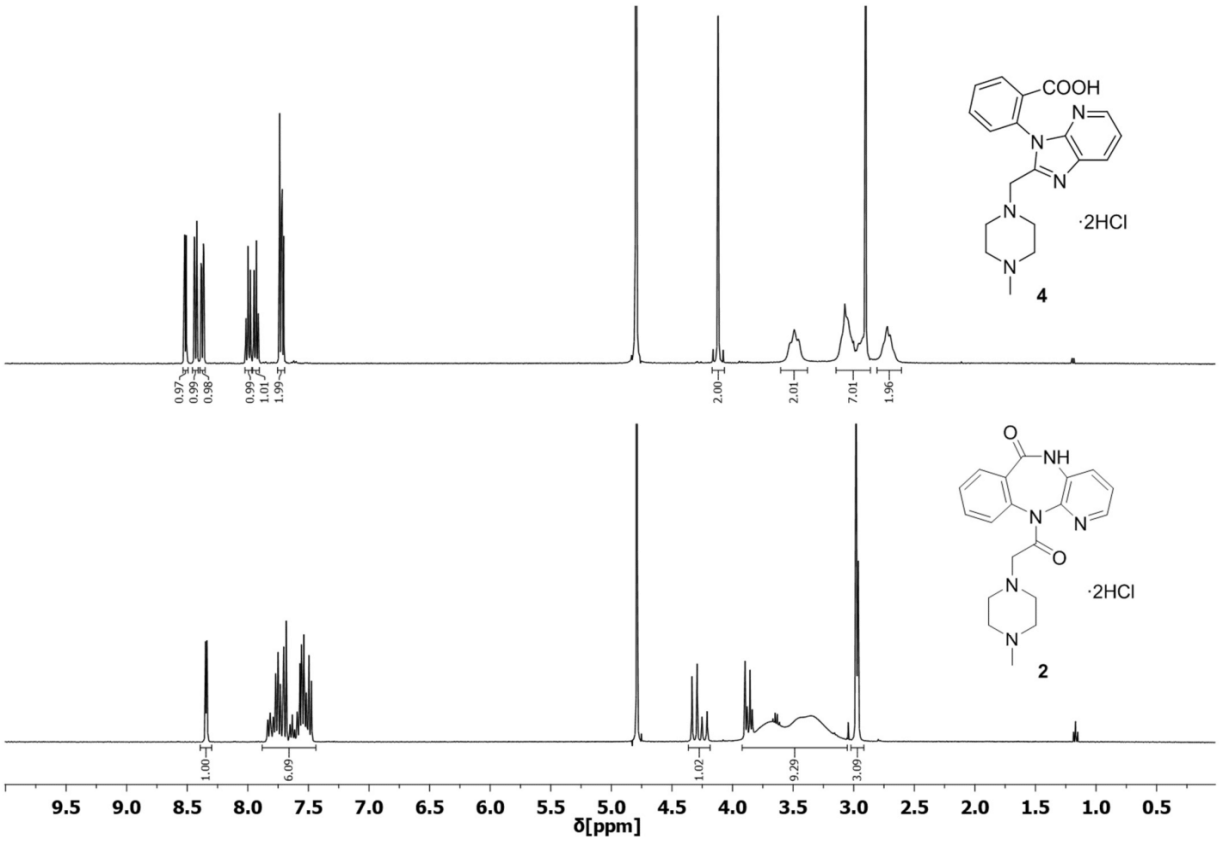


Figure S1: *^{1}H-NMR spectra of **2** (top, sample #2) and **4** (bottom, sample #4) in D_2O at 400 MHz.*

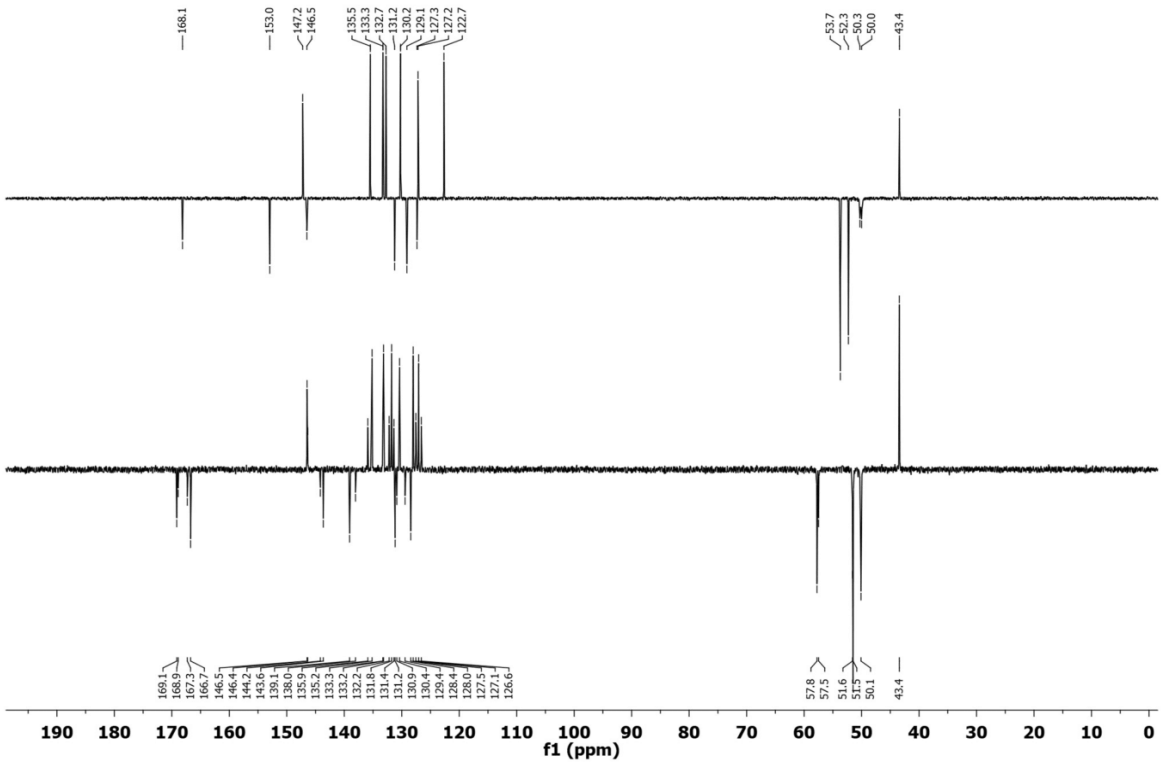


Figure S2: *^{13}C-NMR spectra of **4** (top, sample #2) and **2** (bottom, sample #4) in D_2O at 100 MHz.*

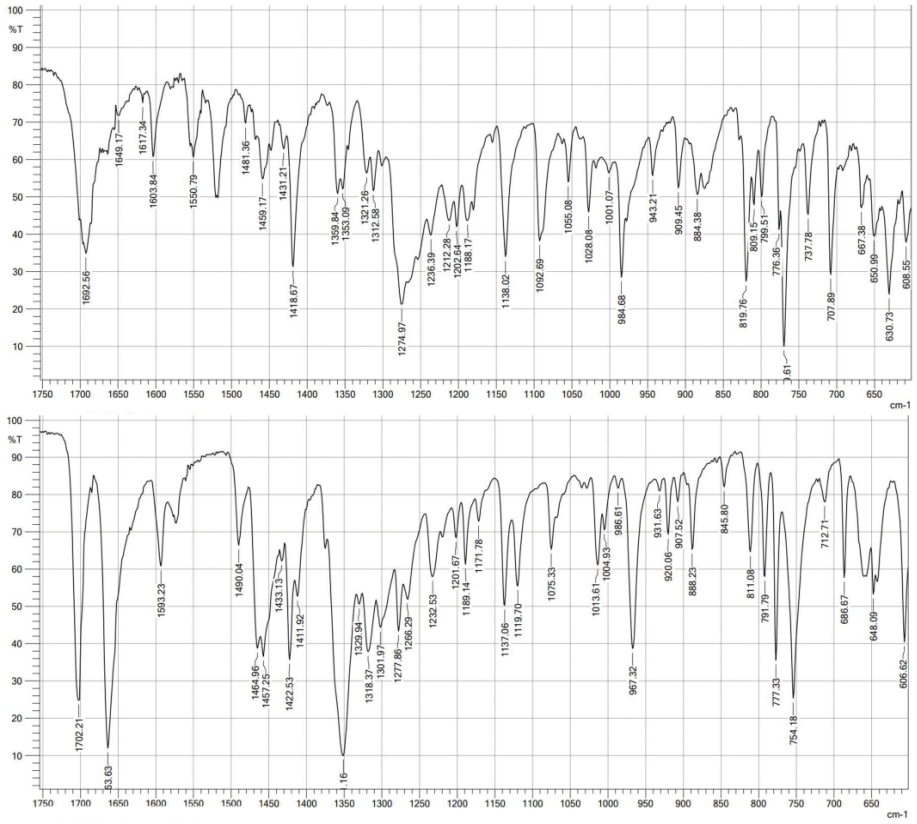


Figure S3: *IR spectra of **4** (top, sample #2) and **2** (bottom, sample #4). Most notable differences are the strong absorptions at 1663 cm^{-1} (**2**), 1351 cm^{-1} (**2**), 1275 cm^{-1} (**4**) and 1093 cm^{-1} (**4**).*

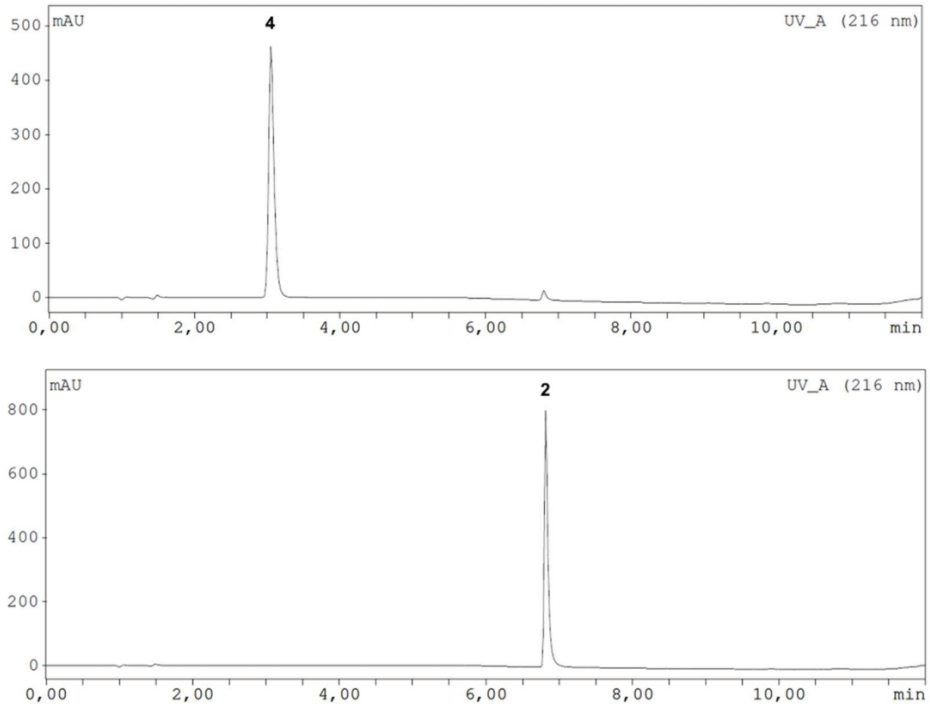


Figure S4: *UV-HPLC traces of **4** (top, sample #2) and **2** (bottom, sample #4).*

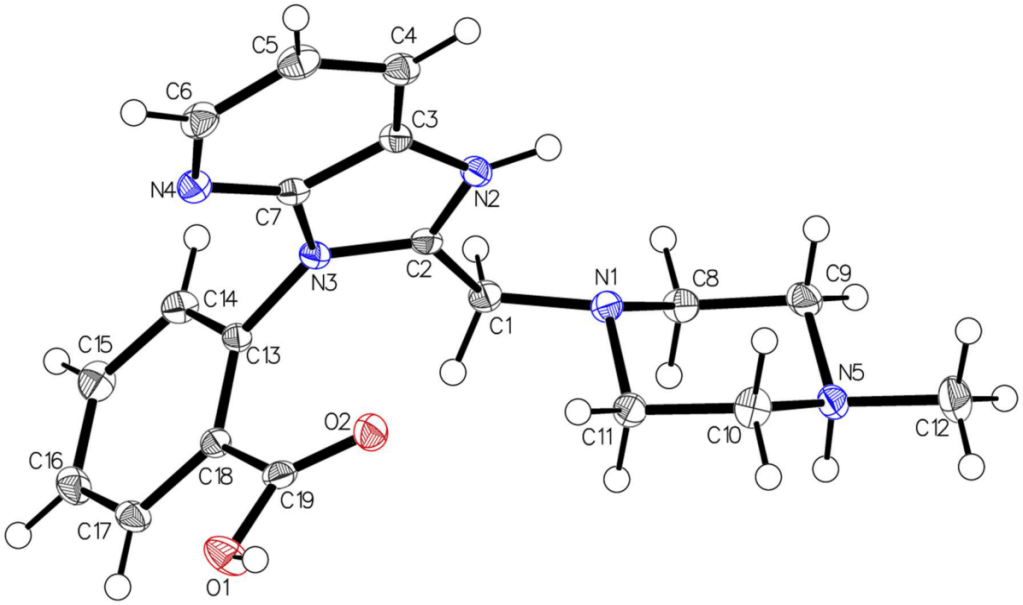


Figure S5: *Crystal structure of **4**, drawn with 50% displacement ellipsoid. The bond precision for C-C single bonds is 0.0017Å. Solvent omitted for clarity.*

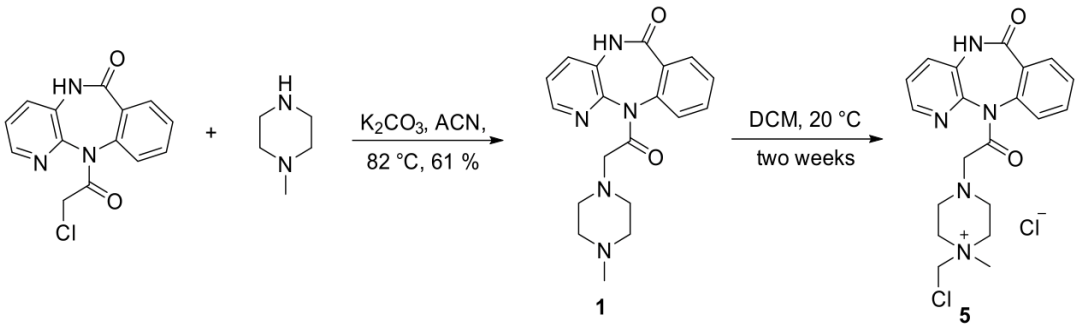
Table S5: *Sample and crystal data of **4**.*

Radiation [Å]	MoKα (λ = 0.71073)	Z	4	Measurement method	\f and \w scans
Crystal habit	clear colourless block	a [Å]	9.5381(5)		
Crystal size [mm³]	0.25 × 0.22 × 0.2	b [Å]	16.2994(9)	Abs. correction type	multiscan
Empirical formula	C19H25Cl2N5O3	c [Å]	14.1925(8)	Abs. correction Tmin	
Formula weight [g/mol]	442.34	α [°]	90	Abs. correction Tmax	
Temperature [K]	100.0	β [°]	106.5352	Density (calculated) [g/cm³]	1.389
Crystal system	monoclinic	γ [°]	90	Absorption coefficient [mm⁻¹]	0.338
Space group	P21/c	Volume [Å³]	2115.2(2)	F (000) [e⁻]	928.0

Table S6: *Data collection and structure refinement of **4**.*

2Θ range for data collection [°]	4.454 to 60.33	Index ranges		Goodness-of-fit on F^2	1.034
Reflections collected	20483	h	-12 ≤ h ≤ 13	Diff. peak and hole [e⁻Å⁻³]	0.45/-0.22
Data / restraints / parameters	6239/0/280	k	-23 ≤ k ≤ 17		
Refinement method	Direct Methods	l	-20 ≤ l ≤ 19	Function minimized	$\Sigma w (F_o^2 - F_c^2)^2$
		all data	R1 = 0.0415, wR2 = 0.0873	Weighting scheme	where
		I>2σ(I)	R1 = 0.0331, wR2 = 0.0820	$w=1/[\sigma^2(Fo^2) + (0.0403P)^2 +0.7619P]$	$P=(F_o^2+2F_c^2)/3$

Synthesis



11-(2-(4-methylpiperazin-1-yl)acetyl)-5,11-dihydro-6*H*-benzo[*e*]pyrido[3,2-*b*][1,4]diazepin-6-one, trivial name: **Pirenzepine (1).** 1-Methylpiperazine (34.8 mg, 0.348 mmol) in acetonitrile (2 mL) was added dropwise to a stirred suspension of 11-(Chloroacetyl)-5,11-dihydro-6*H*-pyrido[2,3-*b*][1,4]benzodiazepin-6-one (100 mg, 0.348 mmol) and K_2CO_3 (72.1 mg, 0.521 mmol) in acetonitrile (2 mL). The suspension was refluxed for 30 min, cooled to room temperature and the solid K_2CO_3 removed by filtration. Evaporation of the filtrate afforded a residue, which was solved in dichloromethane (5 mL). 1 mL of the crude product solution was purified by preparative TLC (DCM:MeOH = 9:1, Rf = 0.19-0.32) to yield pirenzepine as a colorless oil (15 mg, 61%).

^{1}H-NMR (400MHz, $CDCl_3$) δ 9.84 (brs, 1H, CONH), 8.28 (brs, 1H, Ar H-2), 7.96 (d, *J*=7.7Hz, Ar H-7), 7.63 (m, 2H, Ar H-9,10), 7.61 (dd, *J*=7.9Hz, *J*=1.3Hz, 1H, Ar H-4), 7.42 (m, 1H, Ar H-8), 7.31 (dd, *J*=7.9Hz, *J*=4.7Hz, 1H, Ar H-3), 3.58 (d, *J*=14.6Hz, 1H, NCH_2CO), 3.19 (d, *J*=14.6Hz, 1H, NCH_2CO), 2.43 (m, 2H, H-2,6), 2.16 (s, 3H, CH_3) 2.27-2.00 (m, 6H, H-2,3,5,6). ^{13}C-NMR (100MHz, $CDCl_3$) δ 169.7 (NCO), 168.2 (NHCO), 147.4 (Ar C-11a), 144.8 (Ar C-2), 140.8 (Ar C-10a), 133.4 (Ar C-9), 131.1 (Ar C-7), 130.7 (Ar C-4a), 129.8 (Ar C-4), 128.8 (Ar C-10), 128.3 (Ar C-6a), 128.0 (Ar C-8), 123.9 (Ar C-3), 61.1 ($COCH_2N$), 54.7 (Ar C-3,5), 52.8 (Ar C-2,6), 45.9 (CH_3). ^{15}N-NMR (41MHz, $CDCl_3$) δ 301.5 (Ar N-1), 142.8 (Ar N-11), 132.5 (Ar N-5), 37.0 (N-4). HRMS (ESI) calcd for $C_{19}H_{22}N_5O_2$ ($M + H^+$) 352.1768, found 352.1776.

1-(chloromethyl)-1-methyl-4-(2-oxo-2-(6-oxo-5,6-dihydro-11*H*-benzo[*e*]pyrido[3,2-*b*][1,4]diazepin-11-yl)ethyl)piperazin-1-ium chloride (5). Upon leaving the remaining crude product solution standing for 2 weeks colorless crystals formed, which were crystallographically identified as the nucleophilic substitution product of pirenzepine with dichloromethane.

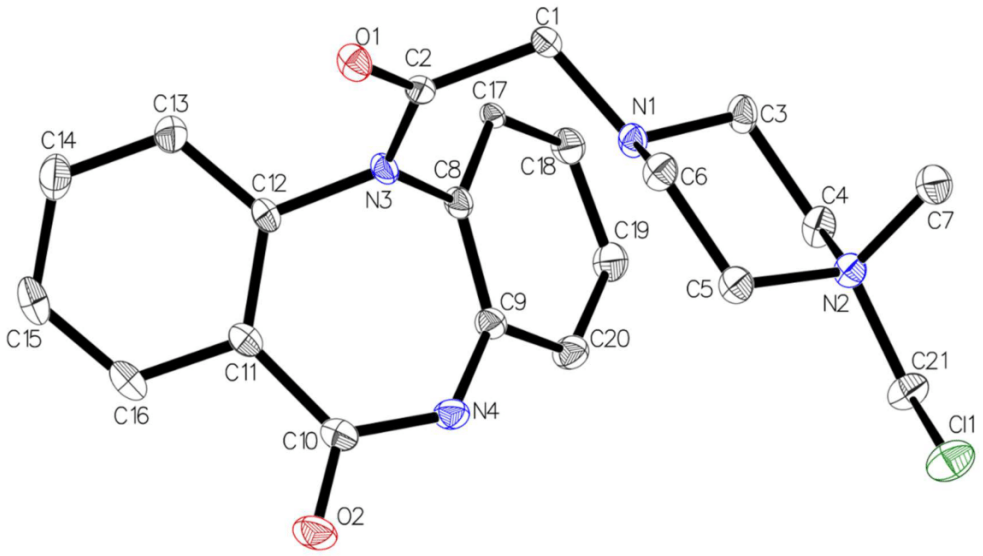


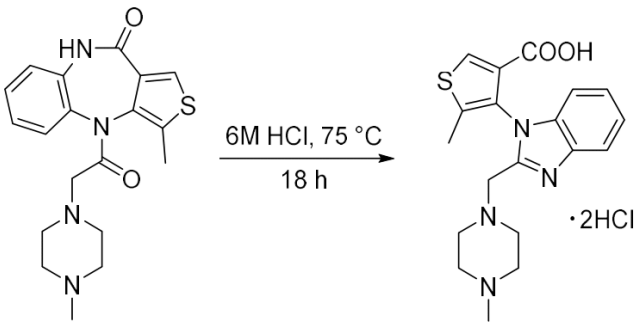
Figure S6: *Crystal structure of **5**, drawn with 50% displacement ellipsoid. The bond precision for C-C single bonds is 0.0020Å. Counter ion, hydrogen atoms and solvent omitted for clarity.*

Table S7: *Sample and crystal data of* ***5****.*

Radiation [Å]	MoKα (λ = 0.71073)	Z	2	Measurement method	\f and \w scans
Crystal habit	clear colourless block	a [Å]	8.9968(4)		
Crystal size [mm^3]	0.25 × 0.2 × 0.2	b [Å]	9.6557(4)	Abs. correction type	multiscan
Empirical formula	C11H13Cl2N2O	c [Å]	13.6354	Abs. correction Tmin	0.7617
Formula weight [g/mol]	260.13	α [°]	80.9712(18)	Abs. correction Tmax	0.8017
Temperature [K]	100.0	β [°]	82.0177(18)	Density (calculated) [g/cm^3]	1.491
Crystal system	triclinic	γ [°]	88.8009(19)	Absorption coefficient [mm^{-1}]	0.539
Space group	P-1	Volume [Å^3]	1158.50(8)	F (000) [e$^-$]	540.0

Table S8: *Data collection and structure refinement of* ***5****.*

2Θ range for data collection [°]	3.054 to 60.706	Index ranges		Goodness-of-fit on F^2	1.037
Reflections collected	74993	h	-12 ≤ h ≤ 12	Diff. peak and hole [e$^-$Å^{-3}]	1.19/-1.08
Data / restraints / parameters	6929/0/290	k	-13 ≤ k ≤ 13		
Refinement method	Charge Flipping	l	-19 ≤ l ≤ 19	Function minimized	Σ w (F$_o^2$ - F$_c^2$)^2
		all data	R1 = 0.0428, wR2 = 0.1185	Weighting scheme	where
		I>2σ(I)	R1 = 0.0388, wR2 = 0.1147	w=1/[σ^2(Fo^2) + (0.0668P)^2 +1.0659P]	P=(F$_o^2$+2F$_c^2$)/3



6

5-methyl-4-(2-((4-methylpiperazin-1-yl)methyl)-1*H*-benzo[*d*]imidazol-1-yl)thiophene-3-carboxylic acid (6). Telenzepine dihydrochloride hydrate (10 mg, 0.0226 mmol) solved in water (750 µL) and reacted with 12 M HCl (750 µL) at 75 °C for 18 h. The solvent was evaporated and the solid residue was solved in ethanol (1 mL). Crystalline **6** was obtained as colorless needles by vapour diffusion with diethyl ether.

^{1}H-NMR (600MHz, D_2O) δ 8.37 (d, 1H, *J*=2.3Hz, thiophene H-2), 7.92 (d, 1H, *J*=7.1Hz, Ar H-4), 7.68 (t, 1H, *J*=7.1Hz, Ar H-5), 7.62 (t, 1H, *J*=7.1Hz, Ar H-6), 7.43 (d, 1H, *J*=7.1Hz, Ar H-7), 4.04 (s, 2H, $ArCH_2N$), 3.50 (brs, 2H, H-2,6), 3.11 (brs, 2H, H-2,6), 3.02 (brs, 2H, H-3,5), 2.90 (s, 3H, NCH_3), 2.67 (brs, 2H, H-3,5), 2.30 (s, 3H, CH_3). ^{13}C-NMR (150MHz, D_2O) δ 164.9 (COOH), 151.2 (Ar C-2), 141.7 (thiophene C-4), 133.6 (Ar C-7a), 133.1 (thiophene C-2), 130.3 (Ar C-3a), 128.9 (thiophene C-3), 127.1 (Ar C-6), 127.0 (Ar C-5), 124.3 (thiophene C-5), 114.6 (Ar C-4), 112.4 (Ar C-7), 53.2 (C-2,6), 51.1 ($ArCH_2N$), 49.5 (C-3,5), 42.7 (NCH_3), 11.4 (CH_3). HRMS (ESI) calcd for $C_{19}H_{22}N_5O_2$ (M + H$^+$) 371.1536, found 371.1541.

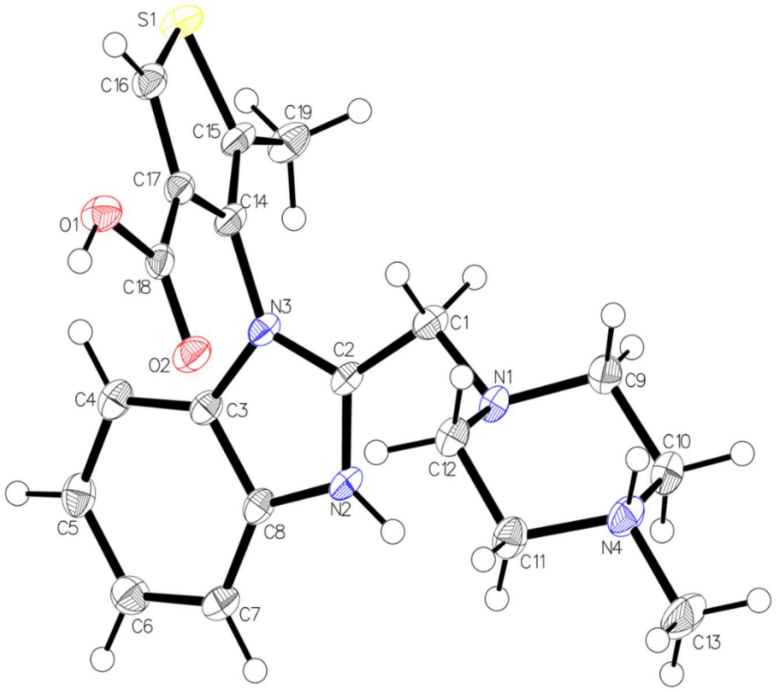


Figure S7: *Crystal structure of* ***6****, drawn with 50% displacement ellipsoid. The bond precision for C-C single bonds is 0.0039Å. Counter ion and solvent omitted for clarity.*

Table S9: *Sample and crystal data of* ***6****.*

Radiation [Å]	MoKα (λ = 0.71073)	Z	4	Measurement method	\f and \w scans
Crystal habit	clear colourless plate	a [Å]	12.8483(5)		
Crystal size [mm³]	0.2 × 0.13 × 0.03	b [Å]	10.8713(5)	Abs. correction type	multiscan
Empirical formula	C19.75H28.51Cl2N4O3.5S	c [Å]	17.7454(7)	Abs. correction Tmin	0.5166
Formula weight [g/mol]	480.97	α [°]	90	Abs. correction Tmax	0.5619
Temperature [K]	100.0	β [°]	101.326(2)	Density (calculated) [g/cm³]	1.314
Crystal system	monoclinic	γ [°]	90	Absorption coefficient [mm^{-1}]	0.383
Space group	P21/c	Volume [Å³]	2430.37(18)	F (000) [e$^-$]	1012.0

Table S10: *Data collection and structure refinement of* ***6****.*

2Θ range for data collection [°]	4.682 to 50.752	Index ranges		Goodness-of-fit on F^2	1.098
Reflections collected	40495	h	-15 ≤ h ≤ 15	Diff. peak and hole [e$^-$Å^{-3}]	0.89/-0.82
Data / restraints / parameters	4441/2/288	k	-12 ≤ k ≤ 13		
Refinement method	Intrinsic Phasing	l	-20 ≤ l ≤ 21	Function minimized	$\Sigma w (F_o^2 - F_c^2)^2$
		all data	R1 = 0.0643, wR2 = 0.1318	Weighting scheme	where
		I>2σ(I)	R1 = 0.0487, wR2 = 0.1174	$w=1/[\sigma^2(Fo^2) + (0.0528P)^2 + 3.9477P]$	$P=(F_o^2+2F_c^2)/3$

Kinetics

An aqueous solution of **2** (50 µL, 100 µg/mL) was combined with aqueous HCl (50 µL, 12 M) and shaken at 37 °C, 55 °C and 75 °C. At 30 min, 60 min, 90 min and 72 h a 5 µL of the reaction mixture were quenched with aqueous $NaHCO_3$ solution (45 µL, 55.5 mg/mL) and analyzed by HPLC. The experiment was performed in three repetitions. The reaction kinetics were studied using the AUC at 216 nm of formed **4** as a function of reaction time. Values were normalized on the AUC of **4** after 72 h, where no more unreacted **2** could be detected. For each temperature data points were fitted with $Y(t) = 1 - e^{-kt}$, with *Y* being the normalized AUC and *t* being the time. The activation energy (E_A) was determined from linear regression based on the linearized Arrhenius equation ($\ln(k) = -E_A/(RT) + \ln(A)$).

Rearrangement using HCl in $[^{18}O]H_2O$

In a three necked round-bottom flask equipped with a dropping funnel gaseous HCl was prepared by adding concentrated aqueous HCl (10 mL) on anhydrous $CaCl_2$. The formed gas was passed through $[^{18}O]H_2O$ (1 mL) using PVC and glas tubings. An aqueous solution of **2** in $[^{18}O]H_2O$ (200 µL, 10 mg/mL) was combined with the prepared HCl in $[^{18}O]H_2O$ solution (200 µL) and shaken at 75 °C for 60 min.40 µL of the reaction mixture were quenched with aqueous $NaHCO_3$ solution (100 µL, 55.5 mg/mL) and 10 µL of the resulting solution were separated by HPLC. A 50 mM NH_4Ac pH 9.3 was used as eluent instead of the $(NH_4)H_2PO_4$ buffer to allow for compatibility with mass spectrometry. Fractions of 2 and 4 were collected and analyzed by ESI-MS.

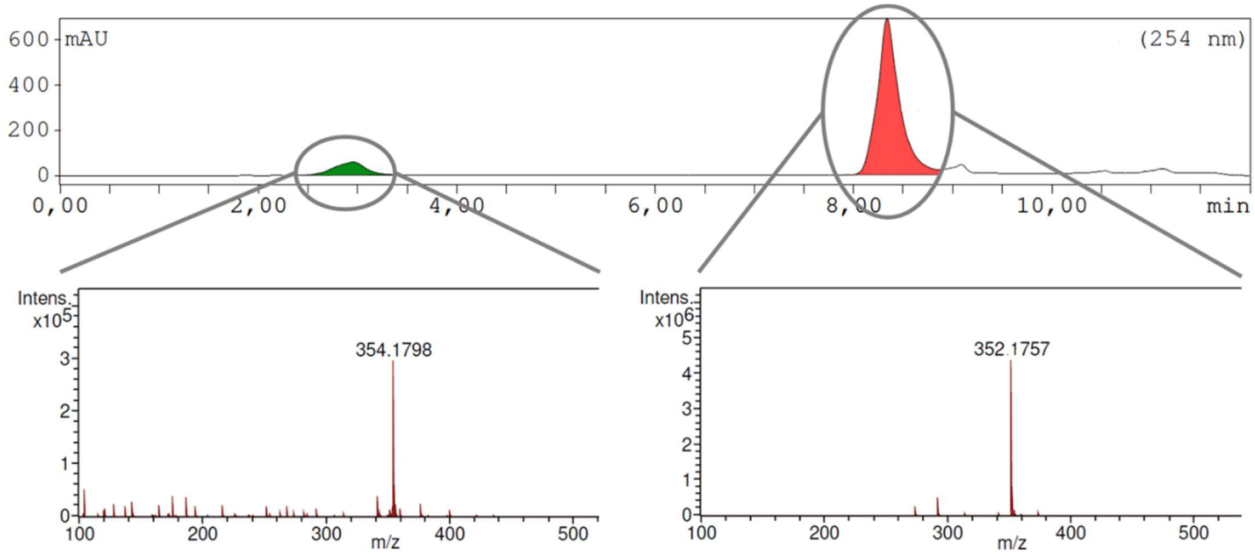


Figure S8: *Isomerization of **2** using HCl in $[^{18}O]H_2O$. The UV-HPLC chromatogram and HRMS spectra of collected fractions after 60 min at 75°C are shown: $[^{18}O]$**4** (t_R = 2.9 min, expected mass: 354.1816 m/z), **2** (t_R = 8.3 min, expected mass: 352.1768 m/z).*

Rearrangement in simulated gastric fluid

The initial concentration of **2** (50 µg/mL) was chosen to mimic the intake of a 50 mg tablet on 1 L of gastric fluid. An aqueous solution of **2** (50 µL, 100 µg/mL) was combined with 2x simulated gastric fluid (50 µL, 0.16 M aq. HCl, 2 g/L NaCl and 3.2 g/L pepsin)[3]x or equimolar aqueous HCl (50 µL) and shaken at 37 °C. At 30 min, 60 min, 90 min and 6 h a 5 µL of the reaction mixture were quenched with aqueous $NaHCO_3$ solution (45 µL, 55.5 mg/mL) and analyzed by HPLC.

Determination of affinities toward mAChR M1-M5

Membrane preparations of mAChR M1, M2, M3, M4 or M5 receptors were produced from the respective cell line as follows. Ten cell culture flasks were processed in parallel. The medium of a confluent T175 cell culture flask was poured off and the cell layer was washed with ice-cold PBS. Cells were scraped off and suspended in 2 mL/flask 10 mM Tris/HCl, 1 mM EDTA buffer (pH 7.4) and 200 µL protease inhibitor cocktail. A cell homogenate obtained from passing

the cell suspension through a G29 needle was centrifuged (10 min, 1,000 g, 4 °C). The supernatant was subjected to ultracentrifugation (30 min, 100,000 g, 4 °C) and the resulting pellet was suspended in 125 µL/flask 50 mM Tris/HCl buffer (pH 7.4) and stored at -80 °C.

A competitive radioligand binding assay using [^{3}H]NMS and variable concentrations of test compounds was performed in assay buffer (50 mM Tris/HCl, 10 mM $MgCl_2$, 1 mM EDTA). Polypropylene tubes were filled with 5 µL aqueous solution of the test compounds, 50 µL radioligand solution in assay buffer and 445 µL membrane suspension in assay buffer (diluted approx. 1:100), shaken and incubated for 1.5 h at 20 °C. Nonspecific binding of the radioligand was determined by using 5 µL of a 1 µM scopolamine hydrobromide solution instead. The concentration of the radioligand solution was chosen as 2 nM, 3 nM, 8 nM, 2 nM and 10 nM for M1-M5, respectively. Membrane bound activity was recovered using a M-36 tygon tubed Cell Harvester (Brandel, Gaithersburg, MD) and GF/B filters (Whatman, GE), presoaked in 0.1% PEI for 1.5 h. After filtration of the assay mixture tubes and hosing were washed with 2x3 mL ice cold 50 mM Tris/HCl buffer pH 7.4. The filter paper was punched out, transferred to scintillation tubes, mixed with 2 mL Ultima Gold scintillation cocktail (high flashpoint LSC cocktail, PerkinElmer), shaken for 15 min and counted in a liquid scintillation counter (HIDEX 300 SL) in CPM mode. Specific binding was calculated as total binding minus nonspecific binding. To delineate the IC_{50} value, specific binding was plotted against the logarithm of the test compound concentration and fitted by a variable slope logistic regression. IC_{50} values were calculated based on at least five different test compound concentrations in technical triplicates with n≥3. K_i values were calculated by means of Cheng-Prusoff equation using K_D values of 0.18 nM, 0.24 nM, 0.23 nM, 0.10 nM, 0.35 nM for M1-M5, respectively.[xi]

Cytotoxicity toward CHO Cell Line

Cytotoxicity was determined by means of a colorimetric microculture assay (MTT assay). For this purpose, CHO-K1 cells were harvested from culture flasks by trypsinization and seeded into 96-well microculture plates (Corning) in densities of 4,000 viable cells/well. After a 24 h preincubation, cells were exposed to dilutions of the test compounds in complete culture medium (200 µL/well) for 72 h. At the end of the exposure period, the compound solutions were replaced with RPMI 1640 medium supplemented with 10% heat-inactivated FBS and 4 mM L-glutamine (100 µL/well) and MTT solution (MTT reagent in PBS, 20 µL/well, 5 mg/mL). After incubation for 4 h, the medium was removed, and the formazan product was solved in DMSO (150 µL/well). Optical densities at 490 nm were measured with a microplate reader (BioTek Synergy HTX multi-mode reader) using a reference wavelength of 690 nm to correct for unspecific absorption. The quantity of viable cells was expressed in terms of T/C values by comparison to untreated controls. Evaluations were based on means from at least three independent experiments, each comprising triplicates for each concentration level.

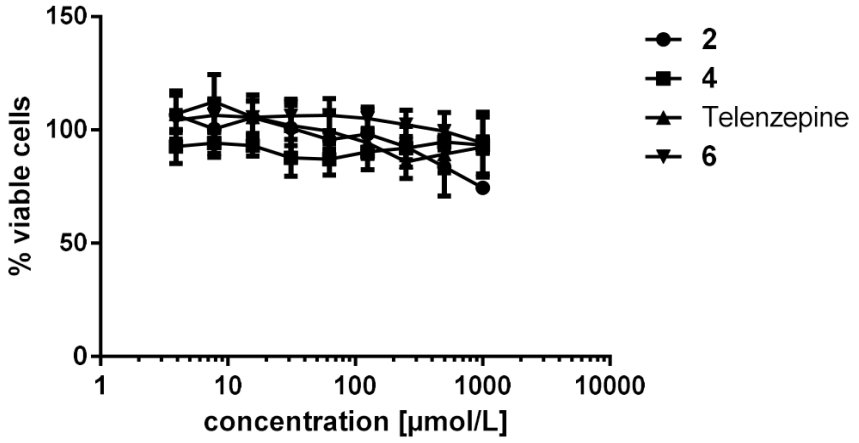


Figure S9: *Log-dose of **2**, **4**, telenzepine and **6** versus cell viability. No cytotoxic effect could be observed for concentrations as high as 1 mM.*

References

[i] ICH Harmonised Tripartite Guideline: Validation of Analytical Procedures: Text and Methodology Q2(R1), **1996**.
[ii] Bruker SAINT v8.38B Copyright © 2005-2019 Bruker AXS
[iii] G. M. Sheldrick, SADABS. University of Göttingen, Germany, **1996**.
[iv] O.V. Dolomanov, L.J. Bourhis, R.J. Gildea, J.A.K. Howard, H. Puschmann, *J. Appl. Cryst.* **2009**, *42*, 339–341.
[v] C. B. Huebschle, G. M. Sheldrick, B. Dittrich, *J. Appl. Cryst.* **2011**, *44*, 1281–1284.
[vi] G. M. Sheldrick, SHELXS v 2016/4, University of Göttingen, Germany, **2015**.
[vii] G. M. Sheldrick, SHELXL v 2016/4, University of Göttingen, Germany, **2015**.
[viii] A. L. Spek, *Acta Cryst.* **2009**, *D65*, 148–155.
[ix] J. Feeney, C. Pascual, *Journal of Pharmacy and Pharmacology* **1984**, *36*, 187–189.
[x] In *U.S. Pharmacopeia*, United States Pharmacopeial Convention, North Bethesda, Maryland, **2005**.
[xi] M. Ozenil, K. Pacher, T. Balber, C. Vraka, A. Roller, W. Holzer, H. Spreitzer, M. Mitterhauser, W. Wadsak, M. Hacker, V. Pichler, *European Journal of Medicinal Chemistry* **2020**, *204*, 112623.